Development and validation of biological monitoring tools for anaerobic (membrane) bioreactors

Iason PASSARIS

Supervisors:
Prof. dr. ir. Ilse Smets (promotor)
Prof. dr. ir. Ivo Vankelecom (co-promotor)

Members of the Examination Committee:
Prof. dr. ir. Hugo Hens (chair)
Prof. dr. ir. Kristel Bernaerts
Prof. dr. ir. Dirk Springael
Prof. dr. ir. Lise Appels
Prof. dr. ir. Vincent O'Flaherty

Dissertation presented in partial fulfilment of the requirements for the degree of Doctor of Engineering Science (PhD): Chemical Engineering

July 2018

© 2018 KU Leuven – Faculty of Engineering Science

Uitgegeven in eigen beheer, Iason Passaris, Celestijnenlaan 200F, box 2424, B-3001, Leuven, Belgium

Alle rechten voorbehouden. Niets uit deze uitgave mag worden vermenigvuldigd en/of openbaar gemaakt worden door middel van druk, fotokopie, microfilm, elektronisch of op welke andere wijze ook zonder voorafgaandelijke schriftelijke toestemming van de uitgever.

All rights reserved. No part of the publication may be reproduced in any form by print, photoprint, microfilm, electronic or any other means without written permission from the publisher

Preface

Het is een lange onderneming geweest, maar eindelijk is het af! Na meer dan 4.5 jaar spreken en dromen in termen van bioreactoren en cofactoren kan ik vandaag dit hoofdstuk afsluiten. Het lijdt geen twijfel, ik ben niet meer dezelfde onderzoeker, noch dezelfde persoon, als toen ik dit doctoraat aanvatte. Verwachtende dat een doctoraat "wel in het verlengde van een master thesis zal liggen", besefte ik uiteraard redelijk snel dat die twee niet vergelijkbaar zijn. Ten slotte heb ik over deze periode zelf een zevental thesissen begeleid. Laat ik het erop houden dat dit doctoraat me heeft geholpen om inzicht te krijgen in waar ik goed en minder goed in ben en me ook de kans heeft gegeven om deze werkpunten aan te pakken. Daarnaast heb ik, ondanks (of dankzij?) de ups en downs, ook een zeker idealisme in me herontdekt dat ik ook in de praktijk heb gebracht. Nu moet ik mezelf even inhouden om deze pagina niet vol te schrijven (ik ben niet zo voor kort en bondig…) en vooreerst een aantal mensen bedanken zonder wie dit doctoraat niet tot stand had kunnen komen.

Ten eerste wil ik mijn promotoren, Ilse en Ivo, bedanken voor de kans die ze me gaven om dit doctoraat aan te vatten. Ik klopte eerst bij Ivo aan, als begeleider van mijn thesis, en vond uiteindelijk bij Ilse een onderzoeksthema dat bij me pastte. Bij deze dank ik ook het IOF AnMBR kennisplatform (KP/13/004) voor de financiering van dit werk (iets zegt me dat ik nog vaker met dat IOF in aanraking zal komen…). Ilse, bedankt voor de fijne samenwerking. Ik denk dat we wel kunnen stellen dat mijn doctoraat van begin tot eind een team effort was en ik ben dan ook blij dat ook jij zeer tevreden bent met het finale werk. Dirk en Kristel wil ik ook graag persoonlijk bedanken omdat ze doorheen deze 4.5 jaren met hun kritische vragen en opmerkingen mijn werk mee richting hebben gegeven.

Via o.a. een stuurgroep en andere formele en informele contacten, waren er uiteindelijk ook een hoop externe stakeholders betrokken bij mijn werk. Bij deze zou ik dan ook de volgende mensen willen bedanken die elk op hun eigen manier een bijdrage aan mijn werk leverden: Roy Rosink, Geo Smith, Barry Heffernan, Thierry Arnaud, Frank Van der Zee, Rewin Pale, Santiago Pacheco-Ruiz, Walter "de operator", Marianne Van Wambeke, Kristof Cuadros, Veerle Van Malderen, Wouter Baekelant, Björn Dieu, Dirk Stockx & Prof. Lynn Vanhaecke,…

Zonder enkele interessante samenwerkingen zou mijn werk minder uitgebreid zijn geweest. In eerste instantie wil ik hiervoor Lynn, Dries & Vimac bedanken. Futhermore, thank you Johannes, Fabian and Conall for the nice collaborative experiments we managed together. All the best in the final stages of your PhDs.

Uiteraard heb ik doorheen deze jaren ook een hele hoop collega's gekend die minstens even belangrijk waren als het onderwerp van mijn doctoraat of de onderzoeksomgeving. Iedereen die me kent, weet dat ik graag met mensen omga en ik moet zeggen dat ik mijn werkomgeving als zeer aangenaam heb ervaren. Vooreerst dank ik de allereerste collega's die mijn eerste stappen in het doctoraat, ondanks moeilijke omstandigheden, in het oude CIT gebouw zo aangenaam mogelijk maakten. Een aantal mensen heb ik bijna van begin tot eind aan mijn zijde gehad en zou ik dan ook in het bijzonder willen bedanken. Jeroen (ping-pong, voetbal & pokébrother), Beatrice, Glenn, TheAhn en Hoang, jullie waren

aangename collega's! Aan de "nieuwere" aanwinsten; Kenneth (The Grinch), Wouter (ping-pong trainee), Lynn, Liesel, Koen, Robert, Armin, Armen, Pieter (x2), Kobe en Kjerstin ook een dikke merci om mijn flauwe moppen te ondergaan.

Hoewel ze vaak als vanzelfsprekend worden beschouwd, wil ik hier ook alle thesisstudenten die ik zelf begeleid heb, of waarmee ik in het labo stond, bedanken. Ilse beseft, volledig terecht, dat zonder goede thesisstudenten een onderzoeksafdeling niet draait. Bovendien zorgen ze voor een dynamiek en een structuur doorheen het jaar die ook de doctoraatsstudenten ten goede komt. Geen wonder dat ik op zijn minst eenmaal werd ingezet om een specifieke thesisstudent te rekruteren (you know who you are) ☺. Dus, bedankt Natalia, Riet & Piet, Charlotte & Kristof en Birte & Joren voor jullie wezenlijke bijdrage aan mijn werk en de fijne samenwerkingen!

Verder wil ik het ondersteunende personeel zeker niet vergeten. Herman & Hanne, jullie hielpen me om beetje bij beetje mijn anaerobe membraan bioreactoren in elkaar te steken (chapeau om geduld te hebben met mijn twee linkerhanden), ondanks het feit dat jullie overbevraagd zijn. Een paar extra Hermannen en Hanne's zijn zeer welkom! Ook Kenneth wil ik persoonlijk bedanken voor zijn ondersteuning in het labo en hulp met allerhande apparatuur. Of ik een paar extra Kenneth's aankan, weet ik dan wel weer niet…

Aan mijn vrienden in Lier en omstreken, studiegenoten uit Antwerpen (Patrons! Michiels, Domien, Jakob, Wouter, Janne, Linus), de YWP-crew (Marjo & co), de huisgenootjes van Kessel-Lo en het slakkenhuis en alle voetbalploegmaats, bedankt voor de meer dan welkome afleiding!

Ook bedankt aan al mijn fijne familieleden én schoonfamilie. Eén persoon in het bijzonder zal ik op mijn verdediging het meest missen. Tante Maria, je bent er niet meer. Ik zal me mijn laatste doctoraatsjaar helaas ook herinneren als het jaar waarin je overleed. Bedankt om er mee voor te zorgen dat dat "frank joenk" toch nog op zijn pootjes is terechtgekomen.

Μπαμπα, σε ευχαριστω για την ευκαιρια που μου εδωσες για να σπουδασο αυτο που ηθελα και να τελειωσω αυτο το διδακτορικο. Επισης σε ευχαριστω για ολες τις φορες που με πηγες σε ματς και προπονησης ποδοσφαιρου τοσα χρονια.

Johan, beste brother-from-the-same-mother, bedankt voor al je tips and tricks. Niet alleen doorheen mijn doctoraat maar doorheen heel mijn universitaire opleiding (wanneer ik weer eens in je kamer stond met een wiskunde-vraag). Bij AOS hadden we beide toch een goede uitlaatklep voor die doctoraatsfrustraties ;). Ik kijk er naar uit om terug vaker te kunnen afspreken wanneer jullie terug zijn. Dat brengt me bij het mooiste cadeau dat je me tot dusver hebt gegeven, namelijk mijn allerliefste petekindje, Ophilia P.☺! Het relativeren in mijn laatste doctoraatsjaar ging zoveel beter dankzij haar en elk moment dat we samen kunnen doorbrengen is een genot. O'tje, luister altijd flink naar je papa en je peter want dat zijn slimme dokters…Bedankt ook Charlotte voor de fijne muzikale momenten die we al samen beleefd hebben. Mogen er nog vele volgen!

Bedankt mama om me altijd alle kansen te hebben gegeven en me te steunen bij eender welke keuze die ik ook nam. Ik twijfel er niet aan dat je dat zal blijven doen en ik doe van mijn kant hetzelfde! Ondertussen besef ik wel degelijk in welke uitzonderlijke omstandigheden Johan en ik zijn mogen op groeien. We behoren letterlijk tot 's werelds

meest geprivilegeerde 2% en dankzij jouw opvoeding zal ik deze positie ook proberen te gebruiken om iets terug te geven aan de rest van de wereld.

Last but (zeker) not least wil ik uiteraard Laura bedanken. Laura, je was erbij vanaf het begin en (verbazingwekkend genoeg) ben je niet veel later hetzelfde pad ingeslagen. Eigenlijk typeert dat ons wel omdat we nu al ruim 6 jaar quasi alles samen doen en dat is eigenlijk een zeer fijne gewoonte geworden ☺. Bedankt om mijn steun en toeverlaat te zijn maar ook om me af en toe te "schoolen" in realistische planningen op te stellen! Vooral bedankt om keer op keer naar mijn gezaag te blijven luisteren en me te prikkelen om mijn passie voor voetbal & muziek te blijven volgen, ook in moeilijkere momenten. Wees er maar zeker van dat je op mij kan rekenen tijdens de rest van je doctoraat maar ook nog lang daarna, … Ik zie je graag.

Abstract

Anaerobic treatment is a well-established, environmentally friendly and economically viable process for the degradation of organic waste. The main practical concern when using anaerobic technologies is process instability leading to treatment failure. Research on improved reactor start-up and especially on recovery of failing reactors (e.g., as a result of changed influent characteristics) is, hence, fundamental to further boost anaerobic treatment technology. To improve reactor management, there is a demand for accurate monitoring tools for both daily reactor follow-up and in-depth process troubleshooting. Current monitoring tools are generally not predictive and do not allow process upsets to be alleviated. Furthermore, they are insufficiently targeted at methanogens and, if they are, require complex and time-consuming quantification methods. Anaerobic membrane bioreactors (AnMBRs) are a specific variant of high-rate anaerobic wastewater treatment systems that combine an anaerobic bioreactor with a membrane filtration unit. Although these reactors have been successfully implemented in full-scale during the last decade, an important aspect hampering their more widespread application is membrane fouling, which increases operational costs.

The overall aim of this PhD thesis is to provide useful monitoring tools to tackle the aforementioned limitations of anaerobic (membrane) bioreactors and increase their applicability. The current work is structured into two main research parts. In **Part I**, the use of methanogenic cofactors (cofactor F_{420} and F_{430}) is assessed for the improvement of biological monitoring. In **Part II**, the application of semi-automated quantitative microscopic image analysis is investigated for the improvement of membrane fouling monitoring. With respect to the first part, the main objective was the assessment of cofactor monitoring for both short- and long-term (industrial) applications, by unravelling the link between cofactor concentration and methane production dynamics. An additional objective was to determine whether cofactor monitoring could replace, or complement, commonly used monitoring methods. In the second part, the objective was to use an in-house developed activated sludge image analysis software for the impact assessment of sludge morphology (i.e., bioflocculation status) on membrane filterability in AnMBRs.

To accomplish the objectives of **Part I**, first, suitable extraction and quantification procedures for cofactor F_{420} and F_{430} need to be available. Therefore, methods from literature were refined and the resulting protocols were validated for use in anaerobic bioreactor experiments. For cofactor F_{430}, a protocol consisting of mechanical cell lysis, purification on a C18 cartridge and quantification using high-performance liquid chromatography (HPLC) provided satisfactory results. For cofactor F_{420}, two

quantification methods were investigated. Extraction and fluorescence quantification of the extract using a fluorimeter provided satisfactory results, whereas this was not the case for a method using quantitative fluorescence microscopy on fresh samples. In the next chapters, these quantification methods were applied in several anaerobic bioreactor experiments.

First, two experiments were performed to confirm the link between cofactor concentrations, on the one hand, and anaerobic bioreactor performance and methanogenic activity, on the other hand. It was shown that an intended inhibition of methanogenesis led to the reduction, or even absence, of cofactor F_{430}. The inhibition was achieved by overfeeding (i.e., an organic loading rate shock) and by increasing the phenolic content in the wastewater. The results served as a proof-of-principle, indicating that cofactor F_{430} can be used as a biomarker for methanogenic activity.

In the next chapter, again two separate experiments were performed in order to elucidate both cofactors' short-term dynamics. Furthermore, their potential to monitor and help avoid or relieve process disturbances in anaerobic bioreactors was investigated. In both experiments, organic loading rate shocks were induced, albeit using different reactor configurations, types of wastewater and time-scales. In the second experiment, *mcrA* gene copy and transcript numbers complemented the cofactor monitoring and served as a benchmark. It was shown that, in combination with methane gas production measurements, cofactor F_{430} and F_{420} content and their dynamics provide an important indication whether there is remaining methane production potential in anaerobic bioreactors subjected to organic loading rate shocks. Correlations between the two cofactors were found, despite the fact that cofactor F_{420} is expected to be predominantly present in hydrogenotrophic methanogens. This observation indicated that either hydrogenotrophic methanogenesis was the most important pathway, or both acetotrophic and hydrogenotrophic methanogens responded similarly to the applied upsets. *mcrA* copy numbers alone, poorly reflected the methane production dynamics, in contrast to the transcript numbers. Furthermore, both cofactor's and *mcrA* transcript production and degradation kinetics differ. The slower degradation kinetics of the cofactors provide an opportunity for the quantification of remaining methanogenic potential in stressed reactors.

Three additional potential applications for methanogenic cofactor monitoring were assessed in a total of five experiments in the final chapter of Part I. First, the application of cofactor quantification for the long-term monitoring of stable bioreactors was investigated and the trend was compared with that of the commonly applied specific methanogenic activity (SMA) test. To this end, two separate experiments were performed in different reactor configurations and using different types of wastewater (i.e., a "regular" synthetic dairy wastewater and one supplemented with long-chain fatty acids) for a prolonged period of time. Both the SMA tests and the cofactor monitoring method showed limitations in representing the actual trend in methanogenic activity in the bioreactors. The results from these experiments indicated that the common use of SMA test in industry should be re-evaluated, and that monitoring the long-term performance of anaerobic bioreactors poses challenges to cofactor measurements and requires further investigation. Next, cofactor F_{430}'s potential to detect stratification of methanogenesis in bioreactors was

investigated. An industrial-scale anaerobic digester was sampled at different heights and the cofactor content was determined at each height. Small differences in cofactor content were detected but could not be statistically substantiated. Nonetheless, the results provide sufficient incentive to further investigate the application of cofactor F_{430} measurements for identifying regions of higher or lower methanogenic activity in poorly mixed reactors or in certain specific reactor configurations (e.g., with attached and suspended biomass). Finally, the application of cofactor measurements for start-up monitoring was investigated. The follow-up of the failed start-up of two AnMBRs with respect to cofactor concentrations, was performed. The results indicate that it is recommended to include cofactor measurements prior to, and during, start-up in order to avoid bioreactor failure during this crucial phase.

In **Part II**, two AnMBRs were monitored for a period of 165 days for the assessment of anaerobic sludge morphology (i.e., bioflocculation status) quantification as a tool to monitor membrane fouling. Certain limitations of the automated image analysis programme used for the morphology quantification related to the segmentation of objects were uncovered throughout the course of the experiment. These limitations were sufficiently addressed in order for satisfactory results to be obtained, however, further optimization of the procedure may be required in the future. The AnMBRs were operated at different solids retention times (i.e., 20 and 40 days), after the start-up phase, and this resulted in different sludge morphologies. Reactor operation at an SRT of 40 days induced a shift towards more filamentous microorganisms. The longer SRT, and the concomitant higher sludge concentrations, led to reduced sludge loading rates and, hence, substrate limiting conditions. These conditions promoted the growth of filament forming bacteria because of their higher substrate affinity. Despite the difference in filament abundance between the two bioreactors, the main factor linked to membrane permeability was the number of fragments (i.e., very small particles). An increase in fragment number was observed throughout the experiment and coincided with reduced membrane permeability. However, this phenomenon was unrelated to the operation at different SRT. Floc erosion took place as a result of shear-stress imposed to the flocs in the cross-flow operated AnMBRs and, most likely, explains the increased abundance of fragments. Despite this floc erosion, the biological performance in the bioreactors was not significantly affected, indicating that the syntrophic interactions between hydrogen producing and consuming species were not disturbed. Monitoring the evolution of sludge morphology using automated microscopic image analysis proved valuable, since it allowed the changes in morphology to be numerically substantiated and linked to the reduced membrane filterability.

Samenvatting

Anaerobe afvalwaterzuivering is een bewezen, milieuvriendelijk en economisch rendabel proces voor de behandeling van organische vervuiling. De belangrijkste praktische belemmering bij het gebruik van anaerobe technologieën, is procesinstabiliteit, wat leidt tot het falen van het zuiveringsproces. Onderzoek naar verbeterde opstart, en vooral herstel, van verstoorde bioreactoren (e.g., als gevolg van veranderde afvalwaterkarakteristieken) is daarom van fundamenteel belang om de toepassing van anaerobe zuiveringstechnologieën verder te promoten. Voor de verbetering van het reactorbeheer is er nood aan accurate opvolgingsmethodes, en dit zowel voor de dagelijkse opvolging als voor gedetailleerde identificatie van problemen. De huidige opvolgingsmethodes zijn doorgaans niet voorspellend wat betreft reactorperformantie en laten niet toe om procesverstoringen te verhelpen. Voorts zijn ze onvoldoende specifiek voor de cruciale methanogene microorganismen en, wanneer ze dat wel zijn, benodigen ze complexe en tijdsintensieve methodolgieën. Anaerobe membraanbioreactoren (AnMBRs) zijn een specifieke variant van zogenaamde intensieve (*high-rate*) anaerobe afvalwaterzuiveringssystemen die een anaerobe bioreactor combineren met een membraanfiltratiesysteem. Ondanks het feit dat dit type van reactoren het voorbije decennium succesvol geïmplementeerd is, verhindert de membraanvervuiling hun verdere toepassing omwille van de gepaard gaande operationele kosten.

Het algemene opzet van dit doctoraat is om efficiënte opvolgingsmethodes aan te leveren om de bovenstaande beperkingen van anaerobe (membraan) bioreactoren aan te pakken en hun toepasbaarheid te vergroten. Het werk is gestructureerd in twee grote delen: in **Deel I** wordt het gebruik van methanogene cofactoren (cofactor F_{420} en F_{430}) beoordeeld, voor het verbeteren van de *biologische opvolging* en in **Deel II** wordt het gebruik van een geautomatiseerde kwantitatieve microscopische beeldanalyse onderzocht, voor de verbeterde *opvolging van membraanvervuiling*. Wat betreft het eerste deel, is de voornaamste betrachting om het gebruik van cofactor monitoring te beoordelen voor zowel lange- als korte-termijn (industriële) toepassingen, door de link tussen de cofactorconcentratie en de dynamica van methaanproductie te ontrafelen. Een bijkomende doelstelling is om te bepalen of cofactor *monitoring* de standaard gebruikte opvolgingsmethoden kan vervangen of aanvullen. In het tweede deel is de doelstelling om beeldanalyse van actief slib te gebruiken om de impact van de slibmorfologie (i.e., de bioflocculatiestatus) op membraanfiltreerbaarheid in AnMBRs te beoordelen.

Om de doelstellingen van **Deel I** te behalen, moeten eerst geschikte extractie- en kwantificatieprocedures voor cofactor F_{420} en F_{430} beschikbaar zijn. Methodes uit de

literatuur werden daarom verfijnd en de resulterende procedures werden gevalideerd voor gebruik in anaerobe bioreactorexperimenten. Een cofactor F_{430} protocol dat mechanische cellysis, opzuivering op een C18 kolom en kwantificatie met behulp van chromatografie omvatte, gaf bevredigende resultaten. Voor cofactor F_{420} werden twee verschillende kwantificatie methodologieën onderzocht. Extractie en kwantificatie van het extract met behulp van een fluorimeter leverde bevredigende resultaten, terwijl dat niet het geval was voor een methode gebaseerd op kwantitatieve fluorescentie microscopie. In de volgende hoofdstukken werden deze methodes gebruikt in verschillende bioreactorexperimenten.

Eerst werden twee experimenten uitgevoerd om de link te bevestigen tussen cofactorconcentraties enerzijds, en de performantie van anaerobe bioreactoren en hun methanogene activiteit, anderzijds. Er werd aangetoond dat een opgelegde inhibitie van de methanogenese tot een afname of zelfs afwezigheid van cofactor F_{430} leidde. De inhibitie werd in deze gevallen bereikt door het overvoeden van de reactor en het verhogen van de fractie van fenolische componenten in het afvalwater. De resultaten dienden als eerste indicatie dat cofactor F_{430} gebruikt kan worden als een biomerker voor methanogene activiteit.

In het volgende hoofdstuk werden opnieuw twee afzonderlijke experimenten uitgevoerd om de korte-termijn dynamica van beide cofactoren op te helderen. Bovendien werd hun potentieel om procesverstoringen in anaerobe bioreactoren te helpen vermijden, of op te lossen, onderzocht. Verstoringen werden aangelegd door het plots verhogen van de organische belading in het afvalwater. Verschillende reactorconfiguraties, types afvalwater en tijdsintervallen werden gebruikt in deze experimenten. In het tweede experiment dienden *mcrA* genkopieën en -transcripten als een vergelijksbasis voor de cofactor opvolging. Er werd aangetoond dat cofactor F_{420} en F_{430} en hun dynamica, in combinatie met methaangasproductiemetingen, een belangrijke indicatie geven wat betreft de residuele methaanproductiecapaciteit in anaerobe bioreactoren onderhevig aan een verstoring. Correlaties tussen de twee cofactoren werden gevonden, ondanks het feit dat cofactor F_{420} voornamelijk in hydrogenotrofe methanogenen zou voorkomen. Deze observatie impliceert dat de hydrogenotrofe methanogenese de dominante syntheseroute was, ofwel dat zowel acetotrofe als hydrogenotrofe methanogenen een gelijkaardige respons vertoonden op de procesverstoring. De *mcrA* genkopieën reflecteerden de methaanproductie dynamiek matig, in tegenstelling tot de transcripten. Voorts verschillen de productie- en degradatiekinetieken van beide cofactoren en de *mcrA* transcripten. De tragere degradatiekinetiek van de cofactoren biedt een opportuniteit voor de kwantificatie van het residuele methaanproductiepotentieel in verstoorde reactoren.

Drie bijkomende potentiële toepassingen voor methanogene cofactor monitoring werden, in een totaal van vijf afzonderlijke experimenten, beoordeeld in het laatste hoofdstuk van Deel I. Eerst werd de toepassing van cofactor kwantificatie voor de lange-termijnopvolging van stabiele bioreactoren onderzocht en werd de trend vergeleken met de veelgebruikte specifieke methanogene activiteitstest (SMA). Hiervoor werden twee afzonderlijke experimenten uitgevoerd in verschillende reactorconfiguraties en met verschillende types van afvalwater (i.e., een "gewoon" synthetisch zuivelafvalwater en een afvalwater waaraan lange-ketenvetzuren werden toegevoegd). Zowel de SMA test als de cofactor opvolgingsmethode toonden gebreken in het weerspiegelen van de werkelijke

methanogene activiteit in de reactoren. De resultaten van deze experimenten tonen dan ook aan dat het veelvuldig gebruik van SMA testen in de industrie herbekeken moet worden. Voorts blijkt dat monitoring van de lange-termijnperformantie van anaerobe bioreactoren uitdagingen inhoudt voor cofactor opvolging en dat hier bijkomend onderzoek naar nodig is. Vervolgens werd het potentieel van cofactor F_{430} om stratificatie van methanogenese in anaerobe bioreactoren te detecteren, onderzocht. Stalen werden genomen op verschillende hoogtes van een industriële vergister en de cofactorconcentratie werd op elke hoogte bepaald. Kleine verschillen in concentraties werden gevonden maar konden niet statistisch worden onderbouwd. Niettemin sporen de resultaten aan tot het verder bewandelen van deze onderzoekspiste. Cofactor F_{430} metingen zouden gebruikt kunnen worden om gebieden met een hogere of lagere methanogene activiteit te indentificeren in onvoldoende gemengde reactoren, of in bepaalde specifieke reactorconfiguraties. Tot slot, werd de toepassing van cofactor metingen voor de opvolging van reactoropstarten onderzocht. De mislukte opstart van twee AnMBRs werd opgevolgd met behulp van cofactormetingen. De resultaten wijzen aan dat het aan te raden is om ook cofactor metingen uit te voeren vóór en tijdens de opstart van bioreactoren om ondermaatse performantie in deze cruciale fase te vermijden.

Voor het onderzoeken van de kwantificatie van anaerobe slibmorfologie (i.e., de bioflocculatiestatus) als een middel om membraanvervuiling op te volgen, werden twee AnMBRs voor een periode van 165 dagen opgevolgd in **Deel II**. Enkele tekortkomingen van het geautomatiseerde beeldanalyseprogramma, dat gebruikt werd voor de kwantificatie van de morfologie, werden blootgelegd tijdens dit experiment. Deze tekortkomingen werden voldoende aangepakt om alsnog bevredigende resultaten te verkrijgen. Verdere optimalisering van de procedure is echter nodig in de toekomst. De AnMBRs werden na de opstartperiode bedreven op verschillende slibretentietijden (i.e., 20 en 40 dagen) en dit resulteerde in een verschillende slibmorfologie. De langere slibretentietijd leidde tot een lagere slibbelasting door de hogere slibconcentratie, en bijgevolg, tot substraatlimiterende condities. Deze omstandigheden bevoordeelden de groei van filamentvormende micro-organismen omwille van hun hogere substraataffiniteit. Ondanks de verschillen in de overmaat van filamenten tussen de twee bioreactoren, was het aantal fragmenten (i.e., zeer kleine partikels) de voornaamste factor die gelinkt kon worden met membraanpermeabiliteit. Een toename in het aantal fragmenten kon vastgesteld worden doorheen het experiment en viel samen met een daling in de membraanpermeabiliteit. Deze toename was echter niet gerelateerd aan de slibretentietijd. Ten gevolge van de *cross-flow* operatie van de AnMBRs, vond erosie van slibvlokken door wrijvingskrachten plaats, en waarschijnlijk verklaart dit de toename in het aantal fragmenten. Ondanks deze schijnbare deflocculatie, werd de biologische performantie van de bioreactoren niet beïnvloed. Vermoedelijk werden de syntrofe interacties tussen waterstofproducerende en consumerende micro-organismen dus niet verstoord. Het opvolgen van de evolutie van de slibmorfologie, met behulp van geautomatiseerde beeldanalyse, was een meerwaarde omdat het toeliet veranderingen in de morfologie te kwantificeren en te linken aan een verlaagde membraanpermeabiliteit.

List of abbreviations and symbols

(X)DLVO	(extended) Derjaguin-Landau-Verwey-Overbeek
ε	Extinction coefficient (L cm^{-1} mol^{-1})
μ	Specific growth rate (h^{-1})
μ_{max}	Maximum specific growth rate (h^{-1})
A	Absorbance
ACTIAS	ACTivated Sludge Image Analysis System
AGC	Automatic Gain Control
AIEX	Anion Exchanger
AnMBR	Anaerobic Membrane Bioreactor
ANME	Anaerobic Methanotrophic *Archaea*
ANOVA	Analysis of Variance
ASIAP	Activated Sludge Image Analysis Programme
au	arbitrary unit
CAS	Conventional Activated Sludge
cDNA	Complement DNA
CI	Confidence Interval
CLSM	Confocal Laser Scanning Microscopy
CoB	Coenzyme B
COD	Chemical Oxygen Demand
CSIA	Compound Specific Isotope Analysis
CST	Capillary Suction Time (s)
CSTR	Continuously Stirred Tank Reactor
CTAB	Cetyltrimethylammonium bromide
DAD	Diode Array Detector
DCB	Divalent Cation Bridging
D_{eq}	Mean equivalent floc diameter (μm)
dH_2O	distilled water
DNA	Deoxyribonucleic Acid
e	Euler's number
EA	Elemental Analysis
EDTA	Ethylenediaminetetraacetic Acid
EPS	Extracellular Polymeric Substances
F/M ratio	Food-over-microorganism ratio
FA	Free Ammonia (mg NH_3-N L^{-1})
FAD	Flavin Adenine Nucleotide
FD	Mean fractal dimension of flocs
FID	Flame Ionization Detector

FilLength	Mean filament length (μm)
FMN	Flavin Mononucleotide
FWHM	Full Width at Half Maximum
GC	Gas Chromatography
Hdr	Heterodisulfide reductase
HESI	Heated Electrospray Ionization Probe
HPLC	High-Performance Liquid Chromatography
HRT	Hydraulic Retention Time
HSD	Honestly Significant Difference
ICP-MS	Inductively Coupled Plasma-Mass Spectrometry
J	Flux (L m^{-2} h^{-1})
K_m	Affinity constant (g L^{-1})
l	Cuvette path length (cm)
LB-EPS	Loosely-Bound Extracellular Polymeric Substances
LCFA	Long-chain Fatty Acid
M/P ratio	Monovalent over Polyvalent cations ratio
m/z	exact mass
MBR	Membrane Bioreactor
MCR	Methyl-Coenzyme M Reductase
mcrA	Methyl-Coenzyme M Reductase gene α-subunit
MP	Milk Powder
MPT	Methanopterin
MQ	Metabolic Quotient
MRFA	Met-Arg-Phe-Ala acetate salt
mRNA	messenger Ribonucleic Acid
MS	Mass Spectrometry
n	number of observations
N/A	Not Applicable
NAD(P)H	Nicotinamide Adenine Dinucleotide (Phosphate) Hydrogen
NMR	Nuclear Magnetic Resonance
OHPA	Obligate Hydrogen-Producing Acetogen
OLR	Organic Loading Rate
OTU	Operational Taxonomic Unit
P	Permeability (L m^{-2} h^{-1} bar^{-1})
p	Statistical significance
Pa	Pascal
PLC	Programmable Logic Controller
ppm	parts per million
PVDF	Polyvinylidene Fluoride
PVPP	Polyvinylpolypyrrolidone
qPCR	quantitative Polymerase Chain Reaction
r	Pearson's correlation coefficient
R^2	Coefficient of determination
RelFilNum	Number of filaments per megapixel of image ($Megapixel^{-1}$)
RelFlocNum	Number of flocs per megapixel of image ($Megapixel^{-1}$)
RelFragNum	Number of fragments per megapixel of image ($Megapixel^{-1}$)
RNA	Ribonucleic Acid
Rndns	Mean roundness of flocs

RPM	Revolutions Per Minute
rRNA	ribosomal Ribonucleic Acid
RT	Retention Time
RT-qPCR	Real-Time quantitative Polymerase Chain Reaction
S	Substrate concentration (g L^{-1})
sCOD	soluble Chemical Oxygen Demand
SDG	Sustainable Development Goal
SDS	Sodium dodecyl sulfate
SMA	Specific Methanogenic Activity
SMP	Soluble Microbial Products
SPE	Solid Phase Extraction
SPT	Sarcinapterin
SRT	Solids Retention Time
SS	Suspended Solids
T	Temperature
TB-EPS	Tightly-Bound Extracellular Polymeric Substances
TMP	Transmembrane Pressure
T-RFLP	Terminal Restriction Fragment Length Polymorphism
TS	Total Solids
TSS	Total Suspended Solids
UASB	Upflow Anaerobic Sludge Blanket
UHPLC-HRMS	Ultra High-Perfromance Liquid Chromatography-High Resolution Mass Spectrometry
UV-VIS	Ultraviolet-visible spectroscopy
V	Volume or Volt
VFA	Volatile Fatty Acid
VS	Volatile Solids
VSS	Volatile Suspended solids
WWTP	Wastewater Treatment Plant

Contents

PREFACE I

ABSTRACT V

SAMENVATTING IX

LIST OF ABBREVIATIONS AND SYMBOLS XIII

CONTENTS XVII

1 INTRODUCTION AND OBJECTIVES 1

1.1 Challenges for the global water supply 2

1.2 Anaerobic wastewater treatment 3

1.3 Monitoring anaerobic (membrane) bioreactors 4

1.3.1 Biological monitoring 5
1.3.2 Membrane filtration monitoring 6
1.3.3 Objectives of this dissertation 6
1.3.4 Chapter-by-chapter overview 7

2 MONITORING ANAEROBIC (MEMBRANE) BIOREACTORS 9

2.1 Biological monitoring: methanogenesis 10

2.1.1 Anaerobic digestion: the basics 10
2.1.2 Monitoring: definitions and evolution 11
2.1.3 Indirect monitoring 12
2.1.4 Direct monitoring 15
2.1.5 Cofactor assays 19
Cofactor F_{430} 20
Cofactor F_{420} 24
Other methanogenic cofactors 27

2.2 Filterability monitoring: bioflocculation 28

2.2.1 Bioflocculation: fundamentals of a dynamic process 28
2.2.2 Factors affecting bioflocculation 30
2.2.3 Role in membrane fouling 32
2.2.4 Bioflocculation monitoring 33

3 MATERIALS AND METHODS 35

3.1 Analytical methods 36

3.2 Nucleic acid (DNA and RNA) extraction 38

3.3 Statistical analyses 39

PART I ASSESSING METHANOGENIC ACTIVITY USING METHANOGENIC COFACTORS 40

4 METHANOGENIC COFACTOR EXTRACTION AND QUANTIFICATION METHODS: ADAPTATION AND VALIDATION 41

4.1 Cofactor F_{430} 42

4.1.1 Native form and derivatives 42
4.1.2 Extraction and purification procedure 43
4.1.3 Quantification and identification methods 48
Absorbance quantification 49
HPLC quantification 50
Cofactor F_{430} identification 51
4.1.4 Standard preparation, purity check and quantification 53

4.2 Cofactor F_{420} 56

4.2.1 Extraction procedure 56
4.2.2 Quantification methods 57
Fluorimetry 57
Fluorescence microscopy 58

4.3 CONCLUSIONS 60

5 INHIBITION OF METHANOGENESIS INDUCES A REDUCTION IN COFACTOR F_{430} CONTENT: PROOF-OF-PRINCIPLE 61

5.1 Do overfeeding and pH shocks lead to significant cofactor reductions? 62

5.1.1 Materials & methods 62
5.1.2 Results 65
Overall reactor performance 65
Cofactor F_{430} and F_{420} content 68
5.1.3 Discussion 69
The effect of an OLR shock on reactor performance and cofactor content 69
The effect of an alkaline pH shock on reactor performance and cofactor content 70

5.2 Does phenol induced methanogenesis inhibition reduce cofactor F_{430} content? 72

5.2.1 Materials & methods 72
5.2.2 Results 74
Overall reactor performance 74
Cofactor F_{430} content 75
Community structure 76
5.2.3 Discussion 76
The mechanism of phenol induced methanogenesis inhibition 76
Cofactor F_{430} response to phenol induced methanogenesis inhibition 77

5.3 CONCLUSIONS 79

6 METHANOGENIC COFACTOR QUANTIFICATION AS A NOVEL APPROACH TO MONITOR PROCESS DISTURBANCES 81

6.1 Does methanogenic cofactor content reflect the dynamics of methanogenesis in digesters subjected to repeated overfeeding pulses? 83

6.1.1 Materials & methods 83

6.1.2 Results 87
Reactor 1 87
Reactor 2 92
Control Reactor 96
6.1.3 Discussion 99
Response of the methanogens to the induced process upsets 99
Correlations between the different experimental approaches for methanogen monitoring 102
6.2 Do cofactor and *mcrA* gene dynamics reflect the methane production dynamics in an anaerobic membrane bioreactor subjected to organic loading rate shocks? 105
6.2.1 Materials & methods 105
6.2.2 Results 109
Overall reactor performance 109
mcrA gene copy and transcript numbers 111
Cofactor F_{430} and F_{420} content 113
6.2.3 Discussion 114
mcrA gene and cofactor dynamics 114
6.3 CONCLUSIONS 118
7 APPLICATIONS OF METHANOGENIC COFACTOR MONITORING: ANAEROBIC BIOREACTOR START-UP, LONG-TERM OPERATION AND STRATIFICATION 119
7.1 Do SMA and cofactor content reflect the methanogenic activity well during stable, long-term bioreactor operation? 121
7.1.1 Materials & methods 121
7.1.2 Results 123
Overall reactor performance 123
Cofactor contents and SMA 124
7.1.3 Discussion 127
The effect of solids retention time on biomass concentration and activity 127
The relation between in-situ methanogenic activity and SMA on acetate 127
Cofactor F_{430} and F_{420} quantification versus SMA 128
7.2 Does the evolution of cofactor F_{430} content better reflect the long-term acclimatisation of anaerobic bioreactors than SMA tests? 130
7.2.1 Materials & methods 130
7.2.2 Results 133
7.2.3 Discussion 134
Comparison between the evolution of SMAs and reactor performance 134
Comparison between the evolution of cofactor F_{430} content and reactor performance 135
7.3 Can stratification of methanogenic activity in a full-scale digester be detected by cofactor F_{430} measurements? 137
7.3.1 Materials & methods 137
7.3.2 Results 138
Absorbance versus HPLC quantification of full-scale samples 138
Reactor stratification and cofactor F_{430} content 139
7.3.3 Discussion 141
Absorbance versus HPLC quantification of full-scale samples 141
Reactor stratification and cofactor F_{430} content 141

7.4 Can cofactor F_{430} and F_{420} measurements predict or diagnose the failed start-up of anaerobic bioreactors? 143
7.4.1 Materials & methods 143
7.4.2 Results 145
Reactor performance and cofactor content 145
7.4.3 Discussion 148
Main reasons for the failed bioreactor start-ups 148
The evolution of cofactor contents during deteriorating reactor performance 149
7.5 Does cofactor F_{430} content correlate with methane production across individually sampled reactors? 150
7.5.1 Materials & methods 150
7.5.2 Results 151
Variability between the inocula and the replicates 151
Correlation between cofactor F_{430} content and methane production 152
7.5.3 Discussion 153
Correlation between cofactor F_{430} content and methane production rate in 12 individually sampled reactors 153
7.6 CONCLUSIONS 155

PART II ASSESSING MEMBRANE FOULING (POTENTIAL) THROUGH BIOFLOCCULATION MONITORING 158

8 DOES SOLIDS RETENTION TIME INFLUENCE BIOFLOCCULATION AND MEMBRANE FOULING IN ANMBRS? 159
8.1 Materials & methods 160
8.2 Results 162
8.2.1 Image analysis with ASIAP 163
8.2.2 Evolution of the sludge morphology 164
8.2.3 Evolution of the membrane filtration performance 167
8.2.4 Correlations between sludge morphology and filtration related parameters 171
8.3 Discussion 174
8.3.1 The impact of solids retention time on sludge morphology 174
8.3.2 The impact of sludge morphology on membrane filterability 175
8.4 CONCLUSIONS 177

9 GENERAL CONCLUSIONS AND OUTLOOK 179
9.1 Part I - Assessing methanogenic activity using methanogenic cofactors 180
9.2 Part II – Assessing membrane fouling (potential) through bioflocculation monitoring 189

10 BIBLIOGRAPHY 193

11 CURRICULUM VITAE 209

CHAPTER 1

Introduction and objectives

In this chapter, a general introduction is provided, followed by the description of the overall objectives of this PhD thesis. First, the global challenges with respect to water availability are discussed. Next, the concepts of (anaerobic) wastewater treatment and monitoring are introduced. Finally, the overall objectives of the PhD are summarized, followed by a chapter-by-chapter overview of the work.

1.1 Challenges for the global water supply

The 6th United Nations Sustainable Development Goal (SDG) aims to ensure access to water and sanitation for all by the year 2030. At present, water scarcity affects more than 40% of the global population and is expected to rise. Today, 1.7 billion people live in regions where water use exceeds recharge, while more than 80% of our wastewater is discharged without any pollution removal (United Nations, 2015). Furthermore, as a result of the warming climate, both the frequency and the severity of droughts and heavy precipitation are expected to increase (Bates *et al.*, 2008). Floods and other water related disasters, today, already account for 70% of all deaths related to natural disasters (United Nations, 2015). Dry regions will become even drier whereas the opposite will occur in wet regions, creating more extreme regional differences. Apart from water *quantity*, higher temperatures and changes in weather extremes are projected to affect the water *quality* as well, which will affect access and utilisation and food availability (Bates *et al.*, 2008).

Contrary to popular belief, Belgium is regarded as a severely water stressed region (Vlaamse Overheid, 2009), indicating that the water quantity that is extracted is not sufficiently replenished. Figure 1.1 illustrates the baseline water stress in Belgium and surrounding countries according to Aqueducts Water Risk Atlas (Gassert *et al.*, 2014). In the summer of 2017, a long period of drought prompted the Flemish government to issue important measures with respect to water squandering (De Standaard, 2017). A few months later Spain and Portugal were hit by massive droughts and in early 2018 the coastal city of Cape Town, with a population of over 3.7 million inhabitants (more than half of that of Flanders), threatened to completely run out of water.

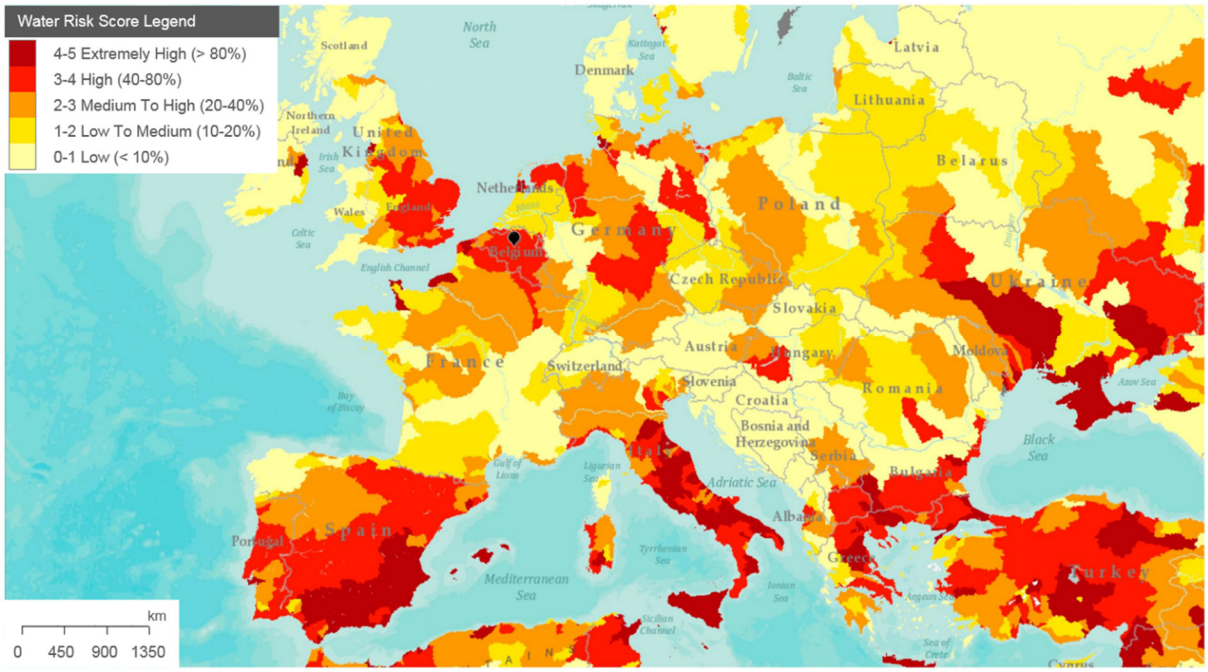


Figure 1.1 Baseline water stress according to Aqueduct's water stress indicators. Baseline water stress measures the ratio of total annual water withdrawals to total available annual renewable supply, accounting for upstream consumptive use. Higher values indicate more competition among users. Belgium is in the high risk zone (Gassert *et al.*, 2014).

These anecdotal examples and Figure 1.1 emphasize the severity of the challenges we face with respect to water quantity and quality and the importance of rational water use in a world suffering from climate change. With the increasing population pressures, wastewater should be regarded as a resource instead of a nuisance since it can be a sustainable source of clean water, energy and nutrients. In the transition towards a circular economy, wastewater treatment will play a key role (United Nations, 2017).

1.2 Anaerobic wastewater treatment

In light of water reuse and resource recovery, anaerobic wastewater treatment is preferred and of particular interest for *industrial wastewaters*. These wastewaters often contain large fractions of biodegradable organic pollutants with a high energy recovery potential. The advantages of anaerobic wastewater treatment compared to aerobic wastewater treatment are the following (Van Lier *et al.*, 2015):

(i) about 1 kWh (fossil *energy*) per kg of COD[1] removed, is *saved*;
(ii) about 1.5 kWh electric *energy* per kg of COD removed, is *produced*;
(iii) over 90% of excess *sludge production* is *avoided*, and;
(iv) spatial and carbon *footprint* are *reduced*.

The biogas (a methane and carbon dioxide mixture) that is produced from the anaerobic digestion of organics present in the wastewater can be used for on-site energy generation and, in combination with the reduction in energy use (since no aeration is required), allows for *energy-positive operation of wastewater treatment plants*. In fact, anaerobic digestion became the preferred method to treat wastewater and sludge in the 1970s because of the oil crisis (United Nations, 2017). By 2020, the market for industrial water treatment technologies is predicted to grow by 50% (GWI, 2015). The implementation of so called *high-rate anaerobic bioreactors* (HRARs) in particular has seen a strong increase over the last four decades. Since the early 1980's, over 1500 of these reactors have been installed, primarily in the agro-food and beverage industry (Van Lier *et al.*, 2015). The key to the success of the HRARs was the *immobilization of microorganisms* which allowed them to be retained inside the reactors (Lettinga *et al.*, 1980). This retention was crucial since these microorganisms perform the biochemical reactions to purify the wastewater and produce the biogas. Since the year 2000, significantly more research was devoted to the combination of high rate anaerobic wastewater treatment systems and membrane technology. The membrane functions as a filter and effectively retains all the microorganisms in the system while producing purified water. The number of research papers on this reactor technology, the *anaerobic membrane bioreactor (AnMBR)*, saw a 900% increase in a time span of just 15 years (2000 – 2015) (Dvořák *et al.*, 2016). Furthermore, in the last decade we have witnessed the full-scale implementation of this technology by leading anaerobic wastewater treatment technology providers, predominantly in food and dairy industry wastewaters (Van Lier *et al.*, 2015). Figure 1.2 provides a simplified schematic representation of the AnMBR technology.

It should be noted that release of the produced methane to the environment may offset the benefits of anaerobic wastewater treatment with respect to avoided greenhouse gas

[1] COD or Chemical Oxygen Demand is a measure of the organic carbon present in the wastewater

emissions when leaks or losses through the effluent are not detected and remediated. Therefore, proper biogas management, both in the gaseous and dissolved phase is required.

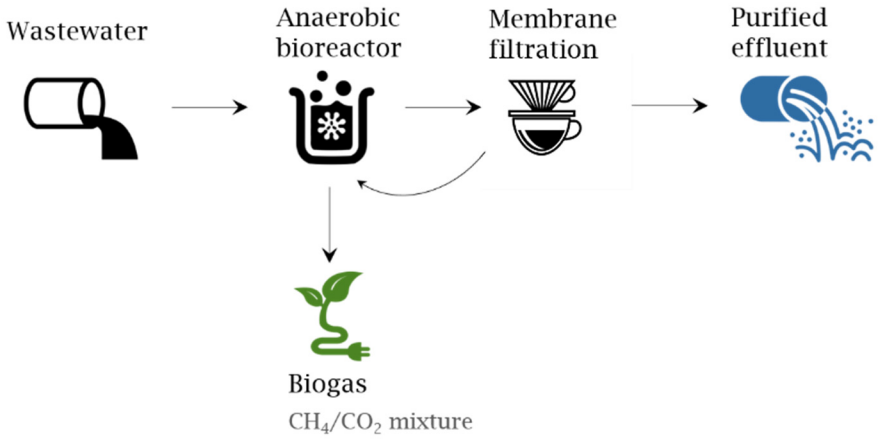


Figure 1.2 Schematic and simplified overview of the anaerobic membrane bioreactor (AnMBR) technology. An anaerobic bioreactor is coupled with a membrane filtration unit in order to separate the microorganisms from the purified effluent. The microorganisms convert the organic pollutants to biogas, which can be used for energy production. Icons from The Noun Project[2].

1.3 Monitoring anaerobic (membrane) bioreactors

To improve reactor management, there is a demand for accurate monitoring tools for both daily reactor follow-up and in-depth process troubleshooting: to measure is to know ("meten is weten"). The INTELSENS project reflects, for example, the significant efforts that are being made with respect to optimal monitoring of conventional (industrial) wastewater treatment in Belgium (TNAV). The project focuses on the smart integration of on-line sensors in order to optimally steer industrial wastewater treatment plants. The smart integration of sensors enforces another important trend, which is the implementation of real-time process monitoring (Nguyen *et al.*, 2015). Systems such as the AQUAVISTA™ Digital Suite (Veolia) provide customers with real-time remote control and monitoring of equipment at a glance, accessible from any device through a secured data cloud. In a similar way, SUEZ's recently launched ModuleTrac/InSight system allows their ultrafiltration membranes to be tracked, monitored and analysed via iOS and Android devices (Suez). Monitoring in anaerobic reactors is even more important than in their aerobic counterparts. Although providing important benefits, anaerobic bioreactors are generally more prone to biological process instability leading to treatment failure (Morris *et al.*, 2013; 2016). Aside from the *biological monitoring*, reducing membrane fouling in anaerobic membrane bioreactors is another important prerequisite in order to boost the implementation of this specific wastewater treatment technology. *Monitoring membrane filtration* and the main parameters that hinder prolonged operation may lead to significant economic benefits because of the operating expenditure related to membranes (Lin *et al.*, 2013).

[2] Waste Water by Alv Jørgen Bovolden, Coffee-filter by Eray Kula, Reactor by Delwar Hossain, Sustainable energy by Blake Thompson, Effluent by Luis Prado from The Noun Project, <https://thenounproject.com>.

1.3.1 Biological monitoring

The anaerobic digestion process takes place in the absence of oxygen and consists of four main steps: hydrolysis, acidogenesis, acetogenesis and methanogenesis. Figure 1.3 shows a simplified schematic overview of the anaerobic degradation of organic molecules to methane and carbon dioxide.

Since the steps of anaerobic degradation are performed in sequence, the microorganisms performing these steps rely on each other's activity in order to successfully produce the end product. Accumulation of intermediate products may occur when the reaction rates of the different groups of microorganisms are not balanced and this imbalance often leads to process failure (Hutschemackers *et al.*, 1982). The microbial group performing the final step, i.e., the production of methane, are the methanogens which belong to the domain of the *Archaea*. This distinct group of prokaryotic microorganisms contains the slowest growing and most sensitive species of the process (Wang *et al.*, 2009; Kangle *et al.*, 2012). Their key-role in the anaerobic digestion process and their sensitivity to environmental stress conditions explains why most of the research regarding biological monitoring in anaerobic digestion focuses on methanogens.

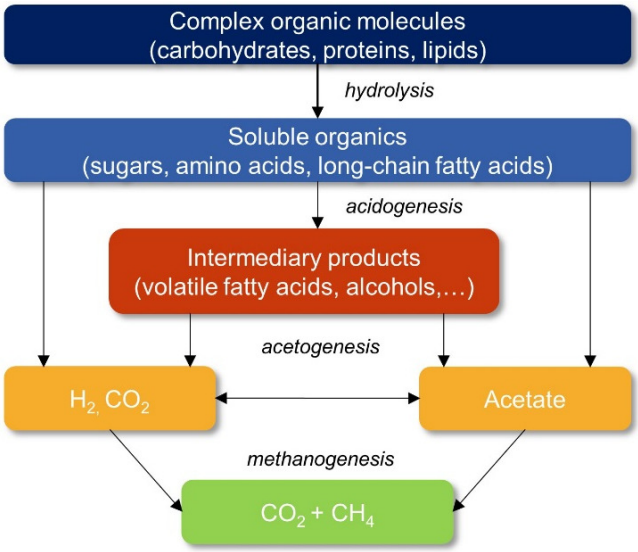


Figure 1.3 Simplified schematic representation of the anaerobic digestion process. Complex organic molecules in the wastewater are converted to methane and carbon dioxide through four main steps: hydrolysis, acidogenesis, acetogenesis and methanogenesis. Figure adapted from Visvanathan *et al.* (2012).

In recent years, different kinds of direct and indirect ways of monitoring the activity of methanogens (i.e., the methanogenic activity) have been developed and investigated. These tools range from relatively simple, physico-chemical analyses using sensors, to complex methods targeting the methanogen's specific genetic code. However, currently, online analysis of, i.e., COD and VFA concentrations is rarely used because of the cost of their implementation. Moreover, molecular genetic biomarkers (i.e., the *mcrA* gene) have been used but a general relation with bioreactor performance is often difficult to establish. Intermediate complexity tools are of particular interest since they may provide the ideal balance between providing detailed information while reducing cost, analysis time and complexity. In general, there is a lack of monitoring tools that specifically target methanogens, have a predictive character, allow process upsets to be alleviated and are

easily and quickly measured. Considering the growing market for anaerobic wastewater treatment technologies, accurate and reliable biological monitoring tools are required in order to unlock the true potential of this remarkable microbial consortium.

1.3.2 Membrane filtration monitoring

As mentioned previously, membrane maintenance and replacement is an important operational cost for MBRs and even more so in the anaerobic variant (Lin *et al.*, 2011). As a result, considerable research effort has been devoted to improving membrane materials, module design and operational strategies in order to allow the prolonged operation of these types of bioreactors. The process through which the membrane performance deteriorates is called *membrane fouling* and results from the interaction between the membrane surface and the bioreactor contents. Chemical engineers focus on achieving the ideal membrane surface characteristics, whereas (micro)biological engineers try to unravel and influence the complex interactions between the microorganisms and the membrane surface. With respect to the latter, the process of *bioflocculation* is of paramount importance. This complex process, of which all of the involved mechanisms have not yet been elucidated, involves the agglomeration of individual microorganisms into larger structures called flocs. The types of microorganisms that are present, their shape, the specific chemicals they excrete and a large number of environmental factors all influence the bioflocculation process (Nielsen *et al.*, 2012). Most research, thus far, has focused on bioflocculation in aerobic wastewater treatment systems. Considering the importance of membrane fouling in the viability of the anaerobic MBR technology and the role that bioflocculation plays in that respect, there is a clear incentive for delving deeper into the interactions between these microorganisms (and the membrane) on a microscopic level.

1.3.3 Objectives of this dissertation

The objectives of this PhD thesis are related to the improvement of biological monitoring, on the one hand, and objectives related to the monitoring of membrane filtration in anaerobic membrane bioreactors, on the other hand.

The first goal is to assess and quantify methanogenic activity in anaerobic reactors using methanogenic cofactors. To this end, the following research steps are proposed:

- *(i)* setting the scene – current state-of-the-art in methanogenesis monitoring;
- *(ii)* refine and validate suitable methanogenic cofactor extraction and quantification protocols;
- *(iii)* provide a proof-of-principle for the use of cofactors in methanogenic activity monitoring;
- *(iv)* compare the dynamics of the cofactors with that of methane production and other commonly used monitoring tools, and;
- *(v)* select the most promising applications for cofactor monitoring in anaerobic reactors.

The second goal is to assess the membrane fouling (potential) in anaerobic membrane bioreactors through bioflocculation monitoring. This goal involves the following research steps:

(i) validate the use of an in-house developed activated sludge image analysis software, for anaerobic sludges;
(ii) influence the bioflocculation process by altering a selected operational parameter, and;
(iii) investigate the impact of sludge morphology on membrane filterability.

1.3.4 Chapter-by-chapter overview

Following this introductory chapter, *the state-of-the-art* with respect to biological and filtration monitoring in anaerobic (membrane) bioreactors is provided in **Chapter 2**. In the first part, after critically assessing the currently available biological monitoring tools, the focus will be shifted to methanogenic cofactors and their application as monitoring tools for methanogenic activity. In the second part of the chapter, filterability monitoring in anaerobic membrane bioreactors is discussed with a specific focus on monitoring the bioflocculation status. From the literature review, knowledge gaps are identified. Figure 1.4 shows a schematic representation of the PhD structure.

Chapter 3 describes the *general materials and methods* that were used. More specific materials and methods are included in the respective results chapters.

In **Chapter 4**, the adaptation and validation of available extraction and quantification methods for two specific cofactors, i.e., cofactor F_{420} and cofactor F_{430}, is elaborated. The *methodology development* described in this chapter is used throughout Chapters 5 to 7.

The results of this PhD thesis are thematically divided into two main parts, based on the distinction between biological and filterability monitoring introduced earlier. **Part I**, the most elaborate part, contains four chapters relating to the *assessment of methanogenic cofactors for methanogenic activity monitoring* in anaerobic bioreactors. In **Chapter 5**, two experiments are described which served as a validation of the extraction and quantification methods described in Chapter 3. More importantly, this chapter provides a proof-of-principle confirming the link between the methanogenic cofactors, on the one hand, and anaerobic reactor performance and methanogenic activity, on the other hand. **Chapter 6** builds further on the proof-of-principle presented in Chapter 5 and investigates the use of methanogenic cofactor quantification for the monitoring of process disturbances in anaerobic bioreactors. To this end, two separate experiments are discussed, of which the second has been published in Passaris *et al.* (2018). In **Chapter 7**, the final chapter of Part I, three additional potential applications of cofactor monitoring are investigated. A total of five separate experiments are discussed in this chapter.

In **Part II**, the *assessment of membrane fouling through bioflocculation monitoring* is tackled. **Chapter 8** presents the results from an experiment in which the impact of an operational parameter (i.e., the solids retention time) on bioflocculation and membrane filtration performance is investigated.

Finally, general conclusions are drawn and future perspectives are provided in the final chapter, **Chapter 9.**

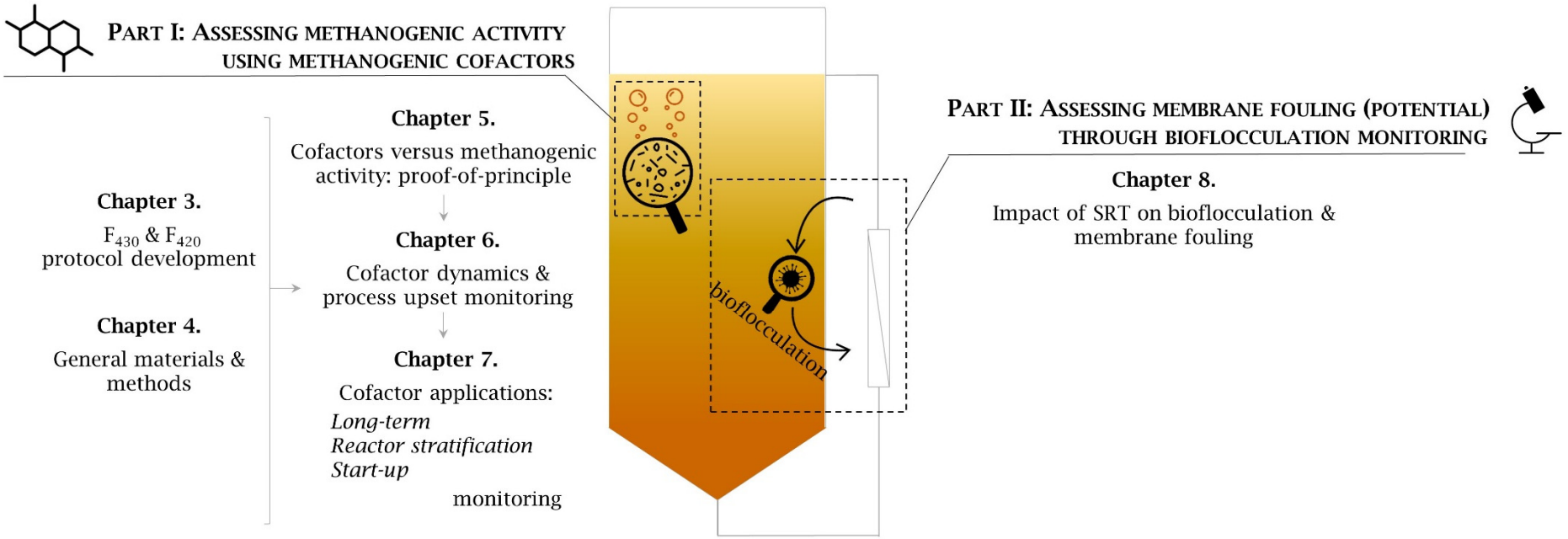


Figure 1.4 Schematic representation of the PhD structure. Part I focuses on monitoring of the biological activity in anaerobic bioreactors, whereas Part II focuses on bioflocculation monitoring in anaerobic membrane bioreactors for the assessment of membrane fouling potential. Icons from The Noun Project[3].

[3] Microscope by AliWijaya, Bacteria by Hugo Alberto, Magnifying Glass by Delwar Hossain, Bubbles by anbileru adaleru, Molecule by mikicon, Arrow by 4B icons from The Noun Project, <https://thenounproject.com>.

CHAPTER 2

Monitoring anaerobic (membrane) bioreactors

In this chapter, the current literature with respect to biological and filtration monitoring of anaerobic (membrane) bioreactors is summarized. At the end of each section, the knowledge gaps are highlighted and these are addressed in the experiments described in the following chapters. The chapter is subdivided into two main parts: Section 2.1 will discuss biological monitoring of the anaerobic digestion process, with a specific focus on methanogenesis, whereas Section 2.2 summarizes the current literature with respect to membrane filtration monitoring in AnMBRs, with a specific focus on bioflocculation.

2.1 Biological monitoring: methanogenesis

In this first part, the state-of-the-art with respect to monitoring of the methanogenic community and its activity, is provided. The focus on this specific group of microorganisms is justified by their aforementioned importance and sensitivity to process upsets. First, a brief summary of the general processes taking place in anaerobic digestion is given. Next, some important definitions and the evolution of commonly used monitoring tools for methanogenesis are described. The final section will zoom in on cofactor assays since these are of particular importance in this thesis.

2.1.1 Anaerobic digestion: the basics

As briefly mentioned in the previous chapter, the anaerobic digestion of organic wastes consists of four distinct steps, which take place in succession. Figure 2.1 shows a simplified schematic of the processes taking place during anaerobic digestion.

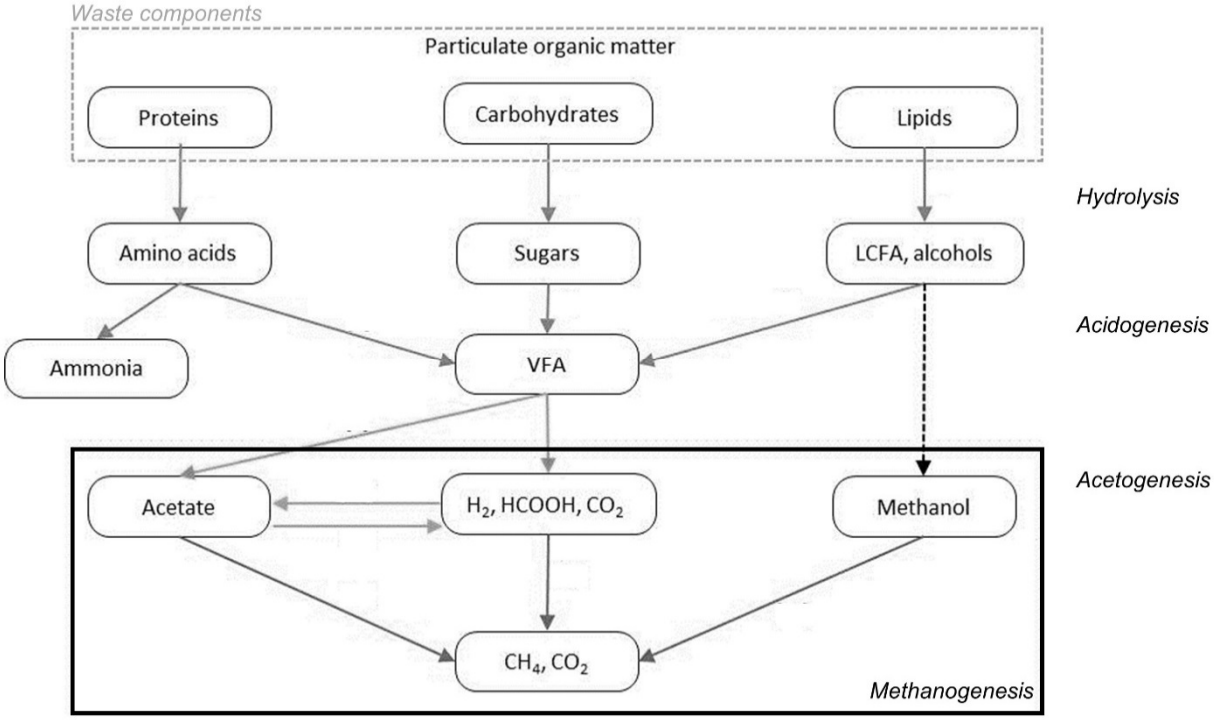


Figure 2.1 Simplified overview of the anaerobic conversion of organic waste to CO_2 and CH_4. The four main steps are the hydrolysis, acidogenesis, acetogenesis and methanogenesis. In this PhD thesis the focus is on the final and crucial step of methanogenesis. Figure adapted from Demirel & Scherer (2008). *VFA = Volatile Fatty Acid, LCFA = Long-chain Fatty Acid.*

First, particulate and other complex organic matter is hydrolysed by extracellular enzymes excreted by hydrolytic microorganisms. The *hydrolysis process* cleaves e.g., proteins, carbohydrates and lipids into their building blocks (i.e., amino acids, sugars and long-chain fatty acids (LCFAs)/alcohols, respectively) using different specific enzymes (i.e., proteases, hydrolases and cellulases, amongst others). For wastewaters with a high particulate matter content and for processes taking place at ambient or lower temperatures, the hydrolysis is generally the rate limiting step (Appels *et al.*, 2008; Kangle *et al.*, 2012). In a process called *acidogenesis* (literally, acid production), fermentative and hydrolytic-fermentative microorganisms convert these building blocks further into intermediates, i.e., short-chain fatty acids such as butyrate and propionate (denoted as

VFA in Figure 2.1), and final products such as acetate, formic acid, hydrogen gas and carbon dioxide. The direct conversion of these building blocks to final products is omitted in Figure 2.1, for the sake of simplicity.

Subsequently, acetate, formic acid, hydrogen and carbon dioxide are also produced in a process called *acetogenesis*, by obligate hydrogen-producing microorganisms. The products of this step, i.e., acetate, carbon dioxide, formic acid and hydrogen can be inter-converted by homoacetogenesis and acetate oxidation. The direction of this reaction mainly depends on the prevailing substrate and product concentrations (Demirel & Scherer, 2008; Ferry, 2010). Finally, the so-called methanogenic substrates, i.e., acetate, hydrogen, carbon dioxide and small methylated compounds like methanol, are converted to methane and carbon dioxide by unique sets of enzymes and coenzymes in the process of *methanogenesis*. The methanogens performing these reactions are, strictly speaking, not bacteria but belong to the domain of the *Archaea*. In the absence of particulate organic matter and at mesophilic and thermophilic temperatures, methanogenesis is generally the rate-limiting step and, thus, the process bottleneck (Rozzi & Remigi, 2004). A more detailed schematic of the crucial methanogensis step is provided further on in this chapter.

2.1.2 Monitoring: definitions and evolution

What defines a good monitoring tool?

According to Switzenbaum *et al.* (1990) an ideal monitoring tool is easy, cheap, fast and on-line applicable. This definition is still valid and Madsen *et al.* (2011) complemented this definition by listing plant operators' expectations for anaerobic digestion process monitoring, i.e., robustness, simplicity, accuracy, precision and reliability. A distinction can be made between retrospective and predictive monitoring tools or biomarkers. It is clear that predictive tools are regarded the holy grail of monitoring since process upsets can potentially be avoided, hence saving troubleshooting costs and optimizing methane yields. Monitoring tools can also be distinguished as *direct* or *indirect* depending on whether (in this case) methanogens are specifically targeted (i.e., based on a methanogen-specific characteristic), or reaction intermediates, substrates and products are used to infer information on their activity (Rozzi & Remigi, 2004). Typically, indirect tools are easy, cheap and fast (often even on-line measurable) but do not provide in-depth information on the (quantities of the) different (active) microbial communities present (Weiland, 2010). Moreover, these tools seldom have a predictive character. The distinction between direct and indirect monitoring tools will be used throughout this chapter.

The ultimate methanogenic monitoring tool

Following the discovery and implementation of high-rate anaerobic reactors and the continuous development of new analytical tools throughout the past decades, monitoring the methanogenic community has been the main focus of researchers. However, up until the widespread application of next-generation sequencing tools, this community remained mostly a black box for reactor operators and researchers alike (Rivière *et al.*, 2009). Process upsets were (and still are), therefore, quite common in methanogenic reactors relying on the implicit experience of their operator (Spanjers & Van Lier, 2006; Madsen *et al.*, 2011). Assays that rapidly monitor the microbial community activity and in particular that of the

methanogenic *Archaea* can provide essential information for operators to optimally manage reactor functions.

Throughout the years, researchers have attempted to, directly or indirectly, and qualitatively or quantitatively, assess methanogenic activity. The following sections of this part will highlight the most important tools that have been developed and will include several of the methods presented in Figure 2.2.

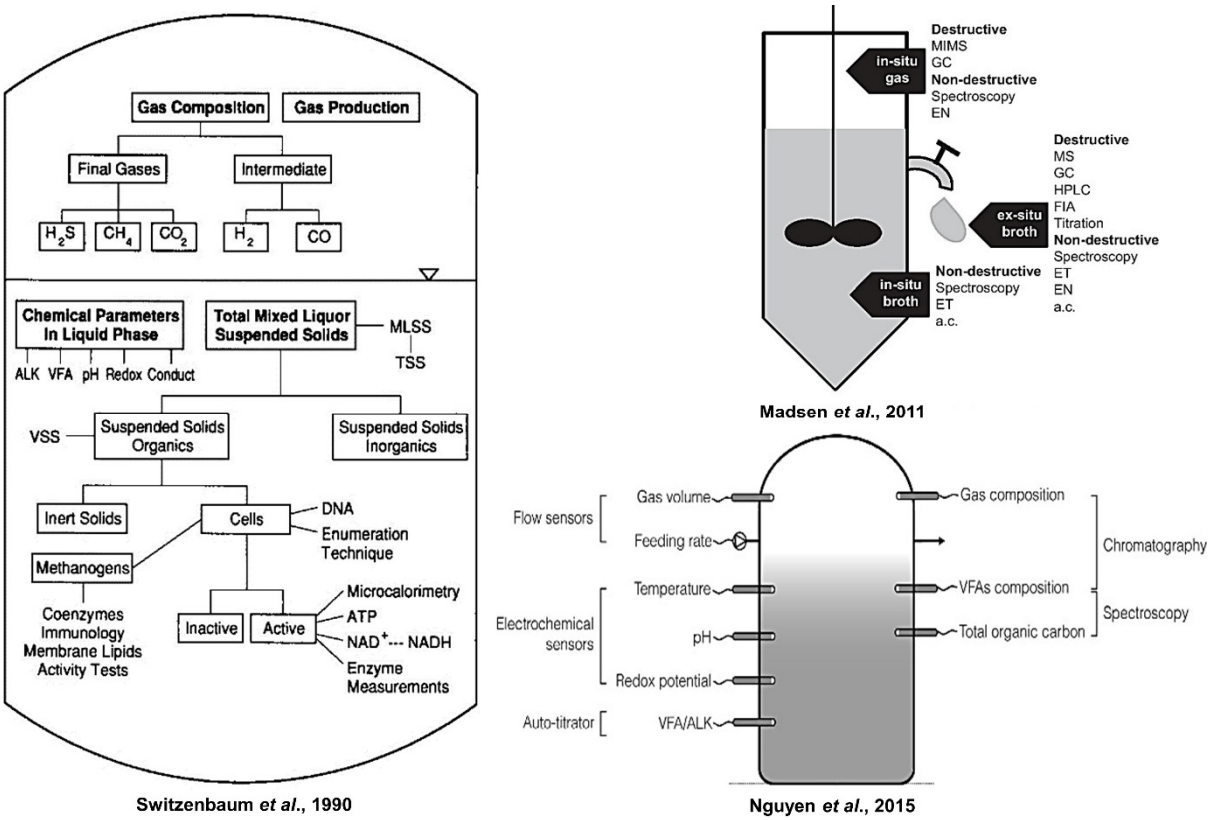


Figure 2.2 Monitoring of the anaerobic digestion process throughout the years according to three separate review papers (Switzenbaum *et al.*, 1990; Madsen *et al*, 2011; Nguyen *et al.*, 2015). Note that Switzenbaum *et al.* (1990) focuses more on *ex-situ* measurements whereas, due to developments in various sensor technologies, more recently the focus has shifted towards automated monitoring and process control methods. For the description of the used abbreviations see the original reference.

2.1.3 Indirect monitoring

As described above, indirect monitoring tools do not focus directly on the methanogens but rather try to infer the methanogenic activity from (the accumulation of) intermediate products and other relatively easily measurable reactor parameters. In what follows, a brief overview of these types of tools is presented.

pH, volatile fatty acids and alkalinity

The reactor pH, volatile fatty acid (VFA) concentrations and alkalinity are three interconnected parameters which have been used for monitoring purposes in anaerobic bioreactors for several decades. Methanogenic bioreactors are generally operated around neutral pH (6.5 – 7.2) in order to avoid inhibition of methanogens (Appels *et al.*, 2008, Lin *et al.*, 2013). In contrast, the fermentative bacteria that produce the VFAs are active in a pH interval ranging from 4 to 8.5 (Appels *et al.*, 2008). As a result, a too low pH is generally

symptomatic of the accumulation of VFAs because of a kinetic imbalance between the activity of fermentative bacteria (acid producers) and the methanogens (acid consumers) (Switzenbaum *et al.*, 1990; Madsen *et al.*, 2011). The mechanism of methanogenesis inhibition (below +/- pH 6.2) is a combined effect of pH and accumulating VFAs. At a lower pH a larger fraction of the acids will be present in the undissociated form which allows them to travel through the cell membrane and reduce the pH intracellularly (Switzenbaum *et al.*, 1990; Weiland, 2010). The effect of the accumulation of VFAs on the reactor pH depends on the buffer capacity. Therefore, the alkalinity has also been used to monitor the anaerobic digestion process. Measuring the ratio of VFAs over alkalinity provides a relatively sensitive parameter which takes into account both the acids and the buffering components (Jobling Purser *et al.*, 2014). Developments in infrared spectroscopy analysis now allow the VFAs and partial alkalinity of reactors to be determined *at-line* (Steyer *et al.*, 2002; Holm-Nielsen *et al.*, 2007; Lomborg *et al.*, 2009) although not all methods provide satisfactory results (Madsen *et al.*, 2011). The evolution of these types of devices towards handheld, mobile and battery-operated configurations is touted by Madsen *et al.* (2011) as the future of monitoring in the anaerobic digestion field. Novel methods using gas chromatography have also been implemented for *on-line* quantification of VFA (composition) (Pind *et al.*, 2002; Boe *et al.*, 2006). Furthermore, *on-line* VFA measurements by means of so-called electric tongues and noses (multiple chemical sensors coupled in arrays) have been proposed (Nordberg *et al.*, 2000). The evolution towards on-line monitoring and process control is driven by the potential errors during sampling and analysis, and human bias (Nguyen *et al.*, 2015).

Hydrogen gas

Hydrogen is an important intermediate in the anaerobic digestion process. It is produced during the degradation of higher weight fatty acids to acetate (acetogenesis) and is consumed by the hydrogenotrophic methanogens to produce methane. Dissolved hydrogen gas is already inhibitive at trace concentrations and, as a result, acetogenic conversions are only able to take place at low concentrations (Spanjers & Van Lier, 2006). High hydrogen concentrations direct the electron flow away from methane production and towards other electron sinks, i.e., propionate, butyrate, lactate or ethanol (Schink, 1997). An increase in partial H_2 pressure may indeed indicate a reduced activity of hydrogenotrophic methanogens. In turn, higher partial H_2 pressures (> 10 Pa) then lead to accumulation of alcohols and higher weight fatty acids since the conversion of these substrates to acetate and hydrogen becomes thermodynamically unfavourable (Worm *et al.*, 2011; Guebitz *et al.*, 2015; Ketheesan & Stuckey *et al.*; 2015). Hydrogen partial pressure, measured in the headspace, has, therefore, been proposed as an on-line measurable parameter which may help steer anaerobic bioreactors (Moletta *et al.*, 1994; Puñal *et al.*, 1999). Although, in theory, an increased concentration of hydrogen in the biogas may indicate (imminent) process failure, effectively steering bioreactors using the H_2 partial pressure alone is currently not common practice because of conflicting results (Whitmore & Lloyd, 1986; Kidby & Nedwell, 1991; Switzenbaum *et al.*, 1990). The discrepancy between the dissolved and gaseous concentration, as a result of mass transfer limitations, has been proposed as a possible explanation (Vanrolleghem & Lee, 2003, Rozzi & Remigi, 2004).

Specific Methanogenic Activity (SMA) tests

Specific Methanogenic Activity (SMA) tests have since long been used as a way to monitor the methanogenic activity of anaerobic sludges. Their use in practice has been proposed for (Cho *et al.*, 2005; Souto *et al.*, 2010):

(i) monitoring the efficiency of the treatment;
(ii) determining seed sludge activity;
(iii) determining the maximum organic load during start-up and normal operation;
(iv) defining the minimum sludge mass to be maintained in the reactor;
(v) evaluating the potentially inhibitory effect of toxic compounds, and;
(vi) verifying changes to the anaerobic sludge after long storage periods.

The maximum specific methane production rate is determined in a (preferably) standardized way and is a measure of the rate of the methanogenic phase (Souto *et al.*, 2010). As such, it represents the maximum capacity of a reactor operating under ideal conditions. When these types of tests are performed with various substrates, which are generally intermediates of the anaerobic digestion process, the combined results may additionally yield information on the importance or activity of the different methanogenic pathways (Dolfing & Bloeman, 1985; Lozano *et al.*, 2009; Alves *et al.*, 2009). It is clear that, since its development in the 1970s, the SMA test has proven its value for the monitoring of anaerobic reactors (Rozzi & Remigi, 2004). However, there are several important drawbacks to this method. Firstly, as already mentioned these tests are performed in *ideal conditions*. Therefore, the relevance of the results for certain applications (i.e., (*i*), (*iii*), (*iv*)) can be questioned. It is still an *ex-situ* method which takes the sludge out of its original context (i.e., operational conditions) and determines the activity *indirectly* by measuring the product, methane (Guebitz *et al.*, 2015). As a result, the test is usually repeated with second and third doses since the first dose serves solely to adapt the biomass to new conditions (Cho *et al.*, 2005). As such, the actual measurement does no longer represent the sludge sample in its operating environment. To take this discrepancy into account, Ince and co-workers (1995; 2001) proposed using the ratio of in-situ determined actual methane production and the ex-situ determined potential methane production based on acetate administration (which is the SMA) as a parameter to ramp-up organic loading rates during start-up. Cho and co-workers (2005) propose to use biomass concentrations, VFA concentrations and mixing intensities that approximate those of the sampled bioreactor, when an indication of the *in-situ* methanogenic activity is desired.

Second, *no standardized protocol* is available that allows the comparison of results. Furthermore, many parameters (e.g., type of mixing, food-over-microorganism (F/M) ratio, nutrient addition, methane quantification method) significantly *influence the outcome of the test*.

A final important disadvantage of the assay is its *duration*. Although specialized equipment has been developed, allowing routine analysis, a couple of days are still required to obtain results, due to the need for multiple feeding doses (Switzenbaum *et al.*, 1990; Cho *et al.*, 2005; Guebitz *et al.*, 2015).

BEAP profiles

One adaptation of the SMA assay is the so-called BEAP assay developed by Refai and colleagues (2017). The test encompasses the determination of the methane production, 24 hours after the incubation with one of four substrates, i.e., butyrate, ethanol, acetate and propionate (the abbreviation, BEAP, refers to the first letter of these substrates). The BEAP profiles allow to pinpoint the bottleneck of the anaerobic digestion process to hydrolysis, acetogenesis or methanogenesis and allows for a distinction between acetotrophic and hydrogenotrophic methanogenesis. The advantages of this approach are the relatively fast results (24 hours) and their predictive character. The BEAP profiles have also been shown to predict upcoming process failures (i.e., ammonia inhibition). Therefore, although still relying on *ex-situ* measurements of parameters indirectly linked to the activity of certain microbial guilds, by adopting a holistic approach using different substrates, the BEAP method appears to be more suitable than SMA tests for process monitoring and steering purposes.

Combinations of indirect parameters

Fdez-Güelfo *et al.* (2012) reports on using volatile solids, dissolved organic carbon and total organic carbon measurements for the calculation of new indirect parameters. The parameters, denoted as *non-solubilized carbon*, *non-acid carbon* and *acidogenic substrate such as carbon*, were applied in a solid waste digester and allowed the evaluation of the efficiency hydrolysis, acidogenesis and methanogenesis step.

2.1.4 Direct monitoring

Today, operators still often exclusively focus on indirect monitoring until the process goes astray (Ramos *et al.*, 2014; Jensen *et al.*, 2015). The implementation of advanced on-line monitoring devices coupled to a shift towards automatic process control may partly solve this problem by taking human bias out of the equation (Madsen *et al.*, 2011; Nguyen *et al.*, 2015). Nevertheless, simultaneously, considerable research efforts have been made in the development of direct monitoring tools. In contrast to indirect monitoring, direct monitoring is based on a distinctive trait of the methanogenic *Archaea* such as a unique metabolite, enzyme or gene sequence. As a result, they are expected to yield information that is more directly related to the activity of the methanogens. The main challenge for such tools is to optimize the quantification method and prove the correlation with methane production. The latter is, of course, crucial considering that the final aim is to maximize methane production in a stable running process. Monitoring tools allowing to capture the *activity* of methanogens, rather than solely their *presence,* are preferred as will be discussed below. Again, ideally the tool has a predictive character allowing it to pinpoint the process' bottleneck such that it can be alleviated in time and process downtime can be avoided.

Enzyme activities

During the past decades the activities of several enzymes related to the hydrolysis, acidogenesis and methanogenesis step were quantified (Switzenbaum *et al.*, 1990; Guebitz *et al.*, 2015). Specific hydrolytic enzymes that have been monitored include amylases, pectinases, proteases and different types of cellulases (Parawira *et al.*, 2005). The esterase activity has also been proposed as a measure of the effectiveness of the overall

fermentation process. Since process disruption was reflected by decreased enzyme activities, it was concluded that the photometric determination of various hydrolytic enzyme activities allowed the anaerobic digestion process to be monitored and controlled with very little effort (Gasch *et al.*, 2013). Furthermore, Gabris and co-workers (2015) quantified the activity of three key acidogenic enzymes.

With respect to methanogenesis, Refai *et al.* (2014) reported on the quantification of the heterodisulfide reductase (Hdr) activity. This enzyme catalyzes the key step for energy conservation in all methanogenic *Archaea*. Interestingly, the different localisation of the enzyme in hydrogenotrophic and acetotrophic methanogens (in the cytoplasm and bound to the cytoplasmic membrane, respectively) allows the separate analysis of the metabolic activity of these types of methanogens. Furthermore, Kern *et al.* (2016) reported that benzylviologen-dependent hydrogenase activities (as a proxy for bacterial activity) correlated positively with methane productivity whereas F_{420}-dependent hydrogenases (as a proxy for methanogenic activity) did not. The quantification of the Methyl-Coenzyme M Reductase (MCR) enzyme activity for practical monitoring purposes has not been reported in literature, despite its crucial role in the final step of methanogenesis. Possible drawbacks of all enzyme activity analyses are the test duration and complexity.

Energy and electron-shuttle related molecules through fluorescence detection

By far the most important fluorophore that is targeted for specifically monitoring the methanogens in anaerobic digestion is cofactor F_{420}. The past and current use of this cofactor in the monitoring of methanogenesis is discussed in Section 2.1.5, in detail. Additionally, Nicotinamide Adenine Dinucleotide (Phosphate) hydrogen (NAD(P)H) has been targeted in this way as a measure of general metabolic activity. Note, however, that this method is not specific for methanogens. Nonetheless, Peck and Chynoweth (1992) reported that the NAD(P)H fluorescence served as an early warning system of process imbalances in AD systems because of organic overloading.

Acetotrophic versus hydrogenotrophic methanogenesis through Compound Specific Isotope Analysis (CSIA)

In recent years, methodologies were developed to use carbon and hydrogen stable isotopes (^{13}C and ^{2}H) of the produced methane for monitoring and control purposes in anaerobic digestion (Nikolausz *et al.*, 2013; Zhang *et al.*, 2014; Mulat *et al.*, 2014; Polag *et al.*, 2015; Gehring *et al.*, 2015). An important advantage of this method is that it allows acetotrophic and hydrogenotrophic methanogenesis to be distinguished based on their specific isotopic signature. This way changes in methanogenic pathways can be detected, which may serve as an early warning for imminent process disturbances (Polag *et al.*, 2015). Polag and colleagues (2015) demonstrated for the first time the feasibility of using laser absorption spectroscopy for the continuous (i.e., *on-line*) high-resolution monitoring of a full-scale anaerobic digester. The authors highlighted the potential of their method as a tool for process automation (i.e., automated feeding based on the isotope profile). The main advantages of the CSIA method seems to be its predictive character and the fact that the measurements can be performed in real-time in the gas-phase. A potential disadvantage is that it does not provide information on the total methanogenic activity or potential.

-omics data through molecular genetic tools

With the development of nucleic acid sequencing techniques in the 80's, the elucidation of (part of) the genetic code of methanogens became possible (Guebitz *et al*, 2015). As sequencing technologies progressed from 1st to 2nd and 3rd generation and computing power increased (Metzker, 2010), high-throughput sequence analysis of PCR amplified target genes and even complete metagenomes became possible. Targeted amplification of the small rRNA subunit (16S rRNA) gene provided information regarding the community's taxonomy and phylogeny, hence, solving the question *"Who is there?"*, while the metagenome answered the question *"What can they do?"* (Guebtiz *et al*, 2015). When RNA instead of DNA is targeted, the metatranscriptome answers the additional question *"What are they doing?"* (Vanwonterghem *et al.*, 2014). Finally, the metaproteome and metabolome, provide information on the synthethized proteins and all low-molecular weight molecules involved in metabolic reactions and required for maintenance, respectively. The metaproteome has the potential to help identify biomarkers as predictive indicators of process failure, whereas the metabolome can provide insights into the key metabolic pathways (Vanwonterghem *et al.*, 2014). Since from a monitoring point of view the activity of methanogens (rather than solely their presence) is most important, targeting the mRNA transcripts of methanogen specific genes coding for, e.g., crucial enzymes leads to interesting monitoring tools. Figure 2.3 provides an overview of the information that can be derived from the different so-called "meta-omics" approaches. From left to right, the derived information relates to potential (i.e., presence), expression, and activity, by targeting different molecules.

Nowadays, often quantification by means of Real-Time quantitative Polymerase Chain Reaction (RT-qPCR) on specific genes is used. Although the reliability of this method has been improved throughout the years, problems or uncertainty still exist particularly with quantitative analyses of prokaryotic messenger RNA (Vanwonterghem *et* al., 2014; Guebitz *et al.*, 2015). Other limitations for monitoring purposes include the need for specialized laboratory equipment. Furthermore, *on-line* monitoring using this technique is, thus far, inconceivable since nucleic acid extraction is required. Nonetheless, developments for on-site use are emerging (Guebitz *et a.l*, 2015). The application of one methanogen specific gene, i.e., the *mcrA* gene, for monitoring methanogen number and activity in anaerobic digestion is discussed in more detail below.

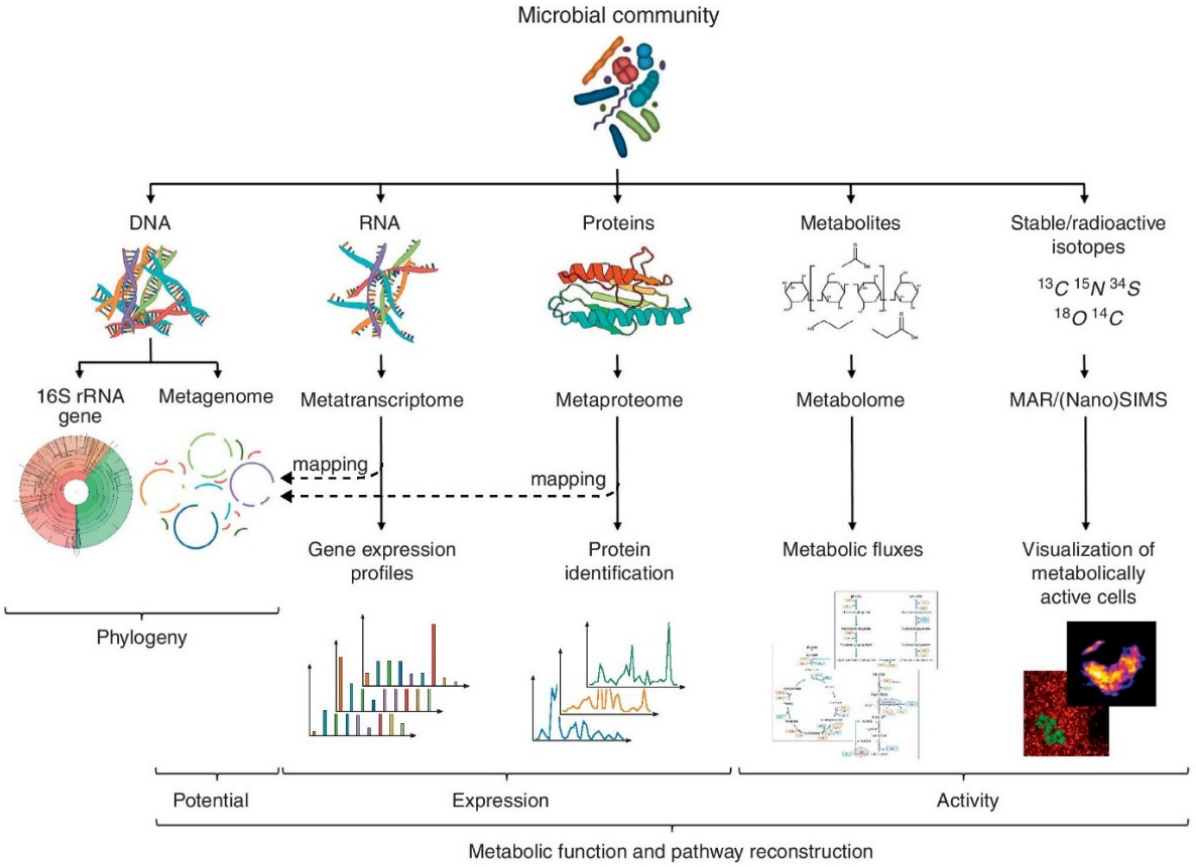


Figure 2.3 Overview of the different "meta-omic" approaches developed throughout the years. Figure taken from Vanwonterghem *et al.* (2014).

The mcrA gene

An interesting molecular genetic technique to assess methanogen presence and activity, is based on targeting the genes coding for the Methyl-Coenzyme M Reductase (MCR) enzyme. The elucidation of partial gene sequences of the *mcrA* gene encoding for the alpha subunit of the MCR enzyme, by Springer and co-workers (1995) lies at the basis of this tool. In fact, they were the first to develop a set of primers for the amplification of this subunit and to propose its use as a marker for the phylogenetic analysis of members of the family *Methanosarcinaceae*. Various primers targeting the *Archaeal* 16S rRNA gene had been developed and the incentive of their work was to eliminate potential problems with non-specific amplification (Alvarado *et al.*, 2014). A number of studies in the early 2000's, focusing on the phyologenetic application, confirmed these results and to date the *mcrA* gene is an established molecular marker for all methanogenic *Archaea* (Lueders *et al.* 2001; Luton *et al.* 2002; Shigematsu *et al.* 2004; Steinberg & Regan 2009). Subsequently, the application of the tool was extended from methanogen presence and community composition to abundance and activity. Methanogen abundance (i.e., DNA copy numbers) alone was not always sufficient to determine methanogenic activity and the inclusion of RNA (i.e., mRNA transcript number) data was shown to be crucial (Watanabe *et al.*, 2009; Ma *et al.*, 2012; Zhang *et al.*, 2014).

While monitoring of the *mcrA* gene initially focused on natural environments, recently, more and focus is on anaerobic digesters. Often, methanogenic activity is inferred from the commonly applied specific methanogenic activity (SMA) test and the correlation with

mcrA gene copy and/or transcript number is investigated. Alternatively, bioreactors are followed up over an extended period of time and dynamics of the in-situ methane production are compared with the dynamics of *mcrA* gene copy and/or transcript numbers. Morris *et al.* (2013; 2016) recently showed that *mcrA* gene copy numbers in methanogenic reactors correlate with SMA on H_2/CO_2 and propionate (SMA on acetate, however, did not correlate). The authors reported that their method provides the operator with information regarding methanogenic activity within 24 hours from receiving the sample, whereas SMA assays take at least 7 to 10 days to complete (Morris *et al.* 2013; 2016). However, they did not find a correlation with *mcrA* transcript numbers. Other studies in paddy field soils did observe changes in *mcrA* transcripts or transcript/gene ratio under different environmental conditions (Watanabe *et al.*, 2009; Ma *et al.*, 2012). Significant changes in *mcrA* transcript numbers or transcript/gene ratio have also been observed in (samples from) digesters. Munk *et al.* (2012) observed significant changes in a pilot-scale digester subjected to an organic shock-load. In lab-scale experiments on sludge from a full-scale CSTR anaerobic bioreactor, Zhang and co-workers (2014) demonstrated that inhibition (induced by ammonium addition) was largely due to repression of gene transcription (RNA) rather than to changes in the total methanogen number (DNA). Munk *et al.* (2012) proposed combining *mcrA* copy numbers (a strictly molecular biological parameter) with methane productivity (a physiological parameter) into the so-called Metabolic Quotient (MQ) as measure of the actual specific methanogenic activity in the reactor. According to these authors, comparing the MQ with a reference standard methanogenic activity at efficient process performance has great potential for monitoring and avoiding process disturbances. They do, however, indicate that "snap-shot" measurements do not necessarily mean very much and gradients of this parameter should be determined (Guebitz *et al.*, 2015). Using the *mcrA* gene to not only determine "Who is there?" but also "Who is active?" yields a powerful tool to determine the dominating active methanogenic species in digesters under various environmental conditions. For instance, it has helped to contradict the widely accepted perception that in general only 30% of methane is produced from H_2/CO_2 (Alvarado *et al.* 2014). In conclusion, the use of *mcrA* copy and transcript numbers (potentially in combination with methane production measurements) have proven their value in monitoring or relieving process disturbances.

Other molecular tools

Additional molecular genetic techniques that are being used for the specific monitoring of methanogens are terminal restriction fragment length polymorphism (T-RFLP), fluorescence in-situ hybridization (FISH) combined with confocal laser scanning microscopy (CLSM) and flow cytometric techniques. The detailed description of these methods does not fall within the scope of this PhD thesis.

2.1.5 Cofactor assays

In this section the use of specific methanogenic cofactors for monitoring of the methanogenesis process is elaborated. First, cofactor F_{430} and cofactor F_{420} (the most commonly used and cited cofactor) are discussed. Next, other more sparsely investigated methanogenic cofactors are briefly mentioned.

Cofactor F_{430}

Discovery & structure elucidation

In 1977 Jean LeGall identified a yellow, non-fluorescent compound while studying cell extracts from *Methanobacterium thermoautotrophicum*. One year later, the compound received its name due to its absorbance maximum at 430 nm (Gunsalus & Wolfe, 1978). The identification triggered a number of studies in the 80's, aiming to elucidate F_{430}'s structure. Whitman & Wolfe (1980) showed that the molecule contained nickel. Diekert *et al.* (1980) showed that cellular F_{430} content depended on the amount of nickel in the growth medium. Basic information regarding the biosynthesis of the compound led to the proposal of a tetrapyrrole structure (Diekert *et al.*, 1980), which was later confirmed by NMR (nuclear magnetic resonance) spectroscopy (Pfalz *et al.*, 1982). In 1990 its structure, shown in Figure 2.4, was entirely elucidated, showing similarities with porphyrin rings found in heme proteins and corrinoids such as vitamin B12 (Dimarco *et al.*, 1990).

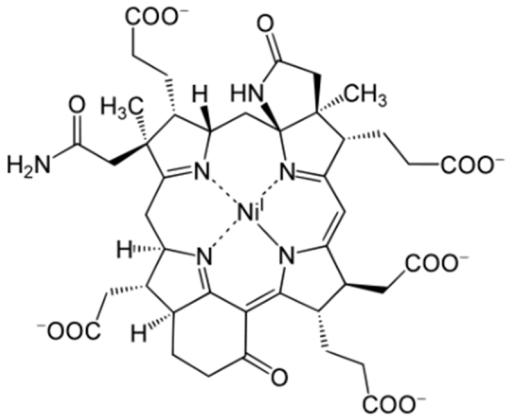


Figure 2.4 Proposed structure of the "native" cofactor F_{430}. An overview of the different variants is provided in Chapter 4.

In 2014, ten F_{430} variants had been described with varying functions and abundancies in different methanogens. F_{430}-4, also known as F_{560}, has been a known F_{430} oxidative degradation product since the early 80's when a shift in absorbance maximum (to 560 nm, hence the name) after heating and contact with oxygen was observed. The native form slowly epimerizes to the 12,13 diepimer, a process that is accelerated by heating. Furthermore, it dehydrogenizes to F_{560}, the 12,13-didehydro variant when in contact with oxygen (Diekert *et al.* 1981, Pfaltz *et al.* 1985). In 2017, the complete biosynthesis pathway of the cofactor was reported by Moore *et al.* (2017). The final piece of the puzzle was the identification of the proteins CfbA and CfBE which catalyse the coenzyme F_{430} synthesis from sirohydrochlorin. According to Moore *et al.* (2017) the understanding of F_{430} synthesis may lead into the development of recombinant MCR systems.

Role in methanogenesis

Simultaneously to the structure elucidation in the mid 80's, considerable research effort was devoted to understanding the role of the cofactor in the methanogenic pathway. These early studies focused on pure cultures and showed that acetotrophic, methylotrophic and hydrogenotrophic methanogens all contained similar amounts of cofactor (Diekert *et al.*, 1980; 1981; Van Beelen *et al.,* 1983; Kida *et al.*, 2001; Jiang, 2006). The results of these studies are summarized in Table 2.1.

Table 2.1 An overview of cofactor F_{430} contents reported in literature. Most experiments were performed on pure cultures.

F_{430} content (nmol g dry cells^{-1})	Sample type and organisms	Reference
5 - 139	*Methanobacterium thermoautotrophicum* strain Marburg	Diekert *et al.*, 1980
800	*Methanobacterium thermoautotrophicum* strain Marburg	Diekert *et al.*, 1981
643	*Methanobacterium thermoautotrophicum* strain deltaH	
307	*Methanobrevibacter smithii*	
227	*Methanococcus vannielli*	
492	*Methanospirillum hungatii*	
800	*Methanosarcina barkeri* methanol grown	
800	*Methanosarcina barkeri* acetate grown	
550 - 620	Anaerobic sludge, mixed samples	Kida *et al.*, 2001
86 - 251	*Methanosarcina barkeri* at different Co concentrations in the feed medium	Jiang, 2006
4.7 - 49	*Methanosarcina barkeri* at different Ni concentrations in the feed medium	
1800	*Methanobacterium thermoautotrophicum* strain deltaH	Van Beelen *et al.*, 1983

Diekert *et al.* (1981), ruled out a potential role of F_{430} in carbon assimilation since *M. smithii* does not grow autotrophically. The combined evidence of this study pointed towards a function shared by all types of methanogens.

The hypothesis was that the cofactor was involved in the methyl-coenzyme M conversion to methane. This reaction was known to be catalysed by the Methyl-Coenzyme M Reductase (MCR) enzyme. A schematic overview, illustrating the different pathways up to the actual methane formation is depicted in Figure 2.5.

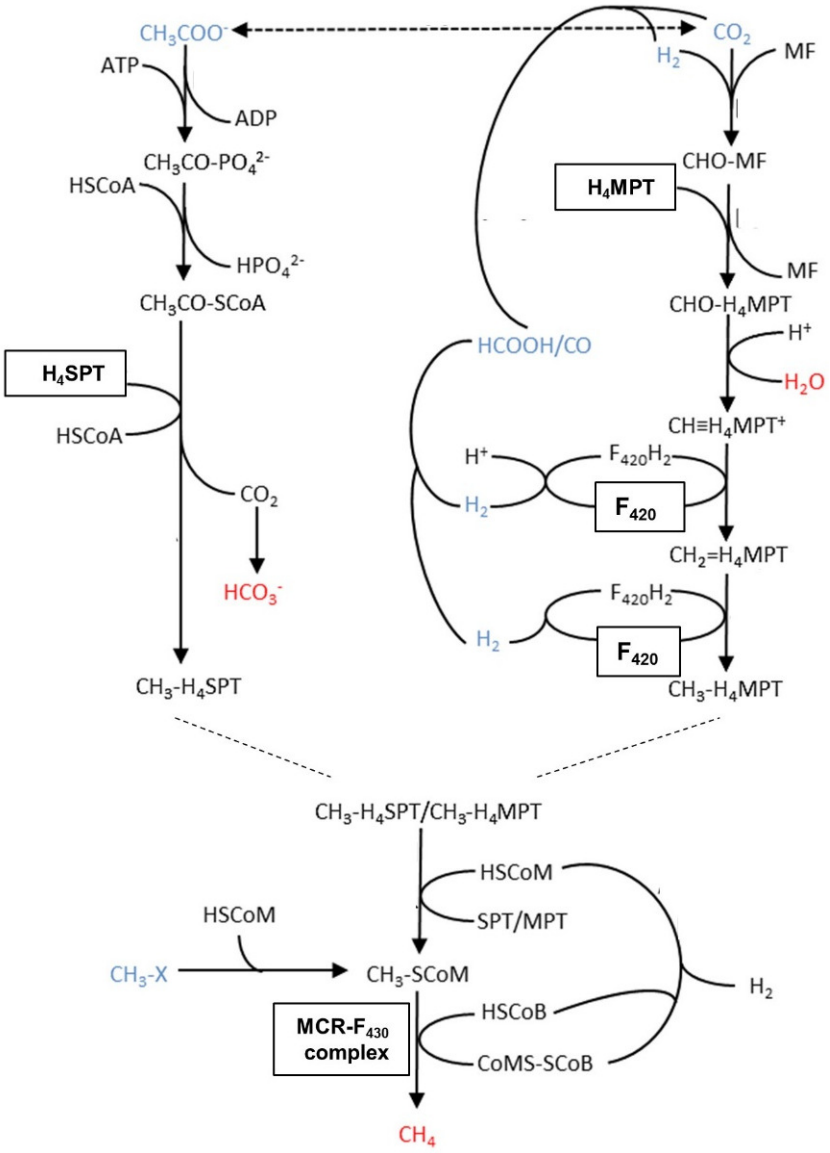


Figure 2.5 Simplified scheme of the different methanogenesis pathways. Methanogenic substrates are shown in blue, products in red. The boxes indicate the cofactors of interest discussed in this chapter. Figure adapted from Duin, 2009; Ferry, 2010; Kaneko *et al.,* 2014.

In 1982, Ellefson *et al.* (1982) provided evidence that one molecule of the MCR enzyme is associated with two molecules of F_{430}. Further experiments established that this association is non-covalent, but the exact catalytic mechanism by which MCR, F_{430} and coenzyme B (CoB) convert methyl-coenzyme M to methane has not been completely elucidated (Hüster *et al.*, 1985; Ermler *et al.*, 1997; Duin, 2009; Scheller *et al.*, 2017). Figure 2.6 shows a molecular surface representation of the MCR enzyme complex with and without the α' subunit (orange). Omitting this subunit exposes the two cofactor F_{430} molecules (yellow) bound with the heterodisulfide CoM-S-S-CoB (white) (Ermler *et al.*, 1997). The enzyme's active site is thought to form a tunnel-like structure with a narrow apex into which methyl-coenzyme M enters first, followed by CoB. The catalytic cycle appears to start with the central Ni atom in the +I oxidation state and most proposed cycles include a covalently bound CH_3-Ni-F_{430} intermediate (Ermler *et al.*, 1997; Craft *et al.*, 2004; Duin, 2009).

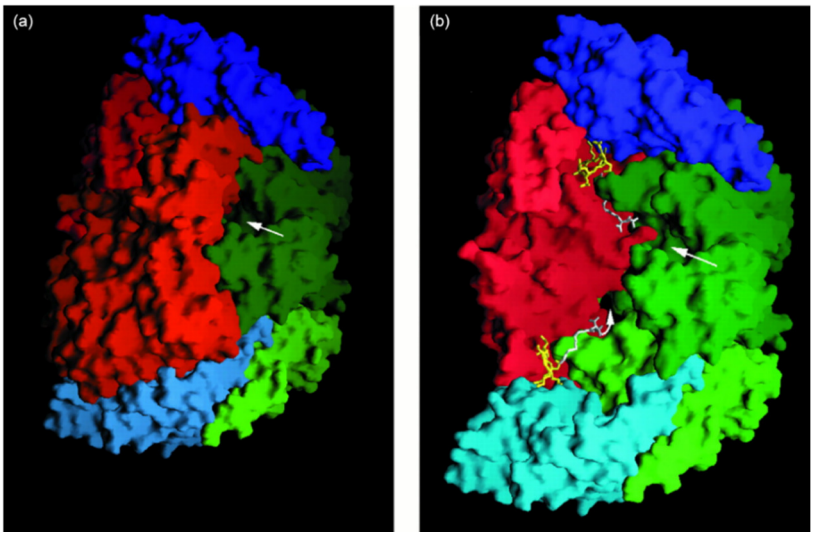


Figure 2.6 Molecular surface representation of the Methyl-Coenzyme M Reductase (MCR) enzyme **(a)** with and **(b)** without the α' subunit (orange). Cofactor F_{430} is shown in yellow and the heterodisulfide CoM-S-S-CoB in white. The white arrows denote two narrow channel entrances to the catalytic sites. Subunit α is shown in red, subunits β and β' in green and light green, and γ and γ' in dark blue and light blue. Figure taken from Ermler *et al.* (1997).

Use as a monitoring tool

Because of its involvement in the terminal step of methanogenesis, F_{430} was proposed for monitoring purposes (Kaneko *et al.*, 2014). Since the elucidation of the cofactor's role and the development and validation of the first extraction and quantification procedures, various attempts have been reported to assess its suitability as a monitoring tool in various applications. Before summarizing the results of these studies, three conditions are defined that need to be met in order for F_{430} to be used to monitor methanogenesis.

(i) Cofactor F_{430} needs to be *present* in, and *restricted* to, methanogenic *Archaea*;
(ii) Cofactor F_{430} content needs to be related to methanogenic *activity*, and;
(iii) Cofactor F_{430} and methane production *dynamics* need to be similar.

The first condition is only partly met. Indeed, apart from methanogens, anaerobic methanotrophic *Archaea* (ANME) are known to contain F_{430} (Dimarco *et al.*, 1990; Allen *et al.*, 2011; Kaneko *et al.*, 2014). The latter organisms, commonly found in marine sediments, perform the opposite reaction of methanogenesis, oxidizing CH_4 to CO_2 (Krüger *et al.*, 2003; Mayr *et al.*, 2008; Allen *et al.*, 2014). However, in typical (high-rate) anaerobic methanogenic systems, methanogens dominate the methanotrophs (Nettmann *et al.*, 2008). None of the bacterial guilds earlier in the anaerobic digestion chain contain F_{430} (Dimarco *et al.*, 1990).

Research regarding the relation between cofactor F_{430} and methanogenic activity in anaerobic reactors has been pioneered by the research group of Kida and Shigematsu at Kumamoto University, Japan. The earliest publication regarding this topic dates back to 1991. However, despite the fact that basic extraction and HPLC procedures were described (Van Beelen *et al.*, 1983; Gorris *et al.*, 1988), F_{430} was not actually quantified by Kida *et al.* (1991) and its influence on methanogenic activity was merely suggested based on nickel consumption (which is required for cofactor synthesis). It took until 2001 for a similar study - this time including cofactor F_{430} quantification - to be published by the same

research group. A lab-scale, continuously fed bioreactor was fed with a synthetic acetate substrate and SMA and cofactor F_{430} content were analyzed at various dilution rates. A link between SMA and F_{430} content was found, both increasing at higher dilution rates (i.e., lower hydraulic retention time). However, these results were not statistically underpinned (Kida *et al.*, 2001). Additionally, the ex-situ determination of the SMA compared to directly monitoring methane production from the reactor vessels may have introduced a potential bias due to different conditions used in the SMA test. In Kida *et al.*'s (2001) study, cofactor F_{420} was also followed-up and from the combined results the researchers suggested that, with an acetate substrate, at higher HRTs a significant level of methane may be produced by the combined activity of the acetate oxidizing microorganisms and the hydrogenotrophic methanogens, whereas at lower HRTs the acetotrophic pathway dominates. Two follow-up studies, performed in continuously stirred tank reactors (CSTRs), focused more on community structure and activity using the *Archaeal* 16S rRNA, acetate kinase, and *mcrA* genes and only briefly reported cofactor contents (Shigematsu *et al.*, 2004; 2006).

The use of cofactor F_{430} as a monitoring tool for methanogenesis or methane oxidation is being investigated by the Japanese researchers Kaneko and Takano, in natural environments. In their most recent work they proposed to derive abundance and activity of methanogens in deep marine sediments in an indirect way through the measured F_{430} content, since direct methane production quantification is impossible for such samples. The abundance was derived based on cofactor contents and prokaryotic cell weights reported in the literature. The activity was estimated by using the methane production per mole of MCR (or F_{430} due to their 1:2 association), determined in cell suspensions in previous experiments. However, the use of literature data led to overestimations compared to other microbiological and ^{14}C tracer methods (Kaneko *et al.*, 2016).

Cofactor F_{420}

Discovery & structure elucidation

Cofactor F_{420} was first isolated in 1972 from a *Methanobacterium bryantii* extract (Cheeseman *et al.*, 1972). The authors described a compound that exhibited blue-green autofluorescence in an oxidized state. Both the pH and oxidation state were shown to influence the fluorescence intensity. Its maximal fluorescence emission occurs at a wavelength of 470 nm, when excited at 420 nm, although the wavelengths may vary depending on the pH of the medium (Cheeseman *et al.*, 1972). The cofactor's name was derived from the distinct peak at 420 nm in its UV-VIS spectrum. A few years after its identification, cofactor F_{420}'s full molecular structure was reported by Eirich *et al.* (1978). It was shown to consist of a (N-L-lactyl-γ-L-glutamyl)-L-glutamic acid phosphodiester of the 7,8-didemethyl-8-hydroxy-5-deasazoriboflavin-5'-phosphate chromophore (Figure 2.7 - a).

This structure is very similar to that of electron carriers such as Flavin Adenine Nucleotide (FAD) and Flavin Mononucleotide (FMN) (Hossain *et al.*, 2015). Since its discovery, various forms of F_{420} have been described, all varying in the number of glutamate residues in the sidechain (varying from one to nine) (Bashiri *et al.*, 2010; Forouhar *et al.*, 2008). F_{420}-2 (the form with two glutamate residues) appears to be the form most often found in hydrogenotrophic methanogens, whereas F_{420}-4 and F_{420}-5 were

mostly found in acetotrophic and methylotrophic species (Reynolds & Colleran, 1987). The different forms exhibit the same functionality.

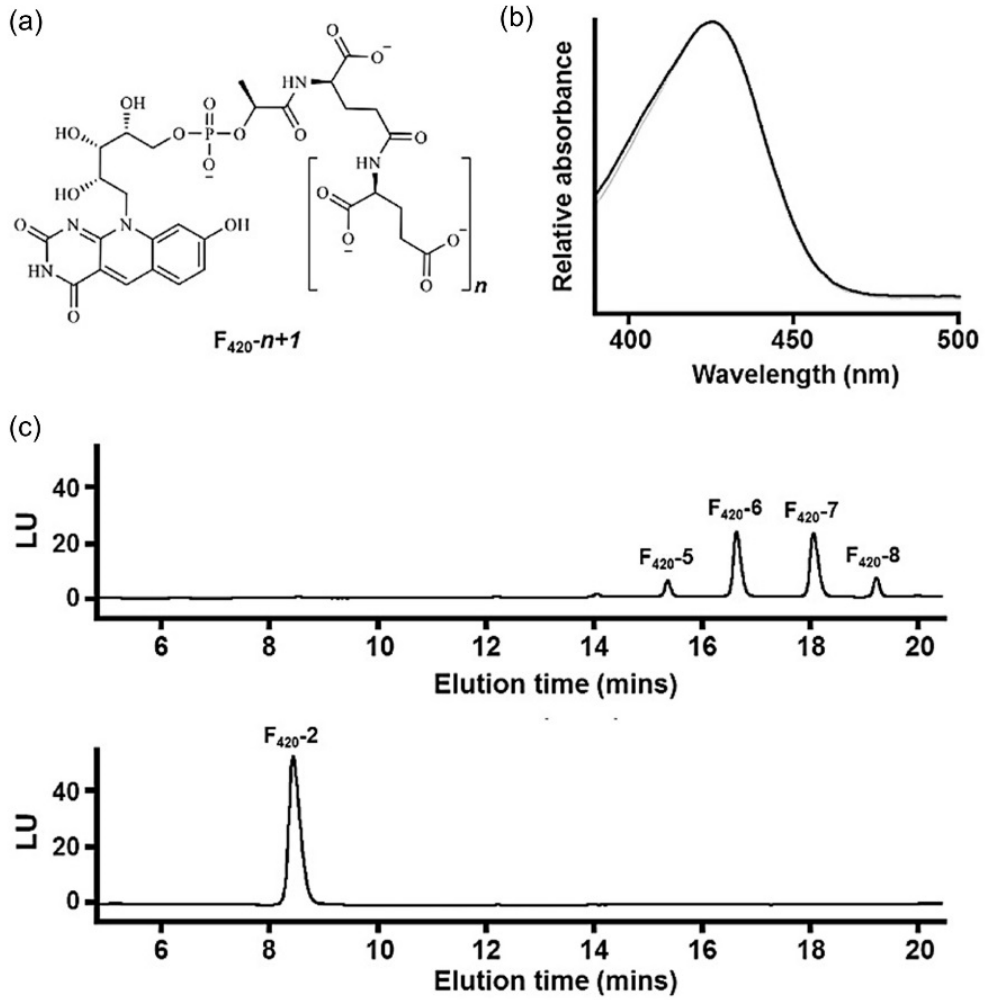


Figure 2.7 (a) general cofactor F_{420} structure, **(b)** typical UV-VIS spectrum, and **(c)** HPLC separation of the different cofactor F_{420} forms. The variants differ in the number of glutamate residues, F_{420}-2 is most commonly found in hydrogenotrophic methanogens whereas F_{420}-4 and F_{420}-5 are mostly found in acetotrophic and methylotrophic species. Figure taken from Ney *et al.* (2017).

Role in methanogenesis

The resemblance of cofactor F_{420}'s structure to that of the abovementioned electron carriers explains its function within the cell. The cofactor is an essential electron carrier in hydrogenotrophic methanogens (Figure 2.5). It is reduced with the addition of two hydrogen atoms at the 1 and 5 positions. In turn, the reduced cofactor ($F_{420}H_2$) supplies reduction equivalents for the formation of methyl-coenzyme M, the final intermediate in methane formation, during which the cofactor is again oxidized by $F_{420}H_2$ dehydrogenase (Bäumer *et al.*, 1998; Hendrickson & Leigh, 2008; Thauer *et al.*, 2008).

Use as a monitoring tool

Because of its relatively simple quantification and its functional importance in methanogenic cells, cofactor F_{420} has, since its discovery, been regarded as an important potential marker for methanogenesis. The same conditions defined for cofactor F_{430}'s application as a monitoring tool, should be met here.

With respect to the cofactor's presence and exclusivity in methanogens, note that F_{420} is not exclusively found in methanogens (or anaerobic methanotrophic *Archaea*) but also in certain non-methanogenic *Archaea*, in *Actinobacteria*, *Cyanobacteria* and in eukaryotic green algae (Lin & White, 1986; Eker *et al.*, 1988; 1990; Li *et al.*, 2009). However, as was the case for F_{430}, these microorganisms are not expected to be present in significant numbers in anaerobic digester communities (Yu *et al.*, 2012; Qiu *et al.*, 2013). The main issue with cofactor F_{420} monitoring is that its concentration varies between the different types of methanogens. Acetotrophic methanogens contain significantly lower concentrations of the cofactor compared to hydrogenotrophic methanogens, because they do not need F_{420} for methane production (see also Figure 2.5) (Kida *et al.*, 2001). Nevertheless, their F_{420} content may not be zero because they may require the cofactor in other metabolic pathways, e.g., for carbon synthesis using the reductive tricarboxylic acid cycle (Zeikus *et al.*, 1977). Table 2.2 lists the cofactor F_{420} content in different methanogen species.

Table 2.2 An overview of cofactor F_{420} contents reported in literature. Both pure and mixed cultures are included. The numbers confirm that species with hydrogenotrophic metabolism generally have higher F_{420} cofactor contents than their acetorophic/methylotrophic counterparts. The references between brackets are the original references for the data (which could not all be retrieved). *UASB = Upflow Anaerobic Sludge Blanket.*

F_{420} content (nmol g dry cells^{-1})	Species	Metabolism	Substrate	Reference
90	*Methanosarcina barkeri*	acetotrophic/ methylotrophic	acetate	Eirich *et al.*, 1979 (de Zeeuw, 1984)
330	*Methanotrix soehngenii*	acetotrophic/ methylotrophic	acetate	Zehnder *et al.*, 1980 (Dolfing & Mulder, 1985)
160	*Methanosarcina barkeri*	acetotrophic/ methylotrophic	methanol	Van Beelen *et al.*, 1983
27	*Methanosarcina acetivorans*	acetotrophic/ methylotrophic	acetate	Sowers *et al.*, 1984 (Dolfing & Mulder, 1985)
3000	*Methanobacterium formicium*	hydrogenotrophic	formate	Eirich *et al.*, 1979 (Dolfing & Mulder, 1985)
1400	*Methanobacterium bryantii*	hydrogenotrophic	H_2/CO_2	Eirich *et al.*, 1979
2400	*Methanobacterium bryantii*	hydrogenotrophic	H_2/CO_2	(de Zeeuw, 1984)
1200	*Methanobacterium formicium*	hydrogenotrophic	H_2/CO_2	
1900	*Methanobacterium thermoautotrophicum*	hydrogenotrophic	H_2/CO_2	
1800	*Methanobrevibacter arboriphilus*	hydrogenotrophic	H_2/CO_2	
40	*Methanobrevibacter ruminantium*	hydrogenotrophic	H_2/CO_2	
700	*Methanogenium marisnigri*	hydrogenotrophic	H_2/CO_2	
1900	*Methanospirillum hungatei*	hydrogenotrophic	H_2/CO_2	
1500	*Methanobacterium thermoautotrophicum*	hydrogenotrophic	H_2/CO_2	Schönheit *et al.*, 1981 (de Zeeuw, 1984)
450	*Methanobacterium thermoautotrophicum*	hydrogenotrophic	H_2/CO_2	van Beelen *et al.*, 1983 (de Zeeuw, 1984)
600	*Methanobacterium thermoautotrophicum*	hydrogenotrophic	H_2/CO_2	
1900	*Methanospirillum hungatei*	hydrogenotrophic	H_2/CO_2	Dolfing & Mulder, 1985 (Reynolds & Colleran, 1987)
55	UASB sludge	mixed	acetate	Dolfing & Mulder, 1985
583	UASB sludge	mixed	acetate/ ethanol	
440	UASB sludge	mixed	acetate/ propionate	
658	UASB sludge	mixed	ethanol	
796	UASB sludge	mixed	propionate	
152	UASB sludge	mixed	sugar	

The significant variability in F_{420} content in different methanogenic subgroups, indicates that a change in cofactor F_{420} content may not necessarily reflect a change in activity but rather a change in methanogenic community structure. Reynolds & Colleran (1987) already mentioned that such changes should be monitored for correct interpretation of the results.

With respect to cofactor F_{420}'s relation to methanogenic activity, links between F_{420} content and *ex-situ* determined SMAs (de Zeeuw, 1984; Dolfing & Mulder, 1985; Gorris *et al.*, 1988; Ahn *et al.*, 2000) or *in-situ* measured methane production (Whitmore *et al.*, 1986; Switzenbaum & Eimstad, 1987) were established. Contradictive results emerged from these studies, which are most likely attributable to the variability of F_{420} content within the different methanogenic groups. Therefore, the use of cofactor F_{420} as a measure of *total* methanogenic activity is unlikely to work in all cases, especially when hydrogenotrophic activity is limited. It is more likely that cofactor F_{420} monitoring can be used (e.g., in combination with F_{430} monitoring) to provide an indication of the presence and activity of hydrogenotrophic methanogens. Indeed, the aforementioned research by Kida *et al.* (2001) linked a relative decrease in cofactor F_{420} content to a shift away from hydrogenotrophic methanogenesis. This correlation was later corroborated by stable isotope analysis (Shigematsu *et al.*, 2004). Nevertheless, despite promising perspectives, the combined monitoring of cofactors F_{420} and F_{430} has rarely been applied.

The current state-of-the art on cofactors F_{420} and F_{430} shows a lack of knowledge on their correlations with other monitoring tools and their combined application in anaerobic bioreactors. Furthermore, knowledge on the dynamics of cofactor content after a process upset is missing for both F_{430} and F_{420}. These topics will be tackled in Chapters 5 and 6 of this PhD thesis.

Other methanogenic cofactors

In addition to cofactors F_{430} and F_{420}, other methanogenic cofactors have been reported in literature. Two interesting cofactors worth mentioning are Sarcinapterin (SPT) and Methanopterin (MPT). Methanopterin was identified in 1978 and originally named factor 342 because of its absorbance maximum at 342 nm (Gunsalus & Wolfe, 1978). The chromophore of this fluorescent molecule was determined to be a pterin (Keltjens *et al.*, 1983). Van Beelen *et al.* (1984) confirmed the proposed structure and identified a closely related coenzyme in *Methanosarcina barkeri*, i.e., Sarcinapterin, which is a L-glutamyl derivative of Methanopterin. Both cofactors function as a one-carbon carrier, a process during which the cofactors are reduced to H_4MPT/H_4SPT (see Figure 2.5) (Graham & White, 2002). Generally, acetotrophic and methylotrophic methanogens contain SPT, whereas hydrogentrophs contain MPT (Gorris *et al.*, 1988). Gorris and colleagues indeed found that SPT was correlated with methanogenic activity on propionate, butyrate and acetate, but not with SMA on hydrogen. Unfortunately, this distinction is not absolute since at least one hydrogenotroph (*Methanococcus voltae*) and one methylotroph (*Methanolobus tindarius)* contain SPT and MPT, respectively (Dimarco *et al.*, 1990). Nevertheless, this potentially, but no absolute, distinctive character is an interesting feature with respect to monitoring these two cofactors. Moreover, whereas both cofactors have the same distinct UV-VIS spectrum, chromatographic methods for their separation have been described, allowing separate quantification (Van Beelen *et al.*, 1984; Dimarco

et al., 1990). Despite these promising properties recent attempts to use these cofactors as markers for the different types of methanogens have not been reported, possibly due to the lack of commercial standards for their quantification and the potential prevalence of methanopterin (and other similar pterins) in non-methanogenic bacteria (Dimarco *et al.*, 1990).

2.2 Filterability monitoring: bioflocculation

In this part, the focus is on filtration performance in anaerobic membrane bioreactors. Although we have witnessed a significantly increased implementation of AnMBRs during the last decade, the main drawback still hampering its widespread application is membrane fouling (Lin *et al.*, 2013). The water flux that permeates through the membrane is a key parameter since it determines the required membrane area, which is an important cost (Liao *et al.*, 2006). As with aerobic MBRs, operation at a flux below the so-called *critical flux* is preferred (Liao *et al.*, 2006). Various definitions of the critical flux have been proposed (Field *et al.*, 1995; Fan *et al.*, 2006). In general, it represents a flux below which the flow does not decline and above which fouling is observed. More recently, other more practical parameters have been introduced, i.e., the *threshold flux* and *sustainable flux*, providing more practical guidance to the operator (Field & Pearce, 2011). A detailed description of the various fouling mechanisms and parameters affecting membrane performance can be found in Lin *et al.* (2013) and Ozgun *et al.* (2013). In what follows, one particular parameter, the *bioflocculation status of the sludge* (i.e., the sludge morphology) and its influence on filtration performance in membrane bioreactors, is discussed. Note that most of the research regarding this subject has focused on aerobic membrane bioreactors

2.2.1 Bioflocculation: fundamentals of a dynamic process

Bioflocculation is a complex and dynamic process involving a multitude of components. It is, in fact, the net result of floc growth and deflocculation or floc decay (Van de Staey *et al.*, 2015). The main components are the microorganisms which interact with multivalent cations, small organic and inorganic particles, dissolved components and extracellular polymeric substances (EPS) in order to form the micro –and macrostructure of sludge flocs (Neyens *et al.*, 2004; Nielsen *et al.*, 2012). The exact underlying mechanisms of the bioflocculation process remain unclear but several theories have been proposed and are being discussed in literature.

General floc structure

According to the *filamentous backbone theory*, flocs have a micro –and macrostructure. Essential in the formation of these structures are two types of microorganisms, filamentous (or filament forming) microorganisms and floc forming microorganisms (Cenens *et al.*, 2000; Nguyen *et al.*, 2007). The latter play an essential role in the formation of the microstructure. These microorganisms form small microflocs which are mechanically weak and, as such, are limited in the size they can attain. The filamentous microorganisms allow the overall floc size to increase by providing a so-called backbone, which is the macrostructure, to which the small flocs can adhere by means of their EPS (Cenens *et al.*, 2000). Considering the abovementioned structure, the amount of filament –and floc forming organisms should be balanced. A shortage of filamentous

microorganisms will result in small and weak flocs, whereas too many filaments may result in a too loose floc structure (Cenens *et al.*, 2002). The resulting floc structure affects the filterability of the sludge. Figure 2.8 visualizes the filamentous backbone theory and the multitude of components involved in the dynamic bioflocculation process.

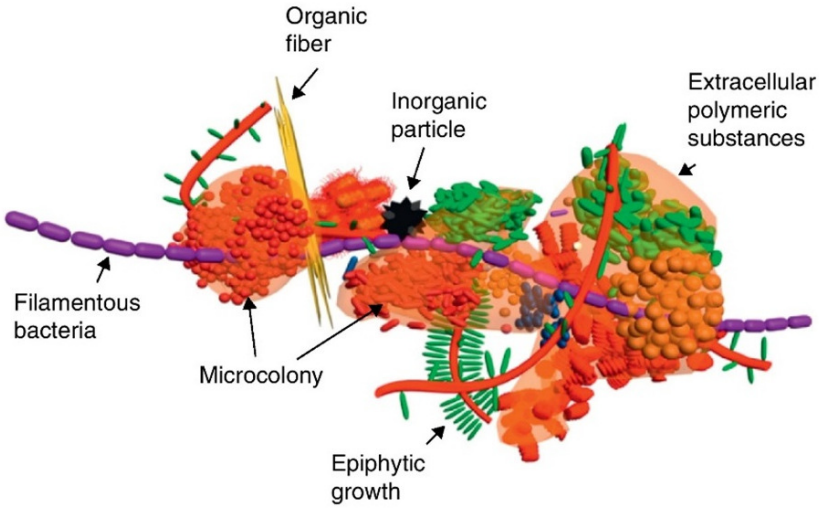


Figure 2.8 Visualization of the two-level micro –and macrostructure of an activated sludge floc. According to the filamentous backone theory, filamentous microorganisms provide the macrostructure to which other components, i.e., small microflocs (microstructures) can adhere. Figure taken from Nielsen *et al.* (2012).

An important operational parameter in achieving the optimal balance between filamentous and floc forming microorganisms is the feeding regime. According to the *kinetic selection theory* (Chudoba *et al.*, 1973) the growth of both types of microorganisms can be described using Monod kinetics as shown in Equation 2-1.

$$\mu = \mu_{max} \frac{S}{S+K_m} \qquad \textbf{Equation 2-1}$$

with μ (h^{-1}) and μ_{max} (h^{-1}) the specific growth rate and maximum specific growth rate, respectively, S ($g\ L^{-1}$) the substrate concentration and K_m ($g\ L^{-1}$) the affinity constant (i.e., the substrate concentration at which μ equals ½ μ_{max}).

The kinetic selection theory states that, since floc forming organisms have a higher μ_{max} than filamentous microorganisms, their growth will be promoted at high substrate concentrations. In contrast, the filamentous microorganisms have a higher affinity (K_m). As a result, these types of microorganisms will thrive at low substrate conditions. Note that substrate is defined here in the broad sense and can refer to organic substrate but also oxygen or nutrients. Due to the promotion of filamentous microorganisms at low substrate concentrations, so called feast-famine cycles are often preferred over continuous feeding regimes (Chiesa *et al.*, 1985), since they allow the formation of a balanced community of filaments and floc formers.

Jorand *et al.* (1995) propose an alternative, three-layer model in which the smallest constituents, i.e., *primary particles* (0.5 – 5 µm) aggregate to first form *microcolonies* and subsequently grow into larger flocs (+/- 125 µm). EPS play a crucial role in the aggregation of the primary particles to microcolonies according to Jorand *et al.* (1995). In general, in all proposed floc structure models, the EPS play an important role.

The role of EPS

EPS is an umbrella term encompassing a wide range of different compounds. In activated sludge systems most of the EPS are proteins and carbohydrates, however, lipids and humic, nucleic and uronic acids are also present to a lesser extent (Frølund *et al.*, 1996; Dignac *et al.*, 1998; Liu & Fang, 2003). A wide range of parameters, e.g., type of wastewater, solids retention time (SRT), nutrient and dissolved oxygen availability, etc. influence the highly variable composition and quantity of the EPS (Liu & Fang, 2003; Lin *et al.*, 2014). Depending on their location, soluble EPS (also known as SMP or soluble microbial products) and bound EPS are distinguished (Van Dierdonck *et al.*, 2012). The latter, which are strongly associated with the cells, are further subdivided into tightly and loosely bound EPS or, TB-EPS and LB-EPS, respectively (Nielsen & Jahn, 1999). The TB-EPS form the stable inner layer around the microbial cells, whereas the LB-EPS are located in the outer layer and form a highly hydrated, loose slime layer (Sheng *et al.*, 2010; Lin *et al.*, 2014; Salama *et al.*, 2016). Most of the EPS measured in bioreactor samples are produced by the microorganisms, but they are also released during hydrolysis of feed components and cellular lysis (Sheng *et al.*, 2010) or can be feed components, adsorbed to the floc surfaces.

As mentioned above, the EPS play an important role in the formation of strong flocs. Since primary particles are known to contribute more significantly to membrane fouling, the formation of such strong and well-formed flocs is of paramount importance to reduce the sludge's membrane fouling potential (Van den Broeck *et al.*, 2012; Van de Staey *et al.*, 2015). Nonetheless, the role of EPS in membrane fouling is ambiguous. Multiple reports have addressed the conflicting results with respect to the role of EPS in membrane fouling. An important explanation for this observation is that the comparison of results from different studies is complicated by the lack of a standardized extraction method for the different types of EPS and the quantification of their constituents (D'Abzac *et al.*, 2010; Kunacheva & Stuckey, 2014).

Bioflocculation mechanisms

An overview of the different bioflocculation mechanisms is found in Sobeck & Higgins (2002). Briefly, the complex bioflocculation mechanism is explained by hydrophobic interactions (with again a crucial role for EPS) and cation interactions. With respect to the latter, three main theories were developed: (*i*) the (extended) Derjaguin-Landau-Verwey-Overbeek ((X)DLVO) theory (*ii*) the divalent cation bridging (DCB) theory and (*iii*) the alginate or *eggbox* theory.

2.2.2 Factors affecting bioflocculation

The bioflocculation process can be influenced by a multitude of operational parameters. In this part, four important factors are discussed.

Wastewater characteristics

Since the characteristics of the wastewater may strongly influence the EPS production and composition, they also have an important impact on the bioflocculation process (Faust *et al.*, 2014). Researchers have observed differences in EPS production when (aerobic) reactors were fed with either glucose or sodium acetate (Li & Yang, 2007), or when particulate substrates (Wang *et al.*, 2014) or different glucose to starch ratios (Van

Dierdonck *et al*, 2013) were used. The differences in EPS production most likely originate from the impact of wastewater characteristics on the microbial community and the metabolic pathways they prefer to use to treat the specific incoming compounds (Van Dierdonck *et al.*, 2013; Faust, 2014).

Because of their aforementioned importance, the amount and composition of cations in the wastewater also have a direct impact on the bioflocculation process. More specifically, the concentration of monovalent over polyvalent cations (M/P ratio) plays a crucial role in the formation of cation-EPS bridges (Bruus *et al.*, 1992; Higgins & Novak, 1997; Sobeck & Higgins, 2002). An M/P ratio higher than two has been shown to induce deflocculation (Van den Broeck *et al.*, 2010; Van de Staey *et al.*, 2015).

Solids retention time (SRT)

Several researchers have investigated the impact of SRT on EPS production and characteristics. Unfortunately, because of the aforementioned issues with EPS quantification, the results are contradictive. Some studies indicate that EPS concentrations increase with increasing SRT (Sheng *et al.*, 2010), whereas others claim that they decrease (Ersahin *et al.*, 2014; Faust *et al.*, 2014) or are unaffected (Liao *et al.*, 2001). One study attributed a worsened membrane fouling to reduced bioflocculation, as a result of an increased SRT and subsequent decreased EPS production (Huang *et al.*, 2011). It should be noted that the different EPS concentrations and characteristics at different SRTs are indirect results of changes in metabolic activity and community structure (Van den Broeck *et al.*, 2012). In general, more research is required in order to establish a clear relationship between SRT, EPS and bioflocculation. In a study where EPS concentrations were not measured, Van den Broeck and colleagues (2012) found that in an aerobic MBR higher SRTs improved flocculation and reduced the amount of primary particles. As a result lower fouling rates were observed. In contrast, in an AnMBR, Pacheco-Ruiz *et al.* (2017) observed improved filterability at lower SRTs. Unfortunately, these authors did not monitor the bioflocculation. Dereli *et al.* (2014) proposed that short SRTs may improve filterability in AnMBRs thanks to the washout of fine particles.

Organic and sludge loading rate (OLR and SLR)

Van Dierdonck *et al.* (2012) investigated the impact of the organic loading rate on the bioflocculation process in aerobic bioreactors. Starting from a nominal reactor loading of 0.7 g COD L^{-1} d^{-1} a lower OLR resulted in more fragmented sludge whereas a higher OLR led to increased floc erosion (a concept explained in the next paragraph). The authors proposed a lower protein-to-carbohydrate ratio of the EPS as an explanation for the more fragmented sludge, whereas the floc erosion may have been caused by increased collisions between the flocs. It should be noted that the sludge concentration in the bioreactor is controlled by means of the SRT and that, in combination with the OLR, this operational setting determines the sludge loading rate (SLR). The SLR, which is essentially the food over microorganism ratio (F/M), reflects the availability of substrate for the microorganisms. As discussed in Section 2.2.1, the prevailing substrate concentration may impact the bioflocculation process by selection for either filamentous or floc forming microorganisms.

Shear rate

In 2009, Jeison *et al.* introduced the "shear rate dilemma" which is now widely accepted in the membrane bioreactor field. The term describes the ambiguous role of the cross-flow velocity in membrane fouling of side-stream operated MBRs. In these types of MBRs the membrane module is located outside the main bioreactor and the sludge is circulated across the membrane loop by means of a pump. The flow rate of the recirculation stream, in combination with the diameter of the membrane module, determines the cross-flow velocity across the membrane module. This cross-flow velocity induces a certain shear rate on the microorganisms. Side-stream or cross-flow operation is popular since it provides simple and direct control over the hydrodynamic conditions at the membrane surface (Lin *et al.*, 2013). In theory, particle deposition on the membrane surface is reduced during cross-flow operation, hence also reducing cake formation on the membrane surface. However, Jeison *et al.* (2009) observed that changes in sludge properties, induced by too high shear rates, may offset this beneficial effect. Figure 2.9 visualizes the shear rate dilemma.

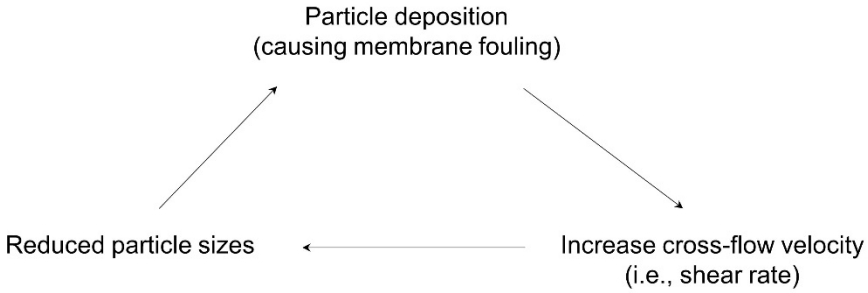


Figure 2.9 Visualization of the shear rate dilemma. Small particles are deposited on the membrane surface and cause membrane fouling, the cross flow velocity is subsequently increased in order to increase back-transport away from the surface but causes an increase in small particles as a result of excess shear, which in turn contributes to membrane fouling. Adapted from Jeison *et al.* 2009.

Van Dierdonck *et al.* (2012) states that deflocculation can occur in two different ways: (*i*) floc erosion and (*ii*) fragmentation. During floc erosion, floc sizes are reduced and the number of free primary particles increases since they are released from the edges of larger flocs. In contrast, fragmentation or floc-breakage implies the splitting up of floc structures, hereby leading to more but smaller flocs, whereas free primary particles only slightly increase. During cross-flow operation of MBRs, floc erosion is more likely to occur and its effect, the increase of primary particles, is expected to lead to the formation of a denser cake layer (Van den Broeck *et al.*, 2012). The challenge lies in selecting an appropriate cross-flow velocity which enhances shear across the membrane surface while limiting size reduction of flocs and disruption of cells (Jeison *et al.*, 2009). Although several researchers have highlighted the potential effect of shear-stress on microbial activity in anaerobic bioreactors (Brockmann & Seyfried, 1996; Choo & Lee, 1996; Ghyoot & Verstraete, 1997), Jeison and colleagues (2009) did not observe a decrease in biological activity.

2.2.3 Role in membrane fouling

In general, membrane fouling is the result of the interaction between the membrane surface and the sludge. Therefore, both the (surface) characteristics of the membrane and the physico-chemical characteristics of the sludge are important to understand fouling phenomena. The previous paragraphs highlighted the ambiguous role of EPS in

membrane fouling because of its role in the bioflocculation process and its potential as a direct foulant. In this PhD thesis the focus is on the physical bioflocculation status of the sludge and its potential impact on membrane fouling. Van den Broeck *et al.* (2010; 2011) concluded that filterability could be predicted by following-up the bioflocculation status of the activated sludge in aerobic MBRs. The general consensus in literature is that small particles and colloidal matter, i.e., (sub-)micron particles, in particular have a high fouling propensity (Ivanovic *et al.*, 2008; Van den Broeck *et al.*, 2011, Gao *et al.*, 2013). These particles tend to fill up small gaps in fouling cake layers, hereby creating a denser cake layer (Van den Broeck *et al.*, 2012). The presence of large and dense activated sludge flocs is preferred over large numbers of (sub-)micron particles which lead to reduced permeabilities (Van de Staey *et al.*, 2016). Van de Staey also found that the shape of flocs has an impact. In general, round flocs with smooth edges had a positive effect in filterability. Moreover, a slightly positive effect of filaments on fouling rates was reported. Having established the importance of bioflocculation in membrane fouling, in the following paragraphs different approaches of monitoring this dynamic process are discussed.

2.2.4 Bioflocculation monitoring

Considering the abovementioned importance of bioflocculation in membrane fouling processes, monitoring the bioflocculation status is an important prerequisite for accurate follow-up of membrane bioreactor systems. Several sludge characteristics that impact bioflocculation, i.e., EPS concentration and composition, hydrophobicity, surface charge, etc. may be measured in order to evaluate the bioflocculation status, however, these are all indirect measures. Other conventional parameters such as sludge volume index, also solely provide indirect information and are not sufficient to characterise evolutions in the bioflocculation status (Van Dierdonck *et al.*, 2012). As a result, more advanced and detailed methods are required. Two such approaches are discussed below.

Microscopy and quantitative image analysis

In recent years, microscopic techniques have become increasingly important for monitoring and controlling the operation of activated sludge systems (Mesquita *et al.*, 2011). The advantages include providing an accurate morphological characterisation of the sludge, allowing the direct assessment of the bioflocculation process (Mesquita *et al.*, 2011; Van Dierdonck *et al.*, 2012). An extensive overview of the various microscopic imaging techniques can be found in Costa *et al.* (2013). Briefly, *brightfield microscopy* is a popular technique but may underestimate the quantity of filamentous microorganisms due to their low absorbance of light. *Phase contrast microscopy* solves this issue by amplifying small phase differences (Davidson & Abramowitz, 1997). Fluorescence microscopy can also be applied to visualize and quantify autofluorescent molecules or to target specific compounds by means of a staining procedure (secondary fluorescence) (Davidson & Abramowitz, 1997). A method using the autofluorescent properties of cofactor F_{420} combined with image analysis for its quantification is assessed in this PhD thesis and described in Chapter 7.

In order to objectify the visual observations from the microscopy images and to be able to quantitatively compare different sludge samples, image analysis can be used. For example, Grijspeerdt & Verstraete (1997) linked morphological parameters to sludge settleability by means of image analysis. More recently, several researchers applied

quantitative image analysis in order to link the sludge morphological characteristics (i.e., the bioflocculation status) to operational conditions in bioreactors (Mesquita *et al.*, 2011). At the KU Leuven such an image analysis programme was developed in MATLAB. The initial programme, i.e. the ACTivated Sludge Image Analysis System (ACTIAS) (Jenné *et al.*, 2002; 2007) was later revised and resulted in the new Activated Sludge Image Analysis Programme or ASIAP (Van de Staey, 2016; Cao, 2016). This programme was used in Chapter 8 (Part II) of this PhD thesis in order to assess the influence of bioflocculation status on membrane fouling in an AnMBR. The fundamentals of quantitative image analysis are elaborated in Costa *et al.* (2013).*Laser-based particle size detection*

An alternative approach to obtain particle size distributions and, hence, an idea on the bioflocculation status of a sludge sample, are laser-based particle size detection methods. Three different methods are used: (*i*) laser diffraction (*ii*) dynamic light scattering and (*iii*) time of transition. The laser diffraction method has been used by several authors in activated sludge research (Jin *et al.*, 2003; Arabi & Nakhla, 2009, Gao *et al.*, 2013,; Shen *et al.*, 2015). Although providing rapid results, because of some important assumptions, the method is not very suitable for activated sludge samples. Noteworthy here are its limitations with respect to monitoring the abundance of small particles (Van de Staey, 2016). In contrast to laser diffraction, dynamic light scattering allows the quantification of (sub-)micron particles. Its application to activated sludge systems has recently been demonstrated by De Temmerman *et al.* (2014; 2015). However, the authors acknowledge the need for separating the primary particles from the flocs prior to the measurement. As a result, the concentration and distribution of particles may be altered, rendering the method only accurate for relative comparison of the tested samples. The third method is based on a combination of size analysis based on the time of transition principle and dynamic size and shape characterization using an online camera (Van de Staey, 2016). Govoreanu *et al.* (2004) used this technique to determine the floc size distribution and concluded that the method has several disadvantages. The most important drawback was that it often failed at separating multiple objects. Based on these reports in literature, it can be concluded that microscopic image analysis remains the most versatile measurement method for the determination of particle size distributions in activated sludge systems (Van de Staey, 2016). Van de Staey found that, together with hydrophobicity, image analysis related information regarding morphology was the most relevant for detecting changes in bioflocculation status.

In general, it can be concluded that the importance of sludge morphology and, hence, of monitoring the bioflocculation status is well-established in membrane bioreactor systems. However, it is also clear that most research thus far focused on aerobic membrane bioreactors and that studies *following-up the bioflocculation process* with suitable techniques (i.e., quantitative microscopic imaging) *in anaerobic membrane bioreactors* are lacking.

CHAPTER 3

Materials and methods

In this chapter the *general* experimental methods used throughout this work are described. The adaptation and refinement of cofactor extraction and quantification methods is described in detail in Chapter 4. Certain specific experimental methods (i.e., molecular genetic techniques and microscopic image analysis) are described in the materials and methods section of the respective experimental chapters.

3.1 Analytical methods

Volatile and total (suspended) solids concentration

Volatile and total (suspended) solids concentrations were determined according to standard protocols (APHA, 2005). For the suspended solids analyses the reactor samples were filtered through a pre-weighed oven dried filter paper (Macherey Nagel, GF-3, pore size 0.6 µm) using a vacuum filtration pump. The filter that retained the suspended solids was then placed into an oven at 105 °C for 2 hours. After cooling in a desiccator, the filter was weighed and the **total suspended solids concentration (TSS)** was calculated using Equation 3-1

$$\text{TSS (g L}^{-1}) = \frac{m_{105\,°C} - m_0}{V} \qquad \textbf{Equation 3-1}$$

with m_0 and $m_{105\,°C}$ the filter weight (g) prior to, and after, drying at 105 °C, respectively. V denotes the filtered sample volume (L).

The **volatile suspended solids concentration (VSS)** was obtained by subsequently placing the same filter in a 550 °C oven for 2 hours. The VSS concentration was then calculated using Equation 3-2.

$$\text{VSS (g L}^{-1}) = \frac{m_{105\,°C} - m_{550\,°C}}{V} \qquad \textbf{Equation 3-2}$$

with $m_{105\,°C}$ and $m_{550\,°C}$ the weight (g) after drying at 105 °C and ashing at 550 °C, respectively. V denotes the filtered sample volume (L).

The **total and volatile solids (TS and VS)** were calculated using the same procedure and equations described above, however, the samples were not filtered but a pre-weighed weighing boat was used.

Chemical Oxygen Demand (COD)

The reactor soluble COD (sCOD) was measured using cuvette test kits (Hach Lange, LCK series) after filtration (Macherey Nagel GF-3, pore size 0.6 µm) and served as a measure of organics concentration. In the cuvette, oxidizable substances react with a sulphuric acid – potassium dichromate solution in the presence of silver sulphate as a catalyst. The green coloration of Cr^{3+} is then evaluated spectrophotometrically (Hach Lange, DR5000). Membrane bioreactor effluent COD concentrations were measured in the same way, without prior filtration.

Ammonium concentration

Ammonium-nitrogen (NH_4^+-N) measurements were performed using cuvette tests (Hach Lange, LCK 302) on filtered (Macherey Nagel GF-3, pore size 0.6 µm) reactor samples. Here, ammonium ions react at pH 12.6 with hypochlorite ions and salicylate ions in the presence of sodium nitroprusside as a catalyst to form indophenol blue, which is spectrophotometrically determined (Hach Lange, DR5000). **Free ammonia concentrations** (FA, mg NH_3-N L^{-1}) were calculated based on the ammonium-nitrogen concentration (mg NH_4^+-N L^{-1}), temperature (T, °C) and pH (Anthonisen *et al.*, 1976; Balmelle *et al.*, 1992) as shown in Equation 3-3.

$$\text{FA } (\text{mg } NH_3 - \text{N } L^{-1}) = \frac{NH_4^+ - N \; 10^{pH}}{e^{\frac{6344}{273+T}} + 10^{pH}} \qquad \textbf{Equation 3-3}$$

Electrical conductivity, pH and temperature

Electrical conductivity was measured with a conductivity probe (Hach Lange) connected to an HQ40d Multi portable meter (Hach Lange). Temperature and pH were monitored and logged using a pH-meter (Knick, Portavo 907 Multi).

Volatile Fatty Acids concentration

Sample preparation for determining individual Volatile Fatty Acid (VFA) concentrations (formic, acetic, propionic, butyric, iso-butyric, valeric and iso-valeric acid) included filtration of supernatant on a Sarstedt Filtropur 0.2 µm cartridge filter. Next, high-performance liquid chromatography (HPLC) analysis was performed with an Aminex® HPX-87H ion exclusion column (300 x 7.8 mm) for organic acid analysis equipped with a pre-filter. This column was installed in an HPLC Agilent technologies 1200 series console. Ion exclusion chromatography is based on the repulsion of dissociated ions (Glod, 1997). The injected volume was 20 µl, operating pressure was 100 bar and the column was heated at 40 °C. Samples were run for 45 minutes using a flow rate of 0.6 mL 5 mM H_2SO_4 min^{-1} and the signal was recorded on a diode array detector at 210 nm. The results were then quantified using an automatic calibration procedure embedded in the Agilent software. Individual VFA concentrations were determined based on standard series of each of the VFAs.

Synthetic feed preparation

For the reactors operated at the KU Leuven, a synthetic feed mimicking dairy wastewater was prepared. The feed composition was adapted from De Vrieze *et al.* (2013) and contained skimmed milk powder (Douwe Egberts) as the main carbon source. The milk powder was a commercially available variant (Douwe Egberts) designed for professional coffee machines and consisted of 12% (w/w) fat, 63% (w/w) carbohydrates (all sugars), 16% (w/w) proteins and 0.5% (w/w) salt. An equivalence factor of 1.278 gCOD g milk $powder^{-1}$ was established based on a linear calibration. Table 3.1 shows the composition of the synthetic feed.

Table 3.1 Composition of the synthetic feed used in the reactors operated at the KU Leuven.

C source	Milk powder		
Buffer	KH_2PO_4	10	mM
	K_2HPO_4	10	
	$NaHCO_3$	20	
Macronutrients	NH_4Cl	500	mg L^{-1}
	$CaCl_2.2H_2O$	200	
	$MgCl_2.6H_2O$	100	
	$Fe_2(SO_4)_3.5H_2O$	122.5	
Trace elements	$NiSO_4.6H_2O$	500	µg L^{-1}
	$MnCl_2.4H_2O$	500	
	$FeSO_4.7H_2O$	500	
	$ZnSO_4.7H_2O$	100	
	H_3BO_3	100	
	$(NH_4)_6Mo_7O_{24}.4H_2O$	36	
	$CoCl_2.6H_2O$	50	
	$CuSO_4.5H_2O$	5	

3.2 Nucleic acid (DNA and RNA) extraction

Total DNA was extracted from bioreactor samples using a method adapted from the cetyltrimethylammonium bromide (CTAB) – sodium dodecyl sulfate (SDS) based isolation method described by Zhou *et al.* (1996). Sludge pellets were mixed with 1 mL of DNA extraction buffer consisting of 100 mM Tris-HCl (pH 8.0), 100 mM sodium EDTA (pH 8.0), 100 mM sodium phosphate (pH 8.0), 1.5 M NaCl and 1% CTAB (preheated to 60 °C) and 0.3-0.5 g of zirconia/silica beads (1.0 mm diameter). After bead beating 3 x 45 s at 5500 rpm with 30 s pauses in a Precellys 24 Ribolyser, the samples were mixed with 150 µL of 10% SDS and incubated on a shaker (450 rpm) at 70 °C for 90 min. After centrifugation at 10 000 x g for 10 min, the supernatant was collected into 2 mL centrifuge tubes, mixed with an equal volume of chloroform-isoamyl alcohol (24:1 v/v) and vortexed for 10 s. The aqueous phase was recovered by centrifugation at 10 000 x g for 10 min and the DNA precipitated with 0.6 volume of isopropanol overnight at room temperature. The nucleic acids were pelleted by centrifugation at 10 000 x g for 25 min, washed with 70% ethanol, dried and dissolved in Tris-EDTA buffer (10 mM Tris-HCl, 1 mM EDTA, RNase A 0.002%, pH 8). The crude DNA extract was purified using self-made columns with polyvinylpolypyrrolidone (PVPP). To this end, 200 µL of a 20% w/v polyvinylpolypyrrolidone in Milli-Q water was packed in a 0.5 mL pierced tube (using a 0.5 mm needle) by centrifugation at 1000 x g for 2 min. The DNA extract was loaded onto the column and the column centrifuged at 1000 x g for 2 min. Quality and quantity of the purified DNA were estimated using a NanoDrop ND-1000 spectrophotometer and a Qubit 3.0 fluorometer, respectively. High quality purified DNA was stored at -20 °C.

Total mRNA was extracted based on the guanidine/phenol method described by Chomczynski & Sacchi (1987), with following adaptations. The homogenization step was performed using 0.3-0.5 g of zirconia/silica beads (1.0 mm diameter) for 45 s at 6500 rpm in a Precellys 24 Ribolyser in a solution containing 4 M guanidium thiocyanate, 25 mM sodium citrate, 0.5% w/v sodium lauryl sarcosinate and 0.1 M ß-mercaptoethanol. Subsequently, 500 µL water saturated phenol in citrate buffer (Sigma-Aldrich, Cat. P4682, pH 4.5), 50 µL 3 M NaAC (pH 5.2) and 200 µL chloroform were added. The first

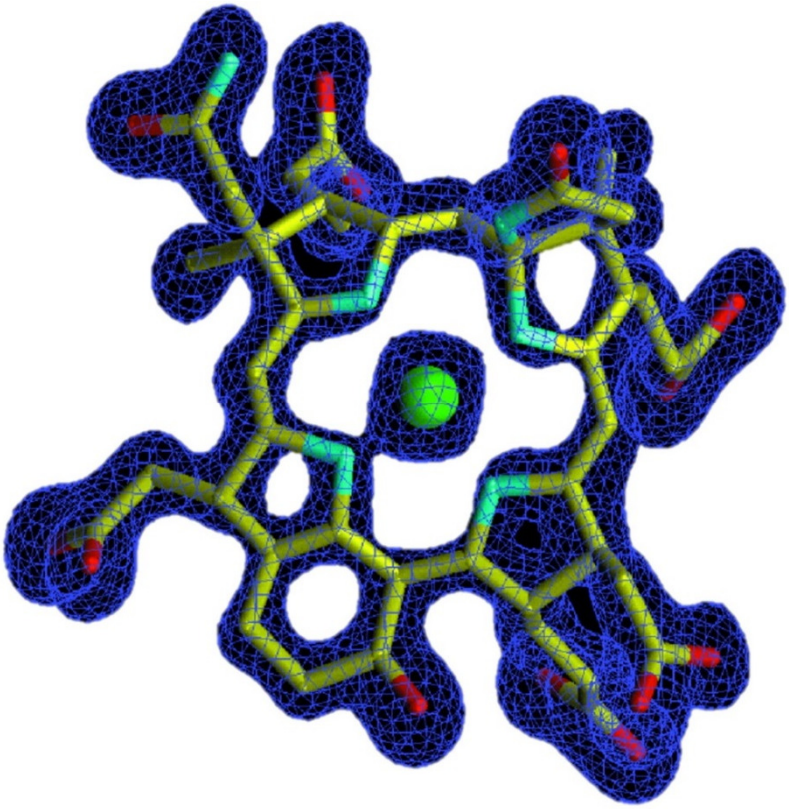
precipitation was performed with chloroform instead of isopropanol, whereas for the re-precipitation 100% isopropanol was used. Furthermore, a second washing step of the obtained pellet with 95% EtOH was applied prior to drying and re-dissolving in THE storage solution (ThermoFisher Cat. AM7000). RNA was treated with DNase (TURBO, DNA-*free*™ Kit, Ambion, CA, USA) at 37 °C for 30 min and purified using the RNA clean & concentrator-5 kit (Zymo, CA, USA). This procedure was repeated twice in order to remove all contaminating DNA. Quantity of the purified mRNA was estimated using the Qubit 3.0 fluorometer and samples were diluted to 70 ng μL^{-1} prior to cDNA synthesis.

3.3 Statistical analyses

The statistical data analysis was performed with the software package JMP Pro® for Windows (version 12.1.0, SAS Institute Inc., Cary, NC, 1989-2007). The Pearson product-moment correlation was used as a measure of the strength of the linear association between two variables. The Pearson coefficient (r) ranges between -1 and +1. A value of -1 or +1 indicates a perfect correlation, whereas a value of 0 indicates the complete absence of correlation. Negative values imply an inverse relation whereas positive values imply a positive relation between the tested parameters. An absolute correlation coefficient value of at least 0.5 indicates a strong correlation. Correlations were considered statistically significant at a 95% confidence interval ($p < 0.05$). Each p-value corresponds to a test of the null hypothesis that the true correlation between the variables is zero. The exact significance values are included in the statistical reports. Note that the Pearson correlation cannot determine a cause-and-effect relation and solely establishes the strength of a linear association between two variables.

Part I

Assessing methanogenic activity using methanogenic cofactors



CHAPTER 4

Methanogenic cofactor extraction and quantification methods: adaptation and validation

In order for the monitoring potential of cofactor F_{430} and F_{420} to be evaluated in anaerobic bioreactors, suitable extraction and quantification procedures need to be adopted. Several methods have been reported in literature for both cofactors. The adaptation of these methods to our specific lab equipment and the samples used in this work, is described separately for both cofactors in this chapter[4].

[4] Image on the previous page taken from Ermler *et al.* (1997)

4.1 Cofactor F_{430}

4.1.1 Native form and derivatives

In Section 2.1.5, the elucidation of cofactor F_{430}'s structure and the existence of several F_{430} variants and derivatives was mentioned. The most recent report describing the various F_{430} variants and how they originate from the native form is that of Allen *et al.* (2014). Figure 4.1 shows an overview of the F_{430} forms described in Allen *et al.* (2014), with the native cofactor depicted in the center.

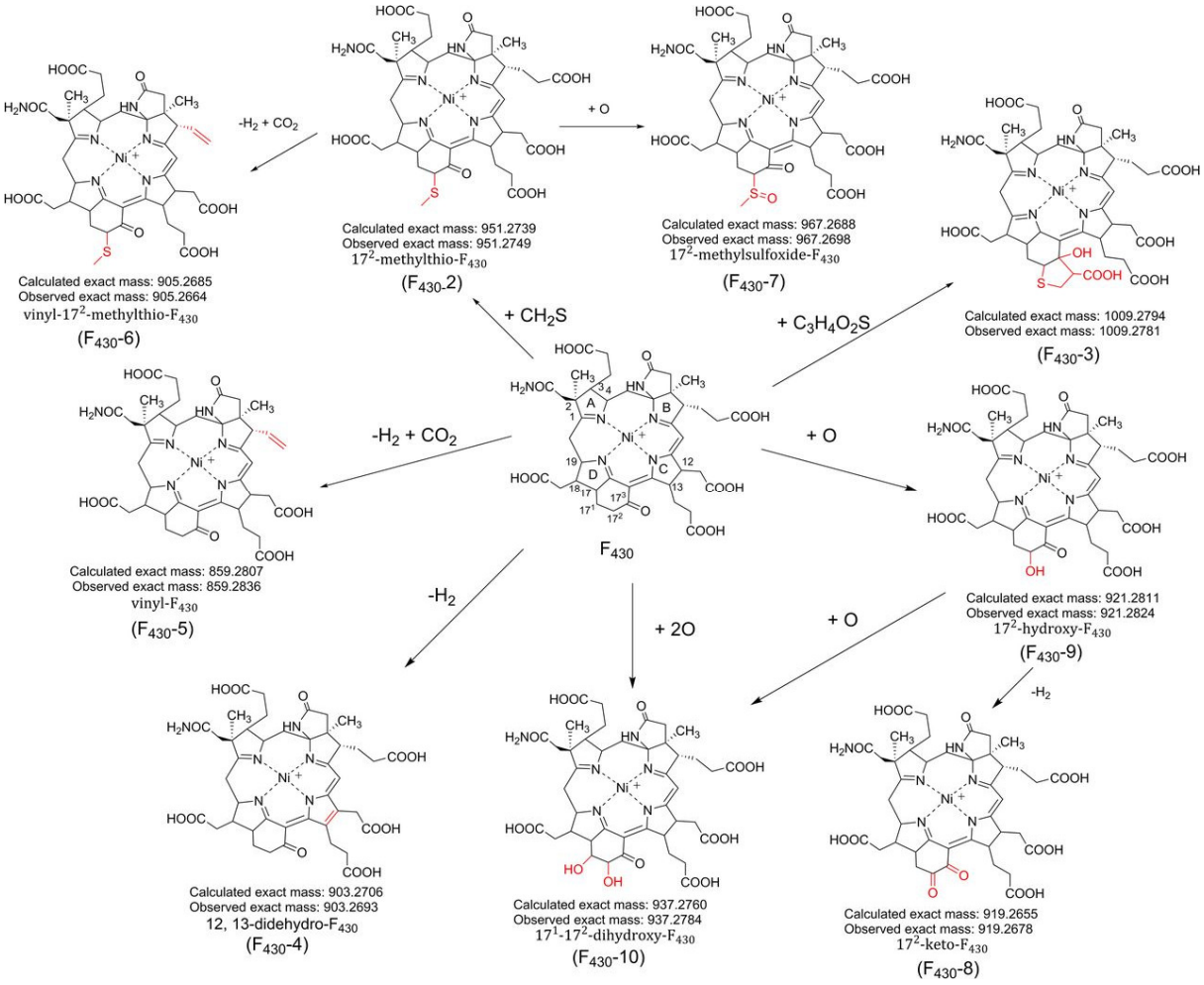


Figure 4.1 The native form of cofactor F_{430} (center) and how it is converted to various derivatives according to Allen *et al.* (2014). Many modifications to the native form (shown in red) are located at the carbon 17 position. Note that the stereo-isomers are not included (i.e., 13-epi-F_{430} and 12,13-diepi-F_{430}).

From Figure 4.1, it is clear that cofactor F_{430}'s biochemistry is complex and that it is important to take into account all possible reactions that might occur intracellularly or during the extraction and quantification procedure. It should be noted that all of these forms, except F_{430}-4, are expected to be functional variants that are produced within the cell (Allen *et al.*, 2014).

With respect to conversions taking place during and after the extraction procedure, the most commonly cited forms are the 12,13-didehydro-F_{430} (also named F_{560} or F_{430}-4) and the stereo-isomers, 13-epi-F_{430} and 12,13-diepi-F_{430} (Shiemke *et al.*, 1988; Kaneko *et al.*,

2014). The last two are not included in Allen's overview (most likely because they cannot be separated by mass spectrometry) but are formed at elevated temperatures and are therefore relevant for the method development described in this chapter. Figure 4.2 provides an overview of the four F_{430} variants that are most commonly found after the extraction procedure. The method development aims to reduce contact with oxygen and excessive temperatures in order to eliminate conversions of the native form to these thermodynamically more stable degradation products as much as possible.

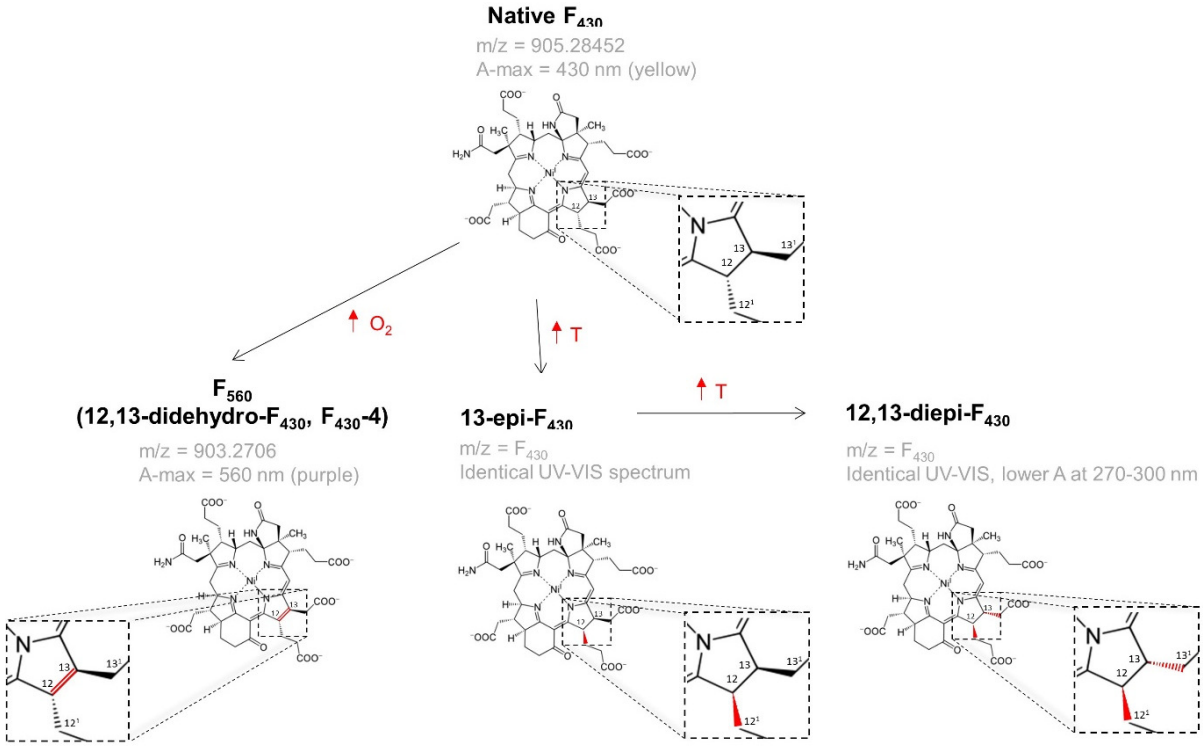


Figure 4.2 An overview of the four most commonly encountered F_{430} variants after extraction. The native form (top) epimerizes at elevated temperatures and dehydrogenizes in contact with oxygen. The exact masses (*m/z*) and basic information with respect to their UV-VIS spectrum is shown in grey (information taken from Allen *et al.*, 2014 and Shiemke *et al.*, 1988).

4.1.2 Extraction and purification procedure

In order to quantify the intracellular cofactor F_{430} content, the first step in the extraction procedure is the cell lysis step. The cell lysis step can be performed by means of a French pressure cell (Shiemke *et al*, 1998), ultrasonication (Mayr *et al.*, 2008), incubation in ethanol at 80 °C (Ketljens *et al.*, 1982), or even boiling. As elaborated above, methods that reduce the temperature and contact with oxygen are preferred since these are expected to maximally preserve the native cofactor form. Figure 4.3 shows the profound effect that excessive contact with air has on the UV-VIS profile of a cofactor extract from one of the experiments from this thesis. The signature F_{430} spectrum disappears, indicating that the native cofactor is degraded.

Following the cell lysis various additional purification steps have been proposed in literature. Typically, an anion exchange resin such as Sephadex (Pfaltz *et al.*, 1987) or Sepharose (Takano *et al.*, 2013) is used first. The use of a hydrophobic resin such as phenyl Sepharose has also been reported (Shiemke *et al.*, 1988).

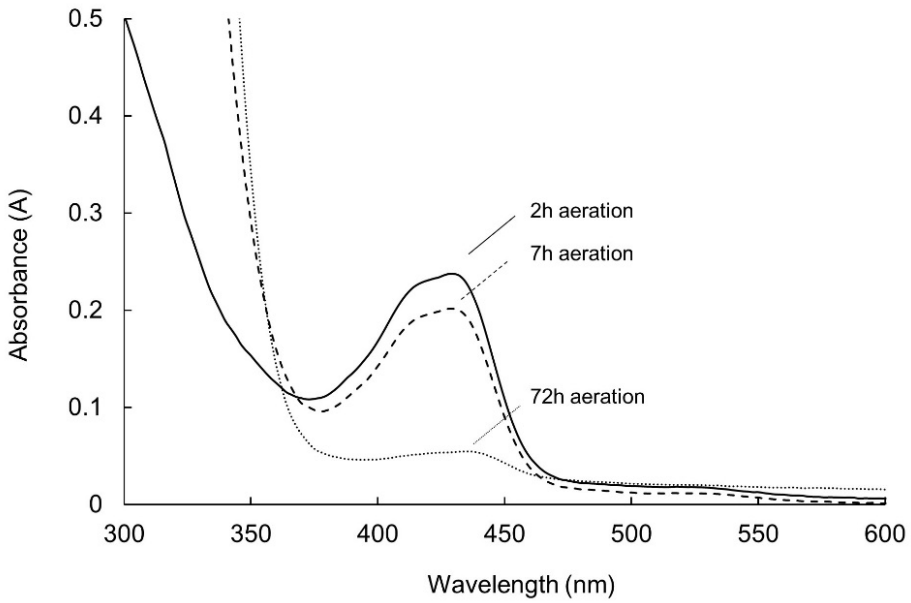


Figure 4.3 The effect of air sparging for 2 hours (—), 7 hours (---) and 72 hours (···) on the UV-VIS spectrum of a cofactor extract from one of the experiments from this thesis. The typical absorbance signature of cofactor F_{430} disappears when the extract is exposed to air.

Several extraction protocols were tested throughout different experiments, resulting in an optimal procedure. Table 4.1 provides an overview of the most important protocols (extraction and purification) that were tested. The initial protocols resemble literature protocols as closely as possible. Ultrasonication (Protocol 1a and b) and heating (Protocol 2) were initially commonly used for the cell lysis. Note that after Protocol 1b the use of the anion exchanger was omitted. Analysis of the run-through and the eluate of this column showed that significant amounts of cofactor were lost in the run-through, indicating that the exchanger was not working properly. For the cell lysis, the use of an ultrasonication probe did not allow multiple samples to be lysed in parallel, which is an important disadvantage. Moreover, a lower F_{430} yield (< 60%) was found compared to the lysis methods based on bead beating. The heating method, on the other hand, seemed to result in high yields, however, the HPLC anlysis indicated that the native cofactor dispersed into several other peaks (all still exhibiting significant absorbance at 430 nm). Figure 4.4 shows an HPLC chromatogram obtained after heating (Protocol 2) and ultrasonication (Protocol 1b). It irrefutably shows that the heat extraction method caused degradation of the native cofactor into thermodynamically more stable variants.

Table 4.1 Overview of some of the tested protocols for cofactor F_{430} extraction and purification. Protocol 4 resulted in the highest cofactor F_{430} yields and allowed twelve samples to be extracted and purified in parallel, in less than half a working day. *AIEX = anion exchanger, SPE = Solid phase extraction.*

Cell lysis	**Protocol 1a[5]**	**Protocol 1b[5]**	**Protocol 2[5]**	**Protocol 3**	**Protocol 4**
Sample preparation	*Centrifugation* 13 000 x g, 10 min, 4 °C	*Centrifugation* 13 000 x g, 10 min, 4 °C	*Centrifugation* 13 000 x g, 10 min, 4 °C	*Centrifugation* 13 000 x g, 10 min, 4 °C	*Centrifugation* 13 000 x g, 10 min, 4 °C
Sample resuspension	217 mM Formic acid (10 mL)	217 mM Formic acid (10 mL)	80% EtOH (v/v) 10 mM KH_2PO_4/K_2HPO_4 (5 mL)	217 mM Formic acid (3 mL)	217 mM Formic acid (3 mL)
Cell lysis method	*Ultrasonication* 15 min (400 W) on ice 2x total (resuspension)	*Ultrasonication* 15 min (400 W) on ice 2x total (resuspension)	*Thermomixer (heating)* 30 min, 80°C 750 rpm 2x total (resuspension)	*Bead beating* Precellys® 24 ribolyser 3x 45 s 5500 rpm Intermittent ice cooling	*Bead beating* Vortex-Genie 2x 10 min 10 000 rpm Intermittent ice cooling
Lysate processing	*Centrifugation* 13 000 x g, 10 min, 4 °C *Decanting*	*Centrifugation* 13 000 x g, 10 min, 4 °C *Decanting*	*Centrifugation* 13 000 x g, 10 min, 4 °C *Decanting*	*Centrifugation* 13 000 x g, 10 min, 4 °C *Decanting* 2x total (resuspension)	*Centrifugation* 13 000 x g, 10 min, 4 °C *Decanting* 2x total (resuspension)
Lysate to purification	Combined supernatant (2x lysis)	Combined supernatant (2x lysis)	Combined supernatant (lysis + wash pellet)	Combined supernatant (lysis + wash pellet)	Combined supernatant (lysis + wash pellet)
Purification					
AIEX	Q sepharose fast flow GE healthcare®	/	/	/	/
AIEX functional group	Quaternary ammonium	/	/	/	/
AIEX equilibration	50 mM Tris/HCl dH_2O	/	/	/	/
AIEX elution	5 mM Formic acid	/	/	/	/
Hydrophobic resin	SPE C18 Resprep®	SPE C18 Resprep®	/	SPE C18 Resprep®	SPE C18 Resprep®
Resin material	C_{18} modified silica	C_{18} modified silica	/	C_{18} modified silica	C_{18} modified silica
Resin equilibration	100% MeOH 217 mM Formic acid	100% MeOH 217 mM Formic acid	/	100% MeOH 217 mM Formic acid	100% MeOH 217 mM Formic acid
Resin elution	100% MeOH 1 bed volume (3 mL)	100% MeOH 1 bed volume (3 mL)	/	100% MeOH 1 bed volume (3 mL)	100% MeOH 1 bed volume (2 mL)
Extract processing	/	/	/	*Centrifugation* 13 000 x g,10 min, 4°C	*Centrifugation* 13 000 x g, 5 min, 4°C

[5] Additional equipment used in Protocols 1a, 1b and 2 includes an ultrasonication probe, a thermoshaker and a Q sepharose column. The ultrasonication probe was a Hielscher UP 400S probe with an H3 sonotrode, typically operated in cyclic mode (0.4 s on 0.6 s off). This sonotrode provides a power density of 460 W/cm² at its tip. The thermomixer employed here was an Eppendorf F1.5 type equipped for 2 mL Eppendorf tubes. The Q sepharose column was custom-made in a 20 mL syringe filled with a glass wool stopper at the bottom. The resin was inserted into the syringe to form the column and stored in a 20% v/v ethanol solution when not in use.

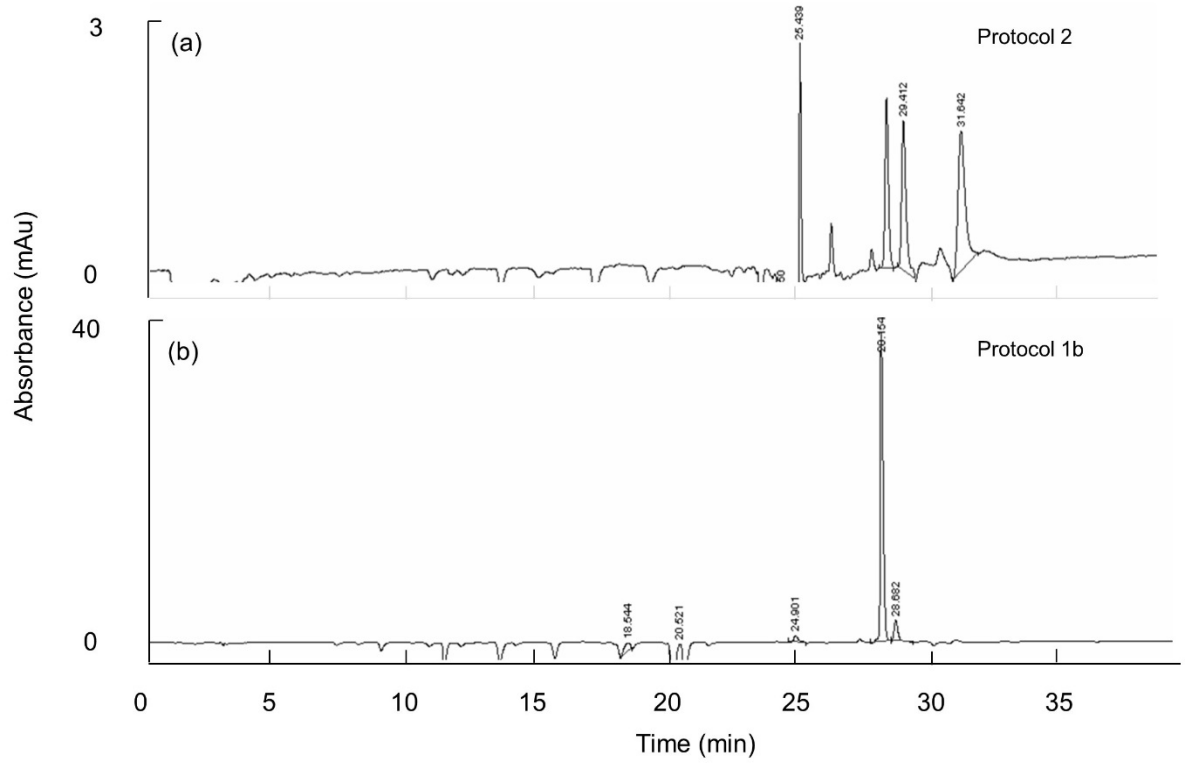


Figure 4.4 Comparison of an HPLC chromatogram after using **(a)** heating (Protocol 2) and **(b)** ultrasonication (Protocol 1b) for the cell lysis step. Heating clearly causes the native cofactor F_{430} peak to be dispersed into several other peaks, indicating that, as expected, excessive temperatures should be avoided when quantifying the native cofactor. The chromatogram was obtained at 430 nm using a Diode Array Detector (DAD).

Because of the abovementioned limitations, a bead beating method using a Precellys® 24 ribolyser (Bertin instruments, Montigny-le-Bretonneux, France) was selected (Protocol 3). When using this protocol for the first bioreactor experiments, several opportunities for optimization were detected which were implemented in Protocol 4. One important disadvantage of Protocol 3 was the requirement of using 1.5 mL micro-centrifuge tubes for compatibility with the Ribolyser. Since a relatively large sludge volume was required in order to obtain sufficient cofactor for quantification, the content of one sample needed to be re-distributed across three micro-centrifuge tubes for the cell lysis, after which the contents were pooled into the original 15 mL Falcon tubes for centrifugation, resulting in losses. This drawback was bypassed by switching to a vortexer with an appropriate tube holder for multiple 15 mL Falcon tubes. As a result, no transferring was required and bead beating was performed in the original sampling tubes. With the vortex set to its maximum rpm setting and with the reduced transferring losses, absorbance signals of around 25% higher were obtained. Figure 4.5 shows the difference in the UV-VIS spectra obtained from Protocol 3 and 4, highlighting the higher cofactor yield in Protocol 4.

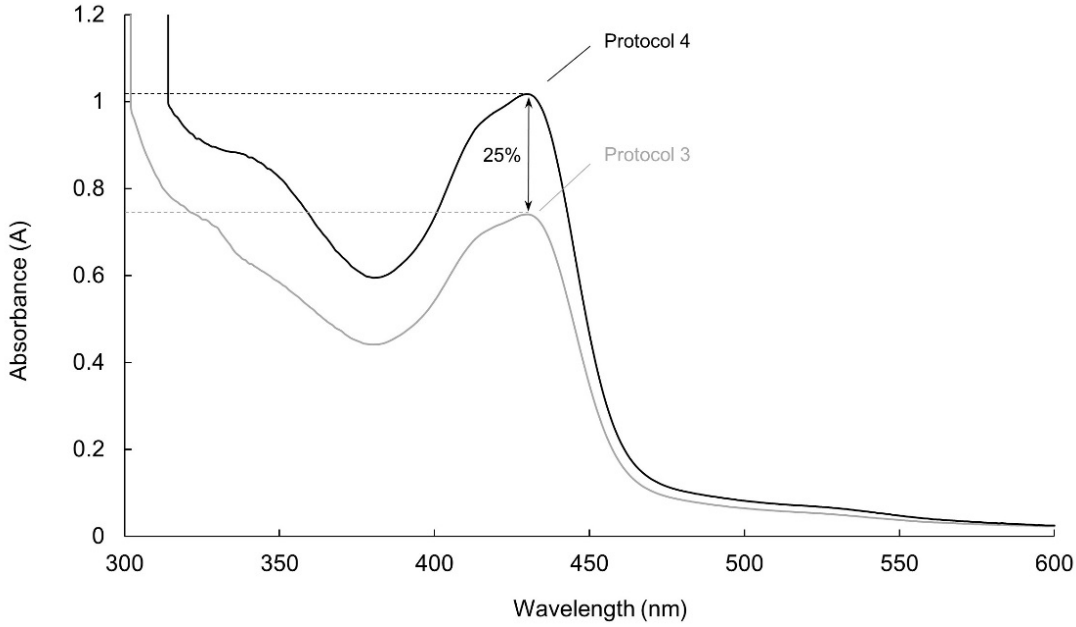


Figure 4.5 The UV-VIS spectra obtained using Protocol 3 (—) and 4 (—) for the extraction of an identical sample. Protocol 4 yields an absorbance signal of about 25% higher, indicating that the cell lysis is more efficient and/or losses are minimized throughout the procedure.

A final optimization implemented in Protocol 4 was the use of a dedicated extraction manifold for use with the C18 purification cartridges. The manifold allowed for the parallel purification of 12 samples, at a uniform flow rate (7 mL min^{-1}) (Figure 4.6). All of the abovementioned tests and optimizations led to the development of Protocol 4, which resulted in the highest cofactor yields while reducing the analysis time. Protocol 4 is described in full in the next paragraph.

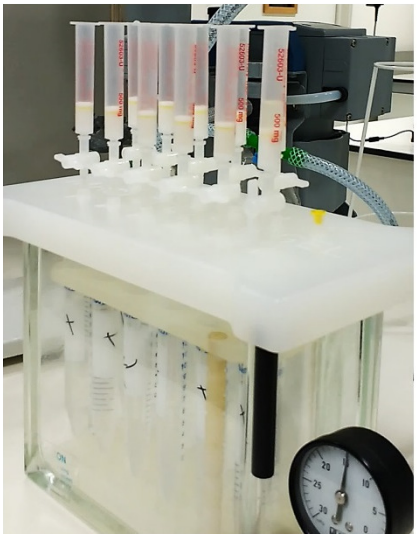


Figure 4.6 The vaccuum extraction manifold used for the parallel purification of multiple lysates. A C18 column is used in order to retain hydrophobic molecules such as cofactor F_{430} (the bright yellow band sorbed on the resin) which is then eluted using pure methanol.

Protocol 4 – the most suitable F_{430} extraction and purification protocol. Sludge samples are centrifuged (Eppendorf 5810 R) at 4 °C for 10 min (13 000 x g) and the pellet resuspended in 3 mL 217 mM formic acid (1% w/w). Subsequently, 1.5 mL of zirconia/silica beads are added (1 mm diameter, Biospec) and bead beating is performed using a Vortex-

Genie 2 (Scientific Industries Inc., Bohemia, NY, USA) at 10 000 rpm (2 x 10 min). Samples are cooled on ice for at least two minutes between the two cycles. Next, the samples are centrifuged (13 000 x g, 4 °C, 10 min) and the clear yellow supernatant (lysate) stored at 4 °C. The pelletized cell debris with the beads is subsequently resuspended in 5 mL 217 mM formic acid and centrifuged to bring any remaining F_{430} in solution and the two supernatants are combined. F_{430} is purified from the supernatant as follows. The supernatant solution is applied to a preconditioned C18 cartridge (Discovery, DSC-18 SPE) which is mounted on a Chromabond® extraction manifold (Macherey-Nagel, Düren, Germany). F_{430} sorbs as a yellow band and is eluted using 2 mL of 100% methanol. After purification, the extract is centrifuged (13 000 x g, 4 °C, 5 min) and the supernatant volume is determined by weight. Finally, the extract is stored at -20 °C in the dark prior to analysis. The extracts are subsequently quantified using the quantification methods described in the next paragraph (Section 4.1.3).

4.1.3 Quantification and identification methods

There are various ways to quantify the total cofactor F_{430} concentration and the relative concentrations of the different variants. Early investigations on cofactor F_{430} content applied absorbance measurements. Two different extinction coefficients (ε) have been reported, i.e., 22 500 L cm^{-1} mol^{-1} (Diekert *et al.*, 1980) and 23 000 L cm^{-1} mol^{-1} (Ankel-Fuchs & Thauer, 1986; Hüster *et al.*, 1985). Thanks to improvements in quantification equipment, more recent reports have conducted more detailed analyses using mass spectrometry and H^1-NMR for identification, often combined with liquid chromatographic techniques for quantification (Krüger *et al.*, 2003, Mayr *et al.*, 2008, Takano *et al.*, 2013, Kaneko *et al.*, 2014, Allen *et al.*, 2014). After identification of the cofactor, the quantification approaches require a standard in order to determine the absolute cofactor concentration. To date, no commercial standard is available and, therefore, such a standard needs to be purified from natural samples. Gorris *et al.* (1988) bypassed this requirement by using a synthetized internal standard (7,8-didemethyl-8-hydroxy-5-deazoriboflavin) in their HPLC method. Furthermore, they attempted to identify the different cofactors by means of relative peak areas at different wavelengths. Table 4.2 provides an overview of the different quantification and identification approaches for F_{430} reported in literature.

It is clear that the continuous developments in analytical technologies have greatly widened the range of applicable quantification methods. Quantification methods evolved from spectrophotometric (UV-VIS) quantification, over chromatographic methods with absorbance detection, to chromatographic methods with mass spectrometry detection and elemental analyses. Furthermore, Nuclear Magnetic Resonance (NMR) spectroscopy allowed the detection and distinction of all variants.

Table 4.2 Quantification and identification approaches for cofactor F_{430} and its variants described in literature. The last row provides two references using or describing the specific technique. *HPLC-DAD = High-Performance Liquid Chromatography – Diode Array Detector, MS = Mass Spectrometry, EA = Elemental Analysis, NMR = Nuclear Magnetic Resonance, N/A = Not Applicable.*

	Spectrophotometry	HPLC-DAD	(HP)LC-MS	EA	NMR
Separation mechanism	no separation	retention time (molecular structure)	retention time (molecular structure) exact mass (*m/z*)	no separation	chemical and magnetic shifts
Distinguished variants	no distinction F_{560} and epimers may slightly alter UV-VIS spectrum	native form, epimers and F_{560} Suitable method required for adequate separation	all forms except epimers based on *m/z* epimers and native form based on retention time	no distinction	all variants
Quantification	extinction coefficient	purified (or synthetic) standard	purified (or synthetic) standard	Nickel concentration (Ni standard)	N/A
Main application	total cofactor quantification (tentative) standard concentration quantification	quantification and identification of most important variants	quantification and identification of all variants standard purification (preparative)	total cofactor and standard concentration quantification	identification and structure elucidation
Reference	Diekert *et al.*, 1981 Huster *et al.*, 1985	Van Beelen *et al.*, 1983 Gorris *et al.*, 1988	Kaneko *et al.*, 2014 Allen *et al.*, 2014	Jiang, 2006 Kaneko *et al.*, 2014	Mayr *et al.*, 2008 Kaneko *et al.*, 2014

In this PhD, thesis F_{430} concentrations were quantified using both the spectrophotometric method (which does not require a standard when the extinction coefficient is used) and an adapted HPLC procedure. In addition, mass spectrometry was used in order to assess the purity of the samples and a standard was synthesized for use in the HPLC procedure. First, the procedures for the spectrophotometric and chromatographic quantification are described. Subsequently, the identification and standard development are discussed.

Absorbance quantification

Absorbance measurement on a spectrophotometer (Lamda 950, Perkin Elmer, Waltham, MA, USA) provided a first indication of the F_{430} content and purity (Diekert *et al.*, 1980; Moura *et al.*, 1983). Spectrophotometry spectra were obtained over a 300 to 600 nm wavelength range. The absorbance was determined using pure methanol as a blank and an extinction coefficient (ε) of 23 000 L cm^{-1} mol^{-1} as proposed by Diekert *et al.* (1980). The calculation of the F_{430} concentration in the extract and in the original sample (on a VSS basis) is shown in Equation 4-1 and Equation 4-2, respectively.

$$F_{430,extract}\,(\text{nmol L}^{-1}) = \frac{(A_{sample} - A_{blanc})}{\varepsilon \times l} \times 10^9 \qquad \textbf{Equation 4-1}$$

$$F_{430,sample}\,(\text{nmol gVSS}^{-1}) = \frac{F_{430,extract} \times V_{extract}}{V_{sample} \times VSS_{sample}} \qquad \textbf{Equation 4-2}$$

with A_{sample} and A_{blanc} the absorbance at 430 nm of the sample and blanc, respectively, ε the extinction coefficient (23 000 L cm^{-1} mol^{-1}), l the cuvette path length (1 cm in this case), $V_{extract}$ (L) and V_{sample} (L) the volume of the extract and the original sludge sample,

respectively, and VSS_{sample} (g L^{-1}) the volatile suspended solids concentration in the original sample (determined using Equation 3-2).

The obtained spectrophotometry spectra were compared with literature spectra and allowed the overall purity of the extract to be assessed. Despite the potential presence of interfering compounds, which are not sufficiently removed during the purification process, the distinct F_{430} spectrum was found in most of the analysed samples. However, as discussed in Section 7.3 the presence of interfering compounds in some full-scale digester samples clearly hampered the applicability of the straight-forward spectrophotometry quantification. In addition, HPLC chromatograms provide more detailed insight in the composition of the extract, allowing the different F_{430} derivatives to be separated. Therefore, additional purification and quantification using HPLC was performed for all samples.

HPLC quantification

After the initial spectrophotometric content and purity check, F_{430} content was quantified after purification by HPLC. Therefore, the extract was evaporated in a Labconco® centrivap concentrator and re-dissolved in 27.5 mM acetic acid (pH 4.7 with KOH) for HPLC analysis using an Agilent technologies 1200 series console equipped with a Prevail C18 Alltech Grace 3 µm column (150x4.6 mm) according to Gorris & van der Drift (1988). A gradient elution was performed using as eluent 1 (E1) 27.5 mM acetic acid (pH 4.7 with KOH) and as eluent 2 (E2) 20% acetonitrile in E1. The elution sequence was as follows, (a) 0-2 min: 10% E2 (b) 2-6 min: 10 to 20% E2 (c) 6-20 min: 20 to 60% E2 (d) 20-25 min: 60 to 95% E2 (e) 25-40 min: 95% E2 (f) 40-43 (95 to 10% E2 and (g) 43-45min: 10% E2. An Agilent 1260 infinity diode array UV detector (G1315D) was used to detect the eluting compound at 425 nm. Figure 4.7 shows a typical HPLC chromatogram with the absorbance spectrum of the native F_{430} in the inset. Note that the separation of the native cofactor and its epimers, i.e., the small peak to the right of native F_{430} was not consistently successful.

Initially, prior to the standard preparation, the cofactor F_{430} contents were compared on a relative basis using the peak areas obtained from the HPLC quantification. To this end, a recalculation similar to Equation 4-2 was used, replacing $F_{430,extract}$ by the integrated peak area and taking into account the dilutions used to prepare the HPLC samples.

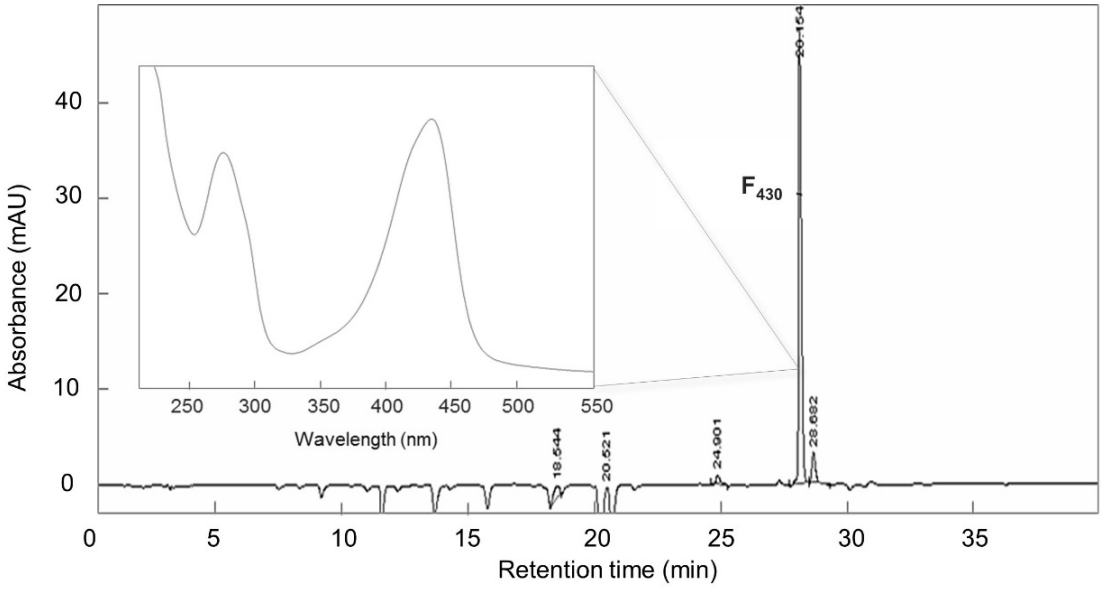


Figure 4.7 Representative HPLC chromatogram and UV-VIS spectrum (inset) of a cofactor F_{430} extract. The HPLC chromatogram shows the cofactor F_{430} peak eluting at approximately 28 minutes. F_{430} is mainly present in its native form and not dispersed into thermodynamically more stable forms. The distinct UV-VIS spectrum shown in the inset matches those reported in literature (Diekert *et al.*, 1980; Dimarco *et al.*, 1990; Allen *et al.*, 2014).

Cofactor F_{430} identification

Although the initial identification based on the retention time and the UV-VIS spectrum seemed to confirm that native F_{430} was quantified in the procedure, mass spectrometry was used for additional verification. To this end, a selection of the extracted samples was subjected to ultra-high-performance liquid chromatography coupled to high resolution mass spectrometric analysis (UHPLC-HRMS) in order to provide additional F_{430} identification based on the cofactor's accurate mass and to assess the purity of the extracts. These analyses were performed at the Lab of Chemical Analysis of the Department of Veterinary Public Health & Food Safety at the Ghent University. The detailed protocol is described in the following paragraph.

The solvent of the selected samples was evaporated under vacuum in a Labconco® centrivap concentrator and re-dissolved in the initial buffer (5% B, 95% A, see below). UHPLC analysis was carried out using a Thermo Fisher Scientific (San Jose, CA, USA) Accela UHPLC pumping system coupled to an Accela Autosampler and Degasser. Separation of the compounds was achieved on an Acquity BEH C18 (1.7 µm, 100 mm x 2.1 mm, Waters, Milford, MA, USA) column. The mobile phase consisted of a mixture of ultrapure water containing 0.1% formic acid (A) and acetonitrile (B). A flow rate of 0.3 mL min^{-1} was used. The applied linear gradient profile started with 5% B for 1 min., rising to 15% B at 3.50 min. Then solvent B was increased to 35% at 9.00 min and to 65% at 9.80 min. Finally, the mobile phase was switched back to the initial conditions in 0.20 min and was kept there for 2 min. An injection volume of 10 µL was used and the column oven and tray temperature were 25 °C and 7 °C, respectively. HRMS analysis was carried out using an Exactive™ benchtop Orbitrap mass spectrometer (Thermo Fisher Scientific, San Jose, CA, USA) equipped with a heated electrospray ionization probe (HESI-II) operating in positive and negative ion mode. The instrumental parameters for the HESI-II probe are

summarized in Table 4.3. An *m/z* scan range of 80 – 1000 was selected, and the resolution was set at 50,000 full-width at half maximum (FWHM) at 2 Hz (2 cycle per second). The automatic gain control (AGC) target was set at the balanced range (1×10^6 ions), and the maximum injection time was 500 ms. Ionization source working parameters are reported in Table 4.3. Initial instrument calibration was done by infusing calibration mixtures for the positive and negative ion mode (Thermo Fisher Scientific). The positive calibration mixture included caffeine, Met-Arg-Phe-Ala acetate salt (MRFA) and Ultramark® 1621, while the negative calibration solution comprised sodium dodecyl sulphate, sodium taurocholate and Ultramark® 1621. These compounds were dissolved in a mixture of acetonitrile, water and methanol, and both mixtures were infused using a Chemyx Fusion 100 syringe pump (Thermo Fisher Scientific). The instrument control and data processing were carried out by Xcalibur 2.1 software (Thermo Fisher Scientific). Mass deviations, expressed in parts per million (ppm), were defined as $10^6 \times$ [(measured mass − theoretical mass)/theoretical mass] and were found to be below 5 ppm.

Table 4.3 Instrumental parameters used for the heated electrospray ionization probe HESI-II.

Instrumental parameters	Value
Spray voltage	4 kV
Sheath gas flow rate	45 au
Auxiliary gas flow rate	2 au
Sweep gas flow rate	0 au
Capillary temperature	175 °C
Heater temperature	350 °C
Capillary voltage	90 (−75) V
Tube lens voltage	180 (−167) V
Skimmer voltage	20 (−22) V

A typical UHPLC-HRMS spectrum and isotope profile from one of the samples is shown in Figure 4.8 and confirmed the identity and purity of the F_{430} samples. Note that the UHPLC-HRMS analysis excludes all F_{430} variants with a different exact mass (i.e., F_{560}) and separates the native cofactor from its epimers based on their different structure and interaction with the column.

The characteristic native F_{430} accurate mass of 905.28564 was found in all analysed samples, also matching the typical F_{430} isotope profiles found in previous studies (e.g., Mayr *et al.*, 2008; Allen *et al.*, 2014). The relative abundances of the native F_{430} peaks to one another were in accordance with those found with HPLC for the same samples. Furthermore, the F_{430} epimers can clearly be distinguished as a shoulder on the right of the native F_{430} peak (Figure 4.8 - a). These epimers could not be sufficiently separated in order to be quantified separately, however, their combined area ranges from 15 to 20% compared to that of the native cofactor. Based on Allen and co-workers' (2014) recent report of multiple alternative forms of F_{430} (see Figure 4.1), the samples were also screened for the specific masses of these components. The 2, -6, -7, -9 and -10 variants of F_{430} were not detected, which is in accordance with Allen's findings for *M. jannaschii*, *M. maripaludis* and *M. vannieli*. F_{430}-5 (vinyl-F_{430}) and -8 (17^2-keto-F_{430}) were detected but at low signal-to-noise ratios, resulting in absence and inconsistency of clear isotopes for confirmative identification. F_{430}-3 (17^2-methylsulfoxide-F_{430}) was not analysed as the *m/z* spectrum was limited to 1000 and its accurate mass is 1009.2794. Finally, F_{430}-4 (12,13-didehydro-F_{430} or F_{560}) was clearly identified in three out of four samples analysed by UHPLC-HRMS, with an absolute area ranging from 2 to 3% of that of native F_{430}. Since

F_{430}-4 is an oxidative degradation product, its low concentration indicates that contact with air during the extraction procedure was sufficiently limited. However, the abovementioned presence of the epimers indicates that additional care needs to be taken in order to reduce excessive temperatures and, thus, thermodegradation of the native cofactor to the epimers. It should be noted that the conversion to these degradation products may also have taken place during sample preparation for UHPLC-HRMS instead of during the extraction and purification procedure. In summary, it is legitimate to say that F_{430} is mainly present in its native form and conversion to its oxidative degradation product (12,13-didehydro-F_{430} or F_{430}-4) is limited during the used lysis and purification protocol (Duin *et al.*, 2009; Kaneko *et al.*, 2014; Allen *et al.*, 2014). The concentration of its thermally more stable epimers (13-epi and 12,13-diepi-F_{430}) was higher but may have originated from sample preparation.

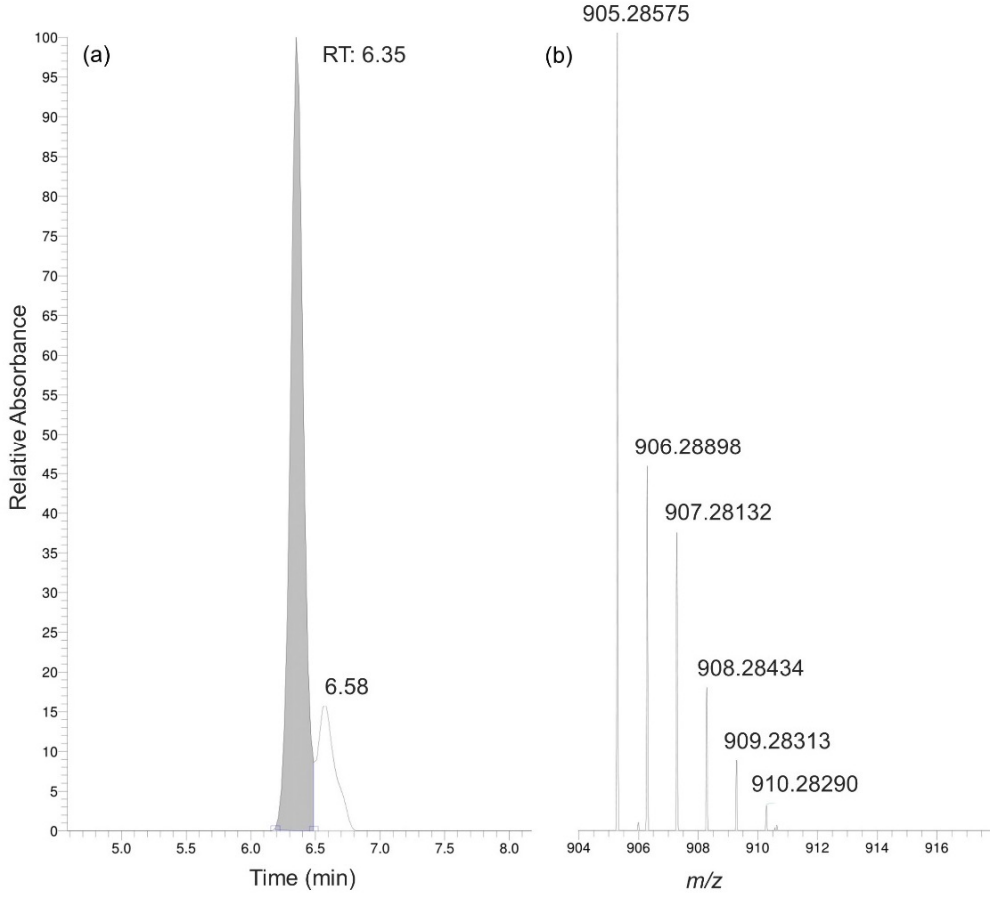


Figure 4.8 Representative **(a)** UHPLC-HRMS spectrum (50.000 FWHM) and **(b)** isotope profile of a cofactor F_{430} extract with the exact mass (*m/z*) set at 905.28575. The mass spectrometric analysis profile shows the distinct peak for native cofactor F_{430}, eluting at approximately 6.35 minutes. The shoulder seen in (a) contains the F_{430} epimers. The isotope profile matches those previously described by Mayr *et al.* (2008) and Allen *et al.* (2014) for native F_{430}. *RT = Retention Time.*

4.1.4 Standard preparation, purity check and quantification

In order to provide absolute quantification of the native cofactor in terms of nmol $gVSS^{-1}$ (for comparison with literature values), a F_{430} standard was tentatively prepared from previous cofactor extracts. To this end, a large amount of cofactor extracts (in pure MeOH, stored at -20 °C) were pooled and the solvent was evaporated under vacuum. Subsequently, the cofactor was re-dissolved in the initial UHPLC buffer (see previous

section) and injected onto the UHPLC. The same procedure as described in the previous section was used for the UHPLC-HRMS quantification but the eluent (containing the purified standard) was collected. Unfortunately, the epimers could not be sufficiently separated from the native form in the current UHPLC procedure, which did not allow the collection of pure native cofactor. Therefore, the cofactor contained an impurity of these stereo-isomers of up to 14%. In addition, approximately the same amount of impurity was present under the form of the 12,13-didehydro variant (F_{560}), yielding a standard purity of around 71%. A possible explanation for the lower purity lies in the vacuum evaporation of the sample which took multiple hours and did not allow simultaneous cooling. Figure 4.9 shows the UV-VIS spectrum of the pooled samples and that of the standard collected from the UHPLC which are also visualized in Figure 4.10.

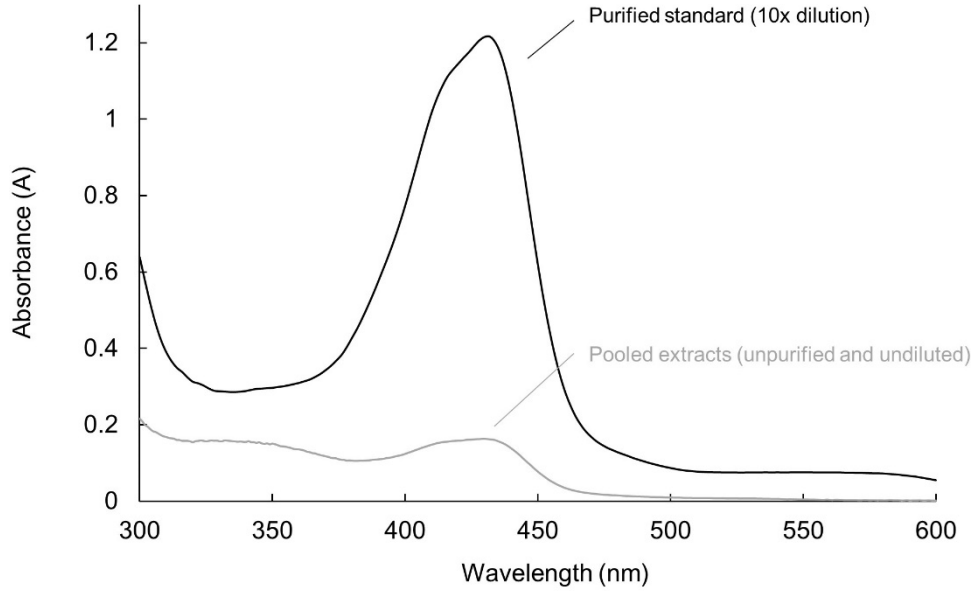


Figure 4.9 UV-VIS spectrum of the pooled F_{430} extracts used to prepare the standard (—) and a 10x dilution of the (semi-) purified standard (—). The UHPLC procedure clearly removed certain contaminants, yielding a highly concentrated and semi-purified F_{430} standard.

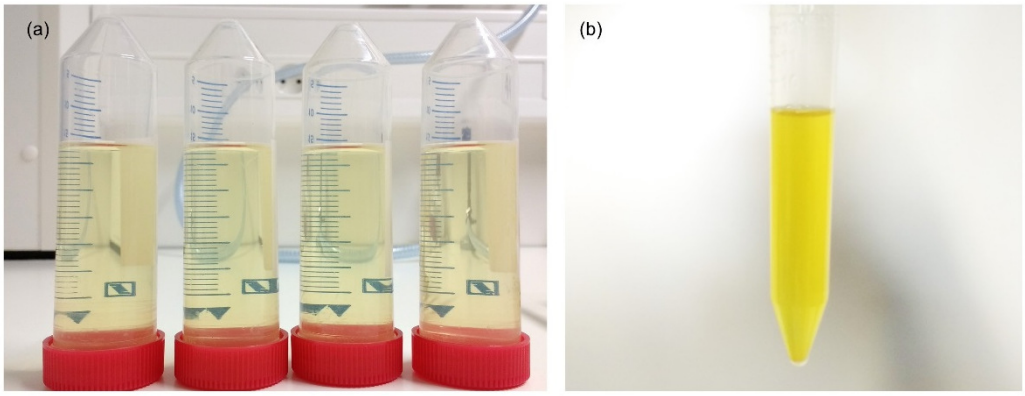


Figure 4.10 The **(a)** pooled F_{430} extracts prior to UHPLC purification and **(b)** the (semi-)purified and upconcentrated standard after preparative UHPLC.

Subsequently, the total cofactor concentration in the extract was determined by measuring the total nickel concentration using inductively coupled plasma mass spectrometry (ICP-MS). To this end, a fraction of the standard was acidified in a 1% nitric acid solution (ultrapure, 67-70%) and injected in an Agilent 7700x ICP-MS (Agilent Technologies, Santa

Clara, CA, USA). The concentration was determined to be 490.65 µmol Ni L^{-1}. Since one F_{430} molecule contains one central Ni atom this concentration equals the total cofactor F_{430} concentration.

Despite the lower purity of the standard, a calibration curve was determined on the HPLC. A standard purity of 85% was assumed since 12,13-didehydro-F_{430} (F_{560}) (present at a relative concentration of 15% in the standard) was successfully separated in all HPLC chromatograms whereas this was not always the case for the epimers. This calibration curve allowed the peak areas to be converted to cofactor F_{430} concentrations and provided approximate cofactor F_{430} concentrations. The recalculation towards F_{430} concentration in the original sample was then again done using Equation 4-2, in which $F_{430,extract}$ was calculated using the calibration curve. The calibration curve was linear (R^2 = 0.9998) in the 0.7 to 210 µM concentration range and is shown in Figure 4.11.

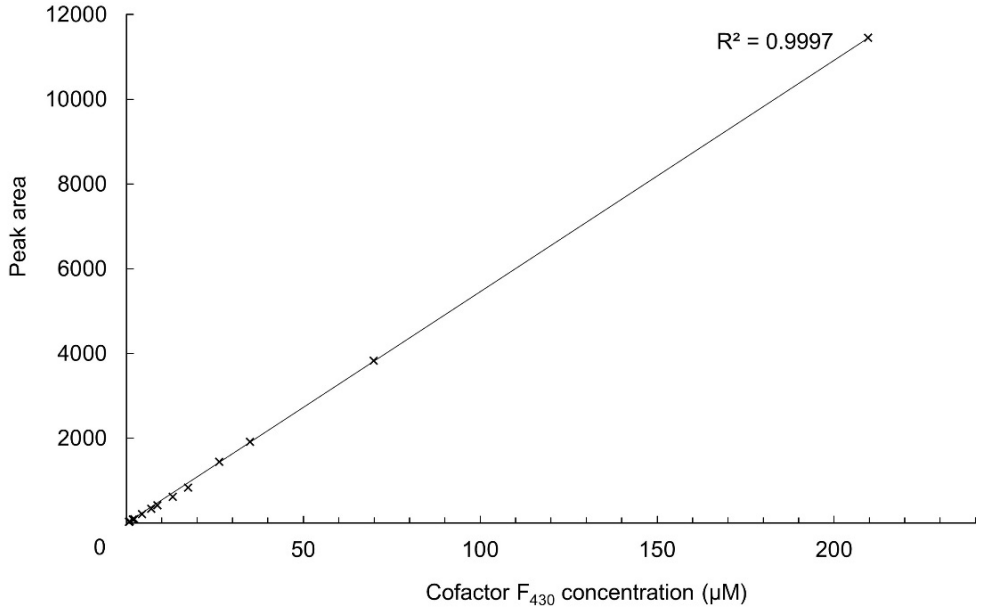


Figure 4.11 The linear calibration curve which relates the peak areas measured on the HPLC-DAD to cofactor F_{430} concentrations using a dilution series of the (semi-)purified standard (R^2 = 0.9997).

4.2 Cofactor F_{420}

Due to its autofluorescent properties and more stable nature, cofactor F_{420} is more easily extracted and quantified than cofactor F_{430}. Various methods have been described in literature throughout the years. Cell lysis by means of heating, boiling, autoclaving and by means of a French pressure cell have been shown to keep the cofactor intact for subsequent quantification (Delafontaine *et al.*, 1979; Eirich *et al.*, 1979; Kida *et al.*, 2001). Prior to quantification the extract can be purified by means of 2-propoanol precipitation of DNA and lipids (Egusa *et al.*, 1983; Hänni *et al.*, 1995). The obvious way to quantify the extract's F_{420} concentration is by measuring its fluorescence intensity. When excited at a wavelength of 420 nm, cofactor F_{420} emits blue-green fluorescent light with a maximum emission at 470 nm. The cofactor exhibits its fluorescence in the oxidized state and the emission spectra depend on the pH of the sample (Cheeseman *et al.*, 1972). Therefore, these two factors need to be taken into account throughout the extraction and quantification procedure since they may influence the measured fluorescence intensity. Photo bleaching is another phenomenon that needs to be taken into since it may decrease the fluorescence intensity when the cofactor is excessively exposed to light. However, the autofluorescence has been reported to be restored after a short period in the dark (Doddema en Vogels, 1978). The fluorescence quantification can be performed *ex-situ* on the cell extract (obtained using the abovementioned extraction methods) by means of spectrofluorimetric quantification (De Zeeuw *et al.*, 1984; Reynolds & Colleran, 1987). Alternatively, fluorescent microscopy or flow cytometry can be used for *in-situ*, non-invasive fluorescence quantification in whole cells (Ahn *et al.*, 2000; Lambrecht *et al.*, 2017). Instead of exploiting the cofactor's autofluorescent properties, some researchers have developed high-performance liquid chromatography techniques with absorbance detection for F_{420} quantification (Van Beelen *et al.*, 1983; Gorris *et al.*, 1988).

In the following sections, the extraction procedure that was chosen and two quantification methods which were used in this PhD thesis, are described.

4.2.1 Extraction procedure

Sludge samples were centrifuged (Eppendorf 5810 R) at 4 °C for 10 min (13 000 x g) and the pellet resuspended in 5 mL miliQ water. The pH was adjusted to 8.5 using 1 M KOH. Next, the samples were transferred into glass reaction tubes and heated to 100 °C for a period of 15 minutes. In contrast to cofactor F_{430}, cofactor F_{420} is stable at increased temperatures, allowing a heating step to be used for the cell lysis. The samples were transferred to centrifugation tubes after cooling and centrifuged for 5 min at 20 °C (13 000 x g). The yellow supernatant (lysate) was decanted and its volume determined by weight measurement. Subsequently, the supernatant was diluted 4 times using pure 2-propanol and shaken vigorously. Next, the supernatant-propanol mixture was centrifuged at 20 °C for 5 min (13 000 x g) and transferred to a new tube while taking care not to transfer any of the impurities (DNA and lipids) which are deposited on the centrifuge tube's wall. If necessary, the extracts were diluted (using miliQ) in order to achieve an absorbance between 0.05 and 0.1 at 420 nm. Finally, the purified F_{420} extracts were stabilized using 1 M KOH (0.1 M KOH concentration in the final extract) at a pH of 13. The tubes containing the F_{420} extracts were wrapped in aluminium foil (in order to reduce photo bleaching) and stored in the dark at -20 °C prior to fluorescence quantification. The fluorescence

quantification was performed no longer than 2 hours after the stabilization of the fluorophore in order to avoid its degradation.

4.2.2 Quantification methods

Two approaches for autofluorescence quantification were taken in this work. The first entailed the quantification of the fluorescent intensity of the cell extracts, obtained as described above, by means of a fluorimeter. With the second approach, the *in-situ* autofluorescence in the fresh samples was tentatively determined by means of fluorescence microscopy. The advantage of the microscopic method was that it allowed images to be simultaneously acquired for autofluorescence determination and morphology quantification, hence reducing analysis time. The microscopic method was compared with the extraction and fluorimetric quantification in order to attempt to validate the procedure.

Fluorimetry

The (diluted) extracts obtained using the abovementioned extraction method were analysed with a fluorimeter (Fluorolog®, Horiba Scientific, NJ, USA). The excitation wavelength was set to 420 nm and emission spectra were recorded in the 450 – 750 nm range. Emission intensities were related to F_{420} concentrations by means of a calibration curve. The F_{420} standard that was used had a concentration of 4.184 mM and was kindly provided by Prof. Deppenmeier (Institut für Mikrobiologie und Biotechnologie, Universität Bonn). The calibration curve was linear for cofactor concentrations between 12 nM and 792 nM ($R^2 = 0.9998$) and is shown in Figure 4.12.

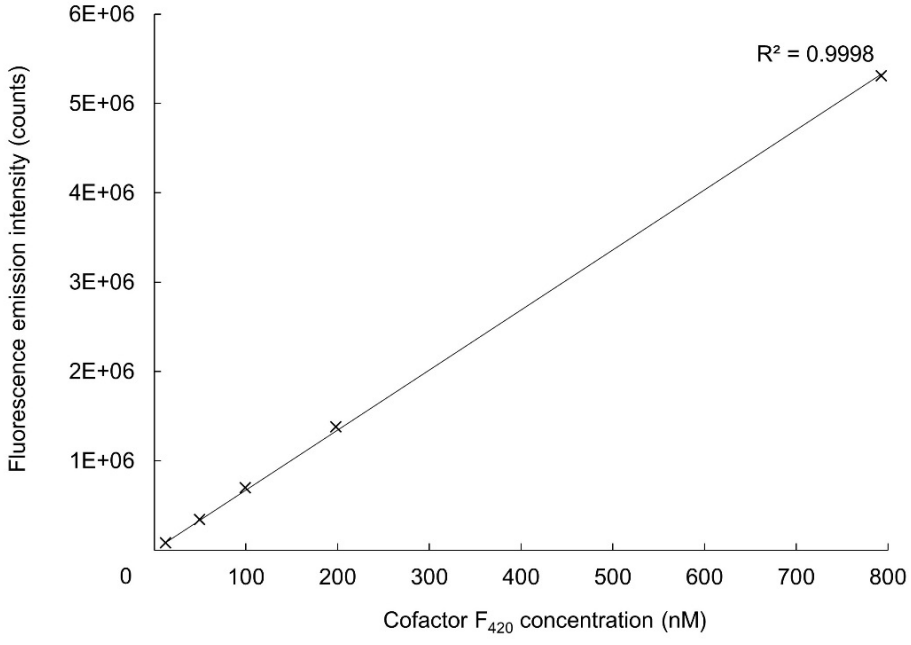


Figure 4.12 The linear calibration curve which relates the fluorescence intensity measured on the fluorimeter to cofactor F_{420} concentrations using a dilution series of the purified standard ($R^2 = 0.9998$).

Figure 4.13 shows the UV-VIS and fluorescence emission spectra obtained using the F_{420} standard (0.1 M KOH, pH 13).

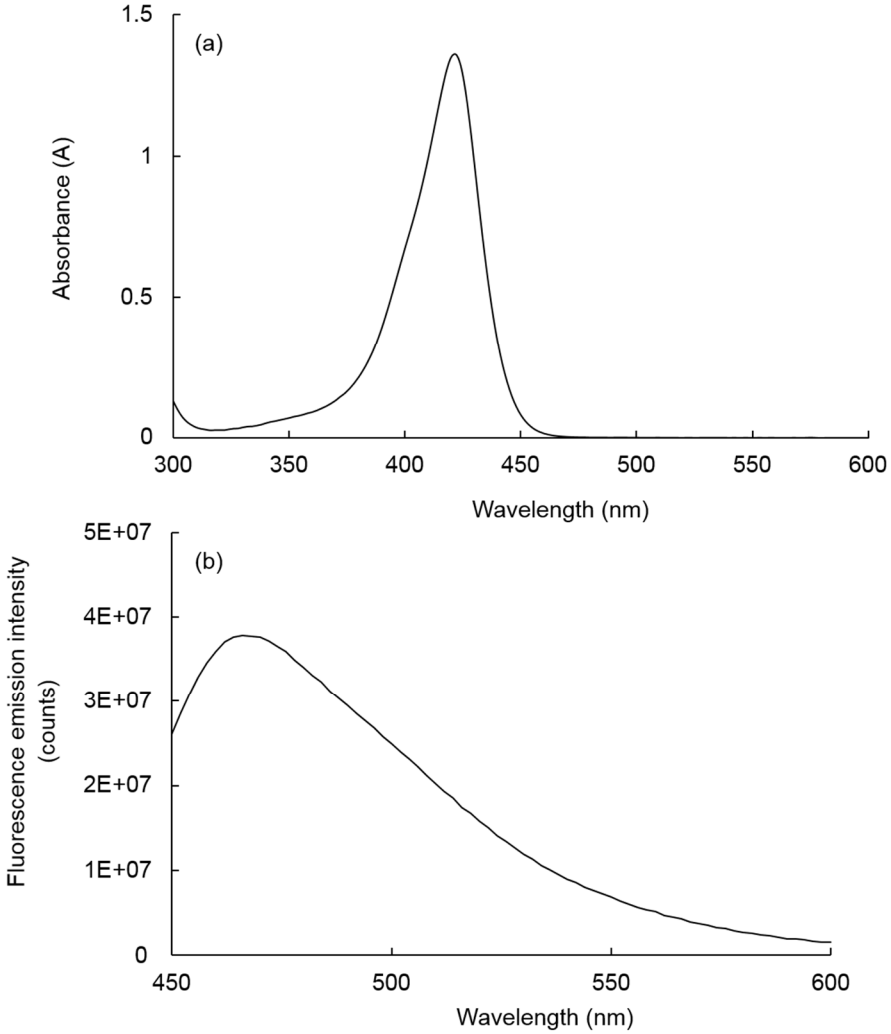


Figure 4.13 The **(a)** UV-VIS and **(b)** fluorescence emission spectum (excitation at 420 nm) of the F_{420} standard. Both spectra were recorded at a pH of 13 (0.1 M KOH). Both spectra are in accordance with those reported in literature (Cheeseman *et al.*, 1972; Eirich *et al.*, 1979).

Fluorescence microscopy

For the fluorescent microscopy fresh samples were diluted to a 1 gTSS L^{-1} concentration using supernatant in order to facilitate comparison across different sludge samples and prevent structural changes of the sludge. Two droplets (8 µL) were applied on a sample glass (Menzel-Gläzer) and covered with a cover slip (Menzel-Gläzer). After sample preparation, 22 images were obtained from each sample using an Olympus IX83 inverted microscope and the accompanying CellSens Dimension software. The excitation light was provided by a 120 W Mercury Vapor Short Arc lamp (X-cite series 120 Q, Lumen dynamics) and a filter cube (ET405/20x and ET460/50m, Chroma, VT, USA) was used (excitation 390 – 420 nm, emission 435 – 490 nm). Each image consisted of 9 photos, taken at a 20 times magnification, stitched together to form one large 3x3 image. The resulting images were analysed with an in-house developed MATLAB software which counted the number of fluorescent pixels and the fluorescence intensity per image. Figure 4.14 shows a typical phase contrast, fluorescence and combined microscopy image. The blue fluorescence indicates the presence of cofactor F_{420}.

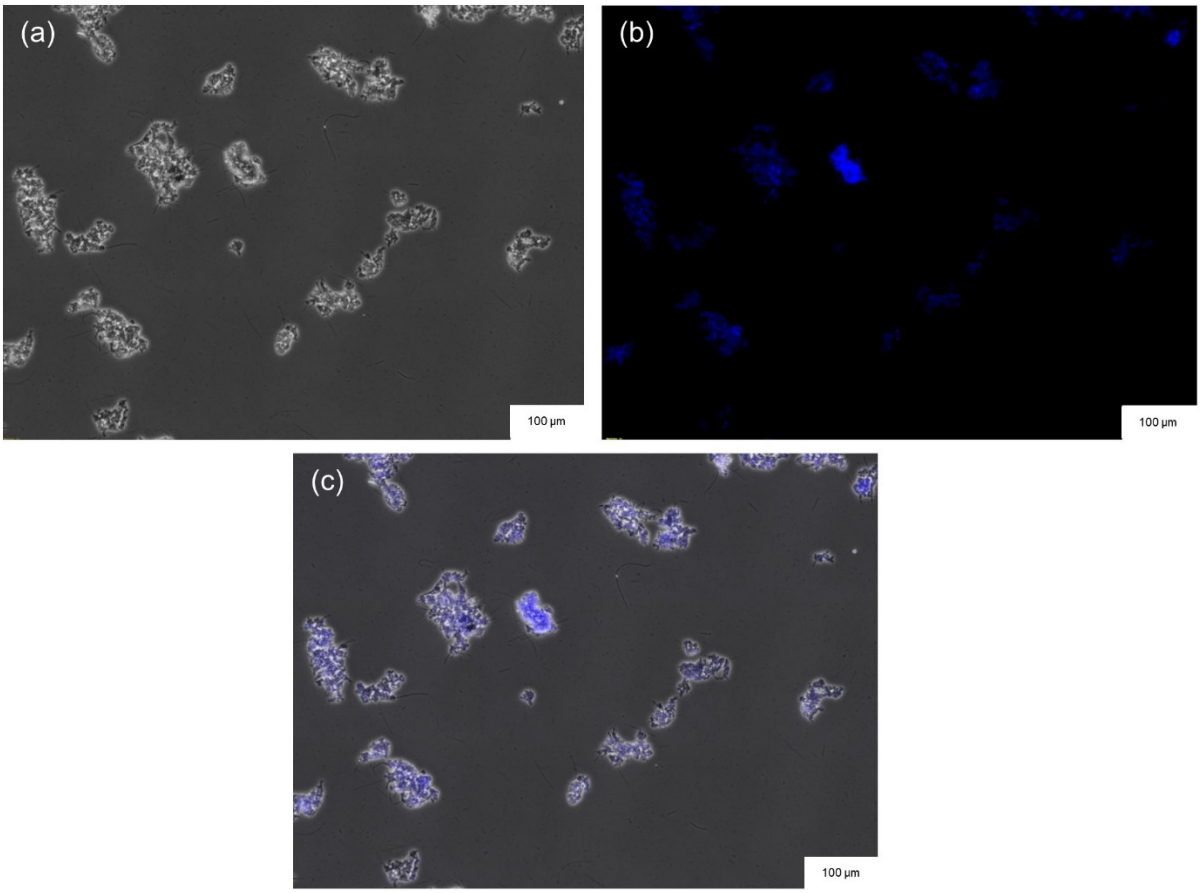


Figure 4.14 Examples of a **(a)** phase contrast **(b)** fluorescent and **(c)** combined image of an anaerobic sludge sample acquired with a fluorescent microscope (20x magnification). The blue fluorescence indicates the presence of cofactor F_{420}.

4.3 CONCLUSIONS

Extraction and quantification protocols for both cofactor F_{430} and F_{420} were successfully adapted from literature and produced satisfactory results. For **cofactor F_{430}** the importance of reducing contact with air and excessive temperatures was demonstrated. A protocol (Protocol 4) using bead beating (in a vortex) for the cell lysis and a vacuum extraction manifold allowed the succesful extraction and purification of up to 12 samples in parallel. Quantification using HPLC required the preparation of a standard. Although the standard's purity was lower than expected, a calibration curve allowed approximate cofactor F_{430} concentrations to be derived. Both the standard and experimental samples contained mainly the native cofactor, however, oxidative (F_{560}) and thermal (13-epi-and 12,13-diepi-F_{430}) degradation products were present to a lesser extent. Heat extraction and quantification using fluorimetry produced satisfactory results for **cofactor F_{420}** quantification. The adapted method will be compared with a fluorescence microscopy approach in Chapter 7.

In the next chapter (Chapter 5), the protocols for both cofactors are first validated using bioreactor samples and then used throughout the experiments described in Chapter 6 and 7.

CHAPTER 5

Inhibition of methanogenesis induces a reduction in cofactor F_{430} content: proof-of-principle

A proof-of-principle is sought to confirm that cofactors F_{420} and F_{430} are closely linked to anaerobic digester performance and methanogenic activity, allowing them to be tested as potential monitoring tools in cases of reactor failure and disturbances. To this end, two experiments were performed in order to determine whether cofactor F_{430} and F_{420} content respond to drastic changes in operational conditions and reactor performance. The experiments also served as a validation of the first versions of the cofactor extraction protocols.

In the first experiment, synthetic dairy wastewater fed lab-scale digesters were subjected to an organic loading rate shock and a pH disturbance to inhibit methanogenesis. Cofactor F_{430} and F_{420} content were followed-up alongside specific methane production and classical performance monitoring tools and their dynamics were investigated.

In the second experiment, a lab-scale digester was inhibited by an increasing phenol concentration in the influent. Cofactor F_{430} content was followed-up alongside classical performance monitoring tools and community structure.

5.1 Do overfeeding and pH shocks lead to significant cofactor reductions?

Cofactor F_{430} and F_{420} content were followed-up alongside classical performance parameters during the operation of 4 fed-batch lab-scale anaerobic digesters. Two reactors were subjected to an organic shock-load whereas the other two served as controls. Subsequently, the control reactors were subjected to a pH shock (pH 9 by addition of base). The aim of the experiment was to assess whether these two process upsets had an important impact on cofactor F_{430} and F_{420} content. If reduced methanogenic activity is reflected by reduced cofactor contents, F_{430} and F_{420} can serve as biomarkers for methanogenic presence or activity.

The organic loading rate (OLR) shock was expected to affect the methanogenesis by the combined effect of acidification and volatile fatty acids (VFAs) accumulation. The accumulation of VFAs results from an imbalance between the methanogenesis, on the one hand, and the hydrolysis/acidogenesis/acetogenesis on the other hand. Indeed, methanogensis is often the rate-limiting step in mesophilic reactors because of the slower growth rate of methanogens compared to the microorganisms active earlier in the degradation chain. A sudden increase in organic loading rate may then allow the acidogenic bacteria to convert the supplied feed into VFAs, whereas the methanogens cannot handle the incoming substrates because of their unfavorable growth kinetics. The effect of the VFAs is that they induce a pH decrease which inhibits methanogens whereas it promotes the activity of fermentative bacteria. The undissociated VFAs (which are more abundant at lower pH) then permeate the cell membrane of methanogens and affect the cellular metabolism by reducing the cytoplasmic pH (see also Chapter 2, Section 2.1.3). The effect of a pH increase is twofold. On the one hand, an alkaline pH above 8 may directly affect methanogenesis (Sandberg & Ahring, 1992). On the other hand, the equilibrium between the ammonium ion (NH_4^+) and the significantly more toxic ammonia (NH_3) is pH dependent and shifts towards the latter at higher pH (Erickson, 1985). An increase in pH results in a more than proportional increase in ammonia concentrations.

5.1.1 Materials & methods

Experimental set-up and feeding strategy

The fed-batch[6] set-up used in this experiment is shown in Figure 5.1. The setup consisted of four 1 L Schott-Duran® bottles containing anaerobic sludge originating from a lab-scale AnMBR treating the same synthetic wastewater (2 in Figure 5.1), placed in a temperature controlled water bath (Julabo SW22) at 35 °C and shaken with an axial movement at a speed of 120 rpm (1 in Figure 5.1). Feeding and sludge purging was performed through a gas tight sampling port compatible with luer-lock syringes.

[6] Strictly speaking this experiment is not purely fed-batch, since the volume remained constant throughout the experiment. The term fed-batch is used here to refer to the discontinuous feeding and wasting and can be seen as equivalent to sequencing batch operation.

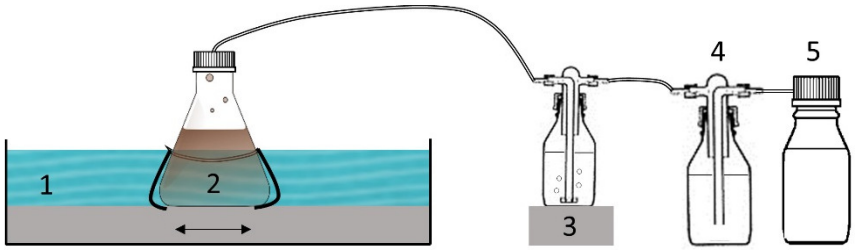


Figure 5.1 Schematic overview of the experimental set-up used in the fed-batch experiments. The set-up included (1) a temperature controlled (35 °C) shaking water bath, (2) a 1 L reactor bottle, (3) an alkaline stripping solution equipped with a bubble diffuser, (4) a liquid displacement system and (5) a bottle to collect the displaced water.

Biogas was directed towards an alkaline stripping solution (3 in Figure 5.1) containing 0.9 M KOH to remove all acid gases (mainly carbon dioxide and H_2S) based on the gas-dissolved acid equilibrium. Sufficient gas-liquid contact was ensured through the implementation of a bubble diffuser at the bottom of the stripping solution. Stripped biogas was then measured using a simple liquid displacement system (4 and 5 Figure 5.1). Gas production rates were normalized to 0 °C and 1 atm. The pressure in the headspace of the sludge bottle was assumed to be 1.0179×10^5 Pa and the temperature of the biogas was 35 °C.

The anaerobic sludge was fed with a synthetic wastewater containing a main carbon source (milk powder), macronutrients, trace elements and buffer compounds adapted from De Vrieze *et al.* (2013). The exact composition of the synthetic feed is reported in Table 3.1. The milk powder was a commercially available variant (Douwe Egberts) designed for professional coffee machines and consisted of 12% (w/w) fat, 63% (w/w) carbohydrates (all sugars), 16% (w/w) proteins and 0.5% (w/w) salt. An equivalence factor of 1.278 gCOD g milk powder^{-1} was established based on a linear calibration. The inoculum for the experiment originated from a lab-scale AnMBR fed with the same synthetic wastewater. Introducing the feed into the reactor was performed three times per week in combination with sludge purging (usually 50 mL every two days to maintain an HRT and SRT of 40 days). The purged sludge was used for all further analyses.

The experimental run was divided into 4 phases: acclimatization from day 0 to day 4 (Phase I), start-up to stable operation from day 4 to day 18 (Phase II), OLR shock in Reactors 1 and 2 (denoted as R1 and R2) from day 17 to day 27 (Phase III) and pH shock in Reactors 3 and 4 (denoted as R3 and R4) from day 27 onwards (Phase IV). Reactors 3 and 4 served as controls during Phase III. Sucrose was used to induce the shock in R1 and R2, and was of analytical purity, whereas a potassium hydroxide solution was used to induce the pH shock in R3 and R4. The synthetic dairy feed concentration was adjusted in order to achieve the desired organic loading rate (OLR). The different phases are depicted in Figure 5.2 in a graph showing the theoretical organic loading rates and measured sludge loading rates.

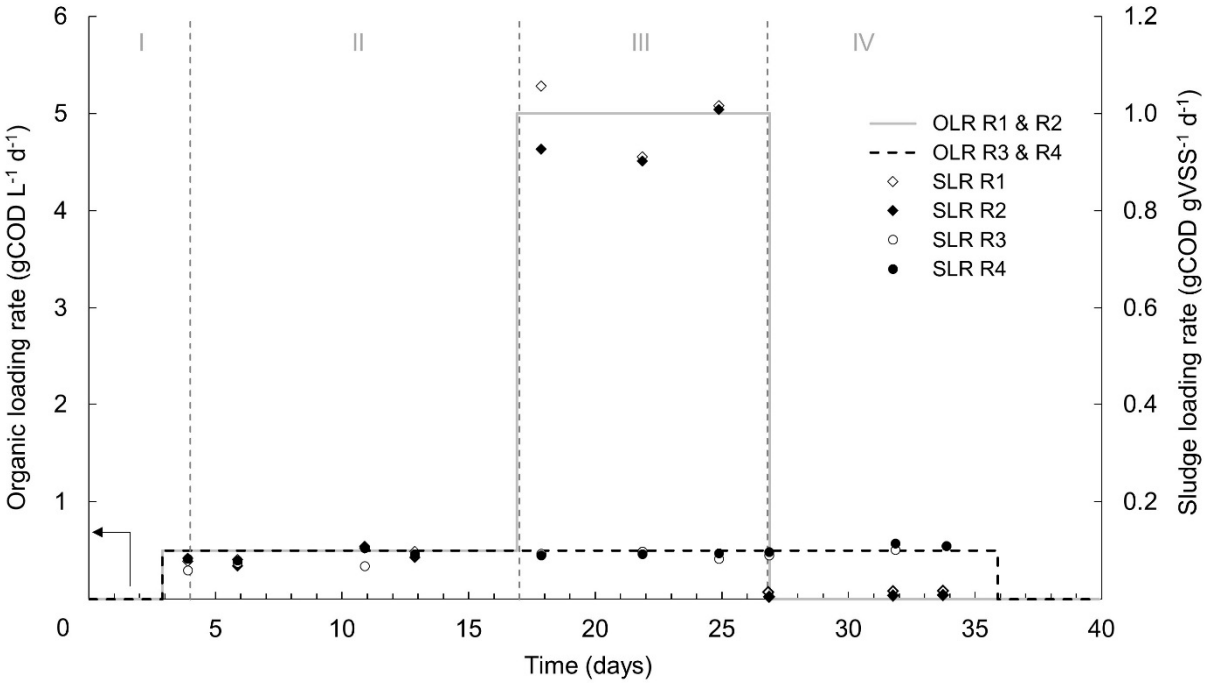


Figure 5.2 Organic and sludge loading rates (OLR and SLR, respectively) applied over the 40 days experimental period. After the acclimatization (I) and start-up (II) phase, an organic shock load was applied to R1 and R2 (—) whereas the OLR was kept constant in R3 and R4 (---) (Phase III). During Phase IV feeding was halted for R1 (◊) and R2 (♦), and R3 (○) and R4 (●) were subjected to an alkaline pH shock.

During the acclimatization period (Phase I), the equivalent of 1 gCOD of milk powder was introduced into the reactor and the sludge was allowed to acclimatize. During Phase II all reactors were fed bi-daily at an OLR of 0.5 gCOD L^{-1} d^{-1} with the synthetic dairy feed and this regime was maintained for two full weeks. From day 18 to 27 (Phase III) R1 and R2 were fed at a 10-fold higher OLR (5 gCOD L^{-1} d^{-1}, sucrose) while the OLR in R3 and R4 was left unchanged. During this period the SLR in R1 and R2 also increased tenfold from around 0.1 gCOD $gVSS^{-1}$ d^{-1} to around 1 gCOD $gVSS^{-1}$ d^{-1}. After maintaining this feeding regime for 10 days, on day 27, the feeding of Reactor 1 and 2 was halted and the supernatant[7] was diluted two-fold with tap water. Moreover, an alkaline solution (8 M KOH) was introduced into Reactor 3 and 4 in order to increase the pH to a value of at least 9. This pH was maintained in these reactors until the end of the experiment, by adding KOH whenever necessary. It should be noted that due to the lack of online pH-control, base addition had to be done manually on an intermittent basis, making it more difficult to maintain the pH at the desired value (pH 9).

Reactor performance and stability were assessed using the conventional parameters such as (specific) methane production, VFA concentrations, pH, and bioreactor soluble COD (sCOD) concentration.

[7] The biomass in the reactor bottles typically settled well, allowing removal of supernatant without loss of biomass.

Analytical methods

The analytical methods used in this experiment have been described in the general material & methods section (Chapter 3). The following parameters were analysed.

- (Volatile) Suspended solids
- COD
- Ammonium
- pH and electrical conductivity
- Total and individual VFA concentrations

Cofactor F_{430} and F_{420}

Cofactor F_{430} was extracted and quantified using Protocol 4 (Table 4.1) as described in Section 4.1.2.

Cofactor F_{420} was extracted and quantified using the fluorimetry method, as described in Section 4.2.2.

5.1.2 Results

The different phases shown in Figure 5.2 are described here in terms of overall reactor performance and cofactor F_{430} and F_{420} content.

Overall reactor performance

The specific methane production rates over the course of the experiment are shown in Figure 5.3. On average the maximum specific methane productions fluctuated between 50 and 70 mL CH_4 $gVSS^{-1}$ d^{-1} (0 °C and 1 atm). The observed sinusoidal pattern in the methane production rates is a result of the discontinuous feeding of the reactors at a low OLR. This pattern indicates that the micro-organisms went through so-called feast and famine cycles.

A significant increase in methane production is observed in reactor R1 during phase III (this data was cropped off the graph for clarity). Rather than resulting from the increased OLR in this period, it is most likely a consequence of a shift to a fermentative metabolism. The fraction of CO_2 in the produced gas significantly increased, hereby exceeding the alkaline stripping solution's capacity. The produced gas was thus in fact more likely carbon dioxide rather than methane in this reactor. In R2 a clear drop in methane production is observed during Phase III. It is clear that the methane production rate never recovered to the values observed prior to the OLR shock. Reactors 3 and 4 showed normal methane production rates throughout Phase I to III and were largely unaffected by the alkaline shock imposed in Phase IV.

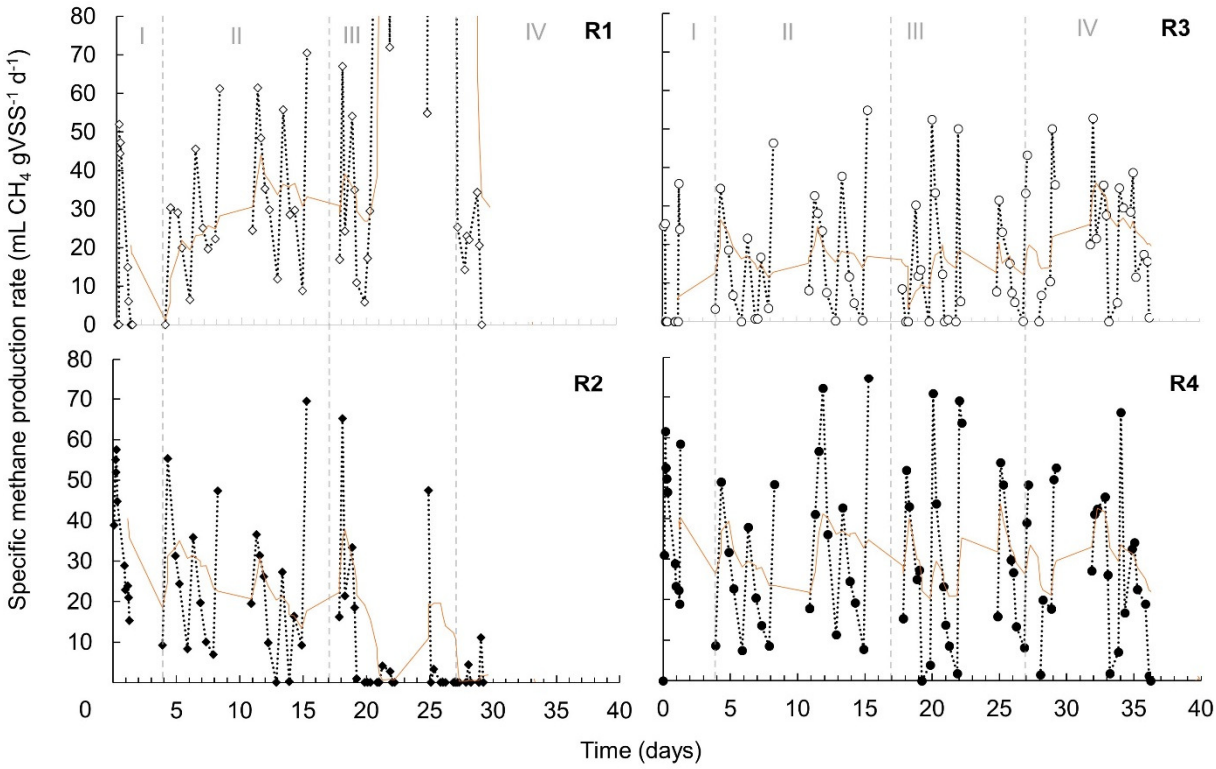


Figure 5.3 Evolution of the specific methane production rates (0 °C, 1 atm) over the 40 days experimental period. The orange line depicts a running average over 9 data points. An HRT and SRT of 40 days was maintained. The observed sinusoidal pattern is a result of the applied discontinuous feeding pattern. Saturation of the alkaline stripping solution explains the very high production rates (cropped off the graph) which were observed for R1 during Phase III, which were most likely a result of CO2 production rather than CH4 production. Methanogenesis was clearly inhibited in R2 as a result of the OLR shock whereas it remained intact in R3 and R4.

Figure 5.4 shows the evolution of (a) VFA concentrations, (b) pH and (c) residual soluble COD concentrations in the reactors during the experimental period. The organic loading rate shock applied to R1 and R2 in Phase III clearly led to an accumulation of VFAs. The pH, which was not controlled, concomitantly dropped from neutral to around 4 over the course of a week as a result of volatile fatty acid production and accumulation. The pH values that were reached and sustained are known to be inhibitory to methanogens (ten Brummeler *et al.*, 1985). However, fermentative bacteria thrive at these lower pH values, which turned R1 and R2 into fermentative reactors rather than methanogenic ones. The COD removal in these reactors decreased as evidenced by the 10-fold increase in soluble COD concentrations during Phase III. The decrease in VFA and sCOD concentrations observed from day 26 onwards was a result of dilution of the reactor supernatant and the halting of the feeding. These observations are all in accordance with the reduced methane production rate measured in R2.

Analysis of the individual VFA concentrations revealed that in Reactor 1 and 2 initially acetic, propionic and butyric acid accumulated during the OLR shock (data not shown). However, when peak total VFA concentrations were attained (up to 12 g L^{-1}), 70% was attributable to butyric acid. The concentrations which were measured contributed directly to the inhibition of the methanogens (Dogan *et al.*, 2005) on top of the indirect pH effect they induced.

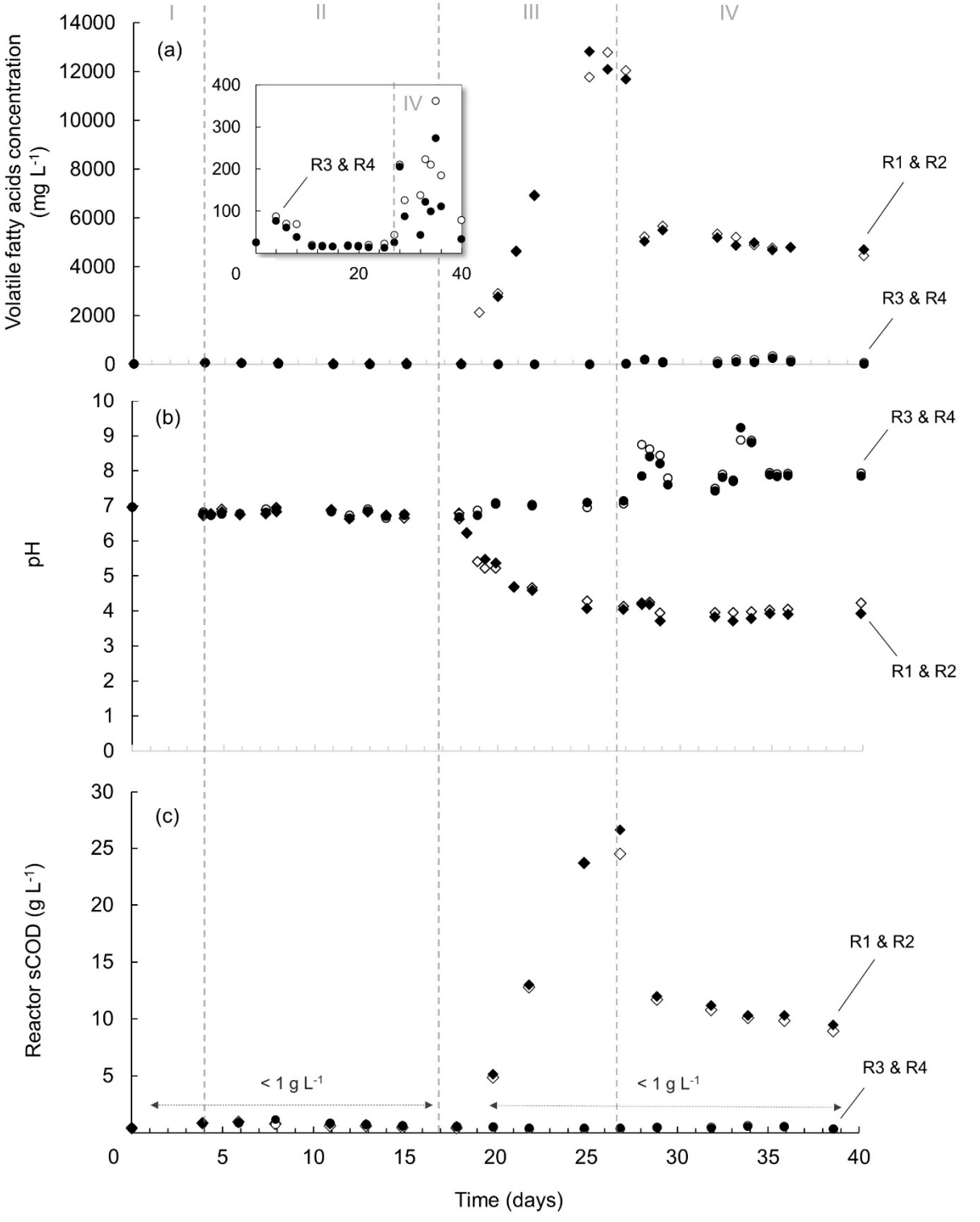


Figure 5.4 The evolution of (a) total volatile fatty acids concentration, (b) pH and (c) reactor soluble COD (sCOD) concentration over the 40 days experimental period. The increased OLR applied to Reactor 1 and 2 (◊ and ♦, respectively) in Phase III, clearly led to the accumulation of VFAs and sCOD and a concomitant acidifcation. Reactor 3 and 4 (○ and ●, respectively), showed stable performance and were not influenced by the pH increase induced in Phase IV. An HRT and SRT of 40 days was maintained.

Reactor 3 and 4 showed stable performance throughout the experiment and their performance seemed largely unaffected by the increased pH in Phase IV, which is in accordance with the observed unaffected methane productions in Figure 5.3. Nonetheless, potentially inhibitory free ammonia concentrations (> 25 mg N L^{-1}) (Omil *et al.*, 1995) were measured on two occasions. On day 29 and 34, free ammonia concentrations of 74 mg N L^{-1} and 223 mg N L^{-1}, respectively, were measured in R3. On the same days, concentrations of 42 mg N L^{-1} and 210 mg N L^{-1} were measured in R4. As expected, the highest free ammonia concentrations were found when the pH was highest.

Cofactor F_{430} and F_{420} content

Figure 5.5 shows the evolution of (a) cofactor F_{430} and (b) cofactor F_{420} during the experimental run.

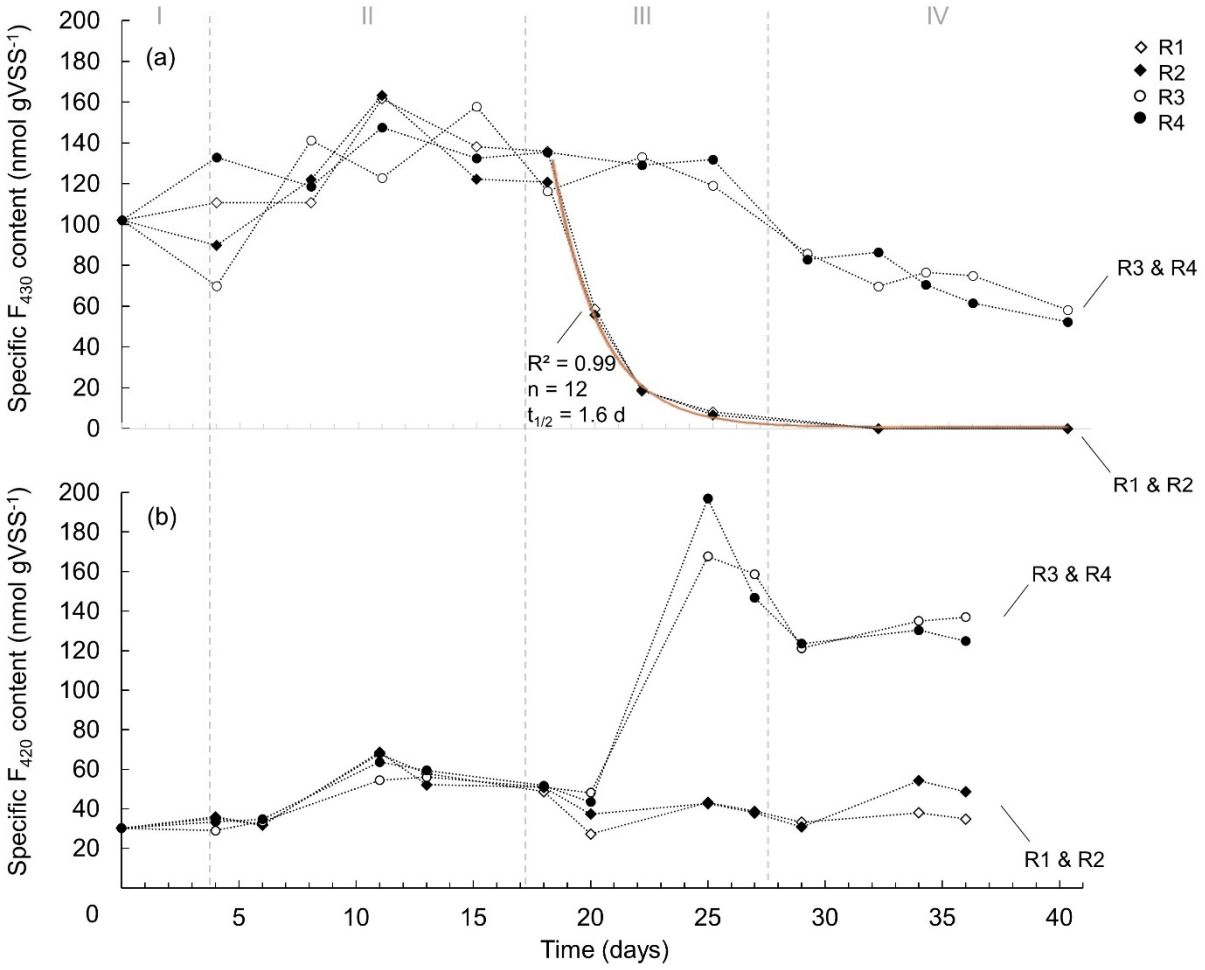


Figure 5.5 The Evolution of specific (a) cofactor F430 content and (b) cofactor F420 content over the 40 days experimental period. The F430 content decreased at an exponential rate during Phase III and IV due to the applied OLR shock in R1 and R2 (◊ and ♦, respectively), whereas it remained constant in R3 and R4 (○ and ●, respectively). The orange line indicates the exponential fit through the combined data of R1 and R2 with its coefficient of correlation (R^2), number of observations (n) and half-life (t1/2). Slightly lower F430 contents were measured in R3 and R4 during the pH shock (Phase IV). Fluctuations in F420 content (i.e., a significant increase followed by a decrease and stagnation phase after day 20) seemed unrelated to operational conditions. An HRT and SRT of 40 days was maintained.

The response of cofactor F_{430} concentration to the induced OLR shock in Phase III in R1 and R2 is clear-cut: approximately 10 days after the onset of the OLR shock, F_{430} has completely disappeared. The data suggests an exponential decay. An exponential fit through the measured data points ($R^2 = 0.99$, n = 12) yields a calculated half-life of 1.6 days[8]. After day 25, a steady but much less drastic decline of the F_{430} content is observed in R3 and R4 as a result of the applied pH shock.

Figure 5.5 – b shows no significant effect of the OLR shock on the F_{420} content in R1 and R2. However, a significant increase of cofactor F_{420} content in R3 and R4 is observed on day 25, without any changes in operational conditions for these reactors during that period. This increase in F_{420} content is followed by a decrease up to day 30, after which a stagnation is visible at a higher level than initially observed.

5.1.3 Discussion

The effect of an OLR shock on reactor performance and cofactor content

The accumulation of VFAs and the inhibitory pH values that were reached in Reactor 1 and 2, likely inhibited or killed-off part of the methanogenic population and this was reflected in a decrease of methanogenic performance and a concomitant reduction in cofactor F_{430} content. The response to the organic overloading is in accordance with Munk *et al.* (2012) which also found that the *mcrA* gene transcript over copy number ratio decreased during periods of acidification in a digester. The stable cofactor F_{430} concentrations in R3 and R4 (which served as control reactors during Phase III) confirmed that the decrease in cofactor content was a result of the OLR shock. From this observation it can be concluded that cofactor F_{430} content is very likely linked to the activity or presence of methanogens, in a similar way as the *mcrA* gene transcript and copy number, respectively (Munk *et al.*, 2012). Although this hypothesis has been occasionally investigated in literature (Kida *et al.*, 2001, Kaneko *et al.*, 2016), here it is clearly demonstrated that the complete disappearance of cofactor F_{430} coincided with an induced destabilization of the methanogenesis process. Moreover, interesting information with respect to the degradation kinetics of the cofactor was obtained. An exponential decay-rate was observed with a half-life of 1.6 days, which is in accordance with a ecent study by Kaneko and co-workers (2017). Because of the complete lack of methanogenic activity during the inhibition period, the decay-rate was dominated by the degradation of cofactor F_{430} molecules rather than the production of new ones. The importance of looking at both the production and degradation kinetics of cofactor F_{430} when investigating its potential use as a monitoring tool is further elaborated in Chapter 6. Note that the absolute cofactor contents were relatively low compared to literature reports (Diekert *et al.*, 1981; Kida *et al.*, 2001; Jiang, 2006).

The sudden increase in cofactor F_{420} concentration in R3 and R4, at a point during the experimental run where no operational conditions were altered and where process performance remained stable, was unexpected. Moreover, since multiple authors have proposed a link between this cofactor and methanogenic activity (Whitmore *et al.*, 1986; Gorris *et al.*, 1988; Ahn *et al.*, 2000), a response to the imposed shocks similar to that of F_{430} could have been expected. Here, a likely explanation is an inconsistency in the

[8] The 6 relevant time points for both reactors were combined, yielding 12 data points to produce the fit.

quantification of this cofactor. After day 20, the fluorimeter's lamp and detector had to be replaced and the remainder of the samples (from day 25 onward) were stored (-20 °C) and extracted and analysed several months later. Due to the lack of a F_{420} standard at the time that the first samples were analysed, the impact of the detector is not taken into account (the impact of the lamp is always taken into account by using a reference signal). Quality controls were re-run and compared with those measured at the time the first samples were analysed but no significant differences were found, ruling out the impact of the detector. Storage at -20 °C did not impact the extracted amounts of cofactors in other experiments and the extraction protocol used before and after lamp replacement was essentially the same. Nonetheless, it is surprising to observe that when shifting the F_{420} baseline (the first analysed samples) upwards (see Figure 5.6), a trend remarkably similar to that of cofactor F_{430} is found. Of course, this result is speculative and is not backed by the actual measured data. The more reliable results obtained for cofactor F_{420} in Section 6.2, however, indicate that the hypothesis of shifting the baseline is reasonable.

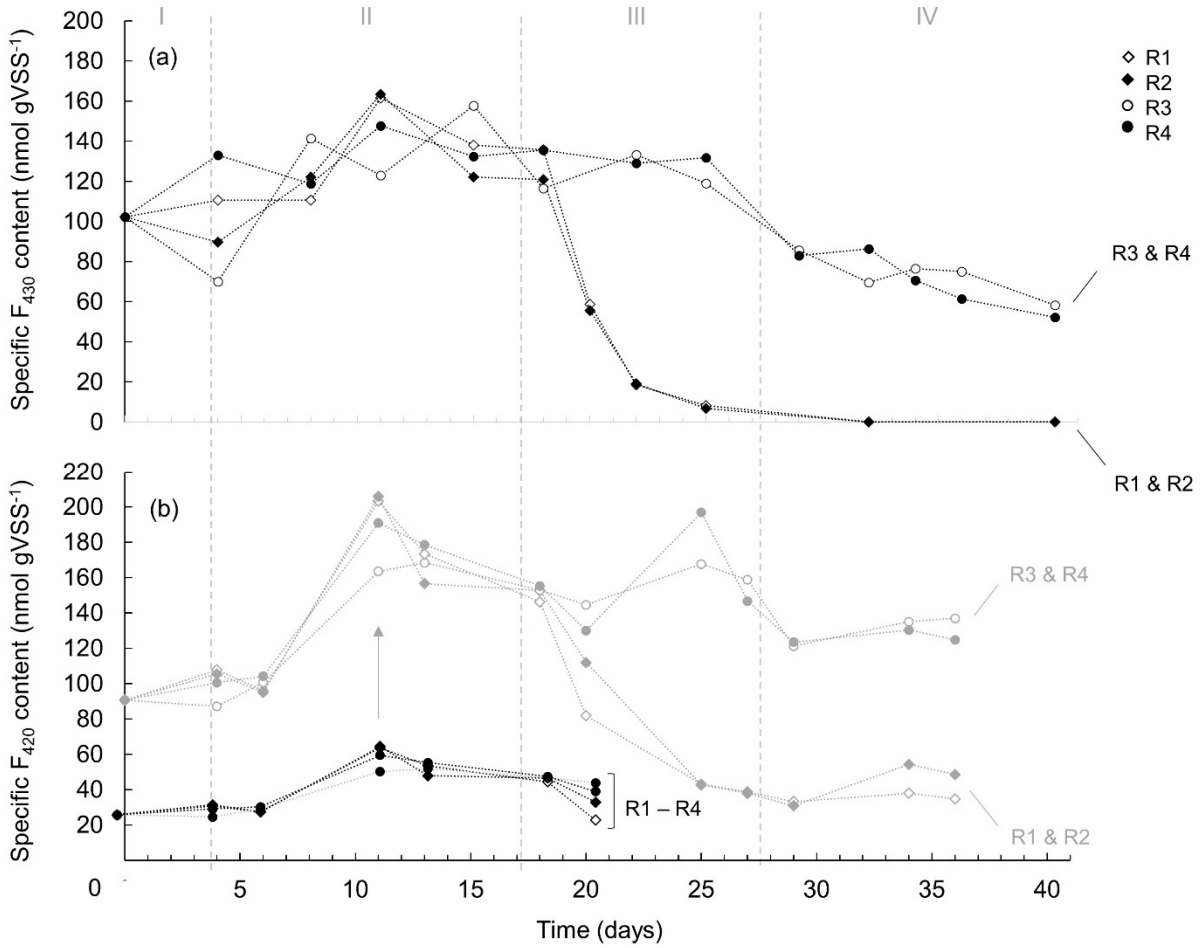


Figure 5.6 The evolution of specific **(a)** cofactor F_{430} content and **(b)** cofactor F_{420} content over the 40 days experimental period. Multiplying the F_{420} contents until day 20 (shown in black) by a factor 3 yields an F_{420} profile (in grey) remarkably similar to that of F_{430}.

The effect of an alkaline pH shock on reactor performance and cofactor content

The methane production rates, sCOD concentrations, VFA concentrations and pH remained relatively stable in R3 and R4 throughout Phase I to III. When these reactors experienced a higher pH as a result of the alkaline dosing during Phase IV, the effect on

performance was limited despite the fact that methanogenesis is expected to be affected at pH values above 8 (Sandberg & Ahring, 1992). In accordance to these findings, a less dramatic decrease in cofactor F_{430} concentrations was observed during Phase IV. In Figure 5.6 (after shifting the baseline), a trend similar to that for F_{430} was observed for cofactor F_{420}, keeping in mind the important assumption made with respect to its measurement.

In summary, the clear decrease in cofactor F_{430} content (and the suspected decrease of cofactor F_{420} content), as a result of an OLR shock, was linked to deteriorated performance and the absence of methane production. The effect of an alkaline pH shock on reactor performance and cofactor content was limited. In the next experiment, it is investigated whether the effect of a process upset on cofactor content can be generalized by looking at yet another mechanism of methanogenesis inhibition.

5.2 Does phenol induced methanogenesis inhibition reduce cofactor F_{430} content?[9]

Having confirmed that cofactor F_{430} content responds to the inhibition of methanogenesis by an OLR shock, the impact of phenol on methanogenesis and cofactor content is investigated. Inhibition by phenol occurs through a different mechanism. Therefore, it is interesting to see whether phenol induced inhibition is also reflected in a reduced cofactor F_{430} content. If so, then it is expected that cofactor F_{430} can serve as a general tool to monitor methanogenesis inhibition by a wide range of process upsets. To this end, a fed-batch lab-scale bioreactor was followed-up over an extended period of time during which the phenolic load in the wastewater was increased. Methane production was followed up and cofactor F_{430} content measurements were spread out over the 265 day experimental period.

A consortium of microorganisms is required to convert phenol to acetate and hydrogen for which different pathways are possible (Léven *et al.*, 2012) but sufficiently high (both acetotrophic and hydrogenotrophic) methanogenic activity is crucial for an efficient degradation of phenolic compounds. The mechanism of phenol inhibition is based on the interference of phenolic compounds with the energy production in the cell (David *et al.*, 2017) and it is, therefore, regarded as a growth-inhibitory toxicant (Veereesh *et al.*, 2005). The process of methanogenesis can be inhibited by a combination of the consortium's inability to convert the excess phenol to acetate and hydrogen (inhibition of acidogenesis and/or acetogenesis) and the direct toxic effect on the involved bacteria and methanogens (Léven *et al.*, 2006). The *Archaea* are more severely affected than the bacteria, however, the acidogenesis has been reported to be the rate-limiting step in the conversion of phenol to biogas (Wirth *et al.*, 2015).

5.2.1 Materials & methods

Experimental set-up and feeding strategy

The set-up used in this experiment was similar to the one described in Section 5.1.1, however, the feeding strategy differed. Only one reactor was used and inoculated with sludge originating from a full-scale installation treating phenol-rich wastewater. The reactor was fed with the same synthetic milk powder (Table 3.1) but was co-fed with phenol. The fraction of phenol with respect to the total COD load was increased throughout the experimental run, whilst the sludge loading rate was also gradually increased.

Table 5.1 shows how the experimental run was divided in three phases based on the COD phenol fraction in the feed. After a start-up period (phase I), the reactor was operated at a 25% phenol fraction for 31 days (phase II) and a 50% phenol fraction for 198 days (phase III). During the first 67 days (phase I and II) an HRT and SRT of 90 days was applied. Afterwards an average HRT and SRT of 49 days was maintained.

[9] This experiment was performed in collaboration with Lynn Lemoine from the KU Leuven Department of Earth and Environmental Sciences – Division of Soil and Water Management, who ran the reactor experiments and performed the molecular genetic analyses.

Table 5.1 The experimental period of 265 days was subdivided into three phases based on the COD phenol fraction in the feed. *MP = milk powder.*

Phase	Days	Influent COD composition
I	0 – 35	100% MP
II	36 – 67	75% MP + 25% phenol
III	67 – 265	50% MP + 50% phenol

Reactor performance was assessed by monitoring the (specific) methane production rate, methane yield, and bioreactor soluble COD (sCOD) and phenol concentration but the results & discussion sections will mainly focus on the methane production rate.

Analytical methods

The analytical methods used in this experiment have been described in the general material & methods section (Chapter 3). The following parameters were analysed.

- (Volatile) Suspended solids
- COD

Phenol concentration

Phenol concentration was monitored using reverse-phase high performance liquid chromatography on a Nexera (Shimadzu Corp) apparatus equipped with an Altima C18 column (100 x 4.6 mm, 3 µm) and a UV-VIS detector at 210 nm. A 1:1 volumetric mixture of Milli-Q water and acetonitrile was used to perform an isocratic elution at a constant flow rate of 1 mL min^{-1}. An injection volume of 1 µl was used and the limit of detection was 0.3 mg L^{-1}. Phenol measurements were performed weekly and sample preparation was done as follows: a 1 mL sludge sample was centrifuged for 5 min at 10 000 x g, the supernatant was filtered over a 0.45 µm filter and diluted with milli-Q to obtain an estimated phenol concentration between 1 and 500 mg L^{-1}.

Community structure analyses

The DNA and RNA based community structure analyses were performed as described in Lemoine (2018).

Sludge samples for DNA and RNA extraction were prepared as follows. One mL of mixed sludge sample was centrifuged (4 °C, 10 000 x g) and the pellet was snap-frozen in liquid nitrogen and stored at -80 °C prior to analysis. Total DNA was extracted using a method adapted from the cetyltrimethylammonium bromide (CTAB) – sodium dodecyl sulfate (SDS) based isolation method described by Zhou *et al.* (1996) while total RNA was extracted based on the guanidine/phenol method described by Chomczynski & Sacchi (1987). Detailed protocols can be found in Section 3.2.

The 16S rRNA gene amplicons were generated by a limited cycle PCR using universal primers adapted from S-D-Arch-0519-a-S-15/S-D-Bact-0785-b-A-18 (Klindworth *et al.*, 2013). The hypervariable V4 regions of both bacterial and A*rchaeal* 16S rRNA genes and 16S rRNA transcripts (after reverse transcription to cDNA) were amplified. Sequencing was performed on the Illumina MiSeq platform using the MiSeq v3 reagent kit to generate 300-bp paired-end reads at a sequencing depth of at least 100.000 raw reads per sample. Sequences from contaminant sources (Chloroplast, Mitochondria, Eukaryota) were removed and the remaining sequences were grouped into operational taxonomic units

(OTUs) at a sequence similarity cut-off of 97% using the average neighbour clustering approach. Finally, an OTU table with the amount of sequences in each OTU and a consensus taxonomy for each OTU was created.

Cofactor F_{430}

Cofactor F_{430} was extracted and quantified using Protocol 4 (Table 4.1) as described in Section 4.1.2.

5.2.2 Results

The results and discussion are focused on the relation between methane production rate and cofactor F_{430} content. In the next paragraphs the evolution of the methane production, cofactor F_{430} content and community structure are described. A more detailed description of reactor performance and community structure can be found in Lemoine (2018).

Overall reactor performance

Figure 5.7 summarizes the overall performance of the bioreactor by showing the (a) phenol removal and (b) specific methane production throughout the 265 day experimental period.

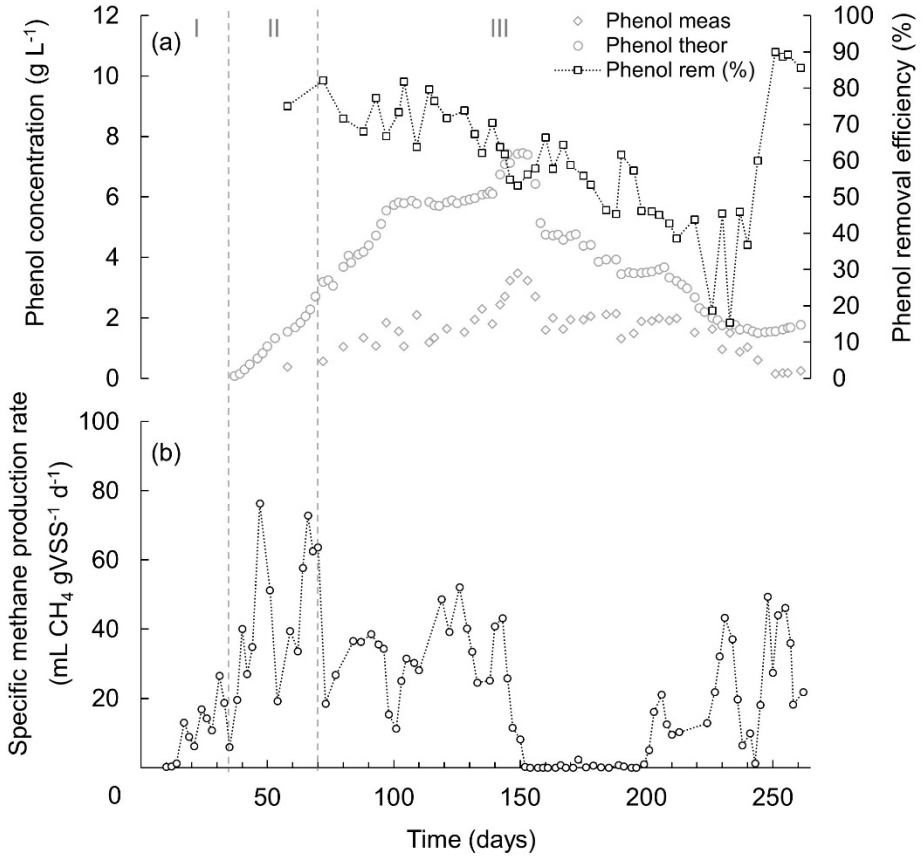


Figure 5.7 The evolution of the **(a)** phenol concentrations and removal efficiency and **(b)** specific methane production rate over the 265 day experimental period. The diference between the theoretical (theor, ○) and measured (meas, ◊) phenol concentrations is used to calculate the phenol removal efficiency (rem, ···□···) which decreases from day 140 onward. Methane production is significantly reduced between day 150 and 200, after which it increases again. During the first 67 days (phase I and II) an HRT and SRT of 90 days was applied. Afterwards an average HRT and SRT of 49 days was maintained.

A gradual inhibition of methanogenesis is observed starting from around day 140 of the experiment. Between day 150 and 200 complete reactor failure is observed, as evidenced by the negligible methane production. Despite the significant reduction of the SLR during this period, phenol removal efficiency continued to decrease over a time span of 50 days. On day 200, however, the methane production started increasing again, albeit with significant variability in performance. Increasingly high phenol removal efficiencies were found from day 240 onward.

The biomass concentration initially increased from around 6.5 gVSS L^{-1} to 9.3 gVSS L^{-1} during Phase I when only milk powder was fed (data not shown). However, once phenol was included in the feed (Phase II – III) the microorganisms' growth was affected and biomass concentration consistently decreased down to around 0.7 gVSS L^{-1} by the end of the experiment. The target sludge loading rate was not attained because of the deteriorating reactor performance. The sludge loading rate was adjusted during the inhibition period in order to recover the reactor performance. Indeed, operation at a significantly reduced loading rate between day 150 and 200 allowed the reactor to recover towards the final part of Phase III.

Cofactor F_{430} content

The reactor was sampled on 7 different occasions over the course of the experiment and Figure 5.8 shows the evolution of the measured cofactor F_{430} content, plotted alongside the specific methane production rate. In the early part of the phase with an increased phenolic load (Phase III), a cofactor content of around 45 nmol $gVSS^{-1}$ was measured. Further on, the data shows a significant increase in cofactor F_{430} content up to a value of 110 nmol $gVSS^{-1}$ on day 138, followed by the complete disappearance of the cofactor by day 166. On day 222 and day 243 very low values of 10 and 7 nmol $gVSS^{-1}$, respectively, were detected. It should be noted that the F_{430} concentration for these last samples was below the lower limit of the calibration curve (< 0.7 μM), so the absolute quantification is tentative.

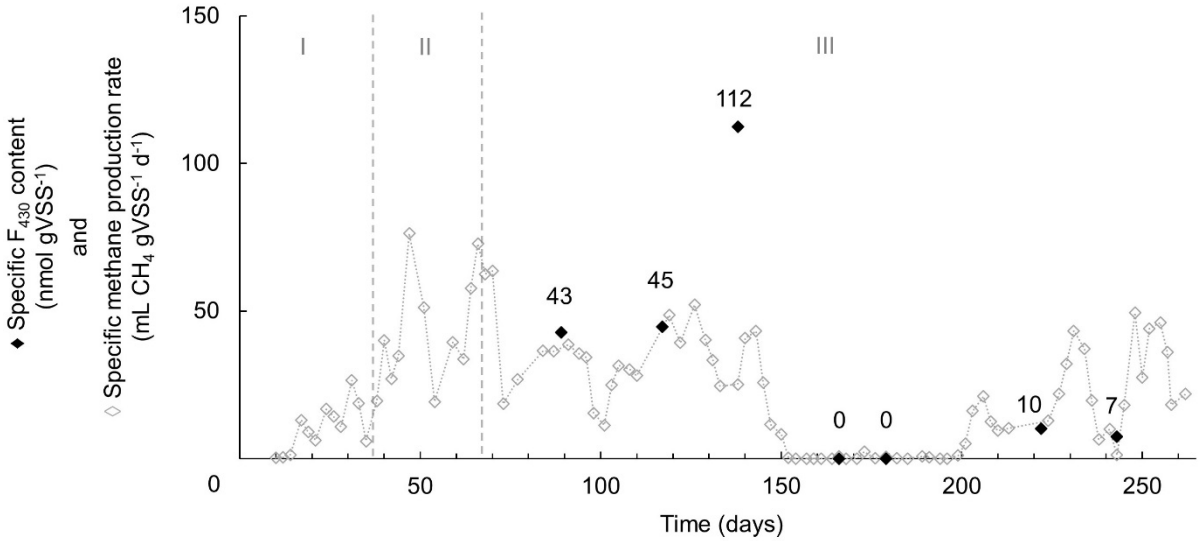


Figure 5.8 The evolution of the specific cofactor F_{430} content (♦) plotted alongside specific methane production rate (◊) over the 265 day experimental period. Data labels indicate cofactor F_{430} content values. Cofactor F_{430} clearly disappears along with the methane production rate during phenol induced inhibition. During the first 67 days (phase I and II) an HRT and SRT of 90 days was applied. Afterwards an average HRT and SRT of 49 days was maintained.

Community structure

The detailed community structure analysis can be found in Lemoine (2018). Several of the most abundant genera found in the reactor (on both DNA and RNA level) are known to be involved in the degradation of phenolic or aromatic compounds. For example, the genus *Cryptanaerobacter*, contains the anaerobic species *C. phenolicus* which uses the 4-hydroxybenzoate route to transform phenol into benzoate (Juteau *et al.*, 2005). Futhermore, the genera *Sporotomaculum* and *Syntrophus* both contain members known to syntrophically degrade benzoate (Qiu *et al.*, 2003; Carmona *et al.*, 2009; Schöcke & Schink, 1999). The abundance of members of the *Cryptanaerobacter* genus (on both DNA and RNA level) was particularly high during periods of effective phenol degradation and even higher after recovery from phenol inhibition (i.e., day 257). However, during reactor failure (i.e., day 159) their abundance was low. Based on the genera that were detected, the degradation pathway via 4-hydroxybenzoate coupled with the benzoyl-CoA pathway for further degradation to acetate, seems to have played an important role. The occurence of the alternative pathway through caproate can, however, not be ruled out. The relative importance of both pathways can only be confirmed through tracer experiments with the addition of labeled phenol (Hoyos-Hernandez *et al.*, 2014). The methanogenic community differed compared to more stable phenol-degrading reactors investigated in Lemoine's study. The genera *Methanobacterium, Methanofollis* and *Methanosarcina* were found to be more abundant in unstable reactors. The first two genera contain hydrogenotrophic methanogens, whereas the latter are acetoclastic methanogens.

5.2.3 Discussion

The mechanism of phenol induced methanogenesis inhibition

During this experimental run a clear, gradual inhibition of methanogenesis was observed. This inhibition resulted from the increasing SLR and COD phenol fraction applied to the reactor. Methanogenic reactors have been reported to be able to adapt to phenol concentrations of up to 2000 mg L^{-1} (Fang & Chan, 1997; Wirth *et al.*, 2015). In this experiment, severe inhibition occurred once phenol concentrations surpassed 2000 mg L^{-1}, with a maximum concentration of 3500 mg L^{-1} measured on day 150. The inhibition manifested itself in severely reduced biomass growth and the complete absence of methane production. However, despite the lower total biomass concentrations measured towards the end of Phase III, the reactor performance recovered, indicating that the sludge was enriched in phenol degrading (and resilient) organisms. Indeed, the community structure analysis showed that, e.g., members of the genus *Cryptanaerobacter*, likely involved in the conversion of phenol to benzoate (Juteau *et al.*, 2005), were most abundant (on both DNA and RNA level) after the inhibition period. However, their abundance during the inhibition period was low, indicating that the accumulated phenol could not be converted to acetate through the 4-hydroxybenzoate/benzoyl-CoA pathway. The metaproteome analysis (data not shown) confirmed the absence of several proteins involved in the degradation of benzoyl-CoA to acetyl-CoA in the reactor. However, many (low abundant) proteins are typically not detected in such analyses and the limited identification is also a common issue (Hettich *et al.*, 2013). Nonetheless, based on these observations, the following two mechanisms may have contributed to the inhibition of methanogenesis in this experiment:

(i) The high phenol concentrations decreased the activity of *Cryptanaerobacter* (and/or similar) species involved in the degradation of phenol to benzoate and possibly also that of species performing the subsequent conversion to acetyl-CoA;

(ii) The accumulation of phenol directly inhibited the methanogens. If the methanogens were not directly inhibited, some methane production would have been expected between day 150 and 200 since acetate was still being produced from the milk powder fraction of the feed.

Therefore, both the acetogenesis and the methanogenesis was likely inhibited in this experiment which is in accordance with literature reports (Léven *et al.*, 2006; Wirth *et al.*, 2015). The 50 days of operation at a significantly reduced SLR allowed the phenol degrading consortium to recover and resume its methane production towards the end of the experiment.

Cofactor F_{430} response to phenol induced methanogenesis inhibition

The data points for cofactor F_{430} quantification were specifically selected in order to know the cofactor content during stable, deteriorated and partially recovered performance. Therefore, a dynamic F_{430} profile was expected with significantly reduced cofactor contents during the inhibition of methanogenesis. Indeed, the cofactor content was below the limit of detection (< 0.2 μM) during the inhibition period, indicating that the absence of cofactor F_{430} reflected well the severely inhibited methanogenic activity. This is an important result since the mechanism of the methanogenesis inhibition was very different from the one occurring in the previous experiment. In Section 5.1, the OLR shock induced the accumulation of large amounts of methanogenic substrates with concomitant methanogenesis inhibition by pH and VFA toxicity. However, in this experiment the amount of substrates being supplied to the methanogens may have decreased due to the inhibition of the phenol degradation to acetate and concomitantly direct phenol toxicity prevented the methanogens from converting the acetate which was being supplied from the milk powder degradation. Nevertheless, in both cases, the cofactor F_{430} content reflected the inhibition well, regardless of the prevailing mechanism.

Despite what might have been expected, the significantly higher cofactor content on day 138 was not reflected in a higher methanogenic activity at this point in time. It is important to note here that in this experiment the sampling points were limited (due to the lack of biomass available to be used for the extraction) and one should be cautious with drawing general conclusions based on such "snap-shot" cofactor measurements. Munk *et al.* (2012) drew a similar conclusion for their quantification of the *mcrA* gene transcript over copy number ratio. In Chapter 6 and 7, the importance of being cautious with these snap-shot measurements of cofactor F_{430} is further elaborated, based on experiments with more sampling points. However, it is interesting to note that despite this outlier and a limited number of data points (n = 7), a significant positive Pearson correlation was found between methane production rate and F_{430} content ($r = 0.78$, $p = 0.0368$). When omitting the outlier, a very strong significant positive correlation is found, albeit with only 6 data points ($r = 0.9905$, $p = 0.0001$). In Chapter 6, this apparent, statistically significant correlation between methane production rate and cofactor content is further elaborated

with more data points. The absolute cofactor contents were, once more, relatively low compared to literature reports (Diekert *et al.*, 1981; Kida *et al.*, 2001; Jiang, 2006).

A final remark relates to the F_{430} extractions. There was significantly less biomass available from the samples taken later during the run (due to the decreasing biomass concentration in the reactor). The amount of biomass used for the extraction of F_{430} was 0.108, 0.147, 0.092, 0.053, 0.050, 0.038 and 0.025 gVSS, for day 89, 117, 138, 138, 166, 179, 222 and 243, respectively. Ideally, the extraction is performed on a similar and sufficient amount of biomass (between 0.06 and 0.1 gVSS typically suffices) in order to extract a measurable quantity of cofactor and to allow for a fair comparison of the cofactor content. For the four last samples, however, this amount of biomass was simply not available. Nonetheless, despite the lower amount of biomass used to extract F_{430} from the last two samples, their F_{430} concentration was higher than during the inhibition period. This confirms that specific cofactor content indeed increased again towards the end of the experiment as process performance and methanogenic activity recovered.

In summary, this experiment demonstrated that the absence of methane production as a result of phenol inhibition coincided with the complete disappearance of cofactor F_{430}, as was the case for the OLR shock in Section 5.1. This observation confirms the potential of cofactor F_{430} to be used as a biomarker for the presence or activity of methanogens during process disturbances, possibly regardless of the inhibition mechanism.

5.3 CONCLUSIONS

Two of the three process upsets that were investigated in this chapter led to an intended methanogenesis inhibition. In those cases, a corresponding reduction or even absence of cofactor F_{430} (and potentially F_{420}) in the biomass was observed.

An **OLR shock** induced a drop in methane production rate with a concomitant accumulation of sCOD and VFAs and acidification. The cofactor F_{430} content decreased during this process upset, whereas it remained stable in the control reactors. The F_{430} concentration showed an exponential decay, implying pseudo-first order degradation kinetics. The combined results from the classical performance monitoring tools and cofactor F_{430} measurements, indicate that the **pH shock** did not severely affect the methanogenesis. Nonetheless, the results showed a slight effect on cofactor F_{430} content, indicating that the methanogens may have been affected by the sub-optimal conditions. In both cases, the results for cofactor F_{420} were inconclusive. However, a similar trend as that of F_{430} might have been observed if all samples had been extracted and measured at the same point in time.

The inhibition imposed by an **increased phenolic content** in the wastewater, led to severe process failure in Section 5.2. The high phenol concentrations likely inhibited both the acidogenesis and the methanogenesis process. Nonetheless, the reactor recovered from the inhibition after around 50 days of operation at a significantly lowered SLR with a reduced phenolic load. The cofactor F_{430} measurements indicate that also in this case, despite the different mechanisms of inhibition, the cofactor's disappearance coincided with the absence of methane production and a positive correlation between the two parameters was found.

The combined results presented in this chapter serve as a **proof-of-principle**, indicating that **cofactor F_{430}** can be used as a **biomarker for methanogenic presence or activity**. Moreover, since cofactor F_{430} is directly linked to the methanogenic metabolism, it has the potential to provide more in-depth information on the activity of the methanogenic community than classical monitoring tools. Furthermore, its relatively simple and fast quantification increases its suitability as a monitoring tool. In the following chapter, cofactor F_{430} dynamics are compared with methane production rate dynamics and the cofactor's potential to monitor OLR shock process disturbances is further elaborated. Moreover, the inconclusive outcome for cofactor F_{420} is addressed and a comparison with other activity related monitoring tools is made.

CHAPTER 6

Methanogenic cofactor quantification as a novel approach to monitor process disturbances[10]

In Chapter 5, the concentration of cofactor F_{430} (and possibly F_{420}) was found to respond to the inhibition of methanogenesis in fed-batch lab-scale anaerobic reactors. This observation served as a proof-of-principle for the cofactors' potential to be used as biomarkers for methanogenic activity in anaerobic digestion. In this chapter, two additional experiments were performed in order to determine *whether the selected methanogenic cofactors can serve as tools to monitor and to help avoid or relieve process disturbances in methanogenic anaerobic bioreactors*. A particular point of interest in these experiments are the cofactor production and degradation dynamics. Moreover, their ability to reflect methanogenic activity is compared with other activity measurements. Furthermore, the evolution of cofactor F_{420} content, in comparison to F_{430}, is followed up more closely and the F_{420} over F_{430} ratio is evaluated as a measure of hydrogenotrophic methanogenic activity.

In the first experiment, two VFA-fed, lab-scale anaerobic digesters were subjected to repeated short-term feeding pulses, inducing organic overloading. Cofactor F_{420} was quantified in two different ways alongside cofactor F_{430}, (methanogenic) cell numbers, *mcrA* gene copy numbers, methanogenic community structure and classical performance monitoring tools.

In the second experiment, a synthetic dairy wastewater fed, lab-scale anaerobic membrane bioreactor (AnMBR) was subjected to two consecutive organic loading rate shocks and the cofactor F_{420} and F_{430} content of the sludge was closely followed up alongside *mcrA* gene copy and transcript numbers as well as classical performance monitoring tools.

As elaborated in Section 2.1.4, several studies have established that *mcrA* gene copy and transcript numbers can be used to quantify the abundance and/or activity of methanogens.

---

[10] The results of Section 6.2 have been published in Passaris *et al.* (2018) Cofactor F_{430} as a biomarker for methanogenic activity: application to an anaerobic bioreactor system. *Applied microbiology and biotechnology, 102(3)*, 1191-1201.

Moreover, the *mcrA* gene can be used to elucidate the methanogenic community structure (Alvarado *et al.*, 2014). Therefore, its quantification was included in these experiments.

6.1 Does methanogenic cofactor content reflect the dynamics of methanogenesis in digesters subjected to repeated overfeeding pulses?[11]

In this first experiment, two lab-scale digesters were deliberately stressed by the application of repeated short-term feeding pulses, which induced organic overloading. The objectives are to:

(i) assess the evolution of the cofactor F_{430} concentration and its relation with a dynamic methane production profile;
(ii) evaluate two cofactor F_{420} quantification methods and compare this cofactor's relation with cofactor F_{430} and methane production rate, and;
(iii) assess the potential of the cofactor F_{420} over F_{430} ratio for reflecting the activity of hydrogenotrophic methanogens.

Two separate experimental reactors and one control reactor were operated and compared in terms of overall reactor performance and cofactor F_{430} and F_{420} content. Additionally, the number of methanogenic cells was determined using flow cytometry as an additional parameter potentially related to methanogenic activity and the total number of cells was used for normalization of the data. Furthermore, the quantification of the *mcrA* gene copy numbers was included.

6.1.1 Materials & methods

Digester experimental set-up and feeding strategy

The digesters used in this experiment were double-walled polyethylene reactors with a transparent acrylate lid and are shown in Figure 6.1. Their total volume was 15 L and the operational volume ranged between 4.5 L and 6 L (due to the applied discontinuous feeding and smapling regime). Water is heated to a fixed temperature of 41 °C and pumped through the heating jacket (MA-4 Umwälzthermostat, Julabo, Seelbach Germany). The digestate's temperature was measured manually with a thermometer and the water flow rate was adjusted with a ball valve to reach the desired working temperature of 37 °C. Once the set point temperature was adjusted, the system was stable. pH was measured externally in samples taken from the reactor using a pH electrode (pH 3110 WTW, Weilheim). Gas production rates were measured hourly using an automated gas counter (Drum-type TG series, Ritter, Bochum, Germany) and gas composition (CO_2, CH_4, H_2S, O_2 and H_2) was determined several times over the course of each experiment by a gas chromatograph equipped with a wide-range Flame Ionization Detector (FID) (AWIFLEX model, AWITE, Langenbach, Germany).

All reactors were inoculated with sludge from lab-scale methanogen-enriched digesters operating at the same HRT, SRT and initial feeding regime as the experimental reactors. These digesters served solely as inoculation reactors and all experimental reactors were essentially "clones" of the methanogen-enriched digesters.

[11] This experiment was performed in collaboration with Johannes Lambrecht and Fabian Bonk from the Department of Microbiology at the Helmholtz Centre for Environmental Research-UFZ, in Leipzig, Germany. They ran the reactors at the Deutsches Biomasseforschungszentrum (DBFZ) in Leipzig. Johannes performed the flow cytometric F_{420} quantification, whereas Fabian performed the molecular genetic analyses.



Figure 6.1 The VFA-fed digesters operated at the Deutsches Biomasseforschungszentrum (DBFZ) in Leipzig.

The reactors were fed with a mixture of acetic, propionic and butyric acid at a fixed 0.45:0.1:45 ratio on a COD basis. This ratio was maintained throughout the entire experiment regardless of the applied organic loading rate. The feed was supplied to the reactor at a constant rate by peristaltic pumps (Hei-FLOW precision, multichannel pump head, HEIDOLPH, Schwabach, Germany). On multiple occasions additional feed was supplemented directly into the feeding port, hereby switching the feeding pattern from continuous to pulse-fed.

Reactor 1 was operated at an HRT and SRT of 20 days and initially fed at a continuous baseline feed rate of 1.86 gCOD L^{-1} d^{-1}. A COD pulse containing the amount normally supplied over the course of the day (11.16 gCOD), supplemented with an extra 49.7 gCOD, was added on time point zero. This amount of COD corresponded to a significantly increased OLR of 5.07 gCOD L^{-1} d^{-1} applied over the next two days. 48 hours after the application of the pulse, continuous feeding at the initial baseline feed rate was re-started. The operation of Reactor 1 is summarized in Table 6.1. The applied OLR is detailed, along with the time span and feeding pattern (continuous or pulse).

Table 6.1 Summary of Reactor 1 operation. Continuous feeding was interrupted by the application of a COD pulse. 48 hours after the application of the pulse, continuous feeding was resumed.

HRT & SRT = 20 days		
Time (hours)	**Feeding pattern**	**OLR (gCOD L^{-1} d^{-1})**
-24 to 0	Continuous	1.86
0 to 48	Pulse	5.07
48 to 168	Continuous	1.86

Since Reactor 1 recovered well from the single pulse applied in the experiment, an identical reactor, Reactor 2, was subjected to additional pulses in order to achieve the desired acidification (reactor failure). The experiment was performed in a separate reactor

in order to exclude effects related to the history of operation. In contrast to Reactor 1, Reactor 2 was operated at an HRT and SRT of 5.5 days and initially fed at a continuous base feed rate of 6.76 gCOD L^{-1} d^{-1} (hereby achieving the same COD feed concentration as Reactor 1). On time point zero, a first COD pulse of 60.9 gCOD was added to the reactor, corresponding to an OLR of 10.14 gCOD L^{-1} d^{-1}. The next two days the reactor was again pulse-fed twice at a rate of 6.76 and 8.36 gCOD L^{-1} d^{-1} 23 and 48 hours after the first pulse, respectively. After 72 hours, the aim was to resume continuous feeding (at the base feed rate of 6.76 gCOD L^{-1} d^{-1}), however, the feeding was stopped due to a pump failure, and thus the reactor did not receive any feed from 72 to 144 hours. Subsequently, the reactor received a fourth pulse containing a total of 140 gCOD (OLR 11.67 gCOD L^{-1} d^{-1}). Finally, continuous feeding was resumed 192 hours after the first pulse and maintained until the end of the experiment. The operation of Reactor 2 is summarized in Table 6.2. The applied OLR is detailed, along with the time span and feeding pattern (continuous or pulse, including the number of the pulse).

Table 6.2 Summary of Reactor 2 operation. Continuous feeding was interrupted by the application of four COD pulses. 192 hours after the application of the first pulse, continuous feeding was resumed.

HRT & SRT = 5.5 days		
Time (hours)	**Feeding pattern**	**OLR (gCOD L^{-1} d^{-1})**
-24 to 0	Continuous	6.67
0 to 23	Pulse 1	10.14
23 to 48	Pulse 2	6.67
48 to 72	Pulse 3	8.36
72 to 144	-	0
144 to 192	Pulse 4	11.67
192 to 240	Continuous	6.67

A control reactor, operated at an HRT and SRT of 5.5 days and fed at a constant rate of 6.67 gCOD L^{-1} d^{-1}, was run in parallel over a period of 168 hours and served as a benchmark for comparison.

Overall reactor performance and stability were assessed using the conventional parameters such as (specific) methane production, VFA concentrations and pH.

Analytical methods

Total and volatile solids content

Total solids (TS) and volatile solids (VS) content were determined as described in Mulat *et al.* (2016) with modifications. The TS and VS content measurements were modified in such a way that a CSTR sample was not added directly to a crucible, but only the pellet after centrifuging 100 mL CSTR content (10 000 × g, 10 min, 10 °C) to increase the amount of biomass per analysis and to reduce the potential error induced by the VFAs in the CSTR sample.

Total and individual VFA concentrations

Total and individual VFA concentrations were determined as described in Mulat *et al.* (2016). Briefly, 2.5 mL supernatant of the centrifuged digestate (10 000 × g, 10 min, 10 °C) was diluted with 2.5 mL dH_2O (1:2) inside 20 mL Gas Chromatography (GC) vials to meet the calibration limits for the main analytes. 1 mL of 2-methlbutyric acid (184 g mL^{-1}) was added as the internal standard and 1 mL phosphoric acid (21.25%) was added. The vials

were prepared as triplicates, closed with aluminium caps and stored at 4 °C. The Headspace Sampler (TurboMatrix110, PerkinElmer, Waltham, Massachusetts, USA) penetrated the septum cap of the vials to transport the headspace gases into the GC System (7890 A, Agilent Technologies, Santa Clara, California, USA).

Flow cytometric methods

Total and autofluorescent (F_{420}+) cell numbers were determined at the Helmholtz Centre for Environmental Research-UFZ, in Leipzig, by means of flow cytometry according to Lambrecht *et al.* (2017). In addition to the number of autofluorescent cells, the bulk fluorescent intensity per sample was calculated as a measure of the total F_{420} content in each sample. All analyses were performed in triplicate and the mean and standard deviations were calculated based on these replicates.

Molecular genetic analyses

mcrA gene copy number analysis

Using the mlas (GGTGGTGTMGGDTTCACMCARTA) and *mcrA*-rev (CGTTCATBGCGTAGTTVGGRTAGT) primers for methanogens (Steinberg & Regan, 2009), qPCR was executed. Template DNA was diluted to 1 ng μL^{-1} and analyzed using a BioRad CFX C1000 (Hercules, USA) targeting bacteria and methanogens, separately, using the primers specified above. DNA concentrations were determined using the Qubit™ dsDNA HS Assay Kit (ThermoFisher Scientific Inc., USA). Each 10 µL well contained 5 µL KAPA SYBR®FAST qPCR Master Mix (2X) Universal (Kapabiosystems, USA), 1 µL of template DNA, 0.5 µL of each primer (diluted to 2 pmol μL^{-1}) and 3 µL nuclease-free water. For methanogens, the qPCR program was as follows: initial enzyme activation at 95 °C for 3 min, denaturation at 95 °C for 5 s, simultaneous annealing and extension at 60 °C for 30 s. The reaction was continued for another 35 cycles. The copy number of the target genes were calculated based on the one-point calibration method by Brankatschk *et al.* (2012) and a standard curve. The standard curve was constructed from a PCR product of a similar reactor sample (same primers, PCR product cleaned with SureClean Plus, Bioline, Germany).

T-RFLP analysis

The methanogenic community composition was assessed by Terminal Restriction Fragment Length Polymorphism (T-RFLP) analysis of *mcrA* gene amplicons as described previously in Sträuber *et al.* (2016). The database of Bühligen *et al.* (2016) was used for the taxonomic assignment. Primers were the same as described in the qPCR procedure. The restriction enzyme used was BstNI (New England Biolabs).

Cofactor F_{430} and F_{420}

Cofactor F_{430} was extracted and quantified using Protocol 4 (Table 4.1) as described in Section 4.1.2.

Cofactor F_{420} was extracted and quantified using the fluorimetry method, as described in Section 4.2.2.

An approximate experimental error on the extraction and quantification of both cofactors was determined. To this end, at least 5 replicates were analysed and the relative error on

the mean was determined, taking into account all potential experimental errors from sampling to quantification. This analysis was performed separately for the two experimental reactors in order to take into account any matrix effects. The relative experimental error on the cofactor F_{430} quantification was 9.3% and 4.7% in Reactor 1 and 2, respectively. The relative experimental error on the cofactor F_{420} quantification was 7.5% and 5.4% in Reactor 1 and 2, respectively. Since the analysis could not be performed on the Control Reactor due to the lack of sufficient replicates, the highest relative errors (9.3% and 7.5% for cofactor F_{430} and F_{420}, respectively) were assumed for the quantification of these samples.

6.1.2 Results

The two experimental reactors and the control reactor will be discussed separately in terms of overall reactor performance, cell numbers and community structure, and cofactor F_{430} and F_{420} content. The applied pulses and periods of continuous feeding described in Table 6.1 and Table 6.2 will be indicated on the figures for clarity. Due to a lack of frequent and accurate VS data, all relevant parameters are normalized on the basis of total number of cells determined by flow cytometry, since this is the most accurate approximation of biomass concentration available in this experiment. Flow-cytometric quantification of total bacterial cell counts is routinely used in drinking water producing plants (Hammes *et al.*, 2008). In full-scale digesters volatile solids originating from the feed may introduce error in volatile solids concentration measurements as a measure of biomass concentration, hence, justifying the use of cell counts determined by flow cytometry.

Reactor 1

Overall reactor performance. Figure 6.2 shows the evolution of (a) the specific methane production rate and (b) the pH and total VFA concentration in Reactor 1. It should be noted that, unfortunately, gas composition was measured discontinuously and that CO_2 outgassing occurred from time to time, rendering the methane production rates rather unreliable. The specific methane production rate (per number of cells) significantly reduced shortly after the pulse applied at time point zero. Simultaneously, the pH dropped more than one unit while the total VFA concentration increased due to their addition through the feed. Around 12 hours after the pulse, methane production had almost completely halted and VFA concentrations were still elevated (more than 90% of the added amount). One day after the application of the pulse the methane production rate started increasing again until 111 hours into the experiment. This increasing trend was unaffected by the re-introduction of VFAs in the reactor during continuous feeding after 48 hours. Both pH and total VFA concentrations recovered towards their initial values during this period. A significant decrease in methane production rate was observed from 111 hours onward, without altering any operational condition. This likely resulted from the fact that all the (residual) VFAs added during the pulse were consumed at this point and the reactor dropped back to its initial methane production rate based on the continuous feed.

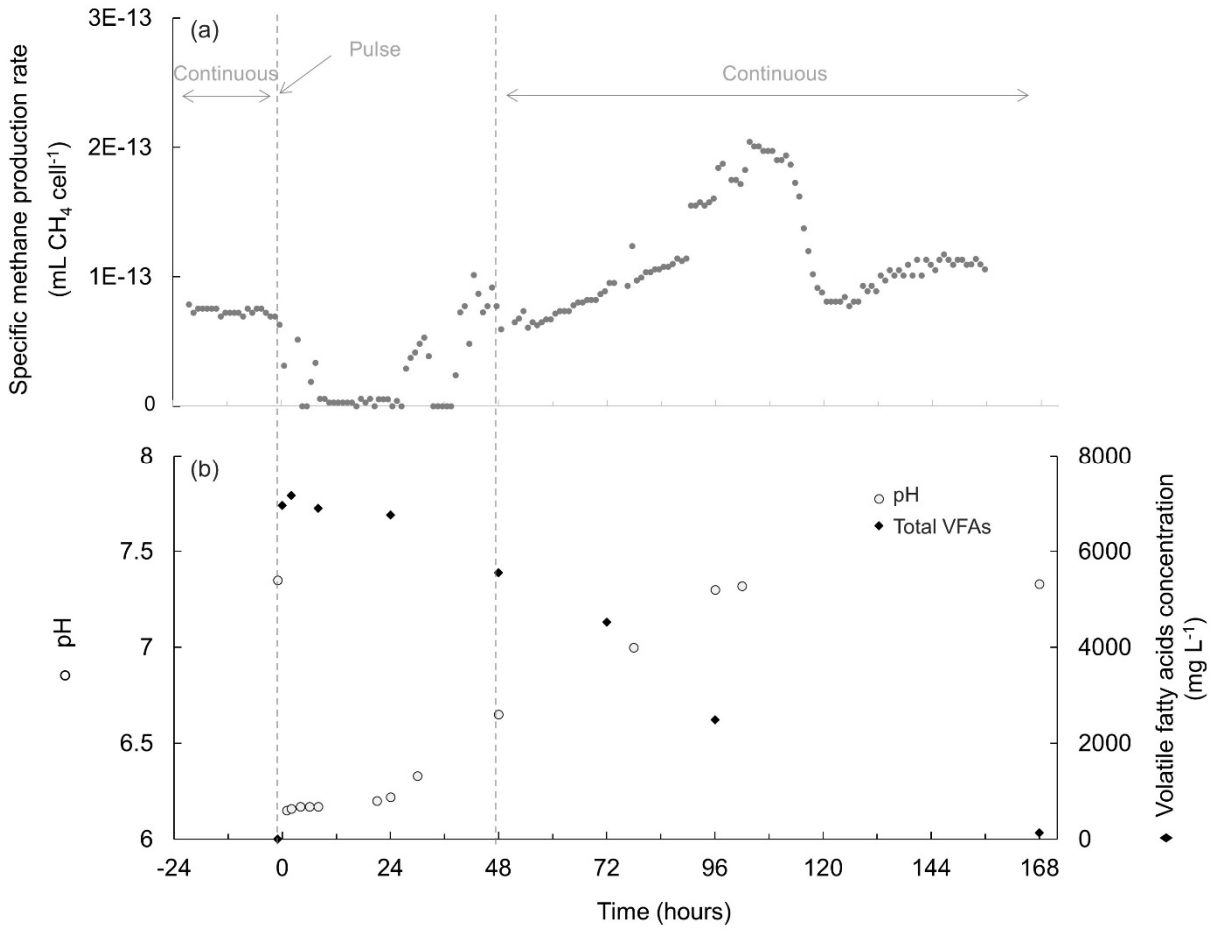


Figure 6.2 The evolution of the **(a)** specific methane production rate (●) and **(b)** pH (○) and total volatile fatty acids concentrations (VFAs) (♦) over the course of the 168 hours experimental period in *Reactor 1*. The pulse applied at time point zero clearly affected the methanogenic activity but the reactor gradually recovered.

Cell numbers and cofactor content. Figure 6.3 shows the (a) total and F_{420}+ cell numbers, (b) F_{420}+ over total cell number ratio, (c) cofactor F_{430} normalized per number of cells, (d) cofactor F_{420} normalized per number of cells, and (d) the F_{420} over F_{430} ratio, plotted alongside the specific methane production rate for Reactor 1.

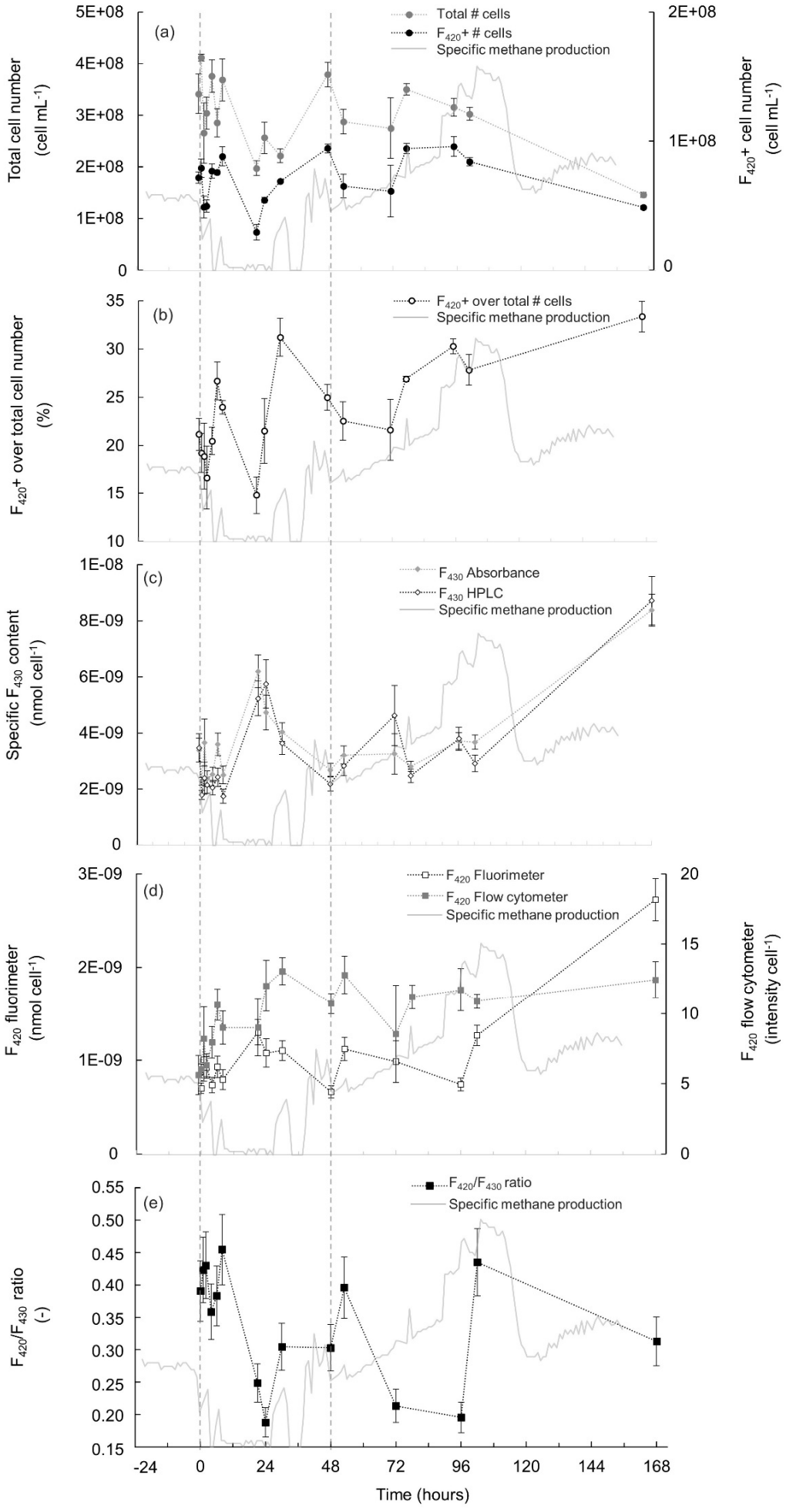

(a)
Total # cells
F420+ # cells
Specific methane production
Total cell number (cell mL-1)
F420+ cell number (cell mL-1)
5E+08
4E+08
3E+08
2E+08
1E+08
0
2E+08
1E+08
0
(b)
F420+ over total # cells
Specific methane production
F420+ over total cell number (%)
35
30
25
20
15
10
(c)
F430 Absorbance
F430 HPLC
Specific methane production
Specific F430 content (nmol cell-1)
1E-08
8E-09
6E-09
4E-09
2E-09
0
(d)
F420 Fluorimeter
F420 Flow cytometer
Specific methane production
F420 fluorimeter (nmol cell-1)
F420 flow cytometer (intensity cell-1)
3E-09
2E-09
1E-09
0
20
15
10
5
0
(e)
F420/F430 ratio
Specific methane production
F420/F430 ratio (-)
0.55
0.50
0.45
0.40
0.35
0.30
0.25
0.20
0.15
-24
0
24
48
72
96
120
144
168
Time (hours)

Figure 6.3 The evolution of **(a)** total (●) and F_{420}+ (●) cell numbers **(b)** F_{420}+ over total cell number ratio (○) **(c)** Specific F_{430} content measured by absorbance (♦) and HPLC (◊) quantification **(d)** specific F_{420} content measured by fluorimetry (□) and flow cytometry (■) and **(e)** F_{420} over F_{430} ratio calculated using the fluorimeter and HPLC quantification (■) over the 168 hour experimental period in *Reactor 1*. Error bars represent the (combined) experimental error on cell number and cofactor quantification. The specific methane production rate (–) was added to compare the trends (for absolute values see Figure 6.2). F_{420}+ cell numbers were consistently lower than total numbers but showed a similar trend. Nonetheless, significant differences in their ratio were observed. Both F_{430} quantification methods and the F_{420} quantification using fluorimetry indicate a significantly higher cofactor content at the end of the experiment. Their ratio widely fluctuates.

In Figure 6.3 – a a relatively similar trend is observed for the total and the F_{420}+ cell numbers. The total cell number was consistently higher than the number of F_{420}+ cells and varied between 1.5 x 10^8 cells mL^{-1} and 4 x 10^8 cells mL^{-1}, whereas the F_{420}+ cells varied between 2 x 10^7 cells mL^{-1} and 1 x 10^8 cells mL^{-1}. Despite the similar trend, significant differences in their ratio are observed. The ratio, shown in Figure 6.3 – b, increased from 21.2 ± 1.7% to 33.4 ± 1.6%, with significant fluctuations in between and a minimum of 14.8 ± 1.9% 21 hours after the pulse. The average ratio in Reactor 1 over the entire experimental run was 23.7 ± 1.9%.

In Figure 6.3 – c both cofactor F_{430} quantification methods yield similar results. Moreover, F_{430} content decreases immediately after the applied pulse but recovers to a higher value approximately 1 day after the pulse was applied. Over the following 80 hours some significant fluctuations in cofactor content are observed and at the end of the experiment the highest cofactor content is measured.

In Figure 6.3 – d a relatively similar trend of cofactor F_{420} content measured by fluorimetry as for cofactor F_{430} is observed. However, quantification by flow cytometry yields a different trend, at least between the final and initial point. Note that unfortunately in this experiment the sample one hour prior to the pulse (sample "-1") was not analysed. Nonetheless, for quantification by fluorimetry, the highest F_{420} content was observed at the end of the experimental run.

In order to visualize the differences in evolution of both cofactors in this experiment, the ratio of cofactor F_{420} over cofactor F_{430} was calculated. The fluorimetric and HPLC quantification were used for cofactor F_{420} and F_{430}, respectively. In Figure 6.3 – e significant fluctuations in this ratio are observed. Indeed, the ratio varies between 0.19 ± 0.02 and 0.45 ± 0.05 with an average of 0.34 ± 0.04. In the first 24 hours after the pulse the measured ratios are between 0.3 and 0.5. Subsequently, significantly varying F_{420} over F_{430} ratios are found and a ratio of around 0.3 is measured at the end of the experiment.

In order to objectify the correlations between the different parameters proposed as monitoring tools for methanogenic activity, they were statistically tested using the Pearson's correlation coefficient (r), which is a measure of the linear relation between two variables (Figure 6.4). The results support the strong correlation between both F_{430} quantification methods observed visually in Figure 6.3 - c. Moreover, strong correlations between the fluorimetric quantification of cofactor F_{420} and both F_{430} methods were found. Furthermore, the number of autofluorescent cells (F_{420}+) significantly correlated with the bulk fluorescent intensity as determined by flow cytometry. However, this fluorescent

intensity did not significantly correlate with the fluorimetric quantification of cofactor F_{420} content.

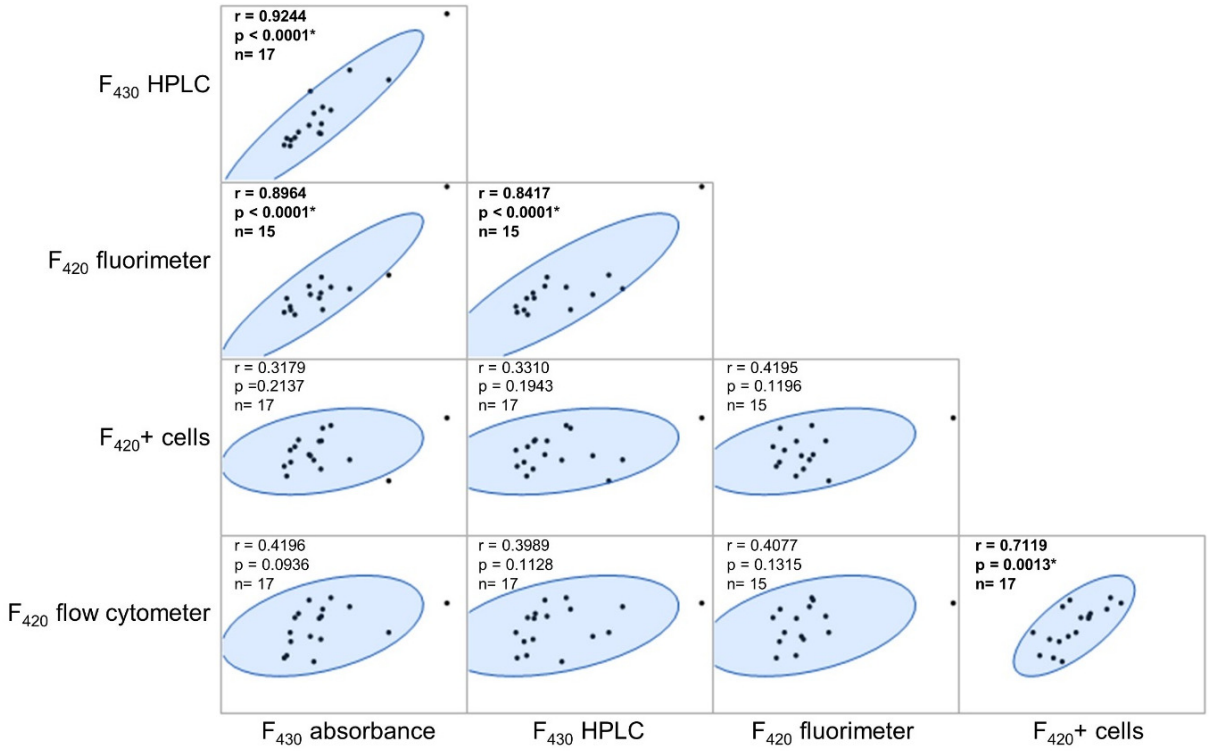


Figure 6.4 Plots showing the correlation coefficient (Pearson r), statistical significance (p), sample size (n) and 95% confidence interval (blue ellipses), between the evaluated monitoring tools for methanogenic activity in *Reactor 1*. Strong significant correlations (highlighted in bold) were found for the two F_{430} quantification methods and between the two cofactors.

Molecular genetic analyses. *mcrA* copy numbers were quantified as an additional measure of methanogen abundance (see Section 2.1.4) in the beginning and at the end of the experiments. These are shown in Table 6.3.

Table 6.3 Average *mcrA* copy numbers and their standard deviations (triplicates), expressed per mL and per ngDNA, at the beginning and end of the experiment in *Reactor 1*. No significant difference is observed.

Sample	Average *mcrA* copy number (copies mL^{-1})	Average *mcrA* copy number (copies $ngDNA^{-1}$)
Reactor 1 – begin (-1h)	$2.0 \times 10^{12} \pm 1.3 \times 10^{11}$	$1.0 \times 10^{6} \pm 6.7 \times 10^{4}$
Reactor 1 – end (168h)	$2.5 \times 10^{12} \pm 4.2 \times 10^{11}$	$1.0 \times 10^{6} \pm 1.7 \times 10^{5}$

The average *mcrA* copy numbers per ng of DNA are similar, indicating that the relative number of methanogens did not significantly increase between the end and the beginning of the experiment.

Having determined a measure of the total number of methanogens by means of the *mcrA* quantification, additionally T-RFLP analysis was performed in order to provide a semi-quantitative measure of the relative abundance of the different methanogenic families. The results for Reactor 1 are shown in Table 6.4 and revealed the dominance of two methanogenic families. Acetotrophic methanogens belonging to the *Methanosaetaceae* family accounted for 50-60% of the methanogens, whereas members of the hydrogenotrophic *Methanomicrobiaceae* family, accounted for the remaining 25-35%. The

relative differences between the beginning and end samples likely fall within the margin of the experimental error on this analysis method.

Table 6.4 Results of the T-RFLP analysis providing a semi-quantitative indication of the relative abundance of acetotrophic and hydrogenotrophic methanogens in *Reactor 1*. Acetotrophic *Methanosaetaceae* and hydrogenotrophic *Methanomicrobiaceae* clearly dominated with relative abundances of 50-60% and 25-35%, respectively. *Methanosarsinaceae* species were present to a lesser extent.

Sample	Methanosaetaceae (%)	Methanomicrobiaceae (%)	Methanosarcinaceae (%)
Reactor 1 – begin (-1h)	57	29	6
Reactor 1 – end (168h)	52	34	6

Reactor 2

Overall reactor performance. Figure 6.5 shows the evolution of (a) the specific methane production rate and (b) the pH and total VFA concentration in Reactor 2.

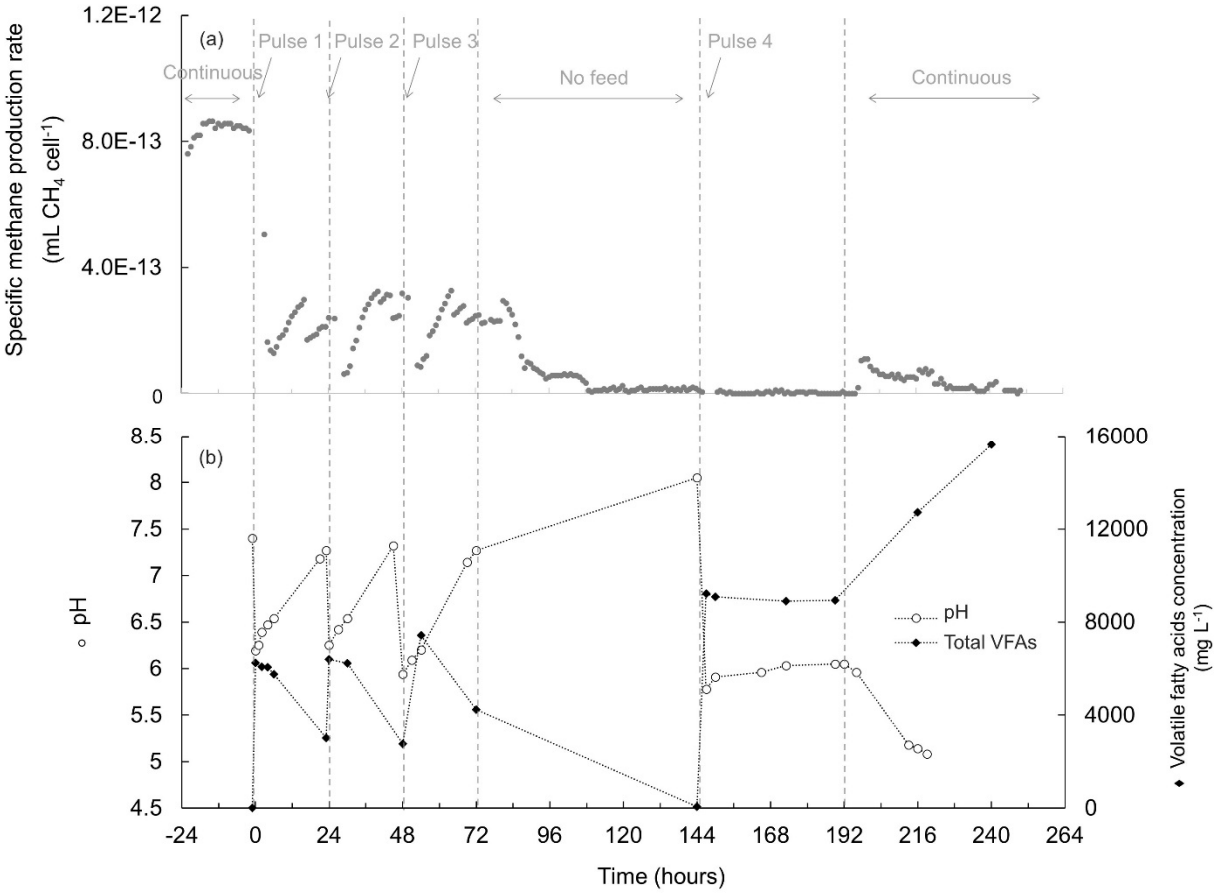


Figure 6.5 The evolution of the **(a)** specific methane production rate (●) and **(b)** pH (○) and total volatile fatty acids concentrations (VFAs) (♦) over the course of the 240 hours experimental period in *Reactor 2*. The applied pulses in the first 3 days of the experiment resulted in distinctive "saw-tooth like" profiles of the methane production rate, pH and VFA concentrations. The reactor recovered from all applied pulses in this period but the large COD pulse applied on 144 hours finally led to the envisaged acidification.

The first three pulses that were applied in Reactor 2 induced similar responses in specific methane production rate, pH and VFA concentrations. Despite the initial decrease in methane production rate, the production recovered around 6 hours after the pulse, albeit to a much lower value. A similar trend is observed for the pH and an opposite trend for

the substrate (i.e., the VFAs). After the accidental halting of the feeding 72 hours into the experiment, VFA concentrations recovered to pre-shock values whilst the pH further increased. Methane production gradually decreased to very low values during this period. The application of the last pulse had little impact on methane production, while VFA concentrations increased and pH decreased due to the feed. In contrast to previous pulses, the pH and VFA concentrations did not recover. Finally, the continuous feeding applied from 192 hours onward induced a temporary increase in methane production rate followed by a decline to almost zero. Simultaneously, VFA concentrations increased. The apparent slight increase in methane production rate is more likely CO_2 which was outgassed due to the declining pH. A lack of gas composition measurement around this time prevents correcting for this. Methane production most likely never recovered from the last applied pulse.

Cell numbers and cofactor content. Total cell numbers in Reactor 2, shown in Figure 6.6 – a, were slightly lower than in Reactor 1 and varied between 1.5 x 10^8 cells mL^{-1} and 3 x 10^8 cells mL^{-1}. F_{420}+ cells were also slightly lower, varying between 2 x 10^7 cells mL^{-1} and 8 x 10^7 cells mL^{-1}. A significant difference between the relative number in the beginning and at the end of the experiment was found. Figure 6.6 – b shows that the relative number decreased from 29.2 ± 2.0% in the beginning to 12.2 ± 0.5% at the end of this run, with significant fluctuations in between. Nevertheless, a similar average of 24.2 ± 1.0% was observed.

Figure 6.6 - c shows that both cofactor F_{430} quantification methods again yield very similar results. Despite the large error margin on the first measurement, F_{430} content seems to decrease immediately after the pulse was applied on time point zero. The relatively large standard deviations in the first 24 hours of the experiment, obscure most of the relative changes in F_{430} content. It seems, however, that cofactor content slightly increased again, after an initial decrease, by the time the second feeding pulse was applied, 23 hours after the first one. The second pulse led to another significant reduction in cofactor content and no recovery was observed by the time the third pulse was applied (48 hours after the first one). The erroneous halting of the feeding, 72 hours after the first pulse, seemed to have a positive effect on cofactor F_{430} content which is reflected in relatively higher measured contents on 72 and 144 hours. The fourth pulse which was then applied, again induced a clear decrease in F_{430} content, followed by recovery of the cofactor up until the re-introduction of continuous feeding 192 hours after the initial pulse. The application of continuous feeding from this point onward, led to a gradual but significant decrease in cofactor content over the course of the last 48 hours of the experiment. 240 hours after the initial pulse, the cofactor present in the sludge was only 3% of its initial value.

In Figure 6.6 – d again significant differences in the trends of both cofactor F_{420} quantification methods are observed. However, when comparing the F_{420} data from the fluorimetric quantification with the F_{430} content, again a very similar trend is observed. The cofactor F_{420} content at the end of the experiment is significantly lower than prior to the first pulse, however, its concentration relative to the initial concentration amounts to 11% which is three to four times higher than what was found for cofactor F_{430}.

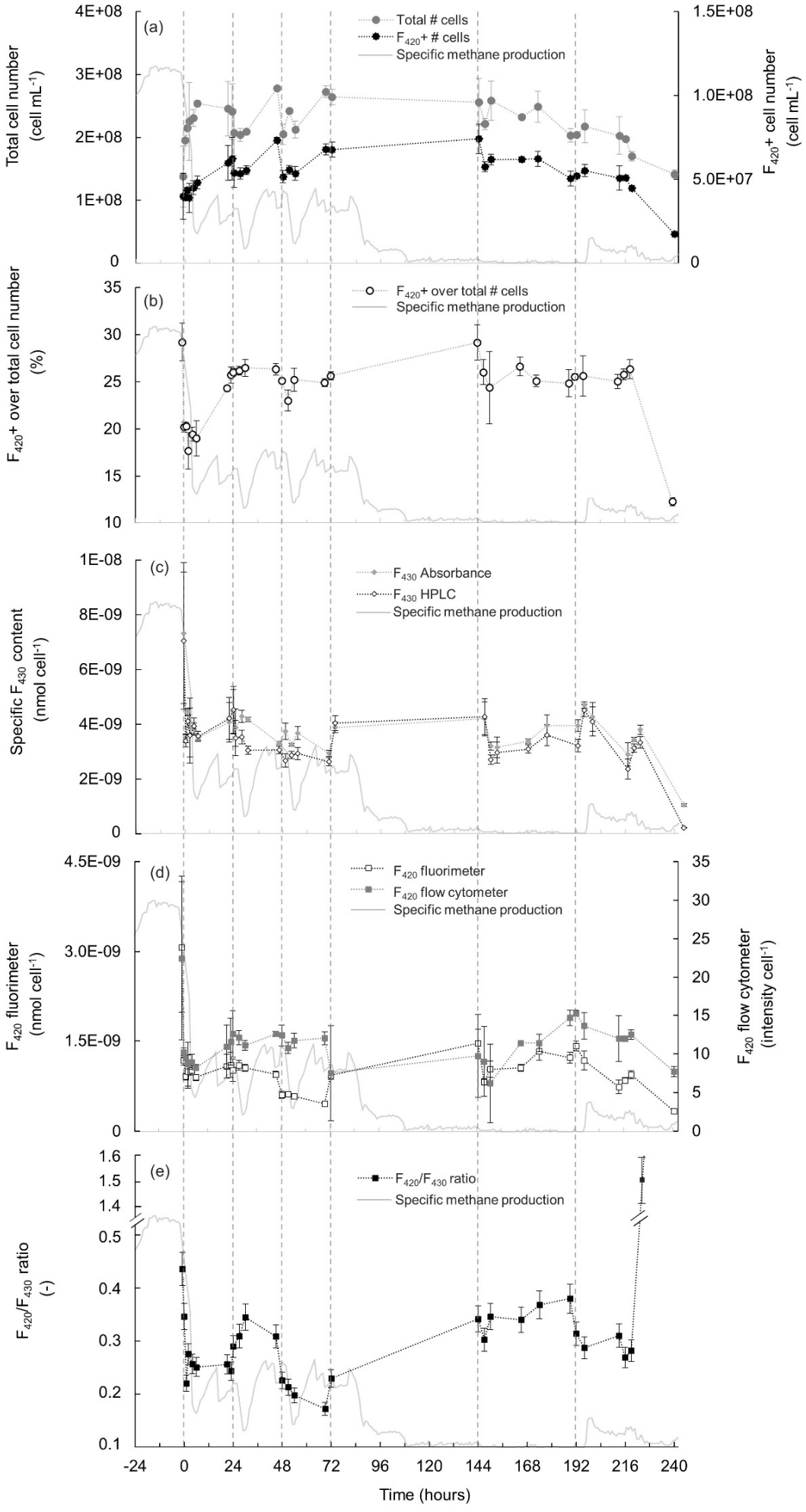

(a)
Total # cells
F420+ # cells
Specific methane production
Total cell number (cell mL-1)
F420+ cell number (cell mL-1)
4E+08
3E+08
2E+08
1E+08
0
1.5E+08
1.0E+08
5.0E+07
0
(b)
F420+ over total # cells
Specific methane production
F420+ over total cell number (%)
35
30
25
20
15
10
(c)
F430 Absorbance
F430 HPLC
Specific methane production
Specific F430 content (nmol cell-1)
1E-08
8E-09
6E-09
4E-09
2E-09
0
(d)
F420 fluorimeter
F420 flow cytometer
Specific methane production
F420 fluorimeter (nmol cell-1)
F420 flow cytometer (intensity cell-1)
4.5E-09
3.0E-09
1.5E-09
0
35
30
25
20
15
10
5
0
(e)
F420/F430 ratio
Specific methane production
F420/F430 ratio (-)
1.6
1.5
1.4
0.5
0.4
0.3
0.2
0.1
-24
0
24
48
72
96
120
144
168
192
216
240
Time (hours)

Figure 6.6 The evolution of **(a)** total (●) and F_{420}+ (●) cell numbers **(b)** F_{420}+ over total cell number ratio (○) **(c)** Specific F_{430} content measured by absorbance (♦) and HPLC (◊) quantification **(d)** specific F_{420} content measured by fluorimetry (□) and flow cytometry (■) and **(e)** F_{420} over F_{430} ratio calculated using the fluorimeter and HPLC quantification (■) over the 168 hour experimental period in *Reactor 2*. Error bars represent the (combined) experimental error on cell number and cofactor quantification. The specific methane production rate (—) was added to compare the trends (for absolute values see Figure 6.5). Significant differences between the relative numbers were found, most notably between the beginning and end of the experiment. Both F_{430} quantification methods and the F_{420} quantification using fluorimetry indicate a significantly lower cofactor content at the end of the experiment. Their ratio widely fluctuates with a disproportionally high value observed at the end of the experiment.

This observation also has important implications for the F_{420} over F_{430} ratio which is plotted in Figure 6.6 – e. The ratio which is typically between 0.17 ± 0.01 and 0.44 ± 0.03 in this experiment, is significantly higher at the end of the run. This is the only data point for which the cofactor F_{420} concentration exceeded that of F_{430}, yielding a relative F_{420} concentration of 1.5 ± 0.1. The average ratio, excluding the last data point, was 0.29 ± 0.02 over the course of the experiment in Reactor 2. Aside from the last data point, significant variations in the ratio were observed also over the rest of the course of the experiment.

The correlation analysis was repeated for Reactor 2 and the results are visualized in Figure 6.7. Considering the larger number of data points and the larger spread on most parameters, more significant correlations were expected.

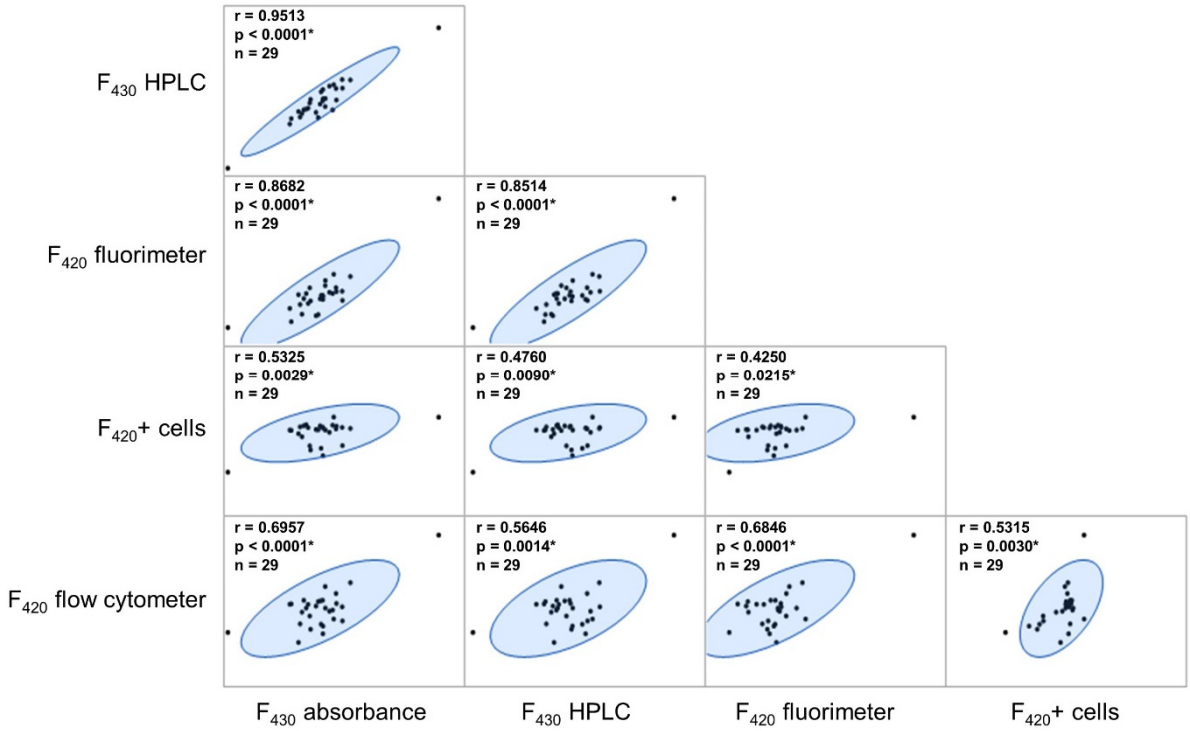


Figure 6.7 Plots showing the correlation coefficient (Pearson r), statistical significance (p), sample size (n) and 95% confidence interval (blue ellipses), between the evaluated monitoring tools for methanogenic activity in *Reactor 2*. Significant correlations (highlighted in bold) were found for all tested parameters, albeit with varying correlation strength and significance.

Indeed, Figure 6.7 shows the 10 significant correlations that were found in Reactor 2. Again, the top correlation pairs are the same as in Reactor 1. In addition to these, all of the tested parameters significantly correlate with one another, albeit with varying

strengths of correlation and significances. Some interesting ones to highlight are the correlation between the fluorescence intensity determined by flow cytometry and the F_{420} content determined by extraction and fluorimetry. Also interesting is the correlation between the number of F_{420}+ cells on the one hand, and F_{430} content, F_{420} content and fluorescence intensity determined by flow cytometry, on the other hand.

Molecular genetic analyses. The *mcrA* copy numbers were also determined in the beginning and end of the experiment in Reactor 2 and are shown in Table 6.5. Despite a relatively similar *mcrA* copy number per mL sample, the copy number per ng of DNA is an order of magnitude higher at the end of the experimental run. Considering that the average *mcrA* copy number per mL is actually lower in this sample, this implies a much lower total DNA concentration in the sample. Most likely an error was made when preparing or reporting on the DNA dilution.

Table 6.5 Average *mcrA* copy numbers and their standard deviations (triplicates), expressed per mL and per ngDNA, at the beginning and end of the experiment in *Reactor 2*. A limited difference is observed between the copy numbers per mL, the clearly higher copy number per ng DNA at the end of the experiment is most likely due to experimental errors.

Sample	Average *mcrA* copy number (copies mL^{-1})	Average *mcrA* copy number (copies $ngDNA^{-1}$)
Reactor 2 – begin (-1h)	$3.2 \times 10^{12} \pm 2.3 \times 10^{11}$	$1.3 \times 10^{6} \pm 9.4 \times 10^{4}$
Reactor 2 – end (240h)	$2.6 \times 10^{12} \pm 1.2 \times 10^{11}$	$1.1 \times 10^{7} \pm 5.3 \times 10^{5}$

Again, T-RFLP analysis was performed in order to obtain a relative abundance measure of the different methanogenic families present in Reactor 2. The results, shown in Table 6.6, indicate that the same families of acetotrophic *Methanosaetaceae* and hydrogenotrophic *Methanomicobiaceae* were most abundant throughout the experimental period. Again, the relative differences between the beginning and end samples likely fall within the margin of the experimental error on this analysis method.

Table 6.6 Results of the T-RFLP analysis providing a semi-quantitative indication of the relative abundance of acetotrophic and hydrogenotrophic methanogens in *Reactor 2*. Acetotrophic *Methanosaetaceae* and hydrogenotrophic *Methanomicrobiaceae* again dominated with relative abundances of 50-60% and 35-45%, respectively. *Methanosarsinaceae* species were not very abundant in this reactor.

Sample	Methanosaetaceae (%)	Methanomicrobiaceae (%)	Methanosarcinaceae (%)
Reactor 2 – begin (-1h)	57	36	1
Reactor 2 – end (240h)	50	45	0

Control Reactor

Overall reactor performance. In the control reactor a stable pH of around 7.3 was measured as well as relatively steady methane production rates (between 2 and 5 x 10^{-13} mL CH_4 $cells^{-1}$). The evolution of the pH and methane production rates in the control reactor are shown in Figure 6.8.

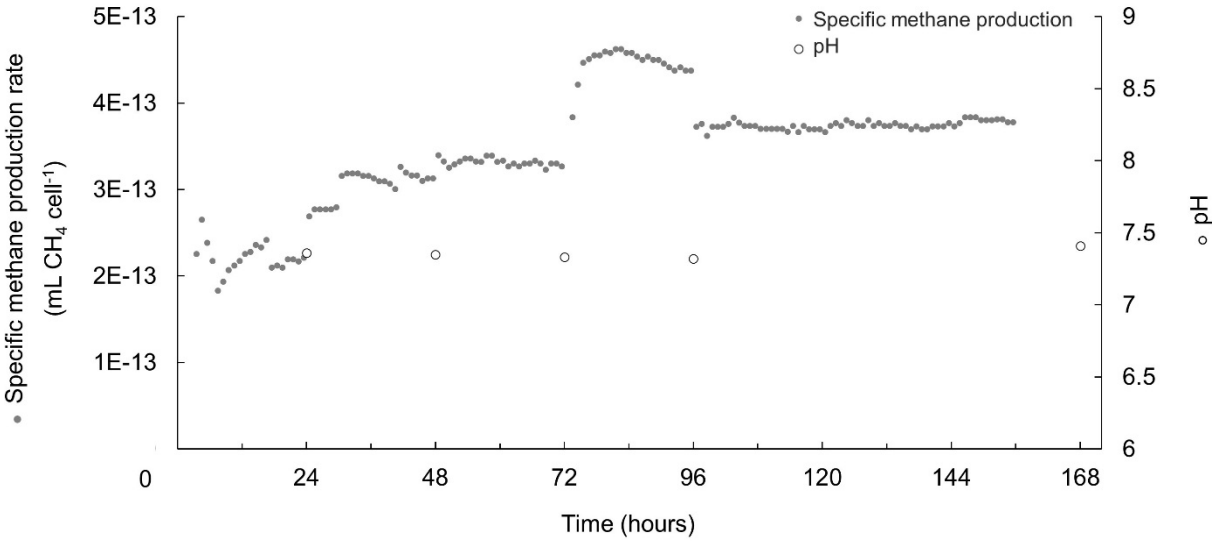


Figure 6.8 The evolution of the specific methane production rate (●) and pH (○) over the course of a 168 hours operational period in the *Control Reactor*. The reactor is characterized by a stable pH and relatively stable methane production rates.

Cell numbers and cofactor content. To be able to ascribe any observed changes in the monitoring tools to operational conditions, the data of the experimental reactors should be compared with that of the Control Reactor. Figure 6.9 shows all the monitoring tools plotted alongside the methane production rate (in grey) in the Control Reactor.

Relatively stable total and F_{420}+ numbers are observed during the 168 hours of stable operation (Figure 6.9 – a). However, some significant changes in the F_{420}+ over total cell number ratios were found (Figure 6.9 – b).

The specific cofactor F_{430} and F_{420} contents are similar to those measured at the beginning of the experiment in both experimental reactors and stable throughout the 168 hours operation of the Control Reactor (Figure 6.9 – c and d). The higher cofactor F_{430} content measured for the last data point could reflect a slight increase in methane production which was observed towards the end of the run. The F_{420} over F_{430} ratio does not significantly vary and is around 0.20 - 0.30 throughout the course of the experiment (Figure 6.9 – e).

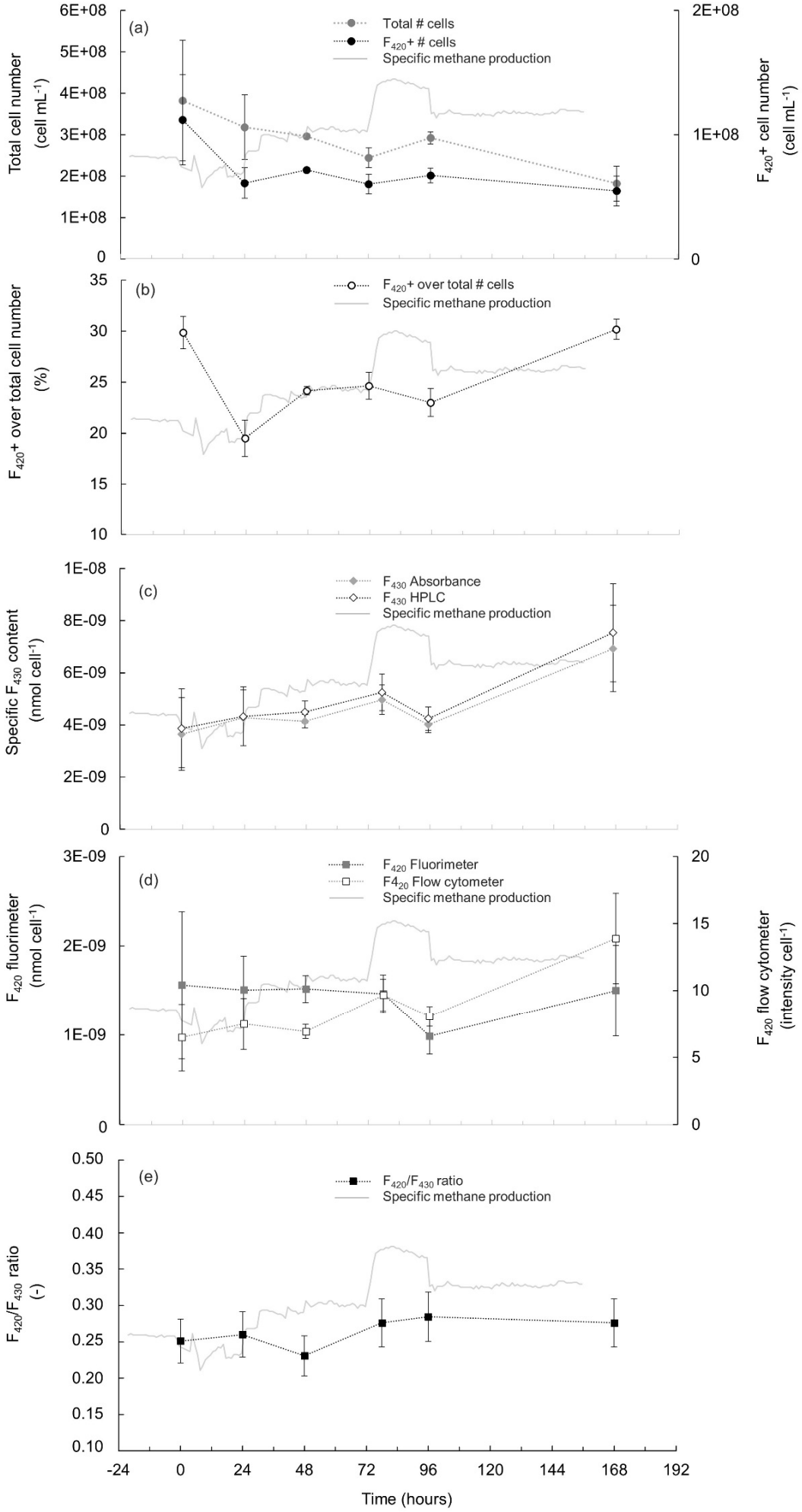

(a)
Total # cells
F420+ # cells
Specific methane production
Total cell number (cell mL-1)
F420+ cell number (cell mL-1)
6E+08
5E+08
4E+08
3E+08
2E+08
1E+08
0
2E+08
1E+08
0
(b)
F420+ over total # cells
Specific methane production
F420+ over total cell number (%)
35
30
25
20
15
10
(c)
F430 Absorbance
F430 HPLC
Specific methane production
Specific F430 content (nmol cell-1)
1E-08
8E-09
6E-09
4E-09
2E-09
0
(d)
F420 Fluorimeter
F420 Flow cytometer
Specific methane production
F420 fluorimeter (nmol cell-1)
F420 flow cytometer (intensity cell-1)
3E-09
2E-09
1E-09
0
20
15
10
5
0
(e)
F420/F430 ratio
Specific methane production
F420/F430 ratio (-)
0.50
0.45
0.40
0.35
0.30
0.25
0.20
0.15
0.10
-24
0
24
48
72
96
120
144
168
192
Time (hours)

Figure 6.9 The evolution of **(a)** total (●) and F_{420}+ (●) cell numbers **(b)** F_{420}+ over total cell number ratio (○) **(c)** Specific F_{430} content measured by absorbance (♦) and HPLC (◊) quantification **(d)** specific F_{420} content measured by fluorimetry (□) and flow cytometry (■) and **(e)** F_{420} over F_{430} ratio calculated using the fluorimeter and HPLC quantification (■) over the 168 hour experimental period in the *Control Reactor*. Error bars represent the (combined) experimental error on cell number and cofactor quantification. The specific methane production rate (—) was added to compare the trends (for absolute values see Figure 6.8). Both the total and F_{420}+ numbers show almost no significant changes in function of time, however, their ratio does change significantly. Both the cofactor F_{430} quantification methods indicate a relatively stable F_{430} content, F_{420} content also remains relatively stable - as does their ratio.

To conclude this part, in Figure 6.10 the correlations between the different parameters proposed as monitoring tools for methanogenic activity are shown over all three reactors lumped together. Based on at least 50 measurements, all monitoring tools and methods correlated significantly with one another. Again, the strongest correlation is found between the two F_{430} quantifcation methods and between cofactor F_{430}, on the one hand, and the quantification of F_{420} by extraction and fluorimetric quantification, on the other hand.

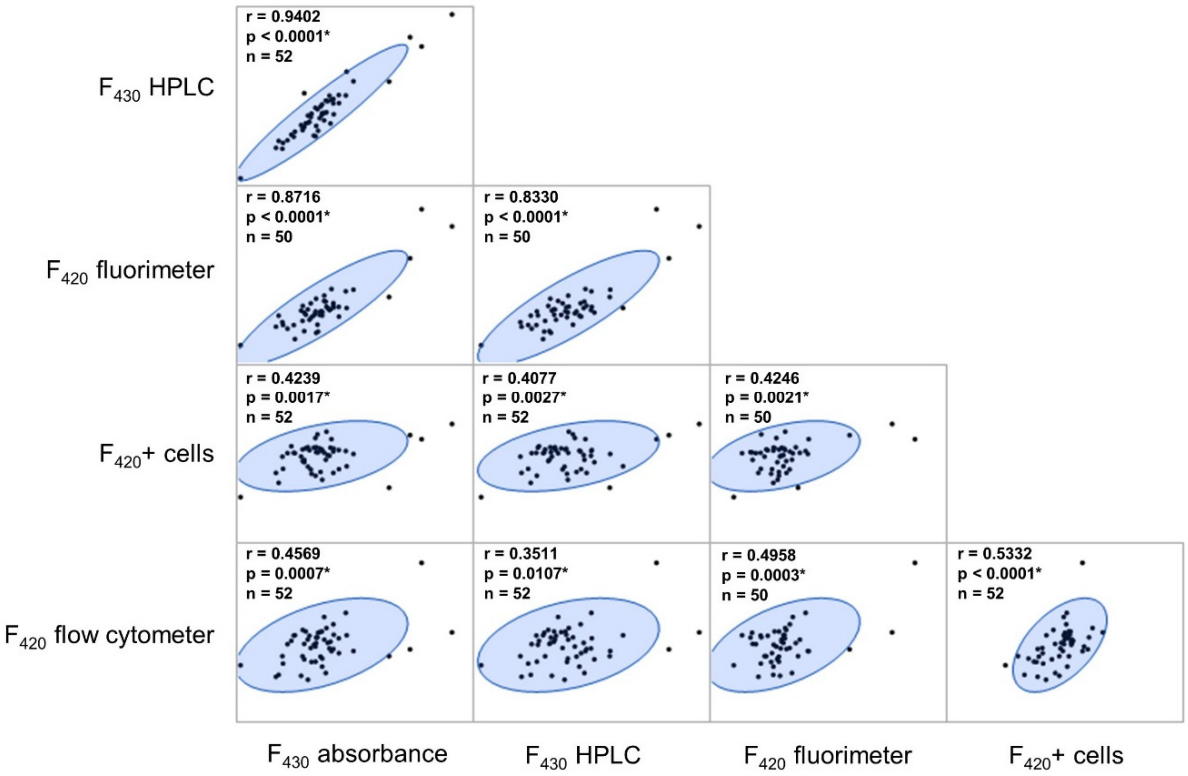


Figure 6.10 Plots showing the correlation coefficient (Pearson r), statistical significance (p), sample size (n) and 95% confidence interval (blue ellipses), between the evaluated monitoring tools for methanogenic activity, lumped *over all three reactors*. Based on at least 50 measurements, significant correlations (highlighted in bold) were found for all tested parameters, albeit with varying correlation strengths and significances.

6.1.3 Discussion

Response of the methanogens to the induced process upsets

The operational data presented in Figure 6.2 and Figure 6.5 clearly suggests varying methanogenic activity in both pulse impacted reactors during the experimental period,

compared to the Control Reactor (Figure 6.8). The saw-tooth like profile of methane production rate, pH and VFAs in Reactor 2 illustrates this most clearly. The total and F_{420}+ cell number data indicates that the pulse applied in Reactor 1 did not lead to the desired reactor acidification and inhibition of methanogenesis. Despite a temporary effect on the F_{420}+ over total cell number ratio, a significantly higher value was measured at the end of the experiment, indicating full recovery and, in fact, possibly higher activity than in the beginning of the experiment. It is also evident that this was not attributable to increased methanogen growth, but rather increased activity, since *mcrA* copy numbers did not significantly increase towards the end of the experiment. Indeed, increased methanogen growth would not have been expected on such short time scales (Zhang & Noike, 1994; Dereli *et al.*, 2012) and recent reports have shown that *mcrA* copy numbers may remain constant whereas the *mcrA* transcript numbers follow the methane production dynamics (Munk *et al.*, 2012). The cofactor F_{430} and F_{420} data confirm the hypothesis of increased activity as significantly higher contents were measured at the end of the experiment. Munk *et al.* (2012) observed similar short-term changes in the *mcrA* gene transcript over copy number ratio, corroborating the *activity* rather than *presence* hypothesis. In the Control Reactor, these parameters remained relatively constant, although a slight increase in cofactor F_{430} content was observed towards the end of its run. In summary, Reactor 1 proved to be resilient towards the applied OLR pulse and the temporary inhibition followed by recovery was well-reflected by the cofactor contents and some of the parameters determined by flow cytometry.

In Reactor 2, the final objective was to completely inhibit the methanogenesis. The operational data (Figure 6.5) indicates that, despite an initial drop in methane production rate, this reactor also showed great resilience to the applied upsets. For instance, the F_{420}+ over total cell number ratio (Figure 6.6) shows a clear initial decrease and then recovers and responds only slightly to the subsequent shocks. The same is true for both cofactor contents. Such short-term dynamic cofactor profiles have not been reported in literature but the resilience after a process upset, which they indicate, is in accordance with reports of similar behaviour of the *mcrA* gene transcript over copy numbers (Munk *et al.*, 2012). Considering that the samples taken on time point zero, were in contact with the added VFAs for only about 10 to 15 minutes (they were taken immediately after adding the substrate and during sample preparation the supernatant was either discarded or replaced), the clear drop in both F_{420} and F_{430} content compared to the "-1h" sample is remarkable. This is an interesting result from a fundamental point of view, since it provides insights into the mechanism of cofactor responses to externally applied stresses. The fast drop in cofactor contents implies that the methanogens immediately reduce their production of both cofactors, as soon as adverse conditions such as low pH and high VFA concentrations are sensed by the cells. Indeed, the reduced cofactor content cannot be attributed to degradation on such a short timescale (considering the expected half-lives) and should therefore be attributed to reduced production. Alternatively, the very sharp decrease in pH may have caused cell lysis of a part of the methanogens. As a result, their cofactors are released extracellularly and are not included in the quantification (which only measures intracellular cofactor). However, given that the number of cells did not decrease in the same way, this hypothesis is less likely.

The accidental halting of the feeding between 77 and 144 hours allowed the reactor to further recover from the previously applied shocks. Indeed, all VFAs were quite quickly consumed (indicating considerable residual methanogenic activity) and, subsequently, the reactor likely went into a starvation period. Despite the lack of substrate and absence of methane production, cofactor contents remained on the same level. In the previous sections it was already shown that although cofactor F_{430} content correlates with methane production rate, it also remains present inside the sludge for some time after methane production has halted. Nonetheless, based on the F_{430} half-life calculated in Chapter 5, at least some degradation was expected. However, in this experiment starvation, and not inhibition, was the cause of the reduced methane production. The residual cofactor contents may then have indicated that the methanogens were expecting additional substrate to be supplied and, therefore, maintained their cofactor concentrations. Despite this residual methanogenic potential, the final pulse which was then applied on 144 hours did not lead to increased methane production. It is likely that the amount of COD that was added at once was just too much to handle for the methanogens and the concomitant pH decrease by 2 units inhibited their activity. Nevertheless, after an initial decrease in both cofactor contents, after 48 hours they recovered, despite the severity of the pulse. Surprisingly, this was not accompanied by a recovery in methane production and VFAs were not consumed, in contrast to the previous pulses. The methanogens were thus not using their cofactors for methane production. Indeed, in this phase of the experiment there seems to be a mismatch between the cofactor concentration present and the methanogenic activity. It was not until the re-introduction of continuous feeding, causing additional accumulation of VFAs and a significant pH decrease that cofactor contents started decreasing towards the end of the experiment. In summary, Reactor 2 showed resilience against several applied overfeeding shocks. Although the cofactor contents did not correlate with the real-time methane production rate at all times, they did indicate the recovery of methanogenic activity after these pulses. In the last part of the experiment, residual cofactor content was present when new substrate was added to the reactor, but methane production rate never recovered, likely due to the severity of this last pulse combined with the re-introduction of continuous feeding, leading to acidification.

In general, cofactor F_{430} and F_{420} concentrations in all three reactors were significantly higher (2 to 5 times) than in previous experiments (between 1000 - 1800 nmol gVS^{-1} and 250 – 600 nmol gVS^{-1} respectively) and in the range of reports for pure cultures (Diekert *et al.*, 1981). This results from the fact that the inocula were enriched in methanogens, which accounted for about 80% of all prokaryotes on genome level. The T-RFLP data suggests that more than half of these methanogens belonged the family of acetotrophic *Methanosaetaceae* whereas 30–40% belonged to the family of hydrogenotrophic *Methanomicrobiaceae* in both experimental reactors. The presence of methanogens belonging to the family of *Methanosarcinaceae* may be attributable to small disturbances in the reactor used to inoculate Reactor 1. These small disturbances may have temporarily increased the VFA concentrations and partial H_2 pressure, which favours the growth of these methanogens, whereas they are generally absent when VFA and H_2 concentrations are low (Conklin *et al.*, 2006).

The rationale for calculating the F_{420} over F_{430} ratio is based on the different prevalence of cofactor F_{420} in hydrogenotrophic compared to acetotrophic methanogens, whereas cofactor

F_{430} is known to be present in all methanogens (see Section 2.1.5). As such, the ratio of F_{420} over F_{430} for a given number of cells may be an indication of presence or activity of hydrogenotrophic methanogens (Kida *et al.*, 2001). Interestingly, the average ratios in all three reactors corresponded quite well with the relative abundance of hydrogenotrophic methanogens measured at the beginning and end of each experiment by T-RFLP. However, the ratio fluctuates widely in both experimental reactors, whereas it is relatively stable in the Control Reactor. This indicates that relative changes in cofactor F_{430} and F_{420} production and degradation occurred over the course of these experiments as a result of the applied pulses. Indeed, the measured cofactor concentrations are expected to be the net result of cofactor production and degradation. Because of the impact of both production and degradation kinetics and due to the fast succession of the pulses it is difficult to relate the changes in the ratios to changes in operational conditions. In some cases, a pulse seems to induce a reduction in the ratio, whereas in others an increase or no significant change is observed. From these results, it is unclear whether the F_{420} over F_{430} ratio reflects the current hydrogenotrophic methanogenic activity well in this type of experiment. It is likely that the observed variations are more related to differences in the degradation kinetics between the cofactors, than to differences in hydrogenotrophic and acetotrophic activity. In fact, the very high F_{420} over F_{430} ratio at the end of the experiment in Reactor 2, reflects that F_{420} degradation was slower than that of F_{430} when production of both had likely halted due to inhibition at low pH (pH < 5.5).

Correlations between the different experimental approaches for methanogen monitoring

Although not all measurements reflected well the methanogenic activity at every point in time, correlations between the different methods were determined. Figure 6.4, Figure 6.7 and Figure 6.10 summarize these correlations between the different parameters proposed as monitoring tools for methanogenic activity. The different approaches can be divided into methods including extraction and quantification of the sample on the one hand, and in-situ quantification on live cells using flow cytometry, on the other hand.

First, it is clear that in these experiments the additional purification on HPLC had relatively little impact on cofactor F_{430} quantification since it correlated very strongly with the simple, preliminary quantification by spectrophotometry. This is because of the very "clean" nature of these sludge samples. Indeed, no suspended solids or other interfering components are introduced via the feed, which consists of completely dissolved VFAs. Early investigations on F_{430} contents in pure cultures also successfully used the spectrophotometric quantification approach (Diekert *et al.*, 1981). Second, both F_{430} quantification methods correlate strongly with the fluorimetric quantification of F_{420}. Thus, in these experiments, both cofactor contents responded similarly to the induced upsets. Nonetheless, small differences in their production and degradation kinetics yielded significant differences in their ratios as discussed in the previous paragraphs.

With respect to the flow cytometric methods, Figure 6.10, indicates that measuring the bulk fluorescent intensity of the samples yields similar information as the extraction and fluorimetric quantification but not in all cases, as is evidenced by the lower Pearson correlation coefficient and significance. Furthermore, the amount of F_{420}+ cells correlates with all of the other cofactor measurements but seems to be inferior since it does not take into account the varying fluorescent intensity of each cell. Based on its very strong

correlation with the cofactor F_{430} content, the extraction and fluorimetric quantification is still preferred. Indeed, a biological hypothesis (i.e., the abovementioned similar response to process upsets of both cofactors) can be formulated as to why F_{430} and F_{420} would correlate and the fluorimetric quantification of F_{420} clearly correlated more strongly with F_{430} than the flow cytometric quantification. The following explanations can be formulated for the differences between fluorimetry and flow cytometry.

(i) The fluorimetric approach relies on the lysis of the cells and the extracellular quantification of the fluorescence. All cofactor molecules in the extracts are expected to be in the oxidized state (which is the fluorescent state) and to experience the same alkaline pH. However, in the flow cytometric approach the cells are intact and the exact F_{420} oxidation state and the pH in the cell are unknown, whereas these are known to influence the fluorescence intensity (Cheeseman *et al.*, 1972). Because of the applied shocks it is reasonable to assume that at least the (intracellular) pH differed throughout the experiments and may have influenced the total fluorescence.

(ii) The flow cytometric method uses a fluorescence threshold in order to determine whether a cell is counted or not, it then takes all of the cells above this threshold and multiplies these by the mean fluorescence intensity. The threshold is chosen manually and is applied to all samples. If, e.g., the pH or redox state has influenced the fluorescent intensity as discussed in *(i)*, then multiple cells may be excluded whereas their actual F_{420} content may not be lower.

(iii) Finally, the clustering of cells is also a general problem in flow cytometric quantification methods. Although this issue is addressed through proper sample preparation it may still be a phenomenon to take into account. Especially if, because of the induced process upsets, the microorganisms e.g., tend to cluster together as a response to the stress they experience. In that case also differences may be induced between samples from stable and disturbed periods.

Regardless of these remarks, the flow cytometric methods have a lot of potential with respect to sorting different communities of methanogens based on their fluorescence (Lambrecht *et al.*, 2017). This "fingerprinting" of the methanogenic communities was not included in this PhD thesis, as the focus is on measures of methanogenic activity rather than the community structure.

In summary, short-term feeding pulses induced organic overloading and were reflected in lower cofactor contents but as long as sufficient cofactor is present, the reactor is resilient and can resume methane production when the adverse conditions are alleviated. Cofactor F_{420} clearly correlated with cofactor F_{430} in these experiments and the extraction and quantification by fluorimetry seemed superior to flow cytometric quantification. The F_{420} over F_{430} ratio related quite well to the relative abundance of hydrogenotrophic methanogens, although this could only be validated for the initial and final measuring points of each experiment. Furthermore, the *mcrA* gene copy numbers seem to not reflect the (changes in) actual methanogenic activity well (admittedly only based on an initial and final value), highlighting the need for *mcrA* transcript number quantification. Finally, due to the frequency of the subsequent pulses, the cofactor's production and degradation

kinetics are obscured in this experiment. In the next experiment less pulses but a very dedicated follow-up, including *mcrA* transcript numbers, will address these unanswered research questions.

6.2 Do cofactor and *mcrA* gene dynamics reflect the methane production dynamics in an anaerobic membrane bioreactor subjected to organic loading rate shocks?

The previous experiment provided additional insights into the use of cofactors F_{430} and F_{420} to monitor process disturbances. As some research questions remain, the aim of the following experiment is to:

(i) re-evaluate the observed evolution of the cofactor F_{430} and F_{420} concentration in a continuously operated AnMBR system subjected to two consecutive OLR shocks;
(ii) assess the evolution of the cofactor concentrations during the critical start-up phase;
(iii) determine the cofactor production and degradation dynamics more precisely, and;
(iv) compare the cofactor F_{430} dynamics to *mcrA* gene dynamics.

The OLR shocks that are applied in this experiment are more gradual and less frequent than the short-term pulses applied in the previous experiment. The reactor is allowed to recover completely and the next OLR shock is applied after a period of stable reactor operation. These operational choices avoid that cofactor and *mcrA* dynamics are obscured by the previous shock. Furthermore, the follow-up of the start-up phase may serve as a first indication whether the proposed tools can be used to more effectively evaluate and steer reactor performance during start-up.

In addition, *mcrA* transcript numbers are quantified on top of the copy numbers. As discussed in Section 2.1.4, recent publications have highlighted the importance of including transcript numbers in order to capture the trends in methanogenic activity (Watanabe *et al.*, 2009; Ma *et al.*, 2012; Zhang *et al.*, 2014). Their ratio is calculated and used as a benchmark tool for methanogenic activity monitoring. Considering the promising results of the *mcrA* gene as a process monitoring tool in anaerobic reactors reported in literature, in this experiment it is investigated whether monitoring on the enzymatic (or metabolic) level (i.e., cofactor F_{430} and F_{420}) may prove to be equally valuable - potentially decreasing analysis time, complexity and cost - while still providing information directly related to methanogenic activity. Indeed, considering cofactor F_{430}'s role as the prosthetic group of the MCR enzyme, monitoring its concentration could yield similar information as MCR enzyme or *mcrA* gene concentration monitoring.

6.2.1 Materials & methods

AnMBR experimental set-up and feeding strategy

A schematic of the used lab-scale AnMBR set-up is shown in Figure 6.11. The reactor consisted of a 12.2 L double-walled glass vessel and was continuously stirred by a magnetic stirrer. The reactor was fed with a milk powder based synthetic feed (see also Table 3.1). The milk powder was used as a carbon source and was pulse-fed separately in concentrated form every 78 minutes. Dilution of the concentrated feed occurred by diluting with tap water by means of a peristaltic pump (Masterflex, Model No. 7518-00) controlled by a vibronic level sensor (Endress+Hauser, Liquiphant T FTL20), thereby keeping the reactor volume constant. A buffer solution (10 mM KH_2PO_4, 10 mM K_2KHPO_4, 20 mM $NaHCO_3$), macro-nutrient solution (500 mg L^{-1} NH_4Cl, 200 mg L^{-1} $CaCl_2.2H_2O$, 100 mg L^{-1}

$MgCl_2.6H_2O$, 122.5 mg L^{-1} $Fe_2(SO_4)_3.5H_2O$) and trace element solution (500 µg L^{-1} $NiSO_4.6H_2O$, 500 µg L^{-1} $MnCl_2.4H_2O$, 500 µg L^{-1} $FeSO_4.7H_2O$, 100 µg L^{-1} $ZnSO_4.7H_2O$, 100 µg L^{-1} H_3BO_3, 36 µg L^{-1} $(NH_4)_6Mo_7O_{24}.4H_2O$, 50 µg L^{-1} $COCl_2.6H_2O$, 5 µg L^{-1} $CuSO_4.5H_2O$) were prepared, according to De Vrieze *et al.* (2013) and supplemented through a Watson Marlow pump (Model No. 205U). The reactor was maintained at 37 °C by circulating warm water originating from an external water bath through its water jacket. Temperature and pH were continuously monitored and logged using a pH-meter (Knick, Portavo 907 Multi). The produced biogas was bubbled through a concentrated (100 g L^{-1}) KOH solution to strip out acid gases (CO_2 and H_2S). The alkaline solution contained 5 mL of a blue pH indicator (80 mg thymolpthalein in 18 mL ethanol and 2 mL distilled water) turning colourless below a pH of 9.3 indicating that the solution had to be replaced when most alkalinity is neutralized. The methane was quantified by a liquid displacement system, coupled to an optical sensor with display, by counting the amount of times a calibrated oil volume was displaced. Methane production rates were normalized to 0 °C and 1 atm. The mixed liquor was pumped through a 2 m long tubular, inside-out polyvinylidene fluoride (PVDF) ultrafiltration membrane (PENTAIR, USA) using a screw pump (Seepex, MD 025-6 L). The membrane had a mean pore size of 0.03 µm and a surface of 0.0327 m^2. Unless otherwise indicated, the membrane was operated at constant flux mode at a low flux of 5 L m^{-2} h^{-1} in order to assure long term operation without excessive transmembrane pressure increases.

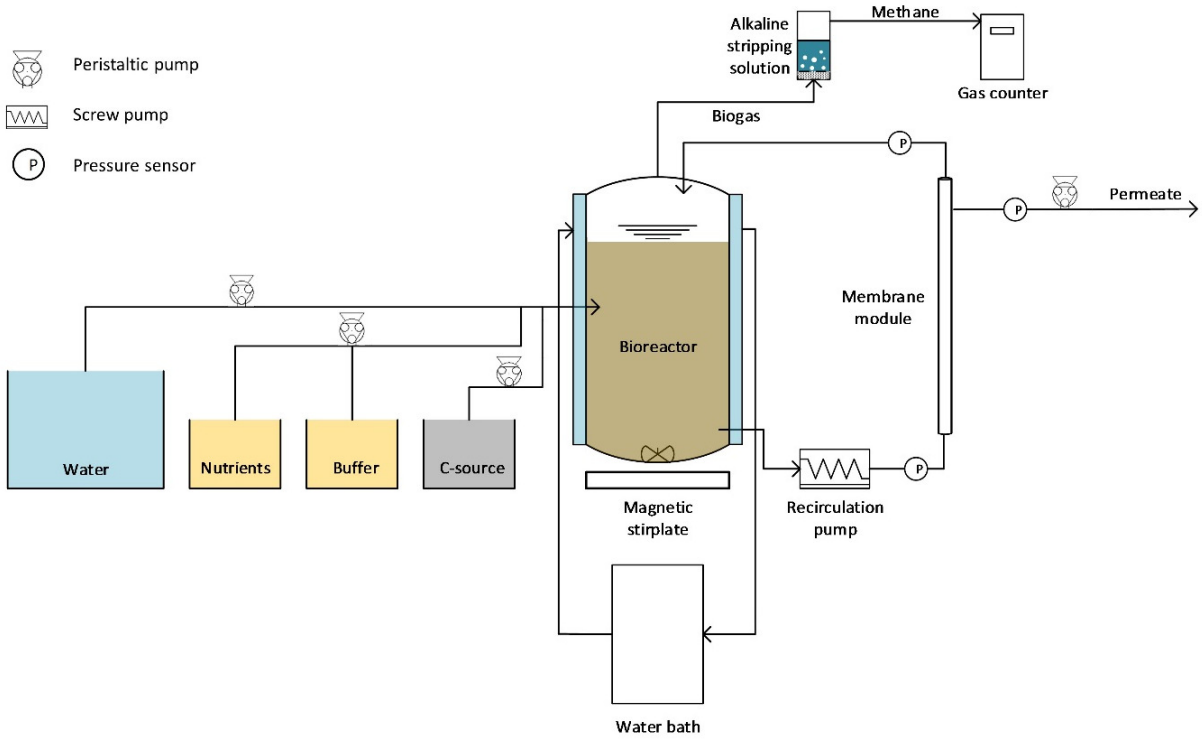


Figure 6.11 Schematic representation of the lab-scale anaerobic membrane bioreactor (AnMBR) setup. An external ultrafiltration membrane module was used to extract the purified effluent while recirculating the biomass to the bioreactor.

Effluent was produced by a peristaltic pump (Masterflex, Model No. 7518-00) with a filtration cycle including a relaxation stage (13.2 minutes filtration, 1.2 minutes relaxation). The transmembrane pressure (TMP) was calculated as the difference between the pressure at the inlet of the membrane module and the pressure on the permeate side,

measured by two pressure transducers (Omega engineering). The pressure measurement data were acquired with a DAQ card (National Instruments, USB-6009) and read-out and logged using LabVIEW (National Instruments, 2015 version).

The lab-scale AnMBR was seeded with granular sludge from a brewery, which was sieved and crushed beforehand to remove coarse particles and, partly, break the granules. The initial total suspended solids (TSS) and volatile suspended solids (VSS) concentrations in the 12.2 L reactor were 8.12 g L^{-1} and 5.04 g L^{-1}, respectively. Sludge was wasted from the system only for sampling during the first 3 weeks of operation, resulting in an average solids retention time (SRT) of 280 days. Afterwards additional sludge was wasted regularly in order to maintain sludge concentrations below 20 g L^{-1}, resulting in an SRT of approximately 60 days.

The organic loading rate (OLR) was gradually increased during the start-up by increasing the concentration of the synthetic milk powder in the feed while keeping the hydraulic retention time (HRT) and membrane flux constant. Evidently, during the OLR shocks, the milk powder concentration significantly increased (i.e., from 6 gCOD L^{-1} to 23 gCOD L^{-1} during the first OLR shock period and from 3 gCOD L^{-1} to 12 gCOD L^{-1} during the second OLR shock).

Based on the applied loading rates, the experimental run can be divided into 5 phases: start-up from day 0 to 21 (phase I), first organic loading rate shock from day 21 to 29 (phase II), recovery toward stable conditions from day 29 to 42 (phase III), second organic loading rate shock from day 42 to 56 (phase IV), and recovery from day 56 onwards (phase V). The different phases are depicted in Figure 6.12 in a graph showing the applied organic and sludge loading rates over time.

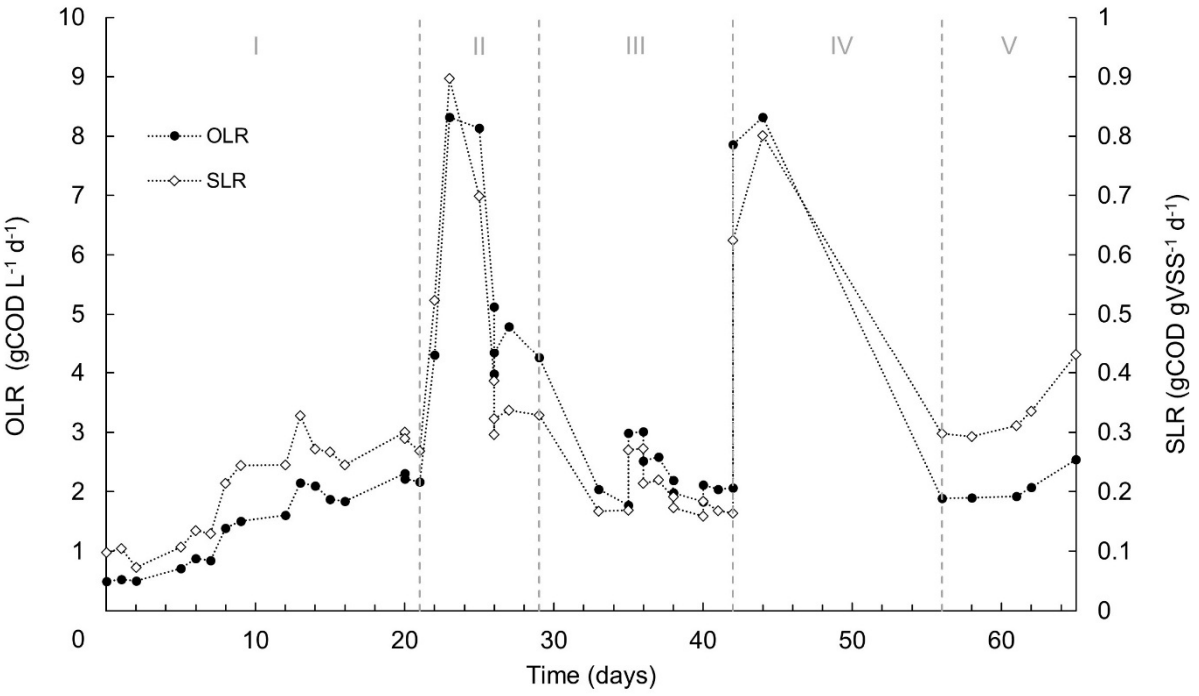


Figure 6.12 The organic (●) and sludge loading (◊) rates (SLR and OLR, respectively) applied over the 65 days experimental period. After the start-up phase (I), two organic OLR shocks were applied (phases II and IV) followed by their respective recovery phases (III and V). Due to variations in sludge concentration organic and sludge loading rates do not evolve in the same way. An SRT of approximately 60 days was maintained after the first three weeks of operation.

Reactor performance and stability throughout these phases were assessed using the conventional parameters such as (specific) methane production, VFA concentrations, pH, and bioreactor and effluent soluble COD (sCOD) concentration.

Analytical methods

The analytical methods used in this experiment have been described in the general material & methods section (Chapter 3). The following parameters were analysed.

- (Volatile) Suspended solids
- COD
- Total and individual VFA concentrations

Molecular genetic analyses

Nucleic acids extraction

The procedure for DNA and RNA extraction has been described in Section 5.2.1.

mcrA gene quantification

Complement DNA (cDNA) was synthesized from community mRNA using the RevertAid H Minus First Strand cDNA Synthesis Kit (ThermoFischer, Cat. K1632). One µL of purified mRNA (70 ng μL^{-1}) and 1 µL of random hexamer primer were incubated at 65 °C for 5 min and subsequently cooled on ice. After adding 4 µL reaction buffer (250 mM Tris-HCl pH 8.3, 250 mM KCl, 20 mM $MgCl_2$, 50 mM DTT), 1 µL RiboLock RNase Inhibitor (10 u μL^{-1}), 2 µL dNTP Mix (10 mM) and 1 µL RevertAid H Minus M-MuLV Reverse Transcriptase (20 u μL^{-1}), reverse transcription (RT) was performed in a Biometra PCR Cycler. The RT reaction conditions were 25 °C for 5 min, 42 °C for 60 min followed by heat-inactivation at 70 °C for 5 min, after which the mixtures were stored at -80 °C prior to qPCR. A no-template negative control and a GAPDH positive control were included. Quantification of *mcrA* gene copies or *mcrA* transcript copies was performed by quantitative PCR (qPCR) on community DNA and cDNA, respectively. The used primer pair consisted of forward primer mcrF (5′-GGTGGTGTMGGATTCACACARTAYGCWACAGC-3') and reverse primer mcrR (5′-TTCATTGCRTAGTTWGGRTAGTT-3') (Luton *et al.*, 2002). The reaction mixture contained 1 µL of 100-fold diluted community DNA extract or community cDNA, 7.5 µL ABsolute qPCR SYBR Green Mix (ThermoFisher, Cat. AB1158B), 0.3 µL of 10 µM forward primer mcrF, 0.3 µL of 10 µM reverse primer mcrR, 1.5 µL of a 1% w/v Bovine Serum Albumin solution and 2.4 µL of Nuclease/DNA-free water. The qPCR was performed in a Rotorgene 3000 (Corbett Research) using the following conditions: 95 °C (5 min) followed by 39 cycles of 20 s at 95 °C, 20 s at 58 °C, 20 s at 72 °C and a final extension step of 5 s at 80 °C. Standard curves were prepared from serial dilutions of a prequantified *mcrA* PCR fragment amplified using primers mcrF and mcrR from a plasmid extract carrying the complete *mcrA* gene using concentrations ranging from $1x10^3$ to $1x10^8$ copies μL^{-1}. Transcript number over gene copy number ratios were normalized on a total nucleic acids concentration basis (DNA and mRNA) from each sample.

Methanogenic community structure

Using the extracted DNA, the abundance of species belonging to the methanogenic orders *Methanobacteriales* and *Methanomicrobiales* as well as the families *Methanosaetaceae*

and Methanosarcinaceae were determined at the Center for Microbial Ecology and Technology of Ghent University. Real-time qPCR was performed on a StepOnePlus Real-Time PCR system (Applied Biosystems, Carslbad, CA, USA). The reaction mixture consisted of 10 µL of GoTaq PCR Master Mix (Promega, Madison, WI, USA), 3.5 µL of nuclease-free water and 0.75 µL of each primer (final concentration of 375 nM), to which 5 µL of template DNA was added. The qPCR program for the order *Methanobacteriales* and the families *Methanosaetaceae and Methanosarcinaceae* consisted of a predenaturation step of 10 min at 94 °C, followed by 40 cycles of 10 s at 94 °C and 1 min at 60 °C. For the *Methanomicrobiales* order an annealing temperature of 63 °C was used. The primers that were used are described in Yu *et al.* (2005).

Cofactor F_{430} and F_{420}

Cofactor F_{430} was extracted and quantified using Protocol 4 (Table 4.1) as described in Section 4.1.2. Additional identification and purity checks were performed as described in Section 4.1.3. Duplicate analysis of eight of the samples indicated an experimental error (standard deviation) of 11% on average on the entire sampling, extraction and HPLC quantification procedure

Cofactor F_{420} was extracted and quantified using the fluorimetry method, as described in Section 4.2.2.

6.2.2 Results

The different phases shown in Figure 6.12 are described here in terms of overall reactor performance, *mcrA* gene copy and transcript number and cofactor F_{430} and F_{420} content.

Overall reactor performance

Figure 6.13 shows that the start-up period was characterized by an increasing methane production (following the step-wise increases in OLR), high biological and total COD removals (higher than 96% and 89%, respectively) and low VFA concentrations (below 100 mg L^{-1}). In contrast, the shock events (phases II and IV) were characterized by a short and slight increase in methane production, followed by a sharp decline as the system was overloaded, concomitant with a steep increase of sCOD and VFA concentrations in the bioreactor.

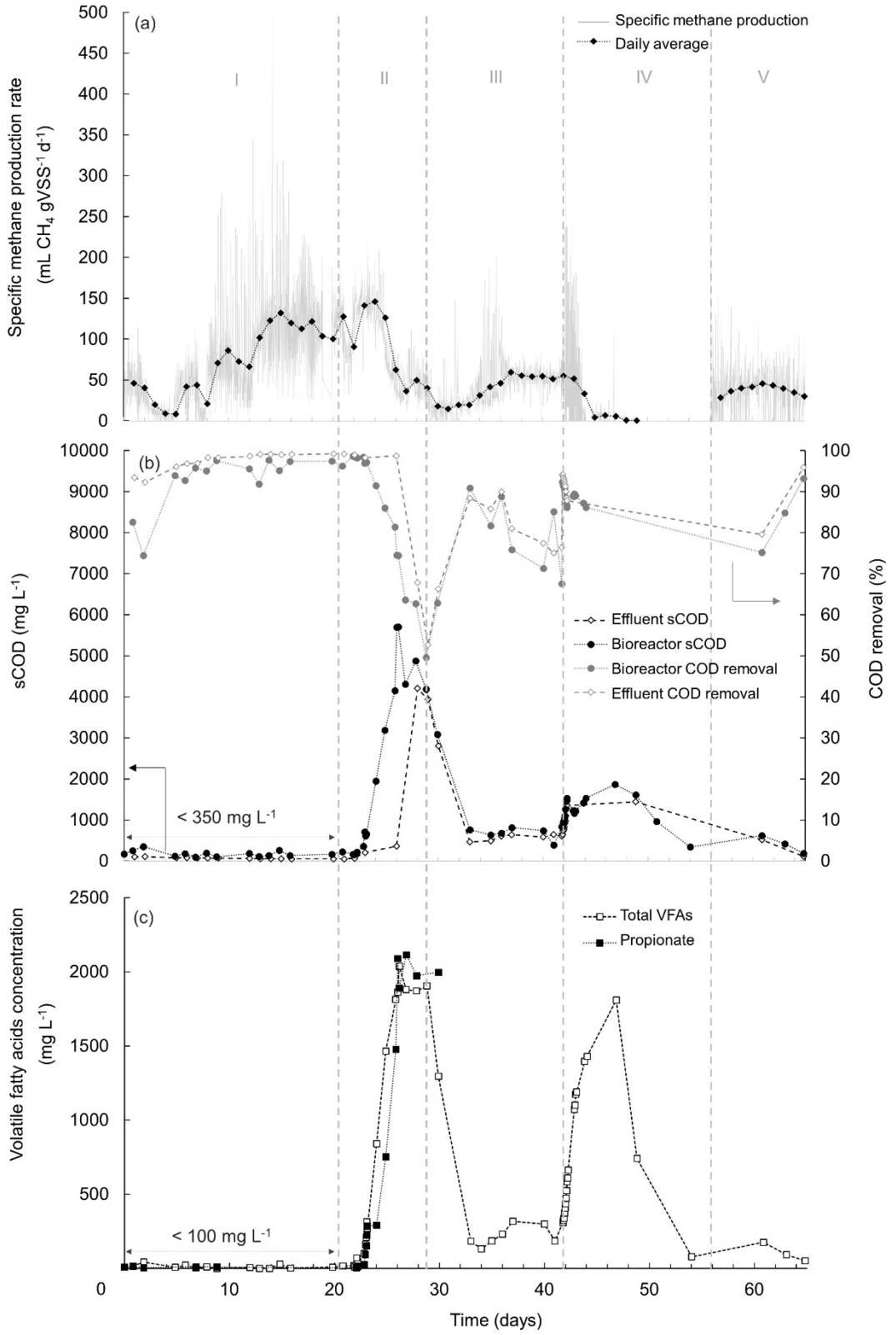


Figure 6.13 The evolution of the **(a)** specific methane production (—) with its daily average (♦), **(b)** reactor (●) and effluent (◊) soluble COD (sCOD) concentrations and COD removal efficiencies (● and ◊), and **(c)** total Volatile Fatty Acids (VFAs, □) and propionate (■) concentrations over the 65 days experimental period. An increased organic loading rate (OLR) induces a short and slight increase in half-hourly methane production rates and daily averages followed by a sharp decline as the system is overloaded. The two OLR shocks can clearly be distinguished by increased soluble COD values. COD removal efficiencies were highest and most stable during Phase I. Stable reactor operation in Phase I (VFAs < 100 mg L^{-1}) was clearly disturbed by the two OLR shocks and led to inhibitive VFA concentrations. In Phase II propionate was the main accumulating VFA. An SRT of approximately 60 days was maintained after the first three weeks of operation.

HPLC analysis of individual VFAs revealed that although during the onset of phase II an initial increase in acetic acid concentration occurred, propionic acid started accumulating, reaching concentrations over 2000 mg L^{-1} which is well above the inhibitory values reported for this particular fatty acid (Wijekoon *et al.*, 2011). Propionate is a known indicator for digestion instability (Nielsen *et al.*, 2007; Weiland *et al.*, 2010). Since the pH was not automatically controlled, its value decreased during the course of the experiment (data not shown). The pH was manually adjusted using 10 M KOH between 6.5 and 7.5 during normal operation (all phases aside from OLR shock phases II and IV). The pH was not controlled during the OLR shock phases in order to achieve and maintain an inhibited system. The transmembrane pressure remained below 130 mbar during the entire experiment. On day 27, the flux was increased from 5 to 7 L m^{-2} h^{-1} to decrease the HRT from around 75 hours to 53 hours in an attempt to faster remove the excess VFAs by dilution. A second increase of the flux to 10 L m^{-2} h^{-1} and a subsequent HRT decrease to 37 days was implemented on day 36. The flux increases had only limited impact on the TMP, which was only slightly higher than when run at a flux of 5 L m^{-2} h^{-1}.

mcrA gene copy and transcript numbers

DNA and mRNA was extracted from a select number of samples in order to assess *mcrA* gene copy and transcript number dynamics. Figure 6.14 shows the evolution of the (a) *mcrA* copy and transcript numbers per gram VSS (on a logarithmic scale), (b) transcript number over gene copy number ratio and (c) F_{430} and F_{420} concentration per gram VSS, plotted alongside a 2-hourly average of the specific methane production. gVSS was used as an approximation of biomass in the bioreactor.

mcrA transcript numbers varied a 100-fold whereas gene copy numbers only varied 3-fold. Moreover, whereas the gene copy numbers show a slightly decreasing trend throughout the experiment, the transcript numbers and transcript number over gene copy number ratio tend to follow the dynamics of the real-time methane production. For instance, in phase IV, the absence of methane production is reflected in the lowest measured transcript numbers and transcript number over gene copy number ratio.

The abundance of two acetotrophic (*Methanosaetaceae* and *Methanosarcinaceae*) and hydrogenotrophic (*Methanobacteriales* and *Methanomicrobiales*) families was determined on DNA level and indicated a higher prevalence of hydrogenotrophic methanogens. The relative abundance of the hydrogenotrophs fluctuated between 65 and 90% with an average of 80 ± 7%. Thus, on average, about 5 times as many hydrogenotrophic methanogens were present compared to the acetotrophic ones.

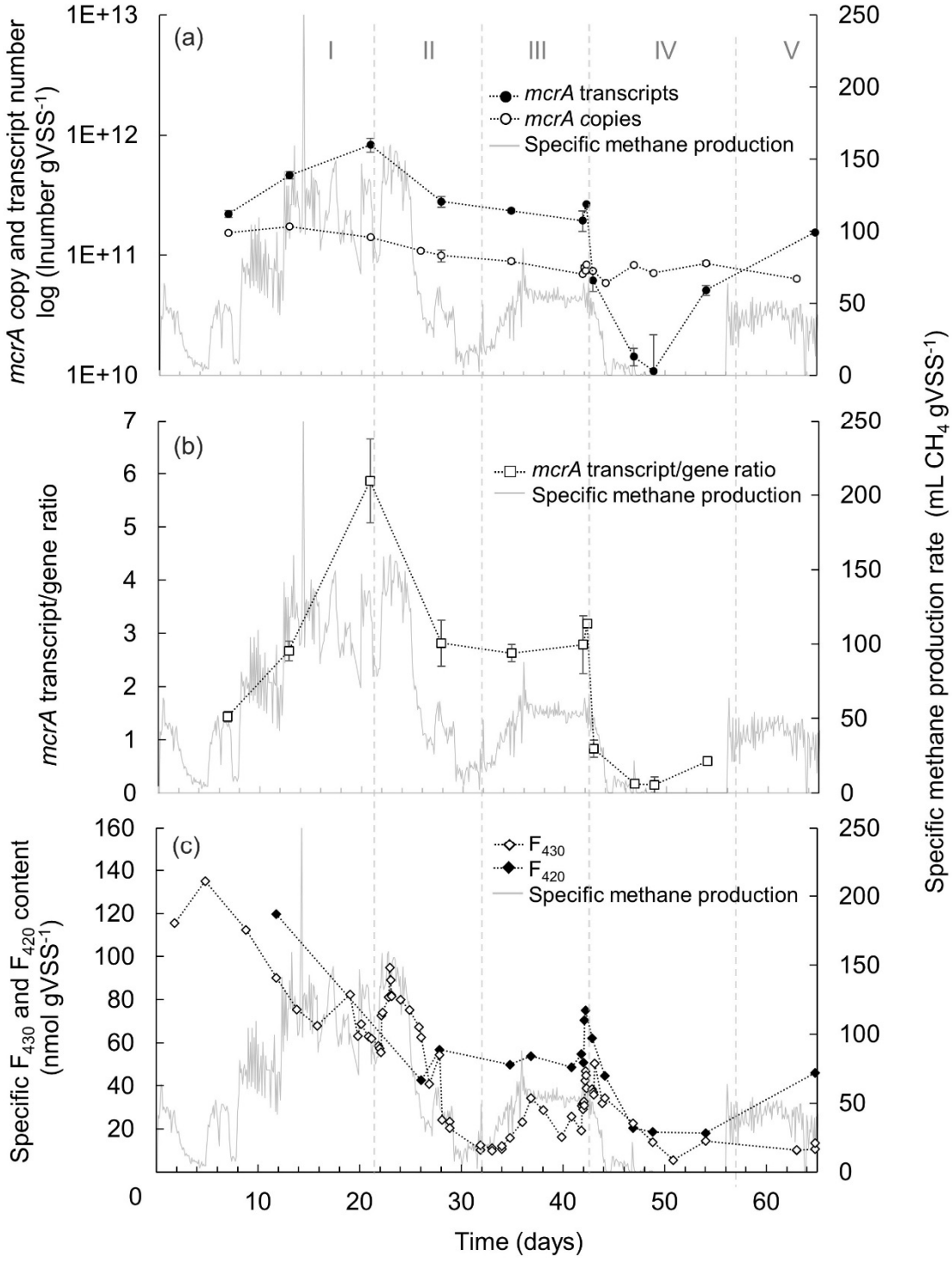


Figure 6.14 The evolution of the **(a)** *mcrA* gene copy (○) and transcript (●) number, **(b)** transcript number over gene copy number ratio (□) and **(c)** specific cofactor F_{430} (◊) and F_{420} content (♦) plotted alongside the 2-hourly average specific methane production (—) over the 65 days experimental period. *mcrA* transcripts, transcript number over gene copy number ratio and F_{430} all follow the methane production rate profile whereas *mcrA* copies do not capture the methane production dynamics. The disproportionally high but declining F_{430} content in the first two weeks is attributed to high cofactor content in the granules stemming from previous (high) metabolic activity and is the net result of (low) production of new and degradation of still present F_{430} molecules. Error bars represent standard deviations of duplicate samples. An SRT of approximately 60 days was maintained after the first three weeks of operation.

Cofactor F_{430} and F_{420} content

Cofactor F_{430}. Over the course of the AnMBR run, 67 F_{430} measurements were performed at different points in time. Sampling was spread out over the entire operational period but the measuring frequency was increased during the OLR shocks (phases II and IV) in order to investigate the short-term dynamics of F_{430} content and the relation to real-time methane production (see Figure 6.14 – c).

The cofactor content steadily decreased during the first two weeks (phase I) whereas methane production increased. From week two until the end of the experiment the cofactor content showed a clear relation with the methanogenic activity. A decrease or increase in methane production related to a decrease or increase of cofactor content. A particular phase of interest is phase II, where the first OLR shock was applied, and the subsequent recovery phase III. In phase II, an abrupt increase in organic substrate causes a temporarily higher specific methane production rate which is reflected in an increased sludge cofactor content in a time span of several hours. Afterwards, methane production decreased with a concomitant decrease in F_{430} content. In phase III, methane production as well as F_{430} content again increased. The second OLR shock (in phase IV) confirmed the reactor behaviour observed in phase II as the system responded similarly. The short increase and subsequent decrease in methane production was again coupled to similar dynamics in F_{430} content as observed during phases II and III. On day 50 the lowest cofactor content was measured, following a period where methane production was completely absent due to inhibition by high VFA concentrations and low pH. F_{430} content only slightly increased again towards the end of the experiment when methane production recovered.

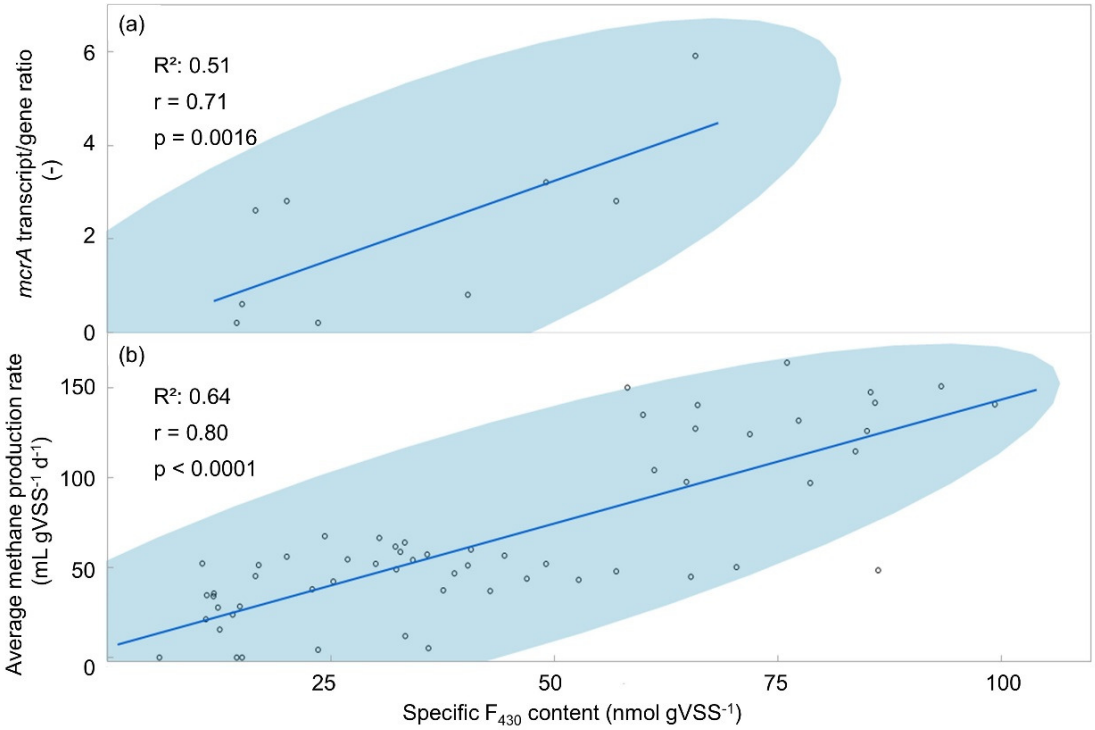
Cofactor F_{420}. Over the course of the AnMBR run, 16 F_{420} measurements were performed at different points in time (see Figure 6.14 – c). The number of data points for this cofactor was considerably lower, however some general conclusions can still be drawn. As for cofactor F_{430}, the F_{420} content was highest in the beginning of the experiment. Based on the data points in phases III, IV and V this cofactor also seems to capture some of the dynamics in methane production. Particularly in phase IV when the second OLR shock took place.

The F_{420} over F_{430} ratio was also determined for 16 samples spread out over the experimental period (data not shown). The ratio fluctuated between 0.68 and 3.41 with an average of 1.8 ± 0.7. However, these absolute values cannot be compared with the ones from Section 6.1 because of the lower cofactor F_{430} extraction efficiency in this experiment.

The relationships between methane production and cofactor contents as well as *mcrA* copy and transcript numbers were further statistically investigated. The Pearson's correlation coefficient (r), which is a measure of the linear relation between two variables, 95% confidence intervals (CI), statistical significance (p), and number of observations (n) are listed in Table 6.7. The positive correlation between the specific methane production rate, on the one hand, and *mcrA* gene copy number, transcript number, transcript number over gene copy number ratio and both cofactor contents, on the other hand, is significant. Furthermore, a positive correlation was found between cofactor F_{430} content and transcript number over gene copy number ratio.

Table 6.7 Correlation coefficient (Pearson r), 95% confidence interval (CI), statistical significance (p) and sample size (n) for the correlations between *mcrA* gene copy numbers, transcript numbers, transcript number over gene copy number ratio and cofactor F_{430} and F_{420} content on the one hand, and 2-hourly average specific methane production rate, on the other. *mcrA* transcript number, transcript number over gene copy number ratio and cofactor contents correlate more strongly than *mcrA* copy number, although all correlations were found to be significant (indicated by *). Note that the first two weeks of the experimental run were omitted to exclude the inoculum effects.

	2-hourly methane production rate average			
	Pearson r	*95% CI*	*p*	*n*
***mcrA* gene copy number**	0.6947	0.2833-0.8902	0.0040*	15
***mcrA* transcript number**	0.9012	0.6780-0.9723	<0.0001*	12
***mcrA* transcript/gene ratio**	0.8293	0.4565-0.9544	0.0016*	11
Cofactor F_{430}	0.8049	0.6925-0.8792	<0.0001*	60
Cofactor F_{420}	0.7850	0.4563-0.9252	0.0005*	15



The correlation of cofactor F_{430} content with transcript number over gene copy number ratio and specific methane production is visualized in Figure 6.15.

Figure 6.15 Visualisation of the correlation between cofactor F_{430} content and **(a)** *mcrA* transcript number over gene copy number ratio (n = 9) and **(b)** average specific methane production (n = 60). Coefficient of determination (R^2), Pearson's correlation coefficient (r) and statistical significance (p) are shown alongside the 95% confidence intervals. Plotting cofactor content versus the *mcrA* transcript number over gene copy number ratio and 2-hourly averaged methane production rate, shows the positive linear relationship between these parameters. Note that the first two weeks of the experimental run were omitted to exclude the inoculum effects.

6.2.3 Discussion

mcrA gene and cofactor dynamics

Theoretically, the *mcrA* transcript number over gene copy number ratio should most closely reflect the activity of the methanogens and, hence, correlate with real-time reactor methane production rate. This hypothesis is corroborated by the data summarized in

Table 6.7. The need to include analysis at the messenger RNA (mRNA) level in addition to DNA analyses was recently proposed in several studies (Watanabe *et al.*, 2009; Ma *et al.*, 2012, Munk *et al.*, 2012). Indeed, in this study, *mcrA* transcript number and transcript number over gene copy number ratio follow the methane production's dynamics, whereas *mcrA* copy numbers alone show very limited variation. Compared to the most recent studies in digester samples, the *mcrA* copy and transcript numbers found in this study, ranging from 4 - 7 x 10^5 copies ng^{-1} DNA and 1 - 10 x 10^6 copies ng^{-1} mRNA, respectively, are about 10 to 100-fold higher (Kampmann *et al.*, 2012; Morris *et al.*, 2013; 2016). In contrast, transcript number over gene copy number ratios ranging from 0.15 to 6, correspond well to what is reported in literature (Freitag *et al.*, 2010, Ma *et al.*, 2012) and are clearly dictated by changes in transcript numbers rather than gene copy numbers. The correlation with methane production rate was the strongest for the *mcrA* transcript numbers, indicating that quantification of copy numbers alone will often not adequately reflect the methanogenic activity since they only focus on abundance rather than activity. These results, including the response profile to an OLR shock, are in accordance with the findings of Munk *et al.* (2012).

In Phase I, the *mcrA* transcript number over gene copy number ratio captures the increasing trend in methane production rate in the first two weeks of the experiment, which was not the case for cofactor F_{430}, which, counter-intuitively decreases while being initially at a very high value. This high initial cofactor content is most likely due to the granular nature of the inoculum. Granular sludge is known to have a high specific activity due to the efficient sharing of metabolites inside the granules and shielding of methanogens in the centre of these structures (De Bok *et al.*, 2004; Fang, 2000). It was observed microscopically that the granular sludge used as inoculum gradually changed in the reactor to a more dispersed sludge. It took the sludge about two weeks to completely lose its granular nature. The cofactor F_{430} content ranged from 70 to 140 nmol $gVSS^{-1}$ in the first two weeks, which is slightly lower compared to contents reported for both mixed and pure cultures (Diekert *et al.*, 1981; Kida *et al.*, 2001; Jiang, 2006). However, considering the suboptimal extraction procedure used in this experiment (see Figure 4.5) the actual cofactor content may have been higher. The relatively low methane production during the reactor start-up phase may have resulted from underfeeding or adaptation phenomena. Insufficient substrate is provided to the methanogens due to either (*i*) the required acclimatization of hydrolytic-fermentative, acidogenic and acetogenic bacteria which convert the complex substrates to the precursors for the methanogens, or (*ii*) just a lack of carbon source supply, hence causing the sludge to lose some of its methanogenic potential (i.e., F_{430} content) over time.

The decreasing trend during the first two weeks is the net result of the production of new F_{430} molecules and the degradation of the still present F_{430} molecules from the active granules (which can be referred to as the metabolic memory or history). Diekert *et al.* (1981) reported specific rates of degradation of F_{430}. In two hours, 96% of the native cofactor epimerized to the 12,13-diepi form at 100 °C and the authors concluded that even at room temperature degradation would occur at day-scale. Recently, Kaneko *et al.* (2017) conducted experiments in the 15-60 °C temperature range and at neutral pH in order to determine the F_{430} degradation rate more precisely. They reported an exponential decrease and hence pseudo-first order kinetics with expected half-lives between 2 and 2.5 days at

37 °C. This value corresponds well to what is observed in this experiment during the two periods with limited methane production where F_{430} degradation clearly dominated over production. Half-lives of 2.8 (R^2 = 0.95, n = 5) and 3 days (R^2 = 0.93, n = 6) were found for the 1st and 2nd shock, respectively. These half-lives are longer than the 1.6 days found in Section 5.1 and the fitted exponentials are less precise. The longer half-lives calculated in this chapter are likely due to the fact that methane production was not completely absent, thus some F_{430} production may still have been taking place, whereas in Section 5.1 methane production had completely halted due to the inhibitory VFA concentrations and low pH. Thus, the less abrupt inhibition of methanogensis in the AnMBR in this experiment is the main reason for the less precise fits and lower R^2 values of the degradation rate plots. In contrast to the F_{430} half-lives, mRNA half-lives are within the minutes-hours range and, hence, much shorter whereas its production changes in the range of minutes (Larson *et al.*, 2009). The initial gradual increase of *mcrA* transcript number is, therefore, not obscured by *mcrA* transcripts from the inoculum that are still present. The faster degradation kinetics of the *mcrA* transcripts versus the cofactor F_{430} molecules is also further on in the experiment evident: the *mcrA* transcript number over gene copy number ratio drops off sharply as soon as the reactor is inhibited and methane production rate declines (i.e., after the second loading rate shock, phase IV), whereas for cofactor F_{430} a clear lag is observed.

While there are not enough samples to substantiate the production kinetics of the *mcrA* transcripts during the start of the OLR shock periods (phase II and IV), an increase in methane production seems to be reflected in an increased cofactor F_{430} content after about 6-8 hours. Since methanogens have doubling-times of more than 6 to 8 hours (Zhang & Noike, 1994; Dereli *et al.*, 2012), the increased F_{430} content cannot be explained by an increase in numbers of methanogens and should, therefore, be interpreted as increased activity of the present methanogens. This is supported by the *mcrA* gene analyses which indicate that not the quantity but rather the activity of the methanogens increased. The 6-8 hours delay in cofactor increase can be explained in two ways. Firstly, as OLR increased, initially the current (methanogenic) community did not require additional cofactor in order to metabolize the incoming excess substrate, indicating that it was not yet fully pushed to its limits. However, with increasing loading rates, methanogens were signalled to increase their cofactor F_{430} content (Kida *et al.*, 2001), hence explaining part of the lag in cofactor production. Secondly, the signalling of increased production starts on the gene level and the production of additional cofactor and the enzymes involved in its synthesis requires time as well, although this goes rather fast for essential metabolites. Despite these remarks, the cofactor content showed a very strong positive correlation with methane production rate ($r = 0.8049$, $p < 0.0001$). Nonetheless, the aforementioned observations have important implications for the use of F_{430} as a monitoring tool in methanogenic reactors. The time gap between methane and cofactor F_{430} production is attributable to kinetics and highlights an important difference with monitoring on the mRNA level whose dynamics are expected to be more closely related to methane production dynamics due to the short half-lives. Indeed, *mcrA* transcripts and transcript number over gene copy number ratio were shown to be more strongly correlated with methane production rate than cofactor F_{430} content, although a limited number of data points were available (Table 6.7). On the other hand, analysis on the mRNA level requires

more complex expertise and equipment. Moreover, although a combined DNA and mRNA extraction and quantification may theoretically be feasible within 24 hours, one should keep in mind that a specific matrix (sludge sample) requires its separate optimization in terms of extraction, serial dilution to avoid inhibition and qPCR conditions. This optimization process and interpretation of the results requires expert knowledge.

The cofactor F_{420} content varied between 20 and 120 nmol $gVSS^{-1}$ during this experiment, which is rather low compared to previous reports on UASB sludge (Dolfing & Mulder, 1985). The remarks formulated for cofactor F_{430} in the previous paragraphs are also applicable to cofactor F_{420}. The F_{420} content decreases after an OLR shock and increases again as the performance recovers. Thus, as observed in Section 6.1, the F_{420} content follows the F_{430} dynamics closely. Since F_{420} has been proposed to be mainly present in hydrogenotrophic methanogens, whereas F_{430} is present in all methanogens (see Section 2.1.5), the similar trends of F_{430} and F_{420} imply that most of the methanogenesis occurred through the hydrogenotrophic pathway in this experiment or that both types of methanogens were similarly affected by the operational conditions. Another possible explanation is that certain acetotrophic methanogenic species are present which do possess significant amounts of cofactor F_{420}, despite what is reported in literature. Based on the methanogenic community structure analysis on DNA level, the dominance of hydrogenotrophic methanogenesis is the most plausible explanation, although analysis on the mRNA level is required to substantiate this hypothesis. It should be noted here that, as discussed in the literature review (Section 2.1.5), F_{420}'s role in methanogens is less directly related to the production of methane compared to F_{430}. Moreover, F_{420} is not exclusive to methanogens. Furthermore, the correlation of cofactor F_{420} with methane production rate was not as strong as for F_{430}. Therefore, in theory, cofactor F_{430} should be regarded a more reliable biomarker of (total) methanogenic activity.

In summary, statistically significant correlations between the methane production rate, on the one hand, and *mcrA* copy and transcript number, transcript over copy number ratio and cofactor F_{430} and F_{420}, on the other hand, were found. The varying degrees of significance and strengths of correlation indicated that measuring the number of methanogenic cells (i.e., *mcrA* copies) does not reflect the methanogenic activity as well as the cofactor contents. However, the *mcrA* transcripts showed the strongest positive correlation. Additionally, the two OLR shocks revealed important information with respect to the production and degradation dynamics of these biomarkers compared to the in-situ methane production dynamics. Both cofactors follow the methane production rate dynamics, however, a lag is observed in their production and degradation. Some cofactor F_{430} still remains after the shock when methane production has already dropped to zero. This observation is in line with Section 6.1 and seems to indicate again that the cofactors may be able to capture reactor resilience after process upsets. Finally, cofactor originating from the inoculum is present during the first two weeks of reactor operation and its concentration decreases whereas methanogenic activity increases during this period. A lack of substrates being supplied to the methanogens is proposed as a possible explanation.

6.3 CONCLUSIONS

In combination with the methane gas production measurements, the **F_{430} and F_{420}** content and their **dynamics**, provide an important indication whether there is remaining methane production potential in anaerobic bioreactors subjected to organic loading rate shocks. Their quantification is therefore proposed as a tool to **monitor process disturbances and methanogen resilience**. The *mcrA* copy numbers alone, clearly do not capture the dynamics in methanogenic activity. Moreover, due to the faster turn-over rate of mRNA and despite the stronger correlation between *mcrA* transcripts and methane production, remaining methanogenic potential may not be detected by monitoring the *mcrA* transcripts, which also entails a more complicated measurement.

During the **start-up phase**, cofactor originating from the inoculum is present and its concentration decreases whereas methanogenic activity increases during this period. A lack of substrates being supplied to the methanogens is proposed as a possible explanation.

Cofactor **F_{420} content correlated well with cofactor F_{430}**, possibly indicating that both hydrogenotrophic and acetotrophic methanogens react similarly to the applied process upsets. However, the cofactor's production and degradation kinetics seem to differ. Whether the F_{420}/F_{430} cofactor ratio reflects the relative activity of the hydrogenotrophic methanogens could not be established with certainty in these experiments, although there are indications that this may be the case.

Extraction and quantification of cofactor **F_{420}** by **fluorimetry** is regarded as more reliable than quantification by **flow cytometry**. Nevertheless, the flow cytometric method definitely has potential since it also seems to capture some of the dynamics in methanogenic activity.

Building further on these promising results, in the next chapter, three additional potential applications of cofactor monitoring will be investigated.

CHAPTER 7

Applications of methanogenic cofactor monitoring: anaerobic bioreactor start-up, long-term operation and stratification

In Chapter 5, a proof-of-principle of cofactor F_{430}'s potential to be used as a monitoring tool for methanogenic activity was shown. Chapter 6 substantiated the correlations between methanogenic activity, cofactor F_{430} and F_{420} content, and investigated whether the cofactor could be used in practice to help better understand and avoid or relieve process disturbances. In this chapter, *three additional potential applications of cofactor monitoring are investigated*. First, the suitability of cofactor F_{430} and F_{420} contents for reflecting the *long-term performance of stable bioreactors* compared to the commonly used SMA tests, is investigated. Second, the potential of cofactor F_{430} to detect *stratification of methanogenic activity* in an industrial-scale reactor is assessed. Finally, the follow-up of a *bioreactor start-up* is described. To this end, five different experiments were performed and are individually discussed in this chapter.

In the first experiment, two synthetic dairy wastewater fed lab-scale AnMBRs were followed-up in terms of cofactor F_{430} and F_{420} content, classical performance monitoring tools and SMA over a period of 165 days of stable operation. The evolution of the cofactor contents was compared with the SMA and was expected to reflect the stable operation and performance of these reactors. In the second experiment, the successful start-up and long-term (351 days) operation of three lab-scale anaerobic bioreactors fed with a long-chain fatty acids (LCFAs) containing feed, was followed-up in terms of cofactor F_{430} content and this was related to *in-situ* methane production and *ex-situ* determined SMAs. These first two experiments were related to the first evaluated application of cofactor monitoring.

In the third experiment, the quantification of cofactor F_{430} at different heights of a full-scale digester was performed in an attempt to map the spatial distribution of methanogenic activity along the height of the bioreactor. A distribution of cofactor F_{430} would imply imperfect mixing and the occurrence of separate (predominantly) methanogenic and acidogenic zones. This experiment was related to the second evaluated application of cofactor monitoring.

In the fourth experiment, cofactor F_{430} and F_{420} concentrations were followed-up alongside classical performance monitoring tools during the failed start-up of two lab-scale AnMBRs. The reactor's performance decreased gradually over a period of 80 days and both cofactors were quantified in order to assess whether the trend of reducing methanogenic activity was reflected by decreasing methanogenic cofactor content. This experiment was related to the third evaluated application of cofactor monitoring.

In the final experiment described in this chapter, cofactor F_{430} content was determined in 12 samples originating from lab-scale reactors inoculated with three different inocula. The methane production and cofactor F_{430} content at the time of sampling were compared in order to determine whether a general relation between methane production and cofactor content can be found across different bioreactors. The main objective of this experiment was to validate the applicability of cofactor measurements (and their link with methane productivity) across different reactors.

7.1 Do SMA and cofactor content reflect the methanogenic activity well during stable, long-term bioreactor operation?[12]

In Chapters 5 and 6, cofactor F_{430} content was shown to accurately reflect the (potential) methanogenic activity of anaerobic bioreactors that were subjected to severe operating upsets. However, in practice anaerobic bioreactors are started-up gently and steered towards stable, long-term performance. It is reasonable to assume that also in those cases the link between methanogenic activity and cofactor content should remain present. In order to examine this hypothesis, this section and the next will describe two experiments during which anaerobic bioreactors were followed up for an extended period of stable operation. An important additional research question was the link between SMA and cofactor content. It is hypothesized that SMA will not always accurately reflect the *in-situ* (potential) methanogenic activity, in which case cofactor quantification could be a valuable alternative or complement.

7.1.1 Materials & methods

Experimental set-up and feeding strategy

Two identical, glass 10 L lab-scale AnMBRs were operated in cross-flow mode using 3 m long polyvinylidene (PVDF) ultrafiltration tubular modules (PENTAIR). Each reactor was mixed by a mechanical stirrer, operated at 35 rpm. The sludge in the reactors was maintained at mesophilic temperature (35 °C) by recirculating hot water from a manually controlled water bath through the double-walled water jacket around the reactors. Online data acquisition of transmembrane pressures (TMP) was controlled by a programmable logic controller (PLC) unit. Both reactors were inoculated with the same granular inoculum originating from an expanded granular sludge bed reactor treating fermentation-industry wastewater. The inoculum was crushed and sieved prior to use. Whole milk, with the addition of a micronutrient mixture, was used for the preparation of the synthetic dairy wastewater used to feed the reactors.

During the first 46 days of the experiment, both reactors were operated at an SRT of 30 days. After 46 days of operation the SRT in both reactors was altered. The SRT was changed to 20 days and 40 days in the reactors that will be denoted as R20 and R40, respectively. To this end, the sludge purging rate was increased in reactor R20 and decreased in reactor R40.

The organic loading rate was gradually increased based on the performance of the reactors using classical monitoring tools such as pH, VFAs, COD removal and methane production rate. Figure 7.1 shows how the organic and sludge loading rates were gradually increased in both reactors. The organic loading rates evolved similarly in both reactors. Towards the end of the experiment OLRs of between 5 and 6 gCOD L^{-1} d^{-1} were successfully sustained. However, the sludge loading rates levelled off in reactor R40 because of the production of additional biomass. Sludge loading rates of up to 0.8 gCOD $gVSS^{-1}$ d^{-1} where reached in R20, whereas those in R40 levelled off at around 0.5 gCOD $gVSS^{-1}$ d^{-1}.

[12] This experiment was performed in collaboration with BIOTHANE in Delft, The Netherlands. The reactors were operated there and the volatile suspended solids and SMA analyses were also performed at BIOTHANE.

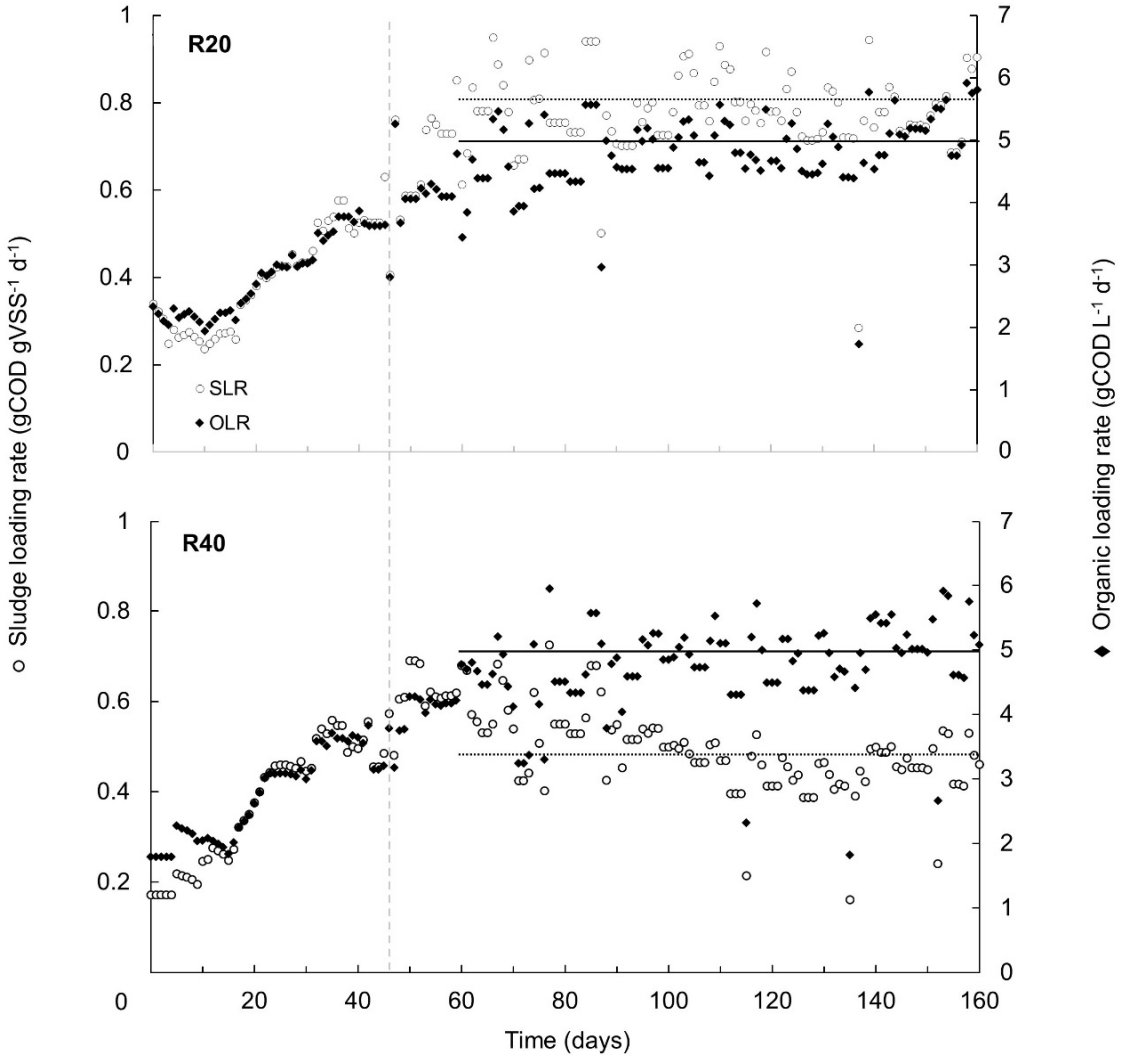


Figure 7.1 The evolution of sludge loading rate (SLR, ○) and organic loading rate (OLR, ♦) over the 165 days operational period in reactors R20 (top) and R40 (bottom). An SRT of 30 days was maintained initially, subsequently, an SRT of 20 and 40 days was maintained in reactor R20 and R40, respectively (indicated by the dashed grey line). Average OLR and SLR from day 60 onwards are indicated by the full black line and dotted line, respectively. Similar OLRs of 5-6 gCOD L^{-1} d^{-1} were sustained towards the end of the experiment. However, significantly higher SLRs of around 0.8 gCOD $gVSS^{-1}$ d^{-1} were able to be sustained in reactor R20 compared to R40 (0.5 gCOD $gVSS^{-1}$ d^{-1}).

Analytical methods

The analytical methods used in this experiment have been described in the general material & methods section (Chapter 3). The following parameters were analysed.

- (Volatile) Suspended solids

Specific methanogenic activity tests

Acetoclastic specific methanogenic activity (SMA) was measured in sealed serum bottles by monitoring the pressure increase with a pressure transducer after the addition of sodium acetate. The SMA value was determined as the slope of the methane production rate in function of time, converted to gCH_4-COD $gVSS^{-1}$ d^{-1}. SMA was measured on average once every two weeks, which is common practice for larger-scale installations.

Cofactor F_{430} and F_{420}

Cofactor F_{430} was extracted and quantified using Protocol 4 (Table 4.1) as described in Section 4.1.2.

Cofactor F_{420} was extracted and quantified using the fluorimetry method and a quantification method using a fluorescence microscope, as described in Section 4.2.2.

Samples for cofactor analysis were taken twice a week, which is a considerably lower frequency compared to the experiments described in the previous chapters. Nonetheless, this frequency is more realistic for the follow-up of larger-scale installations. Eight replicate samples from one of the reactors were analysed prior to the experiment in order to determine an average experimental error on the cofactor quantification of these samples. The experimental error on cofactor F_{430} extraction and quantification was 2.5% (not taking into account the error on the VSS quantification). The experimental error on F_{420} extraction and quantification (based on 10 duplicate samples) was 4.4%. Since no information with respect to the standard deviation on VSS determination was provided, the aforementioned percentages were taken as the approximate experimental error when calculating the normalized (per gVSS) cofactor contents.

7.1.2 Results

The reactor performance will be discussed in terms of (specific) methane production rate, SMA and cofactor F_{430} and F_{420} content in the following paragraphs.

Overall reactor performance

In this experiment, the overall reactor performance was monitored by measuring the methane production rate. Figure 7.2 shows the evolution of the total methane production rate and the specific methane production rate which takes into account the amount of biomass in the reactors.

The methane production rates increased over time because of the increasing OLR. However, the specific methane production rates levelled off in reactor R40 because of the production of additional biomass after the change in SRT. Indeed, after 46 days the biomass concentration in reactor R20 stopped increasing and stabilized between 6 and 7 gVSS L^{-1} due to the increased sludge purging rate, whereas in reactor R40 biomass concentration significantly increased from this point onward, reaching values of up to around 11 gVSS L^{-1} due to the decreased sludge purging rate (data not shown). As a result, the specific methane production rates were twice as high in reactor R20 towards the end of the experiment.

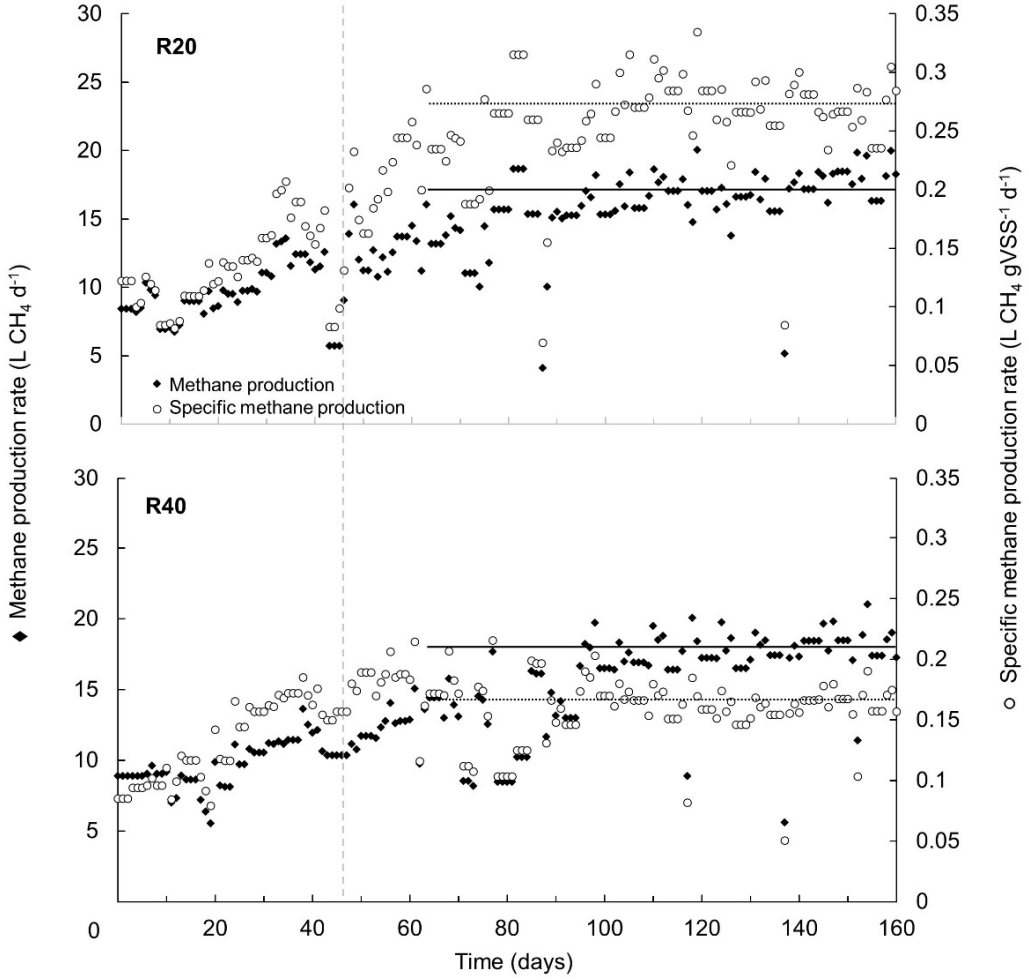


Figure 7.2 The evolution of the methane production rate (♦) and specific methane production rate (○) over the 165 days operational period in reactors R20 (top) and R40 (bottom). An SRT of 30 days was maintained initially, subsequently, an SRT of 20 and 40 days was maintained in reactor R20 and R40, respectively (indicated by the dashed grey line). Average total and specific methane production rate from day 60 onwards are indicated by the full black line and dotted line, respectively. Similar total methane production rates of almost 20 L d^{-1} were reached towards the end of the experiment. However, specific methane production rates were almost twice as high in reactor R20 because of the lower biomass concentration.

Cofactor contents and SMA

Figure 7.3 shows the evolution of cofactor F_{430}, cofactor F_{420} and SMA on acetate plotted alongside the specific methane production rate in reactor R40. In the first 32 days, as the reactor was starting up, an opposite trend is observed for cofactor F_{430} and the methane production rate, whereas the F_{420} content remains relatively stable. Afterwards, for the remainder of the experimental run, the specific cofactor contents and methane production rate both show a slightly decreasing trend.

The trend of the SMA seems to capture some of the increasing trend in specific methane production from day 20 onward. However, on day 48, the SMA sharply decreases, which is not reflected in significantly lower methane production rates. Subsequently, a fluctuating, but slightly decreasing trend is observed, which is more or less in accordance with the relatively stable methane production rates observed for the remainder of the experiment.

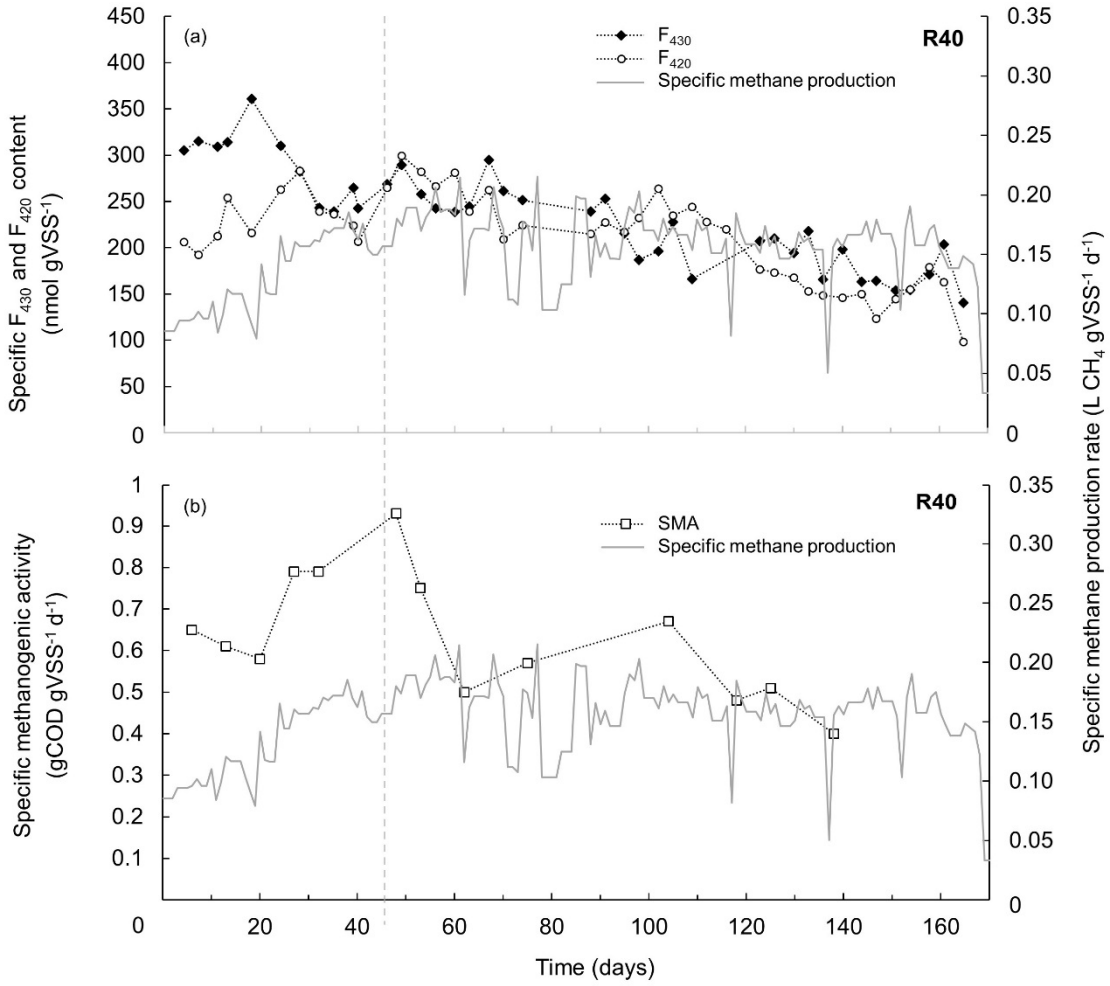


Figure 7.3 The evolution of specific cofactor **(a)** F_{430} (♦) and F_{420} (○) content and **(b)** specific methanogenic activity on acetate (SMA, □) over the 165 days operational period, all plotted alongside the specific methane production rate (–), in reactor *R40*. An SRT of 30 days was maintained initially, subsequently, an SRT of 20 and 40 days was maintained in reactor R20 and R40, respectively (indicated by the dashed grey line). Both cofactor contents do not reflect the evolution of the methanogenic activity well during the first 32 days. In addition, the SMA does not always represent the actual methanogenic activity inside the reactor.

Figure 7.4 shows the evolution of cofactor F_{430}, cofactor F_{420} and SMA compared with the specific methane production rate in reactor R20. Figure 7.2 indicates that the specific methane production in this reactor showed an increasing trend throughout the entire experimental period, indicating that its activity gradually and consistently increased. Therefore, based on the results presented in the previous chapters, an increasing trend was expected for the cofactors. However, this is not what is observed in Figure 7.4 – a. In fact, cofactor F_{430} shows an opposite, decreasing, trend throughout almost the entire experiment. Three separate periods can be distinguished: (*i*) between day 0 and day 26 cofactor F_{430} content decreases whereas methane production rate increases, (*ii*) between day 26 and day 89 F_{430} seems to capture most of the fluctuations in methane production rate, and (*iii*) between day 89 and 165 cofactor F_{430} content is consistently lower than the specific methane production rate, with a particular decrease from day 116 onward. Roughly the same is observed for cofactor F_{420} although in the first two periods combined (0 to 89 days) it seems to better reflect the methane production rate than cofactor F_{430}.

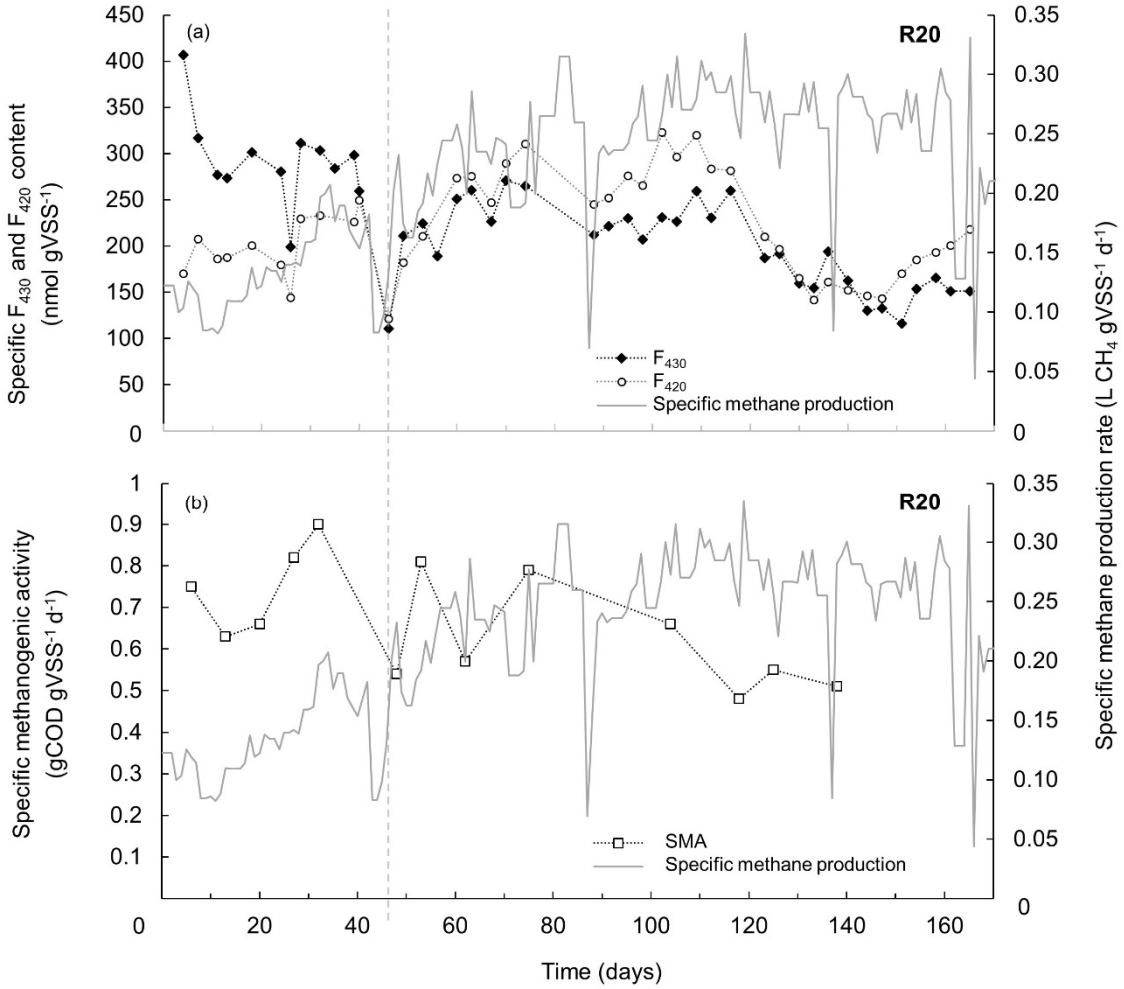


Figure 7.4 The evolution of specific cofactor **(a)** F_{430} (♦) and F_{420} (○) content and **(b)** specific methanogenic activity on acetate (SMA, □) over the 165 days operational period, all plotted alongside the specific methane production rate (—) in reactor *R20*. An SRT of 30 days was maintained initially, subsequently, an SRT of 20 and 40 days was maintained in reactor R20 and R40, respectively (indicated by the dashed grey line). Both cofactor contents do not reflect the evolution of methanogenic activity well and neither does the SMA. The dashed grey line indicates the point at which the solids retention times were altered.

The SMA again partly captures the increasing trend in methane production rate, i.e., between day 20 and day 32. However, afterwards it widely fluctuates with a generally decreasing trend from day 75 onward, not reflecting the in-situ methane production rate well.

In order to objectify the correlations between the different parameters, they were statistically tested using Pearson's correlation coefficient (r). In both reactors, significant positive correlations were found between the two cofactors despite the clear differences observed in the start-up periods ($r = 0.4082$, $p = 0.0081$, $n = 41$ and $r = 0.7190$, $p < 0.0001$, $n = 41$ for reactor R20 and R40, respectively). Furthermore, in accordance with the observations made in Figures 7.3 and 7.4, also significant negative correlations were found between cofactor F_{430} and specific methane production in both reactors ($r = -0.5447$, $p = 0.0002$, $n = 43$ and $r = -0.3778$, $p < 0.0149$, $n = 41$ for reactor R20 and R40, respectively). The SMA showed a significant positive correlation with cofactor F_{430} in R20 ($r = 0.6555$, $p = 0.0207$, $n = 12$) and with cofactor F_{420} in R40 ($r = 0.8019$, $p = 0.0010$, $n = 13$) but correlated

poorly with the in-situ methane production rate in R20 ($r = -0.3200$, $p = 0.3105$, $n = 12$) and R40 ($r = 0.1585$, $p = 0.6051$, $n = 13$).

As explained in the materials and methods section of this experiment, cofactor F_{420} quantification by means of fluorescence microscopy was also attempted in these experiments. These results were not included here because they were not satisfactory. It suffices to mention that both the number of fluorescent pixels and their intensity per pixel did not correlate with the results obtained by extraction and quantification using fluorimetry and the method was, therefore, regarded as unreliable for quantitative F_{420} analysis in its current form.

The F_{420} over F_{430} ratio was also calculated in both reactors and showed a fluctuating, slightly increasing trend over time. Average values of 1.01 ± 0.25 and 0.92 ± 0.18 were calculated for R20 and R40, respectively.

7.1.3 Discussion

The effect of solids retention time on biomass concentration and activity

Both reactors followed-up in this experiment performed similarly in terms of organic loading rates and total methane production, however, reactor R20 managed to do so with less biomass implying an increased specific methanogenic activity. This is in accordance with a similar experiment during which the SRT in an AnMBR was switched from 20 to 40 days (Ersahin *et al.*, 2014). Based on the observations in previous chapters, it is likely that the activity of the methanogens increased rather than their relative abundance. The reason for the increased specific activity is the higher amount of substrate which is supplied per unit of biomass (or methanogens) in R20 (higher SLR). The microbial community in this reactor is pushed to handle the same amount of substrate as R40 but because of their lower abundance they need to increase their activity in order to handle the incoming substrates. On the other hand, in reactor R40, an increasing amount of microorganisms were given the same amount of feed, potentially creating starvation conditions for some organisms. Substrate concentrations were likely kept very low, promoting the growth of some methanogens adapted to these conditions (i.e., *Methanosaetaceae* species) while inhibiting others (Conklin *et al.*, 2006).

The relation between in-situ methanogenic activity and SMA on acetate

Surprisingly, the increased methanogenic activity, reflected by the increasing specific methane production rate, was not reflected well by the SMA on acetate in reactor R20. The SMA fluctuated widely and did not capture the increasing trend in methane production rate. It should be noted that the 13 data points may have been relatively limited, still this corresponds to one measurement every two weeks which is common practice in industry. The SMA reflects a maximum methanogenic activity which can be achieved with the reactor's sludge in ideal conditions and should therefore reveal the methanogenic potential of the sludge (Souto *et al.*, 2010). However, the methanogenic activity increased in reactor R20 indicating an increasing methanogenic potential, whereas the SMA tests indicated a decreasing trend. Indeed, the SMA on acetate correlated poorly with in-situ methane production rate in both reactors. The ex-situ determination of SMA in "ideal" conditions which are very different from those prevailing in the actual reactor may be part of the explanation for these observations (Guebitz *et al.*,

2015). Another possible explanation may lie in the fact that only the SMA on acetate was determined in this experiment and, therefore, the hydrogenotrophic activity was not taken into account. Although acetoclastic methanogenesis is often predominant, the importance of hydrogenotrophic methanogenesis has been reported to be significant in reactors treating synthetic dairy wastewater (Cavaleiro *et al.*, 2009; Bialek *et al.*, 2014). Therefore, in this case the SMA on H_2/CO_2 may have better reflected the increasing methanogenic activity. Based on these results, the SMA on acetate can clearly not always be regarded a reliable tool to steer methanogenic bioreactors since it does not necessarily reflect the sludge's in-situ methanogenic activity, nor its future potential well. Including the SMA on H_2/CO_2 and even on a mixture of ethanol, propionate and butyrate to take into account hydrogenotrophic and syntrophic activity, respectively, is highly recommended with this type of wastewater (Bialek *et al.*, 2014).

Cofactor F_{430} and F_{420} quantification versus SMA

Based on the results obtained in Chapter 6, the two cofactors were expected to show the same increasing trend as the specific methane production rate. As explained in the results section, this was rarely the case over the course of the experimental period. The discrepancy in the beginning of the experiment may be attributable to the adaptation phenomena during start-up previously described in Chapter 6 (Section 6.2.3). Note, however, that this effect seems less pronounced for cofactor F_{420}. Apart from this start-up phase, the two cofactors correlated well in both reactors as substantiated by the correlation analysis. Indeed, they both show the same significant drop after 116 days in reactor R20 which does, however, not coincide with a decrease in methane production rate. The decreasing trend is sustained for a couple of weeks and is only reversed in the last two weeks of operation. The sudden decrease, without any changes in operational conditions or methane production, may suggest a decrease in cofactor extraction efficiency. Unfortunately, the current extraction protocols do not include controls to assess the extraction efficiency and therefore a 100% (or at least a constant) extraction efficiency is assumed. However, as will be seen in Chapter 8 (Part II), some remarkable changes in the morphology and viscosity of the sludges took place throughout the operational period. More specifically, the number of filaments and flocs increased from around 120 days onward and simultaneously the viscosity increased. However, this trend was seen in both reactors and was in fact more pronounced in reactor R40 compared to R20. Thus, although theoretically the changes in morphology and viscosity could have decreased the cell lysis efficiency, since the sudden drop was not observed in R40 it does not explain the decreased cofactor content. Furthermore, the two cofactors are extracted using different methods. The F_{420} extraction is based on cell lysis by heat whereas for F_{430} lysis by mechanical means (microbeads) is used. It is unlikely that both cell lysis methods were affected by the sludge morphology and viscosity in exactly the same way. Problems with the instrumentation used for quantification of these cofactors were also ruled out. A final possible explanation would be a community shift taking place in reactor R20. However, in this case the community shift would need to have been towards methanogenic species which require less of both cofactors to produce the same amount of methane. Based on its involvement in the very last step of methanogenesis, cofactor F_{430} concentration is expected to be independent from the community structure but rather linked to function (i.e., methane production) only. Methanogens are expected to dynamically adapt their cofactor content

to the environmental conditions (e.g., amount of substrate coming in) and a given species is, therefore, expected to produce the same amount of cofactor F_{430} in order to produce a given amount of methane. Indeed, Morris *et al.* (2013; 2016) found that the relationship between methanogenic activity (SMA) and the *mcrA* gene (copy number) was independent of methanogen community structure or composition. It is thus reasonable to assume that the same holds for cofactor F_{430}. Considering these remarks, the community shift hypothesis is unlikely. Unfortunately, the community structure analysis was not performed in these experiments and the hypothesis could not be checked. Therefore, these results remain remarkable and puzzling to this date.

In reactor R40, after about 32 days, the two cofactors seemed to follow the same trend as the methane production rate and therefore did reflect the relatively stable operation in this reactor. However, because of the limited variability in methane production and cofactor contents, in this reactor correlation analysis is less suitable. Nevertheless, because of the inclusion of the start-up samples an overall negative correlation was also found in this reactor, albeit with a lower correlation coefficient and significance than in R20.

The cofactor F_{420} over F_{430} ratios were relatively high in both reactors, compared to those found in the VFA-fed digesters described in Chapter 6. This observation may support the relative importance of the hydrogenotrophic methanogenesis in these synthetic dairy wastewater fed reactors (Cavaleiro *et al.*, 2009; Bialek *et al.*, 2014) as discussed previously, since cofactor F_{420} is expected to be predominantly present in hydrogenotrophic methanogens (Kida *et al.*, 2001). Again, this hypothesis could not be corroborated by community structure analysis in these experiments.

In summary, clear limitations of the SMA test on acetate were highlighted in this experiment. It seemed to not reflect the actual in-situ methanogenic activity, nor the potential, future methanogenic activity in these experiments. Possibly, the SMA on H_2/CO_2 would have reflected the increasing methanogenic activity better. Nonetheless, the common application of SMA in industry should be re-evaluated and the investigation of other tools such as cofactor monitoring is justified. However, the two cofactors also did not reflect the gradually increasing specific activity. The clear discrepancy between cofactor F_{430} and methane production rate in the first two to three weeks of the experiment was in accordance with the findings in Chapter 6 (Section 6.2.3). This phenomenon was less pronounced for cofactor F_{420}. The two cofactors correlated well in both reactors, however, both misrepresenting the actual methanogenic activity in the reactors. A clear explanation for these observations could not be formulated at this point. Based on the results, in these experiments, it cannot be concluded that cofactor measurements provided useful information which could complement or replace SMA tests during the long-term stable operation of bioreactors. However, the SMA tests themselves did not represent the actual methanogenic activity well. Further experiments are required in order to explain these counterintuitive observations.

7.2 Does the evolution of cofactor F_{430} content better reflect the long-term acclimatisation of anaerobic bioreactors than SMA tests?[13]

Similarly to Section 7.1, the aim of this experiment is to relate SMA and cofactor F_{430} content measurements to the real-time performance of methanogenic anaerobic bioreactors. In this particular case, three replicate anaerobic bioreactors were gradually acclimatized to an increasing LCFA (Long-Chain Fatty Acid) load over a period of 351 days. Because of the potentially inhibitory effects of LCFAs on methanogenesis, a gentle start-up and increase in loading rate strategy was adopted. Spread out over the operational period, SMA (both on acetate and H_2/CO_2) and cofactor F_{430} content quantifications were performed. Considering the importance of increasing the loading rate to the reactors only when the community has been sufficiently adapted to the substrate, having monitoring tools which provide more detailed insights on this adaptation is essential. The objective is to investigate the potential of cofactor F_{430} measurements to complement or replace SMA tests for this purpose. In contrast to the previous experiment, both SMA on acetate and H_2/CO_2 was performed. However, due to lack of sufficient sample, only cofactor F_{430} was quantified.

In general, all types of lipids are rapidly hydrolysed to form glycerol and LCFAs, resulting in the accumulation of these components. The LCFAs are eventually converted to acetate and hydrogen by obligate hydrogen-producing acetogens (OHPAs) (Schink, 1997), which in turn rely on the activity of the hydrogenotrophic methanogens to remove the produced hydrogen. The LCFAs act as surfactants at neutral pH and induce granule breakage and sludge flotation. On top of causing the washout of organisms from the reactor, LCFAs can also directly inhibit both the acetogenic and methanogenic communities through metabolic inhibitory mechanisms combined with mechanisms of transport limitations (Alves *et al.*, 2009). The acetoclastic methanogens have been reported to be more severely affected than the hydrogenotrophic ones. One explanation that has been proposed for this phenomenon is related to the transport limitations (Alves *et al.*, 2009). Since H_2 is a smaller molecule than acetate, it more easily penetrates through the LCFA layer which tends to surround the microorganisms, hereby allowing hydrogenotrophic methanogenesis to occur whereas acetoclastic methanogenesis is hampered. Regardless of which inhibitory mechanisms prevail, the inhibition has been shown to be reversible (Alves *et al.*, 2009).

7.2.1 Materials & methods

Experimental set-up and feeding strategy

In this experiment, three identical anaerobic bioreactors were operated as replicates. Figure 7.5 shows a schematic representation of the set-up. The 5 L reactors were constructed in glass and included a sludge retention system in the top part of the reactor to keep the sludge in the system. The reactor design is a hybrid between anaerobic filter and expanded granular sludge bed reactors. The reactors' operating temperature was kept at 37 °C by circulating water from a water bath through the heating jacket. The reactors' recycle lines were altered to ensure a better mixing from position #1 to #2 on day 195.

[13] This experiment was performed in collaboration with Conall Holohan from the Microbial Ecology Laboratory at the National University of Ireland Galway (NUIG), Ireland, who ran the reactors and performed the analytical and SMA analyses.

Biogas was collected in Teflon gas bags. The sludge purging rate (and the SRT) was variable and was adjusted in order to maintain biomass concentrations in the sludge bed at around 20 g L^{-1}. This resulted in an average SRT of 200 days during the first 188 days of operation and of 180 days afterwards. The effective volume of the sludge bed section was variable.

A synthetic feed was supplemented hourly into the recycle line, entering at the bottom of the reactor. The feed, mimicking dairy wastewater, contained 2.5 gCOD L^{-1} of skimmed milk powder (Kerry Co-op) supplemented with 1.0 gCOD L^{-1} sodium oleate (Sigma-Aldrich). Oleate (C18:1) has been reported to be the most abundant unsaturated LCFA, even more so in dairy wastewaters, and was utilised here to represent the long chain fatty acids (Alves *et al.*, 2009). A total feed concentration of 3.5 gCOD L^{-1} (28% of which was sodium oleate) was used throughout the entire operational period.

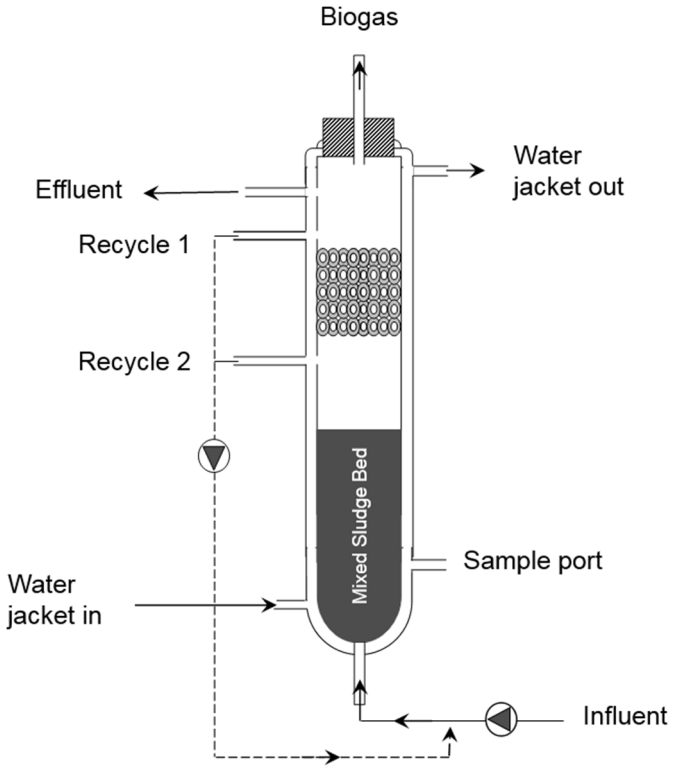


Figure 7.5 Schematic representation of the anaerobic bioreactors operated in this experiment. The reactor design is a hybrid between anaerobic filter and extended granular sludge blanket bioreactors.

The trial aimed to achieve continuous feeding of the lipid-rich substrate from start-up to a high-rate level. To his end, the hydraulic retention time (HRT) was reduced step-wise (~25% steps) throughout the trial, except for one period (increase back to 1.7 HRT on day 189) where a temporary issue (laboratory artefact) of sludge mixing arose. This approach allowed for the continuous increase of the organic loading rate (OLR) while keeping the feed make-up and, thus, COD ratio of LCFAs stable. It, furthermore, ensured a steady development and selective pressure on the microbes and overall system, simultaneously mimicking an applied commercial reactor set-up. The evolution of the OLR and HRT was the same in all three reactors and is shown in Figure 7.6.

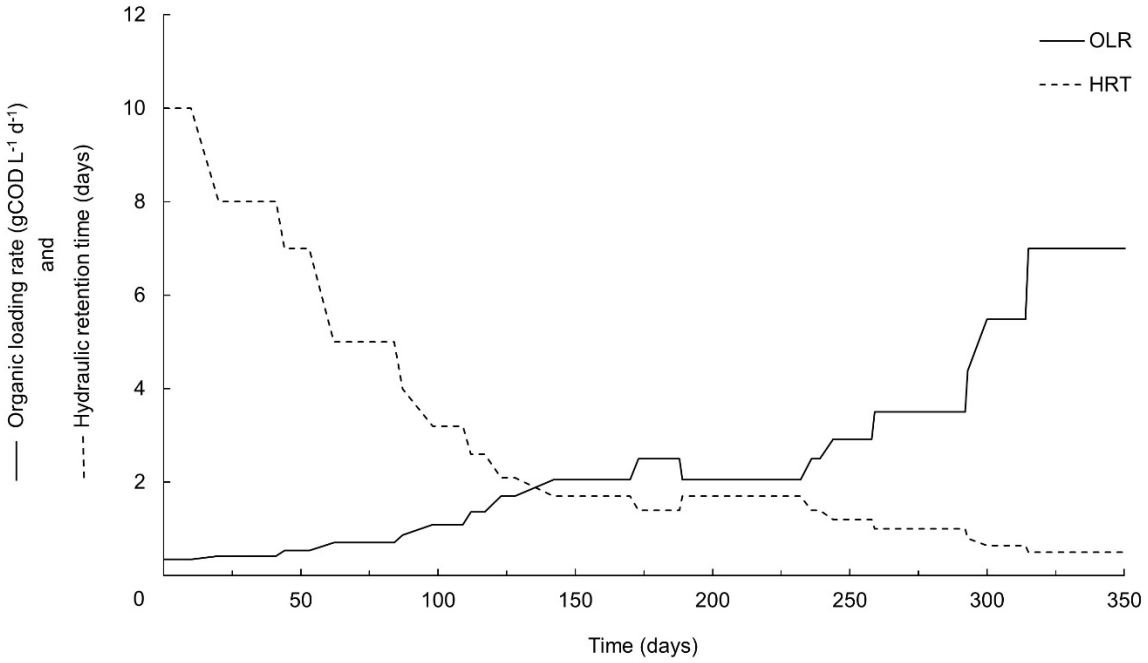


Figure 7.6 The evolution of the organic loading rate (OLR, —) and hydraulic retention time (HRT, - - -) over the 351 days operational period in all three reactors. An average SRT of 200 days was maintained during the first 188 days of operation, afterwards the SRT was 180 days on average.

Analytical methods

The analytical methods used in this experiment have been described in the general material & methods section (Chapter 3). The following parameters were analysed.

- TS and VS

Additionally, biogas composition was quantified approximately three times per week in triplicate via chromatographic analysis on a Varian 3800-CP gas chromatograph equipped with an Flame Ionization Detector (FID) and a Hayesep packed 2 m x 1/8" x 2.0 mm column system.

Furthermore, LCFAs were measured using a Varian 450 GC-FID system with an Aquilant DB50 column (30 x 0.25 mm x 0.25 µm). The detection limit for the individual LCFAs was 30 mg L^{-1} for C18:1 and 25 mg L^{-1} for C16:1 and C14:0.

Specific methanogenic activity tests

SMA was determined using the method described by Colleran *et al.* (1992) and Coates *et al.* (1996) by monitoring the change in biogas pressure within a sealed batch vial in response to substrate degradation. Samples were taken from the sludge bed and the SMA was determined as mL CH_4 gVS^{-1} d^{-1}. These tests allowed the assessment of the activity of acetoclastic and hydrogenotrophic groups through the use of acetate and H_2/CO_2 as substrates, respectively. The SMAs were determined on seven occasions spread out over the operational period.

Cofactor F_{430}

Cofactor F_{430} was extracted and quantified using Protocol 4 (Table 4.1) as described in Section 4.1.2. Samples for cofactor F_{430} extraction were taken from the sludge bed.

7.2.2 Results

The evolution of reactor performance was followed up by means of pH, COD, LCFA concentration, pH, SMA and biogas measurements. In the current work, the focus is on the evolution of the methane production rates and the link with SMA and cofactor measurements. For more details with respect to the overall reactor operation and microbial community structure reference is made to Holohan (2018).

Figure 7.7 shows the evolution of the methane production, SMA and specific cofactor F_{430} content in all three reactors. Based on the applied loading rates (Figure 7.6) and the general trend of the methane production, it is reasonable to divide the experimental period into two main parts: a first part (Part 1) in which the loading rate increase was less steep allowing the biomass to adapt to the substrate, and a second part (Part 2) in which the loading rates more steeply increased. This division is shown visually on the graphs by the grey dashed line. Note that the sludge loading rate and specific methane production were also calculated but for significantly less data point. Their trends aligned with those of the organic loading rate and methane production and, therefore, this data was omitted.

The OLR and SLR were kept low (below 1.5 gCOD L^{-1} d^{-1} and 0.05 gCOD gVS^{-1} d^{-1}) in Part 1 of the experiment in order to allow the microorganisms to adapt to the LCFA-containing wastewater. Afterwards, during Part 2, the loading rates were significantly increased, reaching values of around 7 gCOD L^{-1} d^{-1} and 0.15 gCOD gVS^{-1} d^{-1}, for the organic and sludge loading rate, respectively. The general trend of the methane production rate follows that of the loading rates and is upwards throughout the entire experimental period. However, the increase in methane production is clearly much steeper in Part 2. Note that in this experiment the methane production was not normalized to the reactor's VS concentration. The reason being that the effective volume of the sludge bed varied throughout the experiment, complicating the determination of a total reactor VS concentration. In addition to methane measurements, LCFA concentrations were measured in order to follow-up the reactors' performance. The LCFA concentrations were under the limit of detection for all reactors throughout the entire experimental period, indicating a fast and consistent and adequate degradation of these components.

The upward trends observed in methane production seems to not be reflected well in the SMA measurements. Both the SMAs on acetate and H_2/CO_2 remained relatively constant with only a significant increase towards the end of the experimental period, most notably for the SMA on H_2/CO_2. Furthermore, the SMA on H_2/CO_2 was significantly and consistently higher throughout the entire experimental period, indicating a higher relative activity of hydrogenotrophic methanogens. Overall, the SMA on H_2/CO_2 was between 350 and 1800 mL CH_4 gVS^{-1} d^{-1}, whereas the SMA on acetate varied between 150 and 600 mL CH_4 gVS^{-1} d^{-1}.

The cofactor F_{430} content shows a consistent decrease between the inoculation and day 124 in all three reactors. Its concentration decreases from a relatively high value of around 240 nmol gVS^{-1} to low values of 30 to 40 nmol gVS^{-1}. Subsequently, it increases in all three reactors before levelling off at values that exceed that of the inoculum. In Reactor 1 this trend is less clear and in general the measured cofactor contents were lower in this reactor. Despite the slight differences in the trends, on average the cofactor contents did not significantly differ between the three replicates.

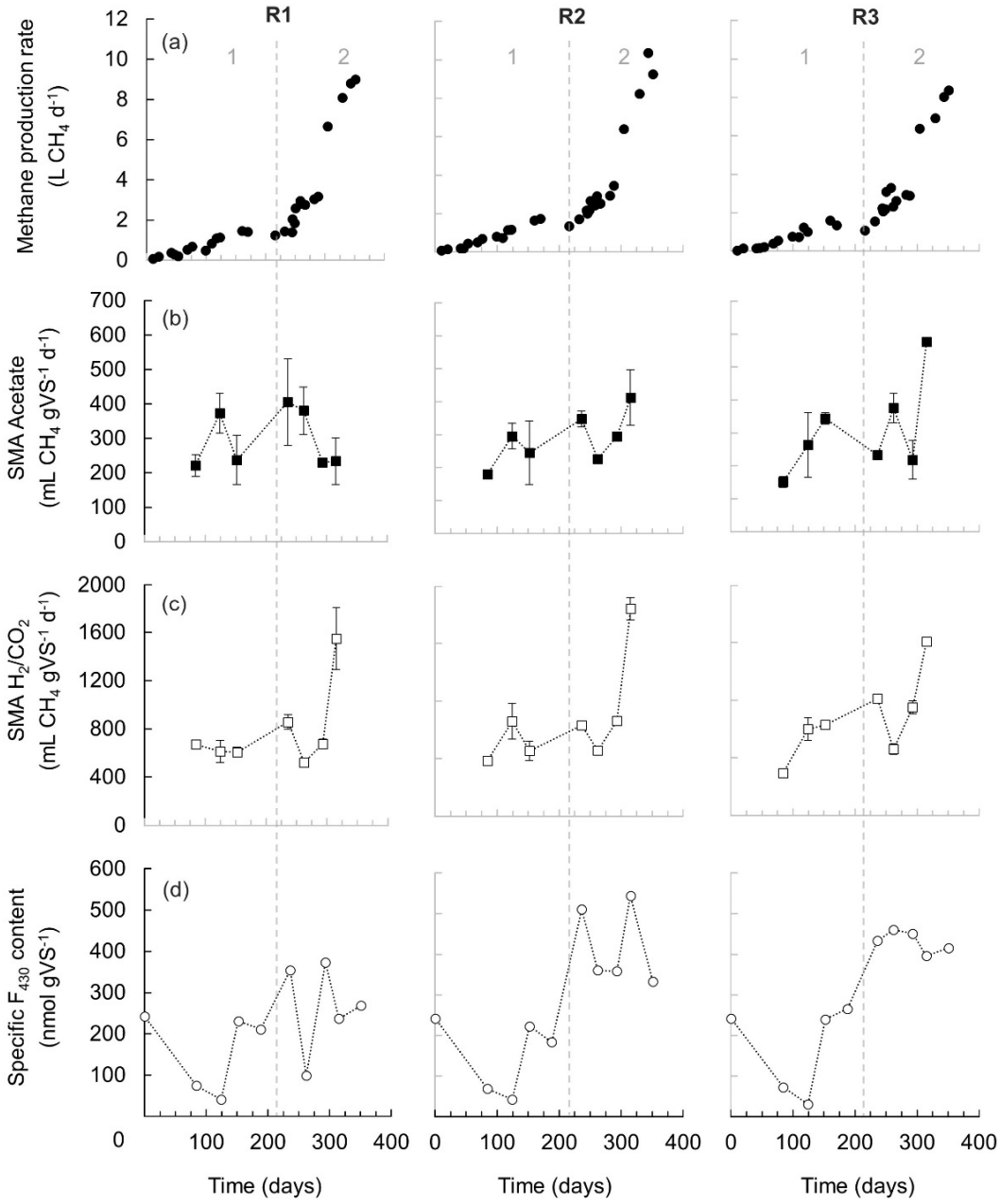


Figure 7.7 The evolution of the **(a)** methane production rate (●) **(b)** specific methanogenic activity (SMA) on acetate (■) **(c)** specific methanogenic activity (SMA) on H_2/CO_2 (□) and **(d)** specific cofactor F_{430} content (○) over the 351 day operational period in reactors R1, R2 and R3 (from left to right). Based on the evolution of the OLR (Figure 7.6) and methane production rate the experimental period is divided into two main parts, denoted here by the dashed grey line. An average SRT of 200 days and 180 days was maintained in Part 1 and Part 2, respectively.

7.2.3 Discussion

Comparison between the evolution of SMAs and reactor performance

The SMAs on both acetate and H_2/CO_2 do not show a clear, consistently increasing trend throughout Part 2 of the experimental period, which might have been expected based on the increasing methane production. Indeed, between day 200 and 300 the methane content (data not shown) and production rate consistently increased whereas in neither of the reactors a similar, gradually increasing trend of the SMAs is observed. Considering the importance of the hydrogenotrophic pathway in the LCFA degradation discussed earlier,

the relatively higher SMAs on H_2/CO_2 compared to acetate are in the line of expectations (Cavaleiro *et al.*, 2009; Bialek *et al.*, 2014). Moreover, the ratio of SMA on H_2/CO_2 and SMA on acetate seems to have increased during Part 2 of the experiment. This observation could indicate that the additional LCFAs, which were introduced, mainly triggered an increased activity of the hydrogenotrophic methanogens, whereas the acetotrophic ones maintained their activity on previous levels. Molecular genetic analyses on both DNA and cDNA level should be performed in order to check the aforementioned observations.

Comparison between the evolution of cofactor F_{430} content and reactor performance

The decrease in cofactor content during the start-up of the reactor is consistent with previous observations. Less than 15% of the initial inoculums' cofactor content was measured after 125 days of operation. The main explanation for this observation is the very low sludge loading rate which was applied in the first phase of the experiment, hence underfeeding the initially active inoculum. Indeed, also the methane production was very limited during Part 1 and the same observation has been reported for the *mcrA* transcripts in a digester subjected to starvation (Munk *et al.*, 2012). The consistent increase in cofactor content in all three reactors in the 150 to 190 days period is remarkable, considering the fact that the SLR was not significantly increased in this period and could not have "driven" this increase in cofactor content as it did in previous experiments (e.g., Section 6.2) and as reported in literature (Kida *et al.*, 2001). Furthermore, no significant increase in methane production was observed during this period. The cofactor measurements here indicate a methanogenic potential which is not in accordance with the actual in-situ methane production. Based on this observation one could ascribe the cofactor measurement a predictive character here, since it seems to indicate that sufficient cofactor is present to accommodate higher SLRs. Considering the fact that previous, more closely monitored, experiments seemed to exclude the possibility of F_{430} to be used in a predictive way, this observation should be interpreted with caution. Nonetheless, despite only having two data points to confirm the upward trend, it is consistent over all three reactors.

Based on the steadily increasing loading and methane production rates and the hypothesized correlation between both these parameters and the cofactor content (Kida *et al.*, 2001), a steadily increasing cofactor F_{430} content was expected in Part 2 of the experiment. However, this is not observed in either of the reactors, as the cofactor content instead levels off. This "plateau" is reached at cofactor contents above 300 nmol gVS^{-1}, which are quite high for non-enriched cultures. The methane production does continue to steadily increase during this period, implying that towards the end of the experiment the same amount of biomass can more effectively use the same (or an even a lower) amount of cofactor to produce the same amount of methane. A possible explanation for this phenomenon is a community shift. However, this hypothesis contradicts the expectation that cofactor F_{430} content would be community independent as stated in the previous section (Morris *et al.*, 2013; 2016). Mechanistically, it makes sense to assume that a fixed amount of F_{430} molecules are capable of producing a certain amount of methane, regardless of which methanogen is producing the F_{430} and performing the reaction. Unfortunately, the community analyses of these experiments have not been performed yet at this point in time. However, certain visual observations imply that such a shift may indeed have taken place. In Part 2 of the experiment a morphological shift was observed in all three

reactors, from mostly granular sludges to more flocculent sludge. It is hypothesized that this shift was induced by the introduction of additional LCFAs in the reactors and potentially coincides with a community shift. The analyses of the community structure data should elucidate these hypotheses.

Despite the abovementioned remarks, the cofactor F_{430} content at least partly captures the trend of increasing methane production. Furthermore, if the community analysis can substantiate that the incoming LCFAs were mainly handled through the hydrogenotrophic route, the observed increased cofactor F_{430} content proves that monitoring on cofactor F_{430} level does not discriminate between hydrogenotrophic or acetotrophic methanogenesis, but rather provides a complete picture of (potential) methanogenic activity. On the other hand, if the community analysis indicates that the shift occurred around the same time the F_{430} curve flattens out, this may again indicate that the new methanogenic community (presumably consisting of mostly active hydrogenotrophic methanogens) requires less F_{430} to achieve the same methane productivity. Considering the suspected importance of the hydrogenotrophs in these experiments, it is highly recommended to include cofactor F_{420} measurements in future experiments. Based on the SMA results, the ratio of F_{420} over F_{430} could be expected to increase over time.

In summary, the relationship between reactor performance and methane production, on the one hand, and SMA and cofactor content, on the other hand, was not clear-cut in this experiment. Both monitoring tools seemed to provide some information on the (potential) methanogenic activity of the sludges but had their limitations. In general, the trend in cofactor F_{430} content was upwards after the start-up period, whereas the SMA only increased at the very end of the experiment. Future experiments should include cofactor F_{420} measurements in order to try to capture the (changes in) activity of hydrogenotrophic methanogens. Moreover, specific methane production rate data would provide a more solid basis to test the SMAs and the cofactor contents head-to-head.

7.3 Can stratification of methanogenic activity in a full-scale digester be detected by cofactor F_{430} measurements?[14]

Considering the link between methanogenic activity and cofactor F_{430} content, in function of time, uncovered in Chapters 5 and 6, the spatial distribution of methanogenic activity and cofactor F_{430} content is investigated in this chapter. Incomplete mixing of full-scale bioreactors is not a well-studied topic, despite its possible implications for the hydrodynamic and biochemical properties of the sludge. In this experiment, a full-scale digester which was suspected to be incompletely mixed, was selected in order to see whether physico-chemical parameters of the sludge differed at different heights. In the case of improper mixing, (predominantly) acidogenic zones on the one hand, and methanogenic zones, on the other hand, may be present. Cofactor F_{430} analysis is investigated as a potential tool to detect the presence and location of these methanogenic zones.

7.3.1 Materials & methods

Sample origin

The samples were obtained from a full-scale anaerobic digester located at a wastewater treatment plant. The reactor had an effective volume of 8935 m^3 and was operated at 35 °C. Sampling ports were located at 5 m, 10 m, 15 m, and 20 m height and at the overflow point (23 - 24 m). The samples were stored at -20 °C after sampling and during transportation. Figure 7.8 shows a schematic of the anaerobic digester.

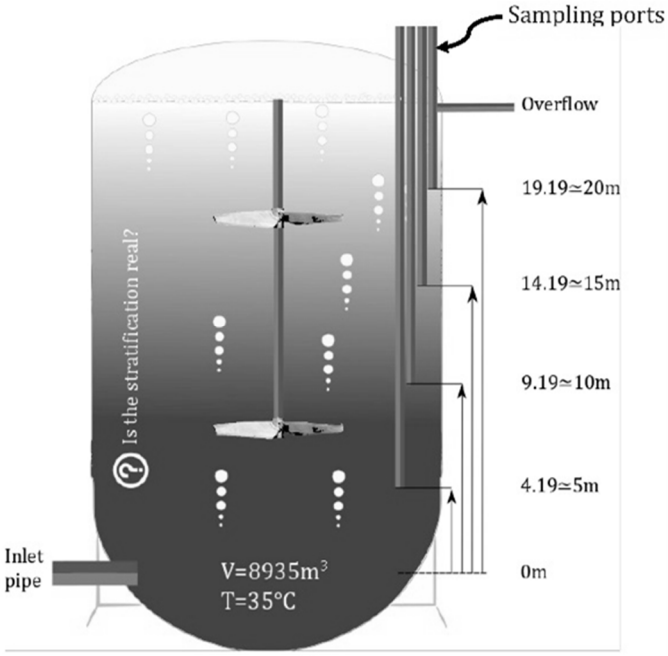


Figure 7.8 A schematic of the full-scale anaerobic digester indicating the sampling points. Taken from Del Pozo *et al.* (2017).

[14] This experiment was performed in collaboration with David Fernandes del Pozo from the Department of Mathematical Modelling, Statistics and Bioinformatics at Ghent University, Belgium, who performed the sampling campaign and the analytical analyses.

Analytical methods

The basic characterisation of these samples was performed at Ghent University. Detailed information with respect to the used methods can be found in Del Pozo *et al.* (2017). The following parameters were determined:

- Total solids (TS) and total suspended solids (TSS)
- Viscosity
- Bulk & floc densities

Additionally, the total solids (TS) and volatile solids (VS) concentrations per g of pellet were determined on the thawed samples at the KU Leuven. To this end, the samples were thawed and approximately 0.4 to 0.9 g of pellet was weighed and added to pre-weighed aluminium recipients. The TS and VS measurement was identical to the TSS and VSS determination described in Chapter 3. However, the samples were kept in the 105 °C oven for a longer period of time in order to assure that all the water had evaporated. The TS and VS calculation was done according to Equation 3-2 but instead of dividing by the volume, the weighed pellet per sample was used.

Cofactor F_{430}

Cofactor F_{430} was extracted and quantified using Protocol 4 (Table 4.1) as described in Section 4.1.2.

In order to more objectively compare the samples, 0.4 to 0.7 g of pellet was weighed for each sample prior to extraction. The exact pellet weights used for the extractions are shown in Table 7.1 alongside the corresponding VS weights.

Table 7.1 Pellet and volatile solids weights used for the cofactor F_{430} extractions. Between 0.4 and 0.7 g of pellet was used per sample, corresponding to a volatile solids range of 0.035 to 0.055 g.

Sample	Pellet weight (g)	Volatile solids (g)
Overflow 1	0.497	0.036
Overflow 2	0.665	0.048
20m 1	0.521	0.043
20m 2	0.499	0.042
15m 1	0.500	0.038
15m 2	0.495	0.037
10m 1	0.485	0.040
10m 2	0.636	0.053
5m 1	0.659	0.051
5m 2	0.608	0.047

The quantification of volatile solids was performed in order to be able to compare the cofactor concentration on both a pellet weight and a VS weight basis. The latter, in theory, better reflects the biomass concentration in the samples. On the other hand, its analysis introduces an additional experimental error which needs to be taken into account.

7.3.2 Results

Absorbance versus HPLC quantification of full-scale samples

Because this experiment was performed on a full-scale digester, it is interesting to compare the results of the preliminary absorbance quantification and the quantification on HPLC which includes additional separation on the C18 column. Figure 7.9 shows the

absorbance spectrum and HPLC chromatogram (with the corresponding absorbance spectrum in the inset) for one of the samples.

The typical F_{430} spectrum (see also Section 4.1.3) is hardly recognisable after the first purification using the C18 cartridges and quantification by spectrophotometry. A feint increase in absorbance is observed from about 450 nm but this is largely obscured by the clear increasing trend from 430 nm to 300 nm. In contrast, the absorbance spectrum corresponding to the F_{430} peak in the HPLC chromatogram shows a much "cleaner" spectrum for the same sample and is in accordance with the F_{430} spectrum known from literature. Furthermore, notice the additional peaks in the chromatogram (e.g., around 27 minutes), which indicate the presence of compounds that also absorb at 430 nm.

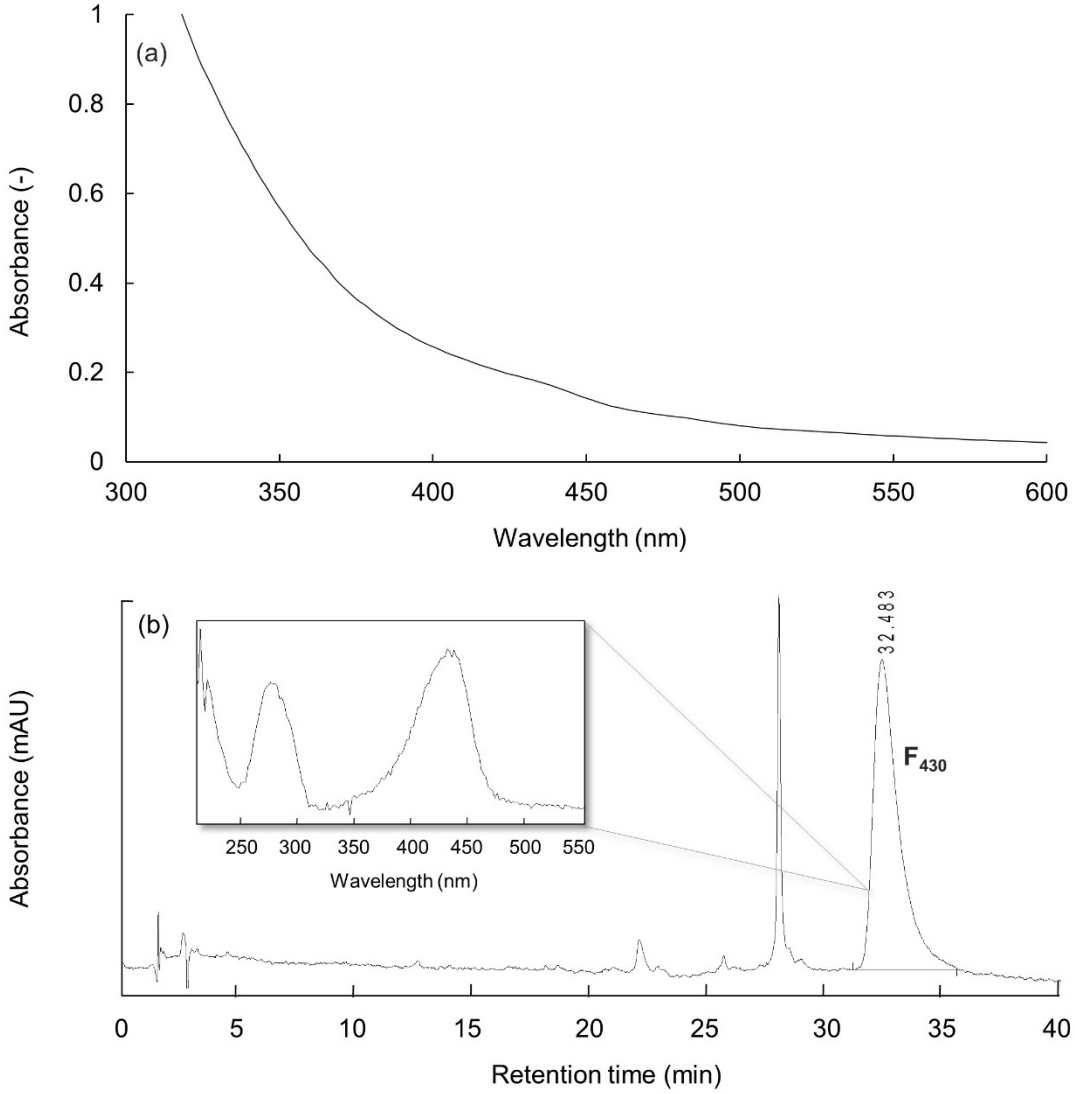


Figure 7.9 A typical **(a)** absorbance spectrum from spectrophotometry and **(b)** HPLC chromatogram with the absorbance spectrum of the F_{430} peak shown in the inset. Interfering compounds clearly distort the typical F_{430} spectrum, rendering the preliminary quantification based on spectrophotometry unreliable.

Reactor stratification and cofactor F_{430} content

Del Pozo and co-workers (2017) analysed the physical characteristics of samples taken from all heights (including the inlet for which the cofactor content was not analysed).

These analyses included concentration (TS and TSS), bulk density, floc density and rheology measurements. Based on their results they suggested a mild stratification below 10 meter depth, a zone encompassing 46.5% of the total reactor volume.

Figure 7.10 shows the cofactor F_{430} contents calculated per gram of pellet and per gram of VS for all tested heights. The average cofactor content across all samples is around 23 nmol gVS^{-1} and differences between the different heights seem to be limited. However, based solely on visual observation, a decreasing cofactor content can be observed towards the bottom of the reactor. This is observed for both the normalization per gram of VS and per gram of pellet. A one-way ANOVA (Analysis of Variance) test performed in order to see whether the means significantly differed, found p-values above 0.05 for both calculation methods (0.0592 for the per gram of VS calculation and 0.0842 for the per gram pellet calculation). A pairwise t-test or Tukey's HSD (Honestly Significant Difference) which would have uncovered the heights that differed significantly, could therefore not be performed.

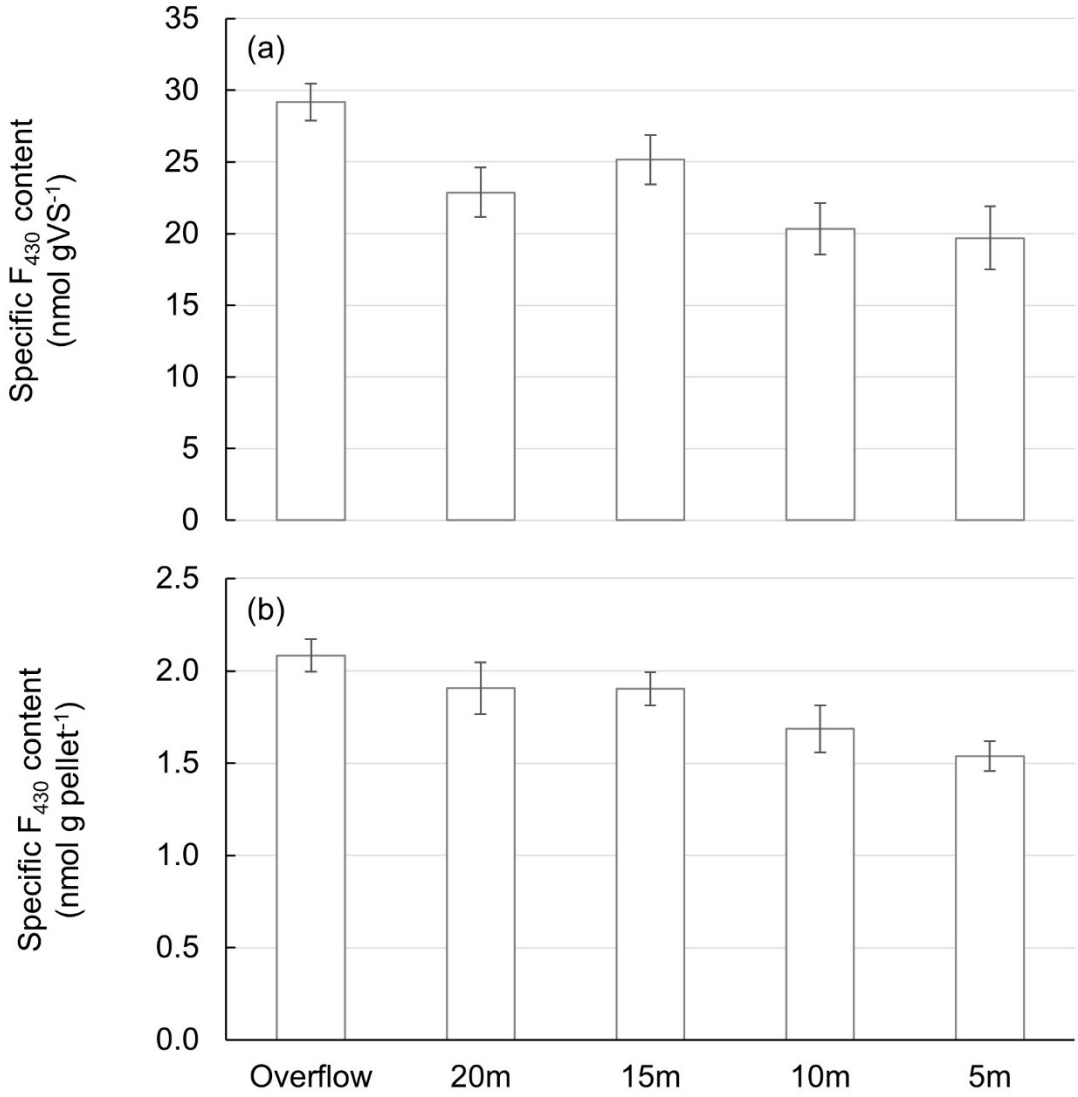


Figure 7.10 Specific cofactor F_{430} content **(a)** per gram of volatile solids and **(b)** per gram of pellet for all tested heights. Both calculation methods indicate a slightly decreasing trend with decreasing height which could, however, not be statistically substantiated. Error bars represent standard deviations of duplicate analyses (of the same sample).

7.3.3 Discussion

Absorbance versus HPLC quantification of full-scale samples

The differences between the absorbance spectrum determined by spectrophotometry after the first purification step, and the one determined by HPLC after additional separation on the C18 column, is clear. Compounds that interfered with the spectrophotometric quantification in the 450 nm to 300 nm were separated by the HPLC and a clear F_{430} peak and absorbance spectrum were observed as a result. This potential interference clearly demonstrates the importance of additional separation and quantification on HPLC for samples originating from industrial reactors fed with complex substrates. Indeed, it is expected that complex substrates and microbial decay products introduced interfering compounds into the sample matrix. The difference with, e.g., the samples from the experiment described in Section 6.1, originating from lab-scale digesters fed with a fully dissolved feed, is considerable. Because of the apparent absence of interfering compounds in those samples, the quantification by spectrophotometry showed a strong linear correlation with the HPLC quantification.

Reactor stratification and cofactor F_{430} content

The results from the physical characterization of the digester imply that it was not fully operating as a CSTR, as is often assumed. Since this may have had implications for the biochemical conditions prevailing at these different heights, zones promoting hydrolysis/acidogenesis/acetogenesis, on the one hand, or methanogenesis, on the other hand, could have been present. Unfortunately, the cofactor F_{430} quantification could not confirm this hypothesis. The differences between the top and bottom of the reactor which seemed to be present, could not be statistically substantiated. The main reason for this is likely the limited number of replicates. Moreover, the sampling ports are located only 1 meter from the reactor wall (the digester has a 24 m diameter), which may reduce the representability of the samples. In order to be able to ascribe the observed differences to actual differences in cofactor content, rather than random variation, multiple samples per location (preferably at least triplicates) should have been taken. Nevertheless, the downward trend observed for both calculation methods is in accordance with the physical stratification suggested by Del Pozo *et al.* (2017). In addition to the remarks made with respect to the statistics, it would also be highly recommended to determine additional parameters related to methanogenic activity at these different heights. For instance, if pH and *mcrA* copy and transcript numbers were determined at every height, these results could again be compared with the cofactor content. Cofactor F_{430} quantification could then be tested as a relatively quick way to pin-point the presence or activity of methanogens at certain regions in the bioreactor.

The absolute cofactor contents which were measured in this digester were very low compared to, e.g., the cofactor contents reported in Section 7.2 and literature reports (Diekert *et al.*, 1981; Kida *et al.*, 2001; Jiang, 2006). Nevertheless, the reactor was performing well with respect to methane production (data not shown). One explanation, related to the quantification, is that the relatively high viscosity of these samples reduced the cell lysis efficiency in the extraction procedure. Another explanation is that a certain fraction of the volatile solids may actually be originating from the feed rather than the biomass and, thus, the volatile solids concentration may not reflect well the actual biomass

concentration (which is in fact lower than what the VS measurement indicates, potentially yielding higher cofactor contents). Finally, a third possible explanation is the presence of a large fraction of biomass which is inactive and does not participate actively in the methane production. This large inactive fraction would imply that the reactor could be able to achieve the same performance with less biomass. Either way, the results imply that the digester seems to have a low specific activity (on a VS basis).

In summary, it was shown that the additional purification on the HPLC column is of paramount importance for industrial samples because of the interfering compounds which remain present after the first purification on the C18 cartridge columns. Furthermore, no statistically relevant differences in cofactor content were found between the different heights. This may have been due to the lack of sufficient replicates, since a decreasing cofactor content toward the bottom of the reactor seemed to be present. Based on the weight of evidence from the previous chapters and the preliminary results of this experiment, it is highly recommended to repeat this experiment on a reactor which is suspected to be stratified in terms of physical or biochemical properties. Additional replicates should be taken and additional parameters, such as pH and *mcrA* copy and transcript numbers should be determined in order to investigate potential differences in methanogenic activity at the different heights. Finally, the approach taken here could be expanded to bioreactor configurations with suspended and attached biomass (such as the reactors described in the previous experiment), since differences in methanogenic activity are also very likely in such cases.

7.4 Can cofactor F_{430} and F_{420} measurements predict or diagnose the failed start-up of anaerobic bioreactors?

In previous experiments (e.g., Section 6.2), a decreasing cofactor F_{430} content during the first 2-3 weeks of operation was observed, despite the successful start-up of the reactor. This decrease was the result of the balance between degrading and newly formed F_{430}. In this experiment, the evolution of the cofactor contents is again followed-up over the course of the start-up of two methanogenic anaerobic bioreactors. By following up the reactors' gradually decreasing performance and measuring the cofactors, additional insights were expected to be obtained. These insights could potentially allow the prevention of future reactor failure during start-up by means of cofactor measurements.

7.4.1 Materials & methods

Experimental set-up & operation

The two lab-scale AnMBRs used in this experiment were based on the experimental set-up described in Section 6.2.1, with slight modifications. The modifications were mainly related to the filtration operation. An additional pressure transducer and slight adaptations to the LabVIEW code improved the reliability of the TMP measurements. Furthermore, the filtration cycle was altered to include a 5 second backflush, every hour, in order to reduce membrane fouling. The net operational flux was kept constant at 12 L m^{-2} h^{-1} in both reactors. At the start of the run, both membranes were cleaned using a 1000 ppm sodium hypochlorite (NaOCl, 35-40 °C for 2h) and 1% citric acid (35-40 °C for 4 h) solution in order to remove, respectively, organic and inorganic fouling. On day 34 of the experiment, the membranes were cleaned again with 1000 ppm NaOCl for 2 h.

The effective operating volumes were 10.55 L and 8.95 L for reactor R1 and R2, respectively. Each reactor was seeded at a total concentration of 8 gVSS L^{-1} using a mixture of UASB sludge from a brewery which was crushed and sieved, on the one hand, and excess sludge from the synthetic dairy wastewater fed AnMBRs described in Section 7.2, on the other hand. During the first 3 weeks only limited volumes of sludge were taken for sampling. Subsequently, sludge was purged on a daily basis in order to maintain a fixed solids retention time (SRT) of 30 days. The imposed hydraulic retention time (HRT) was 27 hours and 23 hours in reactors R1 and R2, respectively.

Both reactors were fed with the synthetic dairy wastewater described in Section 5.1. However, the buffer solution used in this experiment consisted of 4.8 g L^{-1} KH_2PO_4 and 81 g L^{-1} K_2HPO_4 and had a pH of 8. It was used to supply alkalinity to the reactors and to maintain the pH between 6.5 and 7.5. Its supply rate was adjusted according to the reactors' activity. During the first 56 days of the experiment, both reactors were fed in pulses of 1 minute, every 72 minutes. From day 57 onwards, a difference in feeding pattern was applied: reactor R2 was fed for 2 minutes every 6 hours whereas the feeding pattern in reactor R1 was left unchanged.

During start-up the feed COD concentration was adjusted in order to maintain a sludge loading rate (SLR) between 0.15 and 0.25 in both reactors. To this end, the feed COD concentration was adjusted to the amount of volatile suspended solids (VSS) present in

the reactor. Figure 7.11 – a shows the evolution of the SLR over the entire experimental period. The resulting organic loading rates are shown in Figure 7.11 – b.

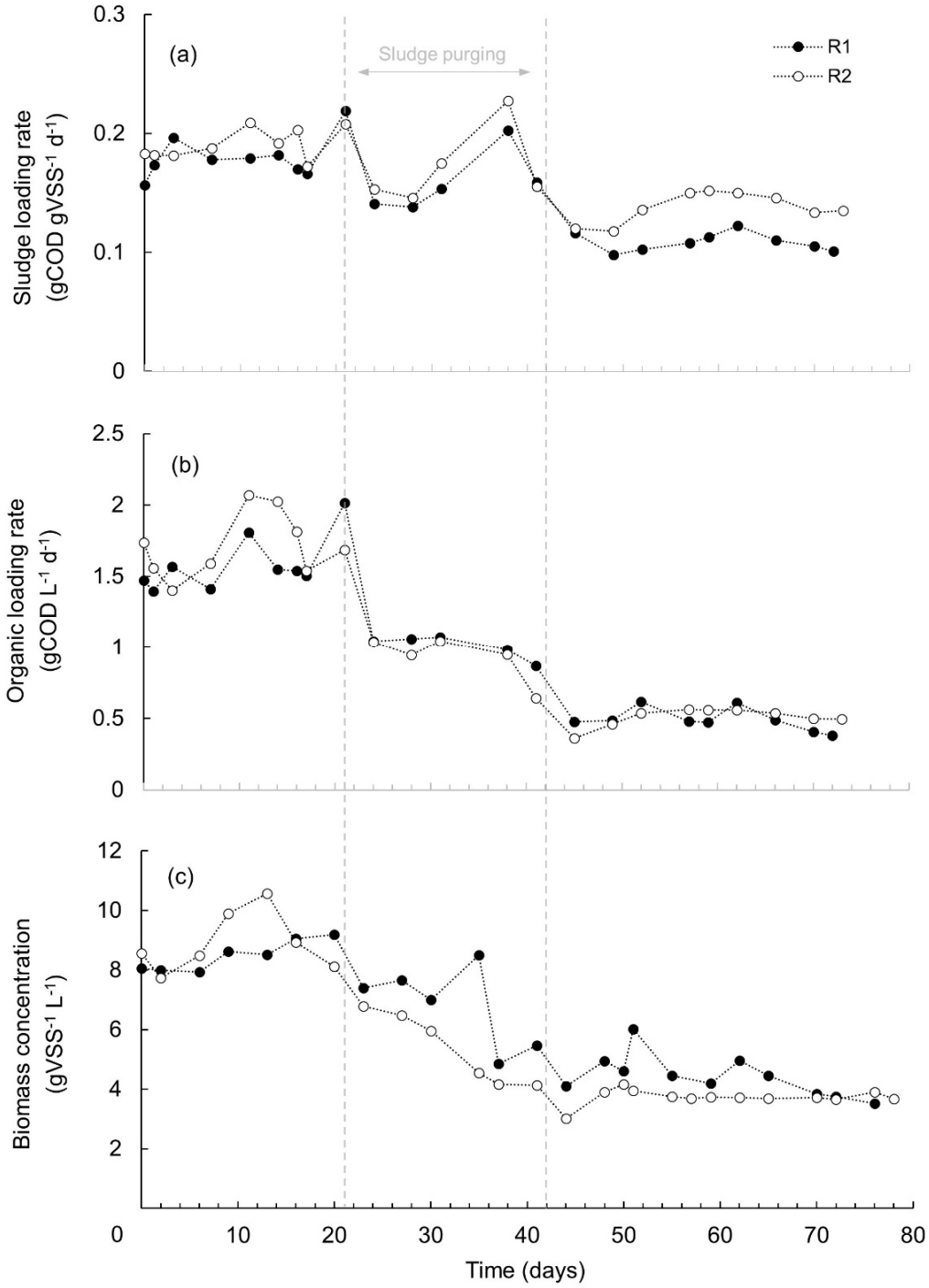


Figure 7.11 The evolution of the **(a)** sludge loading rate (SLR), **(b)** organic loading rate (OLR) and **(c)** biomass concentration expressed as gVSS L^{-1} in reactor R1 (●) and R2 (○) over the 80 days experimental period. Both reactors were operated on an SLR rather than on an OLR target basis. After 21 days of operation, sludge was purged daily in order to maintain a fixed SRT of 30 days in both reactors. Three weeks later, however, sludge purging was halted because of the continuous biomass loss in both reactors.

The expectation was that organic loading rates would be able to be gradually increased after a couple of weeks due to biomass growth and increased activity. However, from day 21 onwards the organic loading rates had to be decreased in order to maintain the same

sludge loading rates. After 41 days both loading rates were further reduced, reaching corresponding values of 0.1 - 0.15 gCOD $gVSS^{-1}$ d^{-1} and 0.5 gCOD L^{-1} d^{-1}. On day 49, it was decided to decouple the SLRs applied to both reactors due to a more significantly decreased reactor performance in reactor R1. The SLRs were maintained at 0.12 gCOD $gVSS^{-1}$ d^{-1} and 0.15 gCOD $gVSS^{-1}$ d^{-1} in reactor R1 and R2, respectively.

Figure 7.11 – c shows that, despite being seeded from the same inoculum and at the same biomass concentration, their concentrations quickly diverged. Therefore, it was decided to mix the contents of both reactors on day 16, yielding again similar biomass concentrations. The subsequent, gradually decreasing trend in both reactors from day 21 onwards resulted from the daily sludge purging applied to maintain the SRT at 30 days. Due to the continuous loss of biomass, from 42 days onwards sludge purging was ceased and the biomass concentrations stabilized between 3 and 5 gVSS L^{-1} in both reactors, with the concentration in reactor R2 being consistently slightly higher. The decrease in biomass concentration explains why from 21 days onwards significantly lower organic loading rates had to be applied in order to keep the sludge loading rates constant.

Analytical methods

The analytical methods used in this experiment have been described in the general material & methods section (Chapter 3). The following parameters were analysed.

- (Volatile) Suspended solids
- COD
- Total and individual VFA concentrations

Cofactor F_{430} and F_{420}

Cofactor F_{430} was extracted and quantified using Protocol 4 (Table 4.1) as described in Section 4.1.2.

Cofactor F_{420} was extracted and quantified using the fluorimetry method, as described in Section 4.2.2.

The reactors were more frequently sampled for cofactor F_{430} than F_{420} analysis.

7.4.2 Results

The experimental period will be described in terms of specific methane production, VFA concentrations, COD removal and cofactor F_{430} and F_{420} contents below.

Reactor performance and cofactor content

In order to assess the daily performance of the bioreactors, the classical performance monitoring tools were used. These served as indicators of methanogenic activity and were intended to be used to decide when, and by how much, to increase the SLR during operation. Figure 7.12 shows the evolution of specific methane production rate, and VFA concentrations and COD removal efficiency in both reactors.

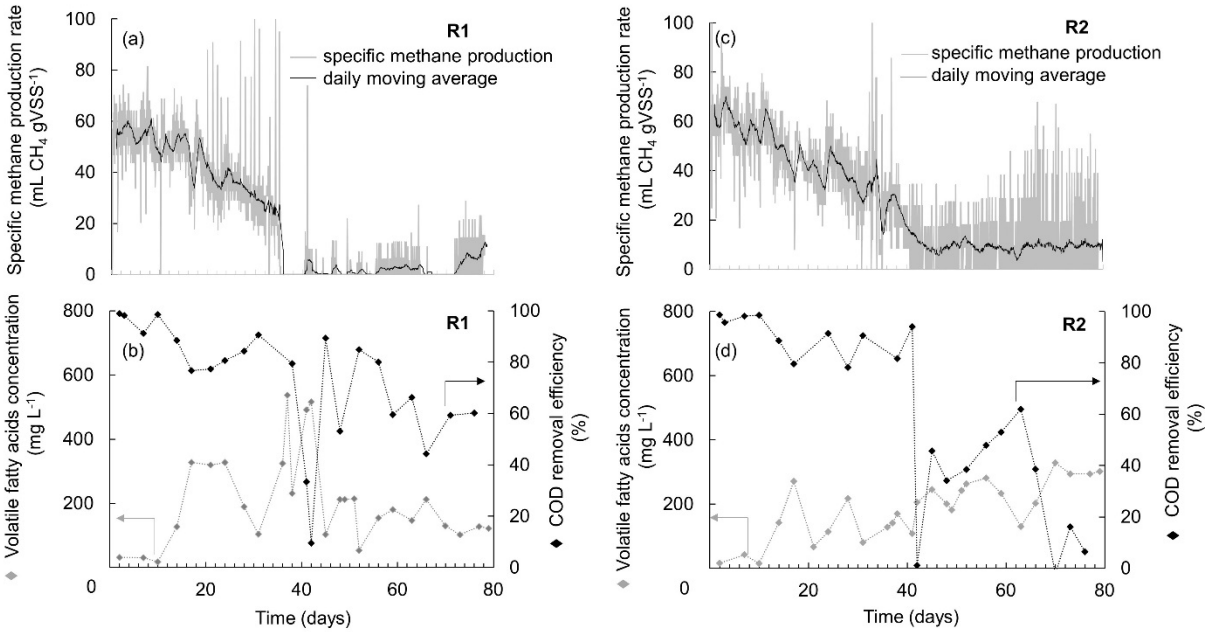


Figure 7.12 The evolution of **(a) (c)** specific methane production rate (—) with its daily moving average (—) and **(b) (d)** total volatile fatty acid (VFA) concentrations (♦) and COD removal efficiency (♦) in reactor R1 and R2, over the 80 days experimental period. After 21 days of operation, sludge was purged daily in order to maintain a fixed SRT of 30 days in both reactors. Methane production rates and COD removal efficiency decreased in both reactors and VFA concentrations were relatively high.

It is evident from Figure 7.12 that from the start of the experiment the performance of both reactors gradually deteriorated. Specific methane production rates almost immediately showed a consistent decrease. Both reactors started around 60 mL CH_4 $gVSS^{-1}$ d^{-1} and their production decreased to almost zero in reactor R1 and around 10 mL CH_4 $gVSS^{-1}$ d^{-1} in reactor R2. Some recovery was observed towards the end of the operation of reactor R1, reflected by slightly increasing specific methane production rates.

The volatile fatty acid concentrations were low and stable before day 10. Subsequently, their concentrations increased and this was accompanied by a decrease in COD removal efficiency. The COD removal efficiencies decreased from at least 90% to below 60% and VFA concentrations concomitantly increased to values of over 300 mg L^{-1} in both reactors. The volatile fatty acids were mainly present in the form of acetic and propionic acid (data not shown).

Based on the aforementioned results, in terms of their performance, the two reactors can be regarded as identical. Considering the clear, gradual decrease in reactor performance in both reactors, it is interesting to see how cofactor F_{430} and F_{420} contents evolved during the experimental period. Figure 7.13 shows a decreasing trend for cofactor F_{430} which then stagnates in both reactors, whereas cofactor F_{420} content fluctuates more widely.

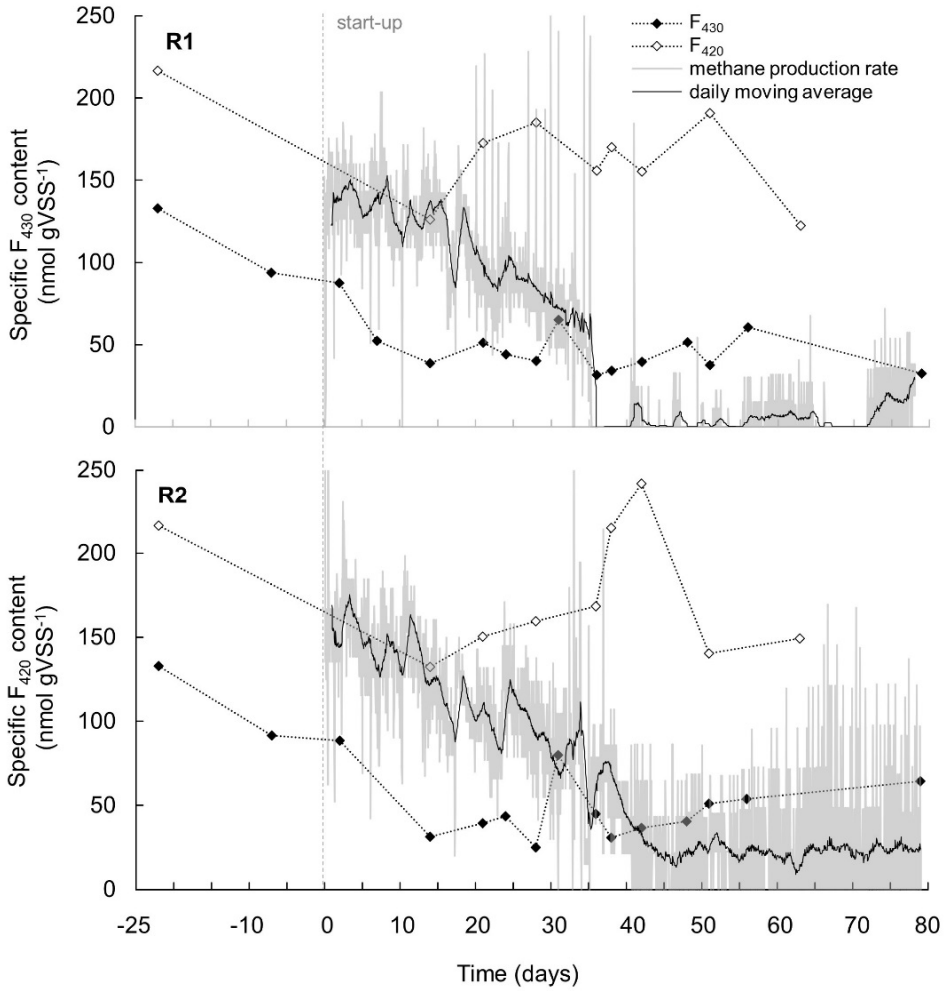


Figure 7.13 The evolution of specific cofactor F_{430} (♦) and cofactor F_{420} (◊) content plotted alongside the specific methane production rate (—) and its moving average (—) in reactor R1 (top) and R2 (bottom) over the 80 days experimental period. After 21 days of operation, sludge was purged daily in order to maintain a fixed SRT of 30 days in both reactors. For absolute values of the specific methane production rates see Figure 7.12 – a and c. Two cofactor F_{430} measurements were performed prior to the actual start-up, which is denoted by the grey dashed line. On day 16 the content of both reactors was mixed and re-distributed over the reactors. Before as well as during the actual start-up, the cofactor F_{430} content decreased in both reactors. Cofactor F_{420} content initially decreased but fluctuated afterwards and was always higher than F_{430} content.

Note that the first two cofactor F_{430} measurements were performed prior to the actual start-up of both reactors (22 and 7 days, respectively, hence the negative values on the x-axis). This is because the start-up of the reactors was delayed on two occasions due to technical problems with the membranes. In between these attempted start-ups, the reactors were fed on an intermittent basis in order to bridge the period to the new start-up.

The initial inoculum (22 days prior to the actual start-up) had a cofactor F_{430} content of around 130 nmol gVSS $^{-1}$ and a higher F_{420} content of around 220 nmol $gVSS^{-1}$. In two weeks' time, the cofactor F_{430} content had reduced by 30% to a value of around 90 nmol gVSS $^{-1}$. The onset of continuous feeding operation did not lead to an increase in F_{430} content and after two weeks, very low cofactor contents of about one third compared to the start of the experiment (30 nmol $gVSS^{-1}$) were measured. Afterwards, the cofactor F_{430} content remained low at 44 ± 10 and 45 ± 15 nmol $gVSS^{-1}$ in R1 and R2, respectively.

Cofactor F_{420} also shows an initial decrease and two weeks into continuous operation, its content was about half of the inoculum's initial content. However, the cofactor F_{420} content increased in both reactors after 14 days of operation. Subsequently, fluctuations are observed, particularly in reactor R2. For the last data point, cofactor contents similar to the first 14 days of operation were measured in both reactors. Note that throughout the experimental period, cofactor F_{420} content was 2 to 7 times higher than cofactor F_{430} content in both reactors, yielding average F_{420} over F_{430} ratios of 3.6 ± 1.2 and 4.3 ± 1.9 in R1 and R2, respectively. The ratio being the lowest for the inoculum measured 22 days prior to reactor start-up.

As in the previously described experiments, the Pearson correlation coefficient was determined as a measure of the linear relation between two variables. However, no significant correlations were found in either of the reactors between the two cofactor contents and specific methane production rate, nor between the cofactors.

7.4.3 Discussion

Main reasons for the failed bioreactor start-ups

The decreasing methane production rates and increasing VFA concentrations clearly indicated that, in these reactors, the microorganisms (and in particular the methanogens) were insufficiently converting the supplied substrates to methane, despite the low SLRs and OLRs and limited sludge purging rates that were applied. Considering the doubling times between 5 and 30 days which have been reported for methanogens (Zhang & Noike, 1994; Dereli *et al.*, 2012), the application of an SRT of 30 days was not expected to interfere with the growth of methanogens. Moreover, multiple experiments have been described successfully operating AnMBRs at this SRT (Huang *et al.*, 2013; Pacheco-Ruiz *et al.*, 2017), including the reactors described in Section 7.1 of this chapter. Nevertheless, the application of sludge purging between day 21 and 42, led to a continuous decrease in biomass concentration and worsened the reactor performance. This indicated that despite the gentle conditions, the methanogens were insufficiently active and, therefore, did not grow fast enough. The decreased methanogenic activity was also evidenced by the increasing acetate and propionate concentrations, indicating limited activity of both acetotrophic and hydrogenotrophic methanogens.

Based on the previous remarks and the cofactor measurements, three main reasons can be identified for the failed start-up: (*i*) the activity of the initial inoculum, (*ii*) the time between its preparation and the actual start-up and (*iii*) the relatively high sludge purging rate applied relatively soon after start-up. Despite using two different sources in order to obtain an as active and diverse as possible initial microbial community, the initial cofactor F_{430} content was not particularly high (i.e., 130 nmol $gVSS^{-1}$). Nonetheless, previously, the AnMBR described in Section 6.2 was successfully started-up with inoculum originating from the same brewery, so a similar performance was expected[15]. Moreover, mixing with waste sludge from the experiment described in Section 7.1 was expected to increase the diversity of the inoculum.

[15] Unfortunately, the absolute values of the initial inoculum cofactor contents between this experiment and the one described in Section 6.2 cannot be objectively compared due to improvements that were made to the extraction protocol used in this experiment.

The evolution of cofactor contents during deteriorating reactor performance

Once the inocula were mixed, they were introduced into the bioreactors and subjected to continuous stirring and heated to the operating temperature. The intermittent feeding of the reactors during the three weeks leading up to the actual start-up may have been insufficient, as evidenced by the 30% decrease in cofactor content over this period, potentially indicating underfeeding of the inoculum. At the time of the actual start-up, the cofactor F_{430} content was relatively low (i.e., 90 nmol $gVSS^{-1}$). If this measurement were to be performed right before start-up as a standard practice, re-inoculation or addition of sufficiently active inoculum should be considered at this point. The inability of the reactors to recover their performance was reflected well in the low cofactor contents that were measured (i.e., around 50 nmol $gVSS^{-1}$). Instead of further decreasing together with the methane production rate, the cofactor contents stabilized around this value, possibly indicating that a "baseline" value was reached.

The cofactor F_{420} trends were less clear and do not seem to provide interesting information with respect to methanogenic activity. Moreover, unfortunately, the F_{420} measurement could not be performed as frequently as the F_{430} measurement. However, the clearly higher cofactor F_{420} contents found in this experiment could, in theory, indicate a relatively high hydrogenotrophic activity (Kida *et al.,* 2001). Interestingly, on the two days on which a clearly higher cofactor F_{420} content was measured in reactor R2 (i.e., day 38 and 42), propionate concentrations were temporarily increased in this reactor. This observation could indicate that hydrogenotrophic activity (and thus an increase in cofactor F_{420} concentration) was triggered by the accumulation of propionate, a mechanism which could be similar as the one described in Section 6.2 for acetate accumulation and cofactor F_{430} production. Further experiments focusing on this phenomenon should be performed in order to confirm this hypothesis. Based on the results, the cofactor F_{420} content seemed to not reflect the significantly deteriorated performance and methanogenic activity as well as cofactor F_{430} did. Moreover, no significant correlation was found between the two cofactors, in contrast to other experiments described in this work.

In summary, this experiment highlighted the importance of a sufficiently high methanogenic activity and cofactor content of the inoculum. Indeed, limited inoculum activity and biomass growth led to deteriorating reactor performance. The relatively low cofactor F_{430} content of 90 nmol $gVSS^{-1}$ at the actual start-up of the reactors only temporarily allowed stable operation and when cofactor content dropped even further (to 30 nmol $gVSS^{-1}$), performance was severely hampered. Clearly, the application of sludge purging complicated the recovery of both reactors and all interventional measures taken to improve the performance afterwards were unsuccessful. A low specific cofactor content, in combination with a low total biomass concentration, yielded a low, total cofactor concentration in the bioreactors, hereby limiting their methanogenic performance. Based on these observations, cofactor F_{430} content may be an interesting additional parameter to quantify prior to, and during, the start-up in order to diagnose and prevent failed start-ups and steer reactors toward stable operation.

7.5 Does cofactor F_{430} content correlate with methane production across individually sampled reactors?[16]

In all previous experiments, cofactor content was followed-up in the same reactor over a prolonged period of time or at different heights. In this section, it is evaluated whether snap-shot measurements of cofactor F_{430} in several stable-performing bioreactors correlate with their methane productivity. As such, the correlation between cofactor F_{430} and methane production rate, which was found in Chapter 6, is re-evaluated across multiple reactors. It is hypothesized that a similar functionality in the bioreactors should be reflected by a similar cofactor F_{430} content.

7.5.1 Materials & methods

Experimental set-up

The set-up used in this experiment was identical to the one described in Section 5.2.1. A total of 12 reactors were started-up with three different inocula. Three sets of four replicate reactors were inoculated with three different inocula originating from a municipal wastewater treatment plant (WWTP) digester, a full-scale dairy UASB and a full-scale brewery UASB. The reactors were fed once every two days and the sludge loading rate and COD concentration in the feed was adapted according to their performance.

All reactors were fed with a synthetic wastewater containing a main carbon source (milk powder or sucrose), macronutrients, trace elements and buffer compounds adapted from De Vrieze *et al.* (2013). The exact composition of the synthetic feed is reported in Table 3.1. The milk powder was a commercially available variant (Douwe Egberts) designed for professional coffee machines and consisted of 12% (w/w) fat, 63% (w/w) carbohydrates (all sugars), 16% (w/w) proteins and 0.5% (w/w) salt. An equivalence factor of 1.278 gCOD g milk powder^{-1} was established based on a linear calibration.

Analytical methods

The analytical methods used in this experiment have been described in the general material & methods section (Chapter 3). The following parameters were analysed.

- (Volatile) Suspended solids
- COD

Cofactor F_{430} quantification

Cofactor F_{430} was extracted and quantified using Protocol 4 (Table 4.1) as described in Section 4.1.2.

Samples for F_{430} quantification were taken during stable operation, which was defined here as a period with stable methane production and a methane yield of at least 70% of the theoretical yield. From day 50 onwards, all reactors showed stable performance until the end of the operational period. The samples were centrifuged and stored at -20 °C prior to analysis.

[16] This experiment was performed in collaboration with Lynn Lemoine from the KU Leuven Department of Earth and Environmental Sciences – Division of Soil and Water Management, who ran the reactor experiments and performed the analytical analyses.

The samples for cofactor F_{430} analysis were taken two days after feeding, except for two samples from the set of the brewery UASB inoculum. For these samples one feed was skipped and the samples were taken 5 days after feeding. The cumulative methane yield was calculated over the 2 or 5 day period and the specific (average) methane production was then calculated by dividing the yield by the biomass concentration and multiplying with the amount of COD fed.

7.5.2 Results

Variability between the inocula and the replicates

First, the means of the sets of reactors inoculated with the different inocula were subjected to an ANOVA (Analysis of Variance) test in order to determine whether the methane production rates and cofactor F_{430} contents differed significantly between each reactor set or between the replicates within the set. Since the reactors were being fed at different sludge loading rates and it has been shown (Section 6.2) that this parameter may influence both methane production and cofactor content, the methane production and cofactor content were also normalized per gram of COD fed and the analysis was repeated. The methane production rate divided by the COD fed is denoted as the specific methane yield. Figure 7.14 shows the data along with their means, 95% confidence intervals and overlap lines.

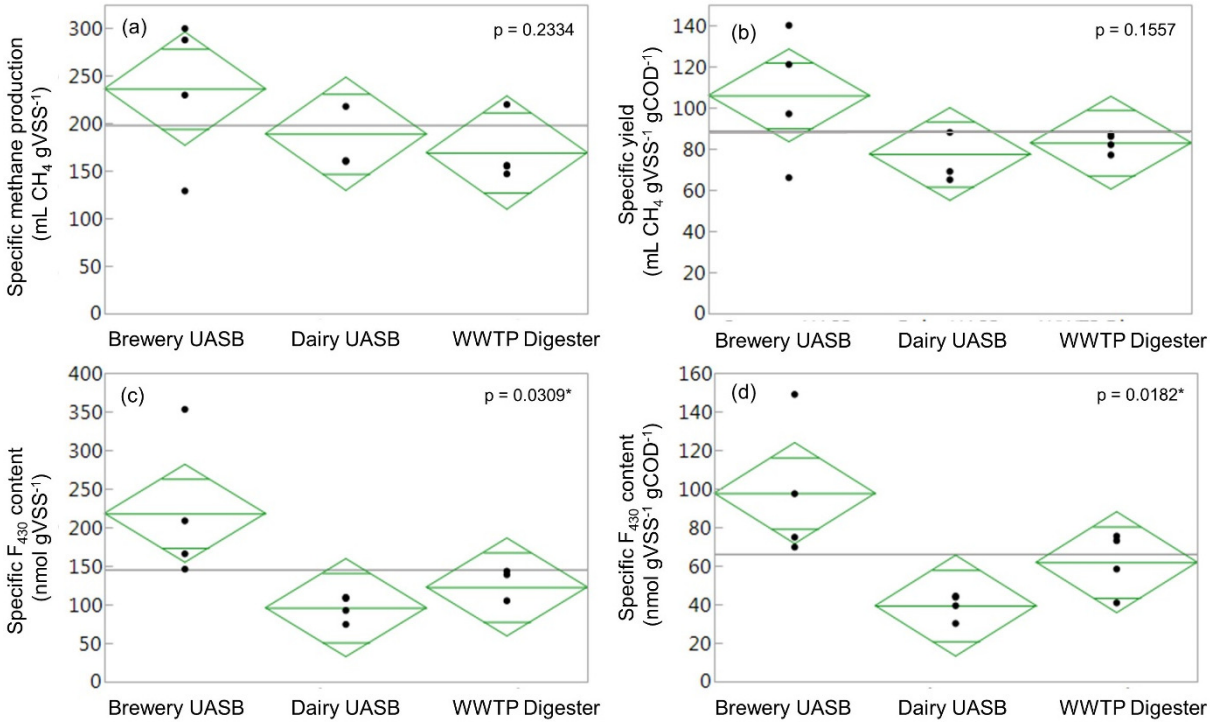


Figure 7.14 ANOVA analysis (n = 12) performed on the means of the **(a)** specific methane production **(b)** specific methane yield **(c)** specific cofactor F_{430} content and **(d)** specific cofactor F_{430} content per g of COD fed in the differently inoculated reactors. Each inoculum had four replicates. A p-value below 0.05 indicates that the means of the different inocula differed more significantly than the four replicates within each set. The top and bottom vertex of the diamonds, horizontal central line and top and bottom lines within the diamonds respectively denote the 95% confidence intervals, means, and overlap lines. Overlapping overlap lines indicate that the two means do not significantly differ (with a 95% confidence interval). The grey horizontal line indicates the grand mean across all reactors. Both cofactor normalization methods indicated a significant difference between at least two of the different inocula.

The ANOVA analysis shows that the methane production (thus the functionality) of the reactors did not significantly differ between the different inocula, even when taking into account the differences in COD fed. However, specific cofactor contents did significantly vary between the different inocula.

Based on the results of the ANOVA analyses, Tukey's HSD (honestly significant difference) test was performed in order to determine which of the inocula differed from one another with respect to the specific cofactor contents. What was expected based on the visual observation of Figure 7.14 was confirmed by Tukey's HSD test. The test revealed only significant differences between the brewery and the dairy UASB inocula ($p = 0.0319$ and $p = 0.0151$ for the specific cofactor content and the specific cofactor content per gram of COD fed, respectively).

Correlation between cofactor F_{430} content and methane production

In Figure 7.15, the specific cofactor F_{430} content and specific cofactor content per gram COD fed is plotted against the specific methane production and specific yield, respectively, for each set of reactors.

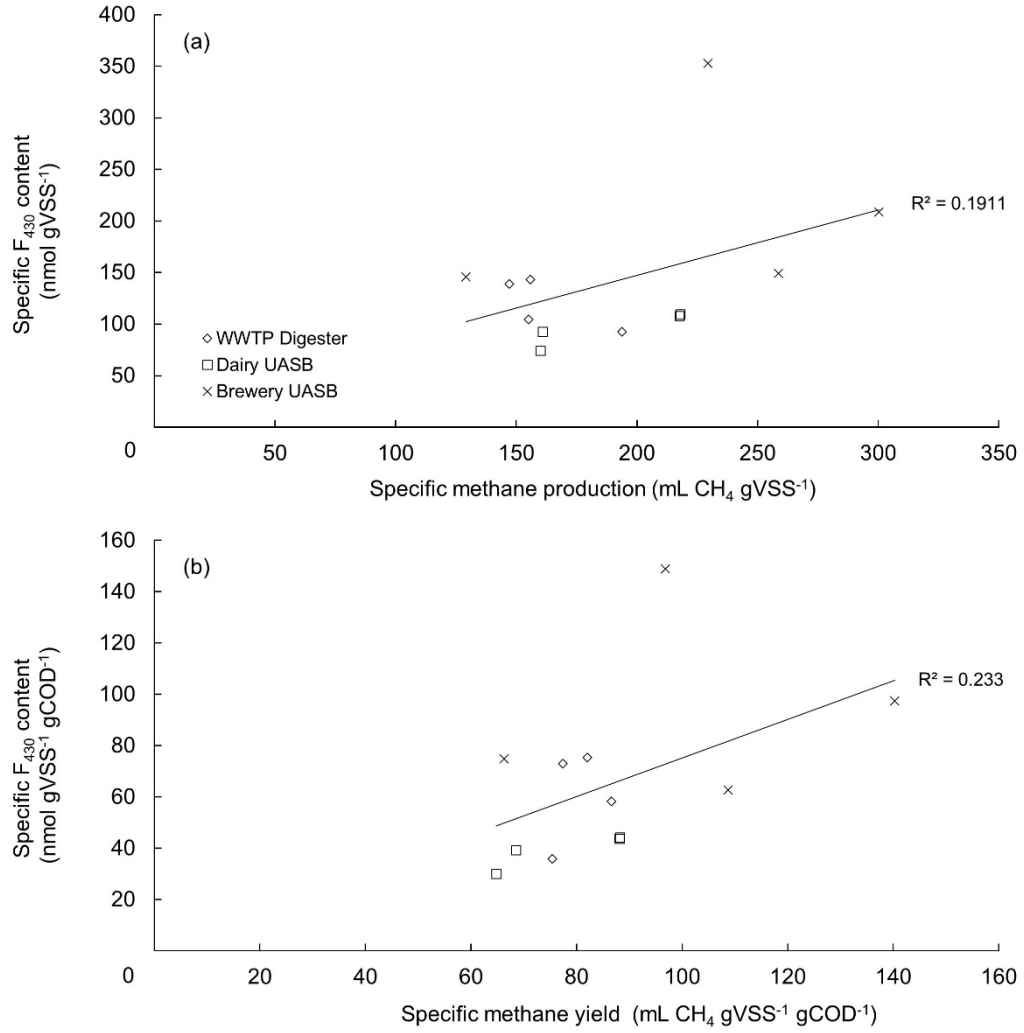


Figure 7.15 The **(a)** specific cofactor F_{430} content plotted against the average specific methane production and **(b)** specific cofactor F_{430} content normalized per gram of COD fed plotted against the average specific yield for the three sets of reactors. The linear correlation between cofactor content and methane production is poor in both cases.

From the spread over the x-axes in Figure 7.15 it is evident that the performance (functionality) at the time of sampling differed between the reactors, despite all being sampled during what was defined as stable performance. Note that in the ideal case of exact identical functionality across the reactors, the cofactor F_{430} content would be expected to also be identical and all samples would cluster together (as is the case for two of the dairy UASB samples). The linear correlation between cofactor content and methane production rate, which was observed in Section 6.2, is very weak in this experiment as evidenced by the poor linear fit and low R^2. One of the brewery UASB reactors is clearly an outlier, even when the normalization per gram of COD is included. Its cofactor F_{430} content is clearly higher than in all other reactors, whereas its methane production rate is relatively low, in comparison. Excluding the outlier still produces a poor fit.

7.5.3 Discussion

Correlation between cofactor F_{430} content and methane production rate in 12 individually sampled reactors

Based on the results presented in Chapter 6, a positive linear relation was expected between cofactor content and methane production rate for the 12 sampled reactors. However, the linear correlations presented in Figure 7.15 are very weak. There are three main explanations for this observation. Firstly, the reactors were fed discontinuously in this experiment, which induces an increased methanogenic activity shortly after feeding and reduced methanogenic activity when most of the feed is consumed (see also the sinusoidal pattern in Figure 5.3, Section 5.1.2). The produced methane was measured at the very end of the feeding period (generally 2 days between feeds) and samples for cofactor F_{430} analysis were also taken at this point. This means that a cumulative, rather than an instantaneous, yield or methane production rate was measured and the same holds for the cofactor F_{430} content.

Second, in Chapter 6, it was explained that cofactor F_{430} production and degradation is a dynamic process and that its production responds to the amount of substrate that is supplied to the methanogens (Kida *et al.*, 2001). Therefore, the correlation between F_{430} and methane production rate was found to be most significant when the latter was averaged out over a period of several hours at the most. In this experiment, the longer methane production measuring interval does not reflect the actual methanogenic activity (and thus cofactor content) well at the time of sampling and this may have affected the correlation. Hence, as also stated in the conclusion of Chapter 6, even in continuously operated reactors where real-time methane production can be measured, snap-shot measurements of cofactor F_{430} have to be interpreted with caution mainly because of the degradation kinetics of the cofactor. A similar conclusion was drawn by Munk *et al.* (2012) for their quantification of the *mcrA* gene transcript over copy number ratio. However, note that *mcrA* gene copy and transcript numbers determined in individually sampled reactors or environments have been reported to correlate with methanogenic activity (Watanabe *et al.*, 2009; Ma *et al.*, 2012; Morris *et al.* 2013; 2016).

Finally, the results could imply that, cofactor F_{430} content is not solely dependent on functionality (methane production) and, thus, not community independent. Indeed, certain, if not most of the reactors will have had a different (methanogenic) community structure and some seemed to be producing more methane than others with similar

amounts of cofactor content (see also Sections 7.1.3 and 7.2.3). Of course, the aforementioned remarks with respect to the (snap-shot) quantification need to be taken into account as well.

In summary, despite all being sampled at stable performance, the functionality of the bioreactors differed. Moreover, the snap-shot cofactor F_{430} quantification did not correlate well with methane production over these 12 individually sampled reactors. The discontinuous feeding pattern, coupled with the time of sampling and the long methane production measuring interval is proposed as an explanation. Furthermore, the results may indicate that cofactor F_{430} content also depends on the (methanogenic) community aside from solely reactor functionality. The cofactor F_{430} content was found to significantly differ between two of the inocula (brewery and dairy UASB) used in these experiments. Only two or three of the replicates, all inoculated from the brewery UASB, had high methane production combined with high cofactor F_{430} content. Thus, based on these experimental results and an approach looking at both methane production and cofactor content at the time of sampling, sludge originating from the brewery UASB would be preferred for the cost-efficient inoculation of new anaerobic bioreactors. Therefore, the choice for this inoculum in the experiments performed at KU Leuven seems justifiable. The potential of cofactor F_{430} measurements to be used as an inoculum selection tool is further elaborated in Section 9.1.

7.6 CONCLUSIONS

In this chapter, three additional potential applications of methanogenic cofactor monitoring were investigated, on top of its application as a tool to monitor process disturbances described in the previous chapters. The following conclusions can be drawn for each potential application.

Cofactor monitoring and SMA tests both showed potential and limitations in long-term reactor operation follow-up

Two separate experiments were followed-up in order to compare the use of cofactor F_{430} (and F_{420}) to that of SMA tests in the monitoring of long-term performance in anaerobic bioreactors. In both experiments, and particularly in Section 7.1, the SMA tests showed clear limitations in representing the actual methanogenic activity in the reactors. However, the cofactor monitoring, again most notably in Section 7.1, also did not perfectly represent (potential) methanogenic activity. Therefore, based on these results, the use of SMA tests in industry should be critically re-evaluated. Moreover, the cofactor monitoring does at this point not seem to provide precise additional information on methanogenic activity in the long-term follow-up of anaerobic bioreactors. Additional dedicated experiments including the analysis of both SMA on acetate and H_2/CO_2 and both cofactor F_{430} and F_{420} measurements should be performed.

Cofactor F_{430}'s potential to be used for the detection of methanogenic stratification could not be confirmed

The spatial distribution of methanogenic activity along the height of the full-scale digester described in Section 7.3 could not be proven using cofactor F_{430} measurements. A decreasing trend in cofactor content was observed towards the bottom of the reactor but this could not be statistically substantiated. Therefore, based on this indication of stratification, it is recommended to perform a dedicated sampling campaign on a reactor suspected or known to be internally stratified because of insufficient mixing. Additional replicates should then be taken and additional parameters, such as pH, *mcrA* copy and transcript numbers and SMA should be determined in order to investigate potential differences in methanogenic activity at the different heights. The approach proposed here could be expanded to bioreactor configurations with suspended and attached biomass, since differences in methanogenic activity are also very likely in such cases.

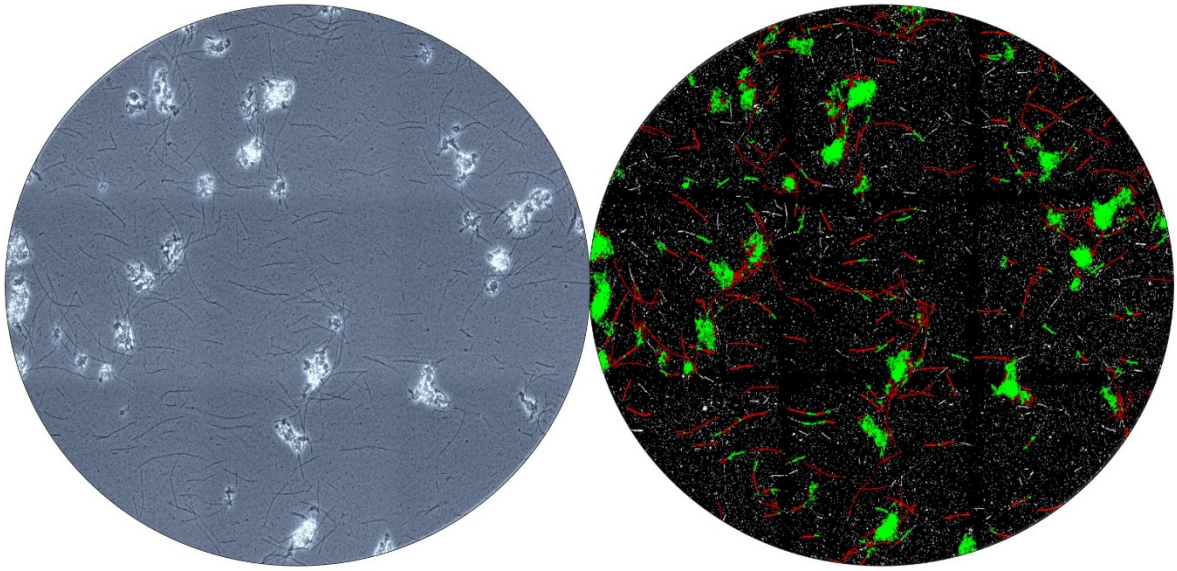
Cofactor quantification is recommended for start-up monitoring

The results of Section 7.4 indicate that the quantification of cofactor F_{430} content prior to reactor start-up could be useful in order to assess inoculum suitability. The reactors started-up with the same inoculum source as in Section 6.2, failed. The inoculum's cofactor content at the time of the start-up was found to be significantly lower than those typically measured in well-performing digesters (Section 7.5). Therefore, the quantification of cofactor F_{430} prior to, and during, the start-up may serve as an early warning for reactor failure. Based on these results, it is recommended to include cofactor F_{430} monitoring during inoculum screening. The quantification of cofactor F_{420}, both SMA on acetate and H_2/CO_2, and *mcrA* transcripts could yield interesting additional information on the inocula

activity. By following-up the subsequent reactor start-ups, the parameters best predicting the most efficient reactor operation, could be selected.

Part II

Assessing membrane fouling (potential) through bioflocculation monitoring



CHAPTER 8

Does solids retention time influence bioflocculation and membrane fouling in AnMBRs?[17]

In this chapter, the impact of an important operational parameter, the solids retention time (SRT), on membrane filtration performance is investigated. Two lab-scale anaerobic membrane bioreactors (AnMBRs) were operated for a period of 165 days at different SRTs and the sludge morphology and viscosity were monitored along with the membrane filtration performance. It was hypothesized that the change in SRT would have an effect on the microbial environment and thereby impact the dynamic bioflocculation process of the microorganisms on a microscopic level (Dereli *et al.*, 2014; Ersahin *et al.*, 2014). This could then change the macroscopic, physical properties of the sludge (e.g., viscosity) and positively or negatively impact the membrane filtration. Selection of a suitable SRT is an important operational choice (Dereli *et al.*, 2014; Ersahin *et al.*, 2014). In this chapter, the importance of taking into account its effect on sludge morphology, rather than solely biological performance, is highlighted.

The importance of SRT selection with respect to activated sludge bioflocculation and membrane performance in submerged aerobic membrane bioreactors was demonstrated in a recent study performed in our research group. Van den Broeck and colleagues (2012) tested three different SRTs (10 - 30 - 50 days) in a pilot-scale MBR and compared the bioflocculation status and fouling rates over a two-year period. They found higher fouling rates at shorter SRTs and attributed this to increased amounts of fragments as a result of deflocculation. In contrast to these results, Pacheco-Ruiz and co-workers (2017) recently reported that membrane filterability improved at shorter SRTs (96 - 40 - 25 - 15 days) in lab-scale submerged anaerobic membrane bioreactors. The latter experiment did not include the follow-up of sludge bioflocculation. Ersahin *et al.* (2014) reported that the SRT had an important impact on filterability in a submerged anaerobic dynamic membrane

[17] This experiment was performed in collaboration with BIOTHANE in Delft, The Netherlands. The reactors were operated there and the volatile suspended solids, capillary suction time, viscosity and membrane permeability analyses were also performed at BIOTHANE.

bioreactor. Furthermore, Dereli *et al.* (2014) reported improved filterability in an AnMBR operated at an SRT of 20 days (compared to 50 days) and attributed this to an increased wash-out of fine particules with the discharged sludge. However, these authors only reported particle size distributions of the sludge. In this experiment, the impact of SRT is re-assessed (in the 20 - 40 days range) in cross-flow operated AnMBRs. The characterization of sludge bioflocculation is included, considering its suspected importance in membrane fouling mechanisms (see also Section 2.2.3). Additionally, the bioflocculation process is hypothesized to be important for the syntrophic interactions between acetogenic bacteria and methanogenic *Archaea* since they need to be in close physical proximity to one another (De Bok *et al.*, 2004; Alves *et al.*, 2009). Several researchers have highlighted the potential negative impact of too high cross-flow velocities in membrane bioreactors on anaerobic biomass activity (Brockmann & Seyfried, 1996; Choo & Lee, 1996; Ghyoot & Verstraete, 1997). This may particularly be the case for the degradation of fats and lipid containing wastewaters (such as the synthetic dairy wastewater used in these experiments) because of the importance of the hydrogenotrophic route for these substrates (Alves *et al.*, 2009).

8.1 Materials & methods

Experimental set-up

The experimental set-up for this experiment has been described in Section 7.1.1. The same anaerobic bioreactors were followed-up, but the focus was shifted from biological performance to membrane performance in this experiment. Briefly, two lab-scale anaerobic membrane bioreactors were initially operated at an SRT of 30 days, after 46 days the SRT was changed to 20 and 40 days in the reactors that will be denoted as R20 and R40, respectively. The reactors were then operated for another 120 days during which the evolution of membrane performance and sludge bioflocculation status was followed-up. The selected SRTs are in the range of those used in Van den Broeck's (Van den Broeck *et al.*, 2012) and Pacheco-Ruiz's (Pacheco-Ruiz *et al.*, 2012) work. Due to the slower growth rates of anaerobic microorganisms, higher SRTs are generally recommended in anaerobic wastewater treatment reactors compared to their aerobic counterparts.

Analytical methods

The analytical methods used in this experiment have been described in the general material & methods section (Chapter 3). The following parameters were analysed.

- (Volatile) Suspended solids

Capillary Suction Time (CST)

The Capillary Suction Time (CST) is defined as a quantitative measure of the release rate of water from sludge (i.e., sludge dewaterability) and was measured with a capillary suction apparatus (Triton Electronics, Model 304M) and standard filter paper (Whatman No.17). It is the time a sample requires to travel a certain distance over a filter paper on the apparatus. A low CST is associated with a good filterability (Chen *et al.*, 1996).

Sludge viscosity

The sludge viscosity was analysed on a regular basis throughout the operational period using a HAAKE VT5500 (ThermoFischer, Waltham, MA USA).

Membrane permeability

The membrane permeability (P) was calculated based on the applied flux (J) and measured transmembrane pressure (TMP) using Equation 8-1.

$$P\ (L\ m^{-2}h^{-1}bar^{-1}) = \frac{J\ (L\ m^{-2}h^{-1})}{TMP\ (bar)} \qquad \textbf{Equation 8-1}$$

Image analysis with ASIAP

In order to quantitatively determine the sludge morphology, microscopic images of the bioreactor samples were taken using an Olympus IX83 inverted microscope and the accompanying CellSens Dimension software shown in Figure 8.1. The mixed liquor samples were first diluted to 1 g L^{-1} using supernatant in order to facilitate comparison across different sludge samples and prevent structural changes of the sludge. Next, two drops of 8 µL were applied on a sample glass (Menzel-Gläzer) and covered with a cover slip (Menzel-Gläzer). After sample preparation, 22 phase contrast images were obtained from each sample. Each image consisted of 9 photos, taken at a 10 times magnification, stitched together to form one large 3x3 image. The resulting images were analysed with the in-house developed MATLAB software, i.e., the Activated Sludge Image Analysis Program (ASIAP).

ASIAP, an adaptation of the original ACTivated Sludge Image Analysis System (ACTIAS) developed by Jenné *et al.* (2002; 2007), recognizes sludge objects and makes a distinction between flocs, filaments and fragments using a segmentation and recognition algorithm. During the *segmentation step*, the phase contrast image is transformed into a black and white segmented image. As illustrated in Figure 8.2 - a, flocs have a brighter colour than the background, while filaments are darker, which results in different intensities. In order to classify the flocs and filaments in the same intensity-range, a top-hat transformation is performed. During this transformation, bright zones (e.g., flocs) are intensified and narrow black elements (e.g., filaments) are removed in the original image to obtain a grayscale closing image. Next, the grayscale closing image is subtracted from the original image resulting in negative values for the flocs and filaments. The contrast between background and objects (i.e., flocs and filaments) is enlarged using an exponential rescaling transformation. Finally, a threshold is chosen to separate objects from the background and a binary file in which object pixels are defined as 1 and background as 0, is created (Van De Staey, 2016).

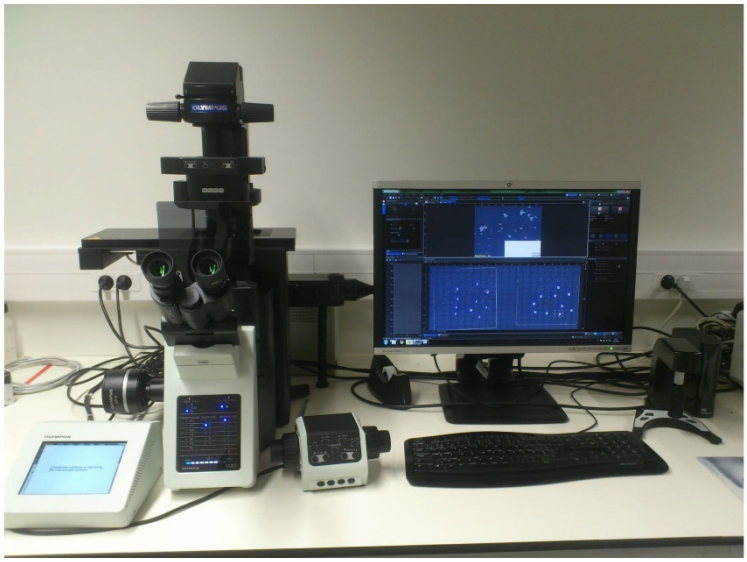


Figure 8.1 The Olympus IX83 fully motorized inverted microscope used to acquire the microscopic images.

In the *recognition step*, each object is classified as a floc, filament or fragment. If an object's equivalent diameter is smaller than 5 µm, the object is classified as a fragment (e.g., microcolonies, debris and small sludge components). To separate filaments from flocs, the ellipse coverage (EC) is calculated which is the ratio between the object area and the area of an ellipse obtained from the minor and major axis length of the object. If the equivalent diameter is larger than 5 µm and the EC is smaller than 21, the object is defined as a filament. All other objects are classified as flocs (Van De Staey, 2016). An overview of the applied criteria is given in Table 8.1.

Table 8.1 Criteria for the classification of the different objects in ASIAP.

Object	Criterion	
	Equivalent diameter (µm)	Ellipse coverage (-)
Fragment	≤ 5	-
Filament	> 5	≤ 21
Floc	> 5	> 21

In the processed images the green, red and white objects represent flocs, filaments and fragments, respectively. Based on the analysed phase contrast images, several output parameters are produced such as, e.g., the mean floc size and diameter, and the relative filament, floc and fragment numbers. A selection of these parameters is used to quantitatively follow-up the bioflocculation process.

8.2 Results

In the following paragraphs, first, problems that arose with the analysis using the automated image analysis software are discussed. Next, the quantitative sludge morphology results in function of time are presented. Finally, the evolution of the membrane filtration performance is presented and the correlation with the sludge morphological characteristics is assessed.

8.2.1 Image analysis with ASIAP

Initially, all phase contrast images were analysed by ASIAP using images taken at 10 times magnification. However, after 40 days of operation problems arose in the segmentation step of the software. Figure 8.2 shows how the processed image did no longer correctly reflect the different object classes and, therefore, rendered the quantitative output erroneous. Both images shown here were taken with exactly the same microscope settings (e.g., exposure time), nevertheless the images taken after 40 days were clearly less bright. This led ASIAP to encounter problems when trying to separate the objects from the background.

Upon closer investigation of these images it seems that mainly an increased abundance of fragments contributed to the reduced brightness, possibly by absorbing a larger fraction of the light. These fragments were grouped together in the segmentation step and recognized as flocs rather than fragments, hereby greatly overestimating the number of flocs while underestimating the number of fragments.

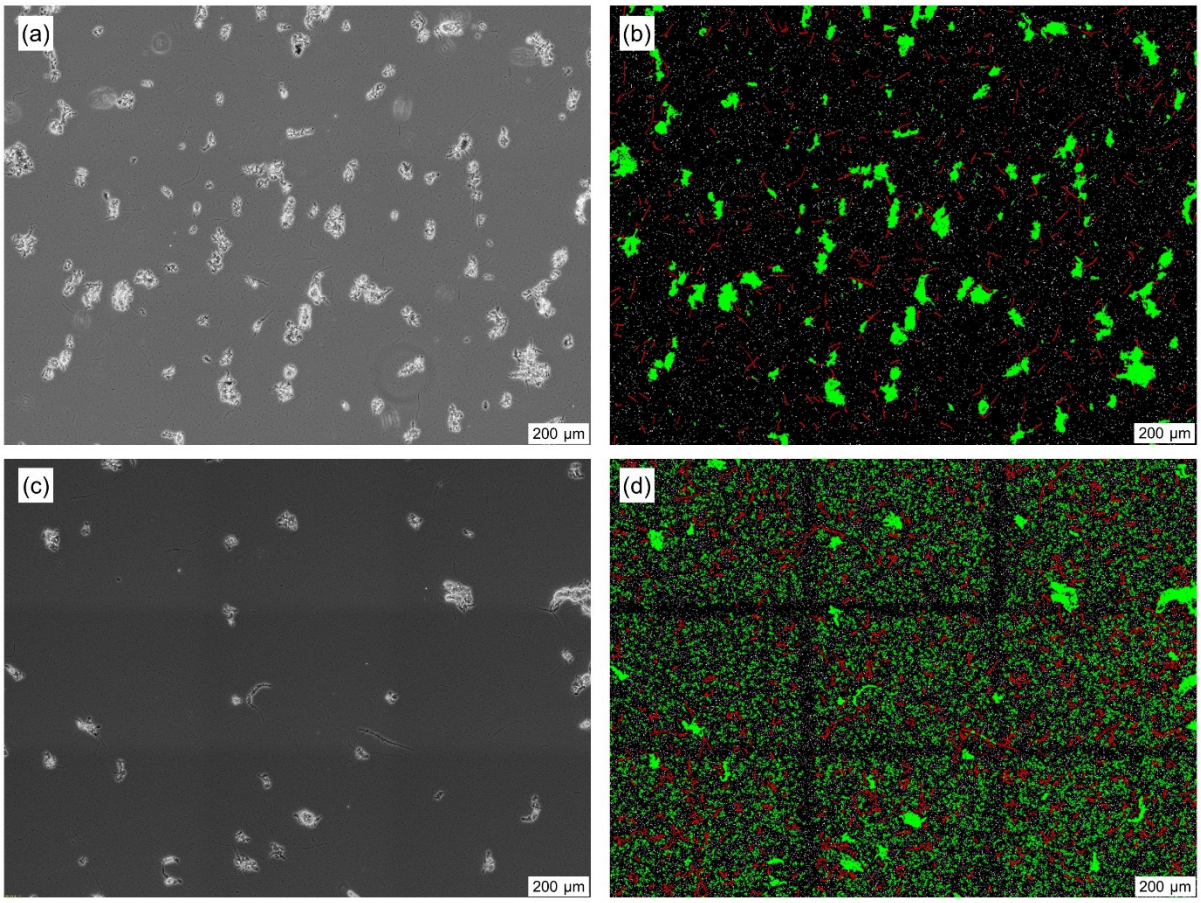


Figure 8.2 The original and processed images of a sludge sample taken before **(a) (b)** and after **(c) (d)** 42 days. Images were taken at 10 times magnification. After 42 days, the image analysis software struggled to separate objects from the background and correctly assign them to the different classes, leading to erroneous quantitative results.

Two approaches were taken in order to solve this issue. First, the original images were optimized by manipulating the contrast and brightness, in order to increase the contrast between the small fragments and the background. This allowed most of the samples taken after 40 days to be correctly analysed, however the same segmentation and recognition problems were encountered again later during the experimental run. Since the automatic

thresholding procedure in the ASIAP code clearly did not produce satisfactory results, the thresholding parameter was set to manual (instead of automatic) allowing it to be fine-tuned for the acquired images. A manual threshold of 0.5 gave the best outcome for most of the images and was, therefore, selected. Despite the significant improvements that were obtained using this dual approach, images taken after 88 days still produced erroneous processed images.

Considering the unsatisfactory results, as a last resort, images which had been taken at 20 times magnification were optimized with respect to brightness and contrast and analysed with a manual threshold of 0.5. Two remarks are in order for these analyses:

(i) Less surface per sample is covered and analysed when using these images, reducing their representability, and;

(ii) ASIAP was optimized for the analysis of 10 times magnification images. Consequently, images taken at 20 times magnification are sub-optimally analysed. Figure 8.3 illustrates the shortcomings of the ASIAP analysis at 20x magnification, showing the faulty recognition of some filaments as fragments or flocs.

Thus, further optimization is required for the analysis at 20 times magnification. Nevertheless, the quantitative results were sufficiently satisfactory to follow-up the relative sludge morphology evolution. Evidently, for the interpretation of absolute output parameters the aforementioned remarks are to be taken into account.

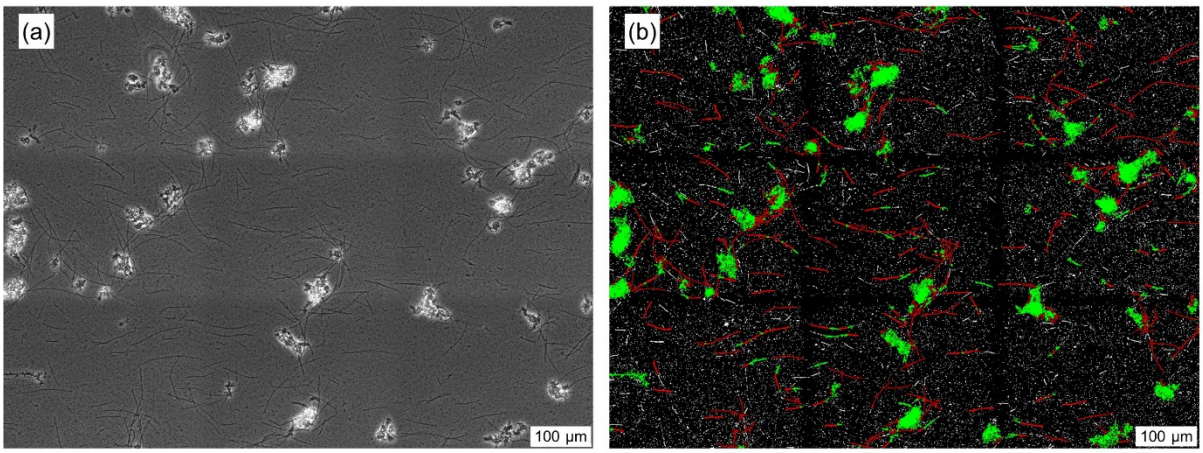


Figure 8.3 An original **(a)** and processed **(b)** image taken with 20 times magnification. Some filaments are wrongly recognized as flocs or fragments, nonetheless, the results were more reliable than those taken at 10 times magnification.

8.2.2 Evolution of the sludge morphology

The quantitative output of ASIAP yields a myriad of morphology related parameters. The most important ones were selected and are shown in Table 8.2. The evolution of the first five parameters in function of time is plotted in Figure 8.4 and Figure 8.5, for both reactors. The dotted vertical line indicates the time at which the SRT in reactor R20 was decreased to 20 days and increased to 40 days in R40.

Table 8.2 Parameters from the ASIAP output chosen to be included in this study. The abbreviations introduced here will be used throughout the results section.

Parameter abbreviation	Description	Unit
RelFragNum	Number of fragments per megapixel of image	$Megapixel^{-1}$
RelFilNum	Number of filaments per megapixel of image	$Megapixel^{-1}$
RelFlocNum	Number of flocs per megapixel of image	$Megapixel^{-1}$
D_{eq}	Mean equivalent floc diameter	µm
FilLength	Mean filament length	µm
Rndns	Mean roundness of flocs	-
FD[18]	Mean fractal dimension of flocs	-

The relative fragment number was comparable in both reactors prior to the change in SRT. Subsequently, it increased more or less simultaneously in both reactors until it levelled off at about twentyfold higher values after 120 days. A slightly decreasing trend was observed in reactor R40 towards the end of the operational period.

The relative filament number fluctuated but remained relatively constant in both reactors until an increase was observed after 116 days. This increase was more pronounced in R40 compared to R20 but was also accompanied by an increase in the error bars (standard deviations of the mean over all images per sample). Towards the end of the operational period a slight decrease was again observed in reactor R40. The relative floc number's evolution was almost identical to that of the filament numbers in both reactors. In absolute terms, the relative fragment numbers increased from about ten to a hundred times higher than the filament and floc numbers.

[18] The fractal dimension (FD) characterizes the complexity of an object's perimeter. The FD increases when the roughness or irregularity of the objects's border increases (Van de Staey, 2016).

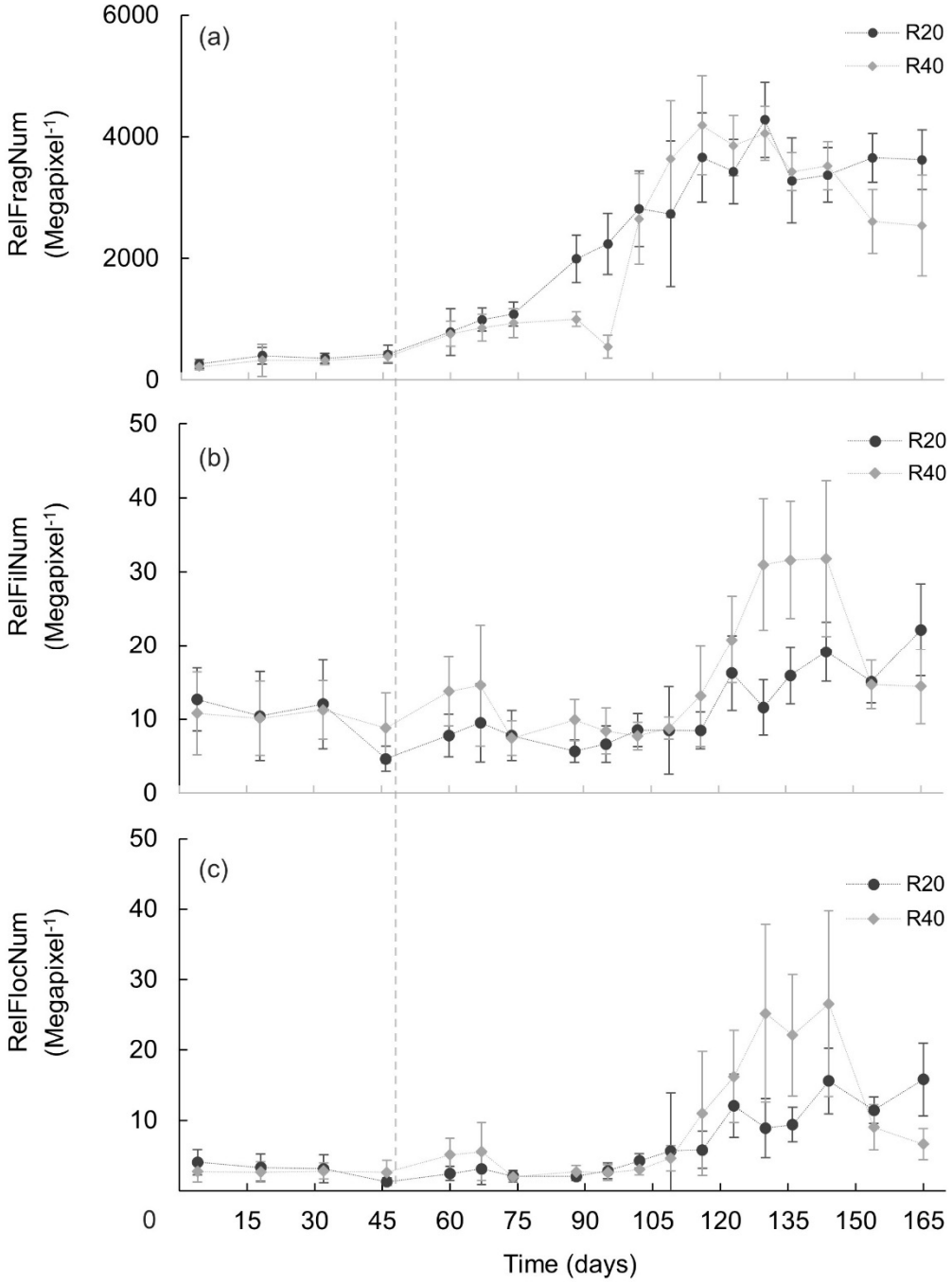


Figure 8.4 The evolution of the relative **(a)** fragment (RelFragNum), **(b)** filament (RelFilNum) and **(c)** floc (RelFlocNum) numbers in reactor R20 (●) and R40 (♦) throughout the 165 days operational period. An SRT of 30 days was maintained initially, subsequently, an SRT of 20 and 40 days was maintained in reactor R20 and R40, respectively (indicated by the dashed grey line). Error bars represent standard deviations of the global mean of 20 images. Increases in all three parameters were observed, however, the increase in filament and floc numbers was more pronounced in reactor R40.

The mean equivalent floc diameter and mean filament length fluctuated between 10 and 35 µm, and 10 and 60 µm, respectively. A decreasing trend of the floc diameter seems to be present throughout the entire operational period, whereas the filament length seems to slightly increase in reactor R40. However, unfortunately, the standard deviations were large. The decrease of the standard deviation on the floc diameter indicates an evolution towards more equally sized (smaller) flocs. In contrast, the increase of the standard

deviation on the filament length indicates an evolution towards a broader distribution of filament lengths over the analysed images per sample.

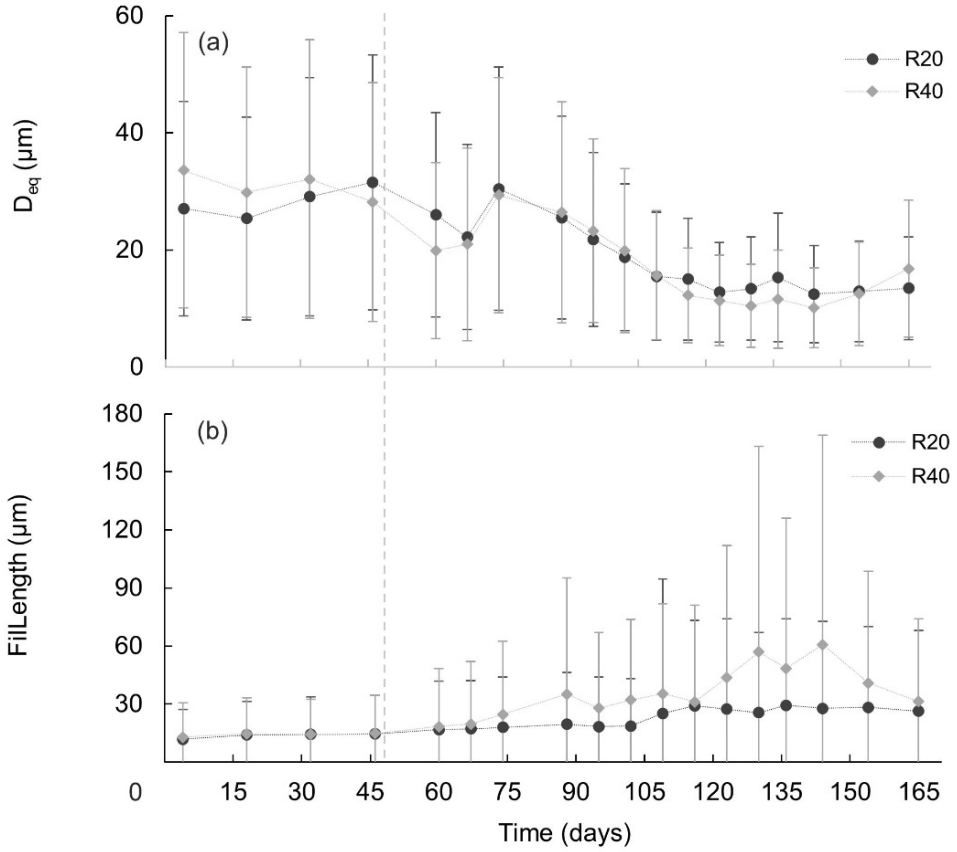


Figure 8.5 The evolution of the **(a)** mean equivalent diameter (D_{eq}) and **(b)** mean filament length (FilLentgh) in reactor R20 (●) and R40 (♦) throughout the 165 days operational period. An SRT of 30 days was maintained initially, subsequently, an SRT of 20 and 40 days was maintained in reactor R20 and R40, respectively (indicated by the dashed grey line). Error bars represent standard deviations of the global mean of 20 images. A slight decrease in floc sizes was observed in both reactors, whereas the length of the filaments slightly increased in reactor R40.

Analysis of Variance (ANOVA) on the 14 data points after the SRT change yielded a significant difference between the mean filament lengths in both reactors ($p = 0.0017$).

8.2.3 Evolution of the membrane filtration performance

In order to be able to assess the evolution of the membrane filtration performance four parameters are discussed: (*i*) the TSS concentration, (*ii*) the membrane permeability, (*iii*) the viscosity and (*iv*) the capillary suction time (CST). Figure 8.6 shows the evolution of the TSS concentration in both reactors.

During the first 46 days the TSS concentration slightly decreased in both reactors from around 10 g L^{-1} to 7 g L^{-1}. Immediately after the change in SRT was applied, the TSS concentration started increasing in reactor R40 because of the reduced sludge purging rate. Its concentration stabilized at about 12 g L^{-1} from day 120 onward. Despite the increased sludge purging rate in reactor R20, its TSS concentration did not significantly decrease and remained stable around 7 g L^{-1}. The two times lower sludge purging rate in reactor R40 resulted in a TSS concentration which was about 1.7 times higher.

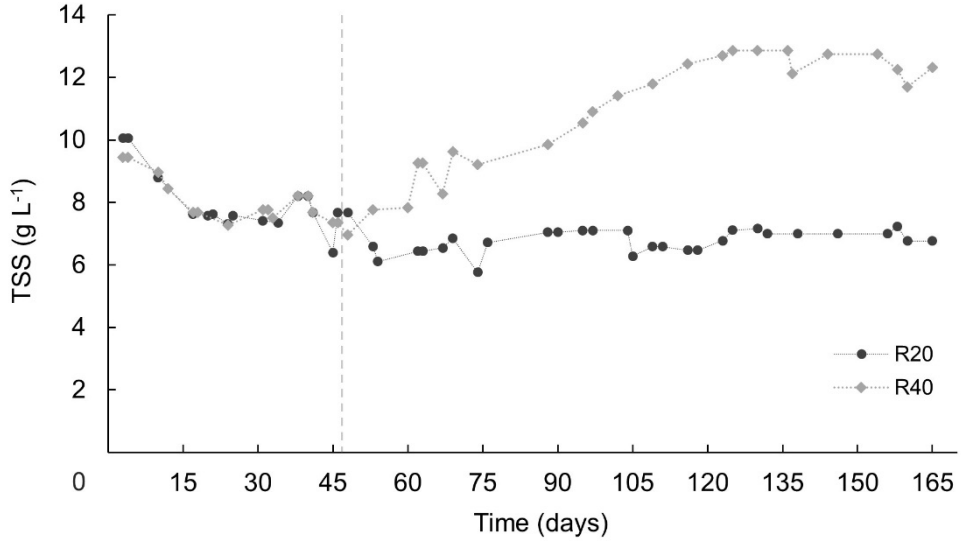


Figure 8.6 The evolution of the TSS concentration in reactor R20 (●) and R40 (♦) throughout the 165 day operational period. The TSS concentration increased in reactor R40 as a result of the increased SRT (indicated by the grey dashed line), whereas it remained stable in reactor R20. An SRT of 30 days was maintained initially, subsequently, an SRT of 20 and 40 days was maintained in reactor R20 and R40, respectively.

The evolution of the membrane flux and transmembrane pressure (TMP) in both reactors is shown in Figure 8.7.

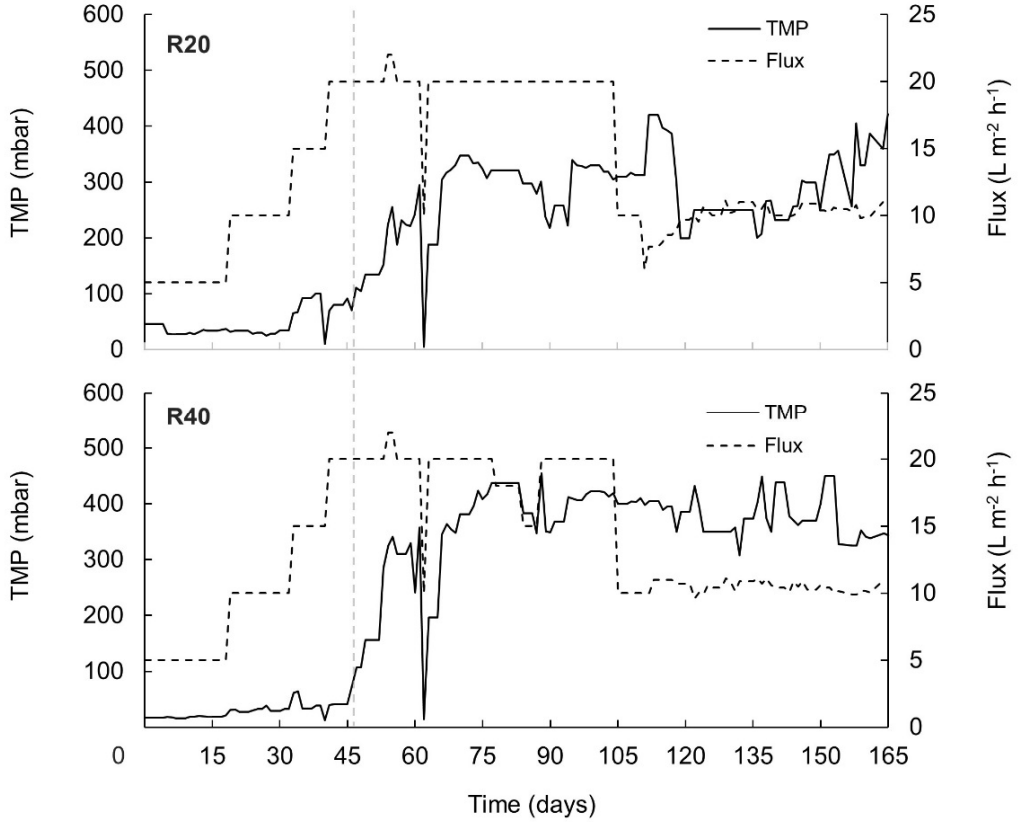


Figure 8.7 The evolution of the transmembrane pressure (TMP, ─) and flux (---) in reactor R20 (top) and R40 (bottom) over the 165 day operational period. An SRT of 30 days was maintained initially, subsequently, an SRT of 20 and 40 days was maintained in reactor R20 and R40, respectively (indicated by the dashed grey line). The flux was increased in a step-wise manner and decreased again on day 106 due to the reduced sludge filterability. Transmembrane pressures increased from day 46 onward and stablized around day 75.

The membrane flux was increased in a step-wise way in both reactors from 5 L m^{-2} h^{-1} to 20 L m^{-2} h^{-1}. After 106 days of operation it was again lowered to 10 L m^{-2} h^{-1} in both reactors due to the decreased sludge filterability.

The membrane permeability, viscosity and capillary suction time where all normalized with respect to the TSS concentration since the biomass concentration is known to influence these parameters. By dividing by the TSS concentration, its impact is taken out of the equation and the evolution of the aforementioned parameters can be compared on the same basis. This equal comparison allows the impact of the sludge morphology on these membrane filtration performance related parameters to be more accurately visualized. The evolution of the TSS normalized membrane permeability, viscosity and capillary suction time is shown in Figure 8.8.

The normalized permeability profile shows two distinct outliers for both reactors. These high permeabilities were observed after chemical cleaning of the membranes, however, they were only sustained for a period of one day. Removing these outliers allows the overall trend (shown in the inset) to be more accurately visualized. In both reactors a generally increasing trend in the first 46 days of operation is observed, after which the permeability in both reactors consistently decreased. Initially, the normalized permeability in R40 was higher than in R20, however after 46 days until the end of the experiment it was slightly lower. The absolute permeability (not shown) varied between 30 and 500 L m^{-2} h^{-1} bar^{-1} throughout the operational period. After the first membrane cleaning on day 40 the permeability recovered to 1500 and 1200 L m^{-2} h^{-1} bar^{-1} in R20 and R40, respectively. After the second membrane cleaning, on day 62, values of 2200 and 720 L m^{-2} h^{-1} bar^{-1} were measured for R20 and R40, respectively. The reduced recovery in reactor R40 indicates that the second membrane cleaning was less effective.

The normalized viscosity was relatively similar in both reactors throughout the entire operational period. A generally increasing trend up to values around 0.13 Pa s $gTSS^{-1}$ can be seen in both reactors. The absolute viscosity (not shown) was clearly higher in reactor R40 after the change in SRT and reached values of up to 14 Pa s. The higher R40 values resulted from the higher TSS concentration in this reactor, which is corrected by the normalization of the viscosity in Figure 8.8.

Similarly, the capillary suction time profile is identical for both reactors. An exponential increase is observed from 94 days onwards and levels off after 120 days of operation. During this short period the CST increased more than a 100-fold from 0.12 to 14 s $gTSS^{-1}$. The absolute values ranged from 10 s to over 1500 s and were again clearly higher in reactor R40 after the SRT change because of the higher TSS concentration. Both the normalized and absolute values are in the range of recent reports from literature (Dereli *et al.*, 2014; Ersahin *et al.*, 2014).

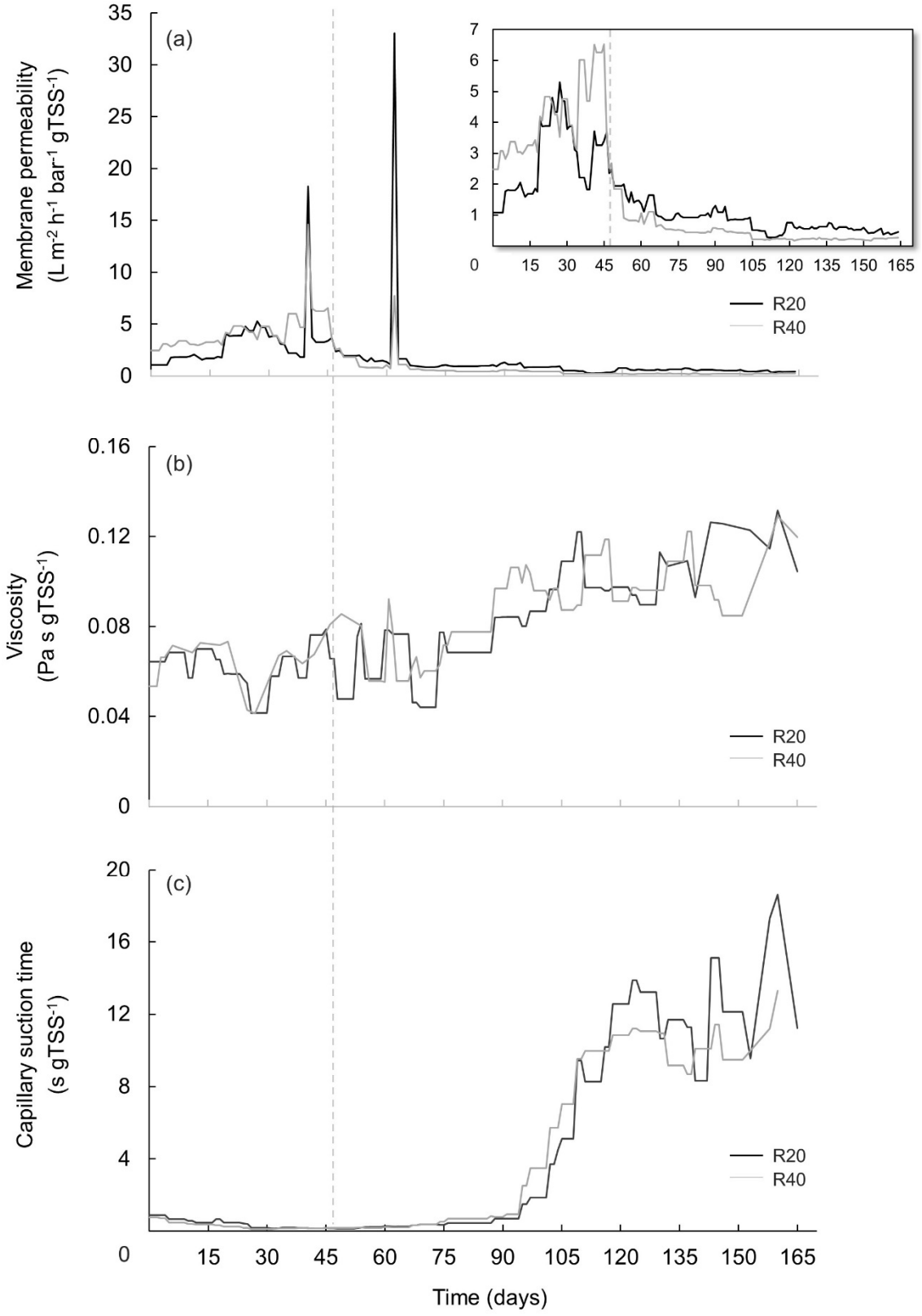


Figure 8.8 The evolution of the **(a)** membrane permeability, **(b)** viscosity and **(c)** capillary suction time in reactor R20 (—) and R40 (–), all normalized per gram TSS, throughout the 165 day operational period. An SRT of 30 days was maintained initially, subsequently, an SRT of 20 and 40 days was maintained in reactor R20 and R40, respectively (indicated by the dashed grey line). The permeability profile omitting the outliers resulting from the temporary effect of membrane cleaning is shown in the inset of figure (a). The permeability decreased over time in both reactors, whereas viscosity and capillary suction time increased.

Analysis of variances (ANOVA) on the 14 data points after the SRT change yielded significant differences between the TSS concentrations and viscosity in both reactors ($p < 0.0001$ and $p = 0.0005$, respectively).

8.2.4 Correlations between sludge morphology and filtration related parameters

Rather than looking at the evolution of their trends in function of time, in Table 8.3 and Table 8.4, the correlations between the three filterability related parameters, on the one hand, and seven selected morphology related parameters, on the other hand, were sought. Note that in this case the normalization per gram of TSS was not performed. Instead this parameter was added to the variables in order to assess its correlation with sludge filterability. Also note that the correlations between the filtration related parameters themselves were included.

In both reactors, several significant negative and positive correlations were revealed. Permeability, viscosity and CST all correlated significantly with one another. However, their correlation with the TSS concentration was only significant in reactor R40.

In reactor R20, all seven morphology related parameters correlated significantly with the three filterability related parameters. The only exception being the correlation between relative filament number and permeability which was not significant. Relative filament, floc and fragment numbers and mean filament length and fractal dimension showed a positive correlation with CST and viscosity and a negative correlation with permeability. Mean equivalent diameter and roundness correlated negatively with CST and viscosity, and positively with permeability. The same is observed in reactor R40, with some select differences. Fractal dimension did not correlate significantly with any of the filterability related parameters. Furthermore, roundness did not significantly correlate with the permeability. Finally, on top of the relative filament number, also the relative floc number did not show a significant negative correlation with membrane permeability in this reactor.

Table 8.3 Correlation coefficient (Pearson r), sample size (n), 95% confidence interval (upper and lower) and statistical significance (p) for the correlations between the capillary suction time (CST), viscosity and membrane permeability on the one hand, and TSS concentration and seven selected morphology related parameters, on the other hand, in *reactor R20*. RelFilNum, RelFlocNum and RelFragNum denote the relative filament, floc and fragment numbers, respectively. D_{eq} and FilLength denote the mean equivalent floc diameter and mean filament length. The last column visualizes the strength of the correlation, a large bar indicates a strong negative or positive correlation. Significant correlations are denoted by an asterisk (*).

						R20	
	Variable	*Pearson r*	*n*	*upper 95%*	*lower 95%*	*p*	*-.8 -.4 0 .4 .8*
	TSS	-0.2782	18	-0.6594	0.2168	0.2637	
	RelFilNum	0.7210	18	0.3832	0.8887	0.0007*	
	RelFlocNum	0.9033	18	0.7547	0.9637	<.0001*	
CST	RelFragNum	0.8760	18	0.6923	0.9531	<.0001*	
(s)	D_{eq}	-0.9210	18	-0.9705	-0.7967	<.0001*	
	FilLength	0.9176	18	0.7886	0.9693	<.0001*	
	Rndns	-0.8702	18	-0.9508	-0.6794	<.0001*	
	FD	0.6918	18	0.3322	0.8758	0.0015*	
	TSS	-0.0309	18	-0.4907	0.4424	0.9031	
	RelFilNum	0.5188	18	0.0686	0.7935	0.0274*	
	RelFlocNum	0.7177	18	0.3772	0.8873	0.0008*	
Viscosity	RelFragNum	0.7718	18	0.4766	0.9105	0.0002*	
(Pa s)	D_{eq}	-0.7646	18	-0.9075	-0.4630	0.0002*	
	FilLength	0.7153	18	0.3730	0.8862	0.0008*	
	Rndns	-0.6825	18	-0.8716	-0.3164	0.0018*	
	FD	0.5325	18	0.0873	0.8004	0.0229*	
	CST	0.8063	18	0.5442	0.9250	<.0001*	
	TSS	0.3607	18	-0.1277	0.7083	0.1414	
	RelFilNum	-0.3159	18	-0.6822	0.1771	0.2016	
	RelFlocNum	-0.4925	18	-0.7800	-0.0332	0.0379*	
	RelFragNum	-0.7083	18	-0.8831	-0.3608	0.0010*	
Permeability	D_{eq}	0.7208	18	0.3828	0.8886	0.0007*	
($L\ m^{-2}\ h^{-1}\ bar^{-1}$)	FilLength	-0.6673	18	-0.8648	-0.2912	0.0025*	
	Rndns	0.6518	18	0.2659	0.8577	0.0034*	
	FD	-0.6948	18	-0.8771	-0.3374	0.0014*	
	CST	-0.5682	18	-0.8180	-0.1379	0.0139*	
	Viscosity	-0.4976	18	-0.7826	-0.0400	0.0356*	

Table 8.4 Correlation coefficient (Pearson r), sample size (n), 95% confidence interval (upper and lower) and statistical significance (p) for the correlations between the capillary suction time (CST), viscosity and membrane permeability on the one hand, and TSS concentration and seven selected morphology related parameters, on the other hand, in *reactor R40*. RelFilNum, RelFlocNum and RelFragNum denote the relative filament, floc and fragment numbers, respectively. D_{eq} and FilLength denote the mean equivalent floc diameter and mean filament length. The last column visualizes the strength of the correlation, a large bar indicates a strong negative or positive correlation. Significant correlations are denoted by an asterisk (*).

		R40					
	Variable	*Pearson r*	*n*	*upper 95%*	*lower 95%*	*p*	*-.8 -.4 0 .4 .8*
	TSS	0.9343	18	0.8290	0.9756	<.0001*	
	RelFilNum	0.6325	18	0.2350	0.8487	0.0049*	
	RelFlocNum	0.7351	18	0.4083	0.8948	0.0005*	
CST	RelFragNum	0.9278	18	0.8132	0.9731	<.0001*	
(s)	D_{eq}	-0.8855	18	-0.9568	-0.7136	<.0001*	
	FilLength	0.8176	18	0.5673	0.9296	<.0001*	
	Rndns	-0.6749	18	-0.8682	-0.3038	0.0021*	
	FD	0.3898	18	-0.0942	0.7248	0.1098	
	TSS	0.9264	18	0.8098	0.9726	<.0001*	
	RelFilNum	0.4917	18	0.0322	0.7796	0.0382*	
	RelFlocNum	0.5954	18	0.1780	0.8312	0.0091*	
Viscosity	RelFragNum	0.8419	18	0.6178	0.9395	<.0001*	
(Pa s)	D_{eq}	-0.7776	18	-0.9130	-0.4878	0.0001*	
	FilLength	0.7474	18	0.4309	0.9002	0.0004*	
	Rndns	-0.5232	18	-0.7957	-0.0746	0.0259*	
	FD	0.2503	18	-0.2452	0.6421	0.3165	
	CST	0.8926	18	0.7298	0.9596	<.0001*	
	TSS	-0.7422	18	-0.8979	-0.4214	0.0004*	
	RelFilNum	-0.2806	18	-0.6609	0.2143	0.2593	
	RelFlocNum	-0.4031	18	-0.7322	0.0785	0.0972	
Permeability	RelFragNum	-0.6617	18	-0.8622	-0.2818	0.0028*	
($L\ m^{-2}\ h^{-1}\ bar^{-1}$)	D_{eq}	0.6185	18	0.2132	0.8422	0.0062*	
	FilLength	-0.6852	18	-0.8728	-0.3210	0.0017*	
	Rndns	0.3085	18	-0.1850	0.6778	0.2129	
	FD	-0.0922	18	-0.5360	0.3915	0.7160	
	CST	-0.6582	18	-0.8606	-0.2762	0.0030*	
	Viscosity	-0.7169	18	-0.8869	-0.3758	0.0008*	

8.3 Discussion

Despite the limitations of the ASIAP analysis in this experiment, some general trends and interesting correlations were revealed.

8.3.1 The impact of solids retention time on sludge morphology

The clear increase in number of fragments observed in this study starts shortly after the change in SRT. However, considering that its increase is similar in both reactors, it is more likely that it is unrelated to the SRT change but rather a result of the prolonged operation in a cross-flow filtration mode. Indeed, the shear rates induced by cross-flow operation are known to potentially disrupt the floc structure in anaerobic sludges (Jeison *et al.*, 2009; Dereli *et al.*, 2014). Nevertheless, the used cross-flow velocity of 1 m s^{-1} is relatively low and its influence on the bioflocculation of the biomass is therefore rather unexpected (Jeison *et al.*, 2009; Lin *et al.*, 2013). Nonetheless, Dereli *et al.* (2014) operated AnMBRs using a cross-flow velocity of 0.5 m s^{-1} and still observed an increase in fragments due to prolonged operation. However, the longer SRT in R40 did not lead to a higher abundance of fragments in contrast to the findings of Dereli *et al.* (2014). From the increase in fragments, and considering the slightly decreasing trend in floc diameter in both reactors, it might be concluded that predominantly *floc erosion* occurred. During this process, small particles break off from the outer surface of the floc and are not re-assimilated into larger floc structures (Van Dierdonck *et al.*, 2012). Alternatively, *floc breakage or fragmentation* may also have taken place, since the relative number of flocs also increased in both reactors. During this process, relatively large flocs break-up into two or more objects which are still large enough to be classified as flocs. It should be noted here that the increase in floc number may also have been partly due to the erroneous ASIAP analysis during which some filaments were misclassified as flocs (see Figure 8.3). Nonetheless, possibly both processes took place over the course of the experiment in both reactors.

In contrast to the studies conducted by Van den Broeck *et al.* (2012) and Pacheco-Ruiz *et al.* (2017), the tested SRTs were likely not far enough apart in order to induce morphological differences which significantly impacted the membrane filterability. The impact of the shear stress inherent to cross-flow AnMBR operation overshadowed the impact of the SRT in the experiments, whereas this was not the case for the submerged configurations used in the aforementioned studies. This should be taken into account at all times when interpreting the results along with the problems encountered with the quantitative ASIAP analysis. Furthermore, it is interesting to note that although the dynamic sludge bioflocculation process was clearly affected, the methanogenic activity was not inhibited. The results presented in Section 7.1.2 showed that the overall reactor performance was stable and not affected by the change in morphology. Thus, no evidence was found for the hypothesis that poor bioflocculation may affect the syntrophic interactions required for the efficient degradation of lipid-containing wastewaters.

Two particular parameters which were less likely to be impacted by the shear caused by the cross-flow pumps, are the relative filament number and the mean filament length. Both parameters were relatively similar in both reactors prior to the SRT change. However, afterwards, both the number and the length of the filaments was consistently

higher in reactor R40. An explanation for this observation may be found in the *kinetic selection theory*. This theory stipulates that the growth of filamentous microorganisms is favoured under substrate limiting conditions due to their larger specific surface area, which increases their substrate affinity compared to floc forming organisms (Li *et al.*, 2009). Indeed, the increased SRT in reactor R40 resulted in an increase in TSS concentration compared to R20. Since the OLR was kept the same in both reactors, the SLR was significantly lower in reactor R40 (see also Figure 7.1 in 7.1.1). As a result, less substrate was available per unit of biomass in R40, potentially creating substrate limiting conditions in which filament forming organisms thrive. Since in both reactors low substrate concentrations were observed (data not shown), this explains why the slightly increasing trend is observed in reactor R20 as well. However, because of the higher sludge purging rate and higher SLR in this reactor, the effect was less pronounced. Also note that the underestimation of filaments by the ASIAP analysis was clearer in R40. The ANOVA revealed a significant difference between the filament lengths (not their number) in R20 and R40 after the change in SRT. From the combined evidence, it is concluded that AnMBR operation at an SRT of 40 days promoted the growth of filament-forming microorganisms. This phenomenon resulted from the operation at a higher sludge concentration and subsequent lower sludge loading rates, creating substrate limiting conditions.

8.3.2 The impact of sludge morphology on membrane filterability

The data obtained in this experiment clearly demonstrated a deteriorated filterability in both reactors. This was evidenced by the decreased membrane permeability. The capillary suction time, an ex-situ indicator of filterability (Chen *et al.*, 1996), also increased. The decrease in permeability started around the same time the SRTs were altered but, as previously mentioned, this was likely not the main cause of the observed trend. The single morphological parameter which clearly increased when the permeability decreased, in both reactors, was the relative amount of fragments. Indeed, small fragments are known to effectively penetrate and block membrane pores and promote the formation of dense cake layers on the membrane surface (Van den Broeck *et al.*, 2012, Ersahin *et al.*, 2014; Dereli *et al.*, 2014; Van de Staey, 2016). Therefore, the increase in fragments as a result of the shear stress on the flocs explains the overall decrease in permeability in both reactors. The decrease in permeability was more pronounced in reactor R40 (even after correcting for the difference in TSS concentrations), whereas the viscosity and CST trend was similar. Part of the explanation may be that higher amounts of filaments were observed in this reactor and this results in the formation of more open and irregularly shaped flocs which more easily accumulate on the membrane (Meng *et al.*, 2006). Moreover, studies in aerobic systems have reported that filamentous microorganisms produce more SMP and EPS, two parameters which have been linked with worsened membrane fouling (Choi *et al.*, 2002; Rushing Pan *et al.,* 2010). The absence of SMP and EPS measurements, in this study, prevents this hypothesis to be confirmed.

The increase in capillary suction time was more pronounced after about 100 days of operation and was similar in both reactors. This increase seems to be linked to the increase in the number of filaments in both reactors, rather than fragments. Again, a concomitant increase in SMP and EPS concentrations as a result of thriving filament-forming microorganisms may explain this observation. Indeed, increases in both parameters have

been linked with increased viscosities (Meng *et al.*, 2006), which in turn led to reduced permeability and increased CST (Nagaoka, 1996; Meng & Yang, 2007). After correcting for the TSS concentration, the higher abundance of filaments in R40 did not lead to higher viscosities or capillary suction times compared to R20.

The correlations determined on the 18 samples taken throughout the entire operational period confirm the link between membrane permeability, CST and viscosity. Although resulting from changes in sludge morphology and concomitant changes in EPS and SMP, the viscosity itself is likely a causal variable which impacts the membrane permeability and CST. The absence of a correlation between the TSS concentration, on the one hand, and permeability, CST and viscosity, on the other hand, in reactor R20 results from the fact that TSS concentration hardly changed and can therefore not explain the observed changes in filterability. However, in reactor R40 the increase in TSS concentration significantly correlated with the deteriorated filterability and increased viscosity. Because of the concomitant changes in morphological parameters, it is unclear whether this correlation is causal. For the morphological parameters the following general conclusions can be drawn from the results obtained from both reactors. The filtration performance (membrane permeability and CST) is generally better and viscosity lower when:

(i) fragments are less abundant;
(ii) filaments are short and less abundant, and;
(iii) flocs are large and round with smooth edges (high roundness and low fractal dimension).

The results presented here are in accordance with the recent findings of Glenn Van de Staey (2016) with one exception. This author reported a slightly positive effect of filaments on fouling rates in cross-flow mode, which was not observed in current study.

8.4 CONCLUSIONS

From the results presented in this chapter it can be concluded that the prolonged operation of two anaerobic membrane bioreactors led to **significant changes in** their **sludge morphology and filterability**. A consistent **decrease in membrane permeability** was observed after 7 weeks of operation and was mainly attributable to an increased abundance of fragments. The increase in fragments likely resulted from floc erosion caused by the continuous shear to which the sludge flocs are subjected in cross-flow operated bioreactors. An increase in capillary suction time and viscosity was mainly linked to an increased abundance of filaments which may also have contributed to the low permeabilities observed in the second part of the experiment. In summary, an increased abundance of fragments, longer and more abundant filaments and smaller and irregularly shaped flocs were linked with reduced sludge filterability. Additionally, higher TSS concentrations and an increased viscosity (likely resulting from the aforementioned morphological parameters and increased TSS concentrations) were linked with poorer sludge filterability.

The AnMBR operation at an **SRT of 40 days induced a shift towards more filamentous microorganisms** compared to operation at an SRT of 20 days. After correcting for the difference in TSS concentration in both reactors, the impact of the increased amount and length of filaments on filterability was limited when comparing the two tested SRTs. It is proposed that, in this experiment, changes in filterability resulting from the operation at different SRTs were **obscured by the influence of the shear induced by cross-flow operation**.

In conclusion, the selection of a suitable cross-flow velocity which limits floc erosion is important in order to avoid reduced sludge filterability in AnMBRs. Operation at an SRT of 20 or 40 days did not yield important differences with respect to sludge filterability, indicating that, in the tested SRT range and with the given cross-flow velocity, the latter was the operational parameter which dominated the membrane filtration behaviour. Moreover, the apparent **deflocculation did not affect the syntrophic interactions** required for adequate reactor performance. Further experiments should focus on more significantly differing (though still operationally relevant) SRTs while altering the cross-flow velocity in order to select its optimal value. The optimal cross-flow velocity should limit deflocculation in order to preserve satisfactory sludge filterability.

CHAPTER 9

General conclusions and outlook

In this chapter, the general conclusions are summarized. These conclusions are subdivided according to the two main parts used throughout this PhD thesis: Part I, which focuses on biological monitoring, and Part II, which focuses on membrane filtration monitoring. An outlook towards future experiments and developments is provided within each section, when relevant, and a general outlook is provided at the end of each part.

9.1 Part I - Assessing methanogenic activity using methanogenic cofactors

In the first part of this PhD thesis, the applicability of methanogenic cofactors for the monitoring of methanogenic activity in anaerobic bioreactors was assessed. The importance of monitoring the methanogenic community and its activity was highlighted in Chapter 1 (Section 1.3.1). Process upsets are still quite common in methanogenic reactors, which often rely on the implicit knowledge of their operator. The main reason for focusing on the methanogens is their greater susceptibility to these upsets and their crucial role in the anaerobic degradation chain. Detailed information on the (activity of) methanogens is therefore important in order to optimally manage methanogenic bioreactors. The main objectives of Part I can be summarized as follows:

(i) refine and validate suitable cofactor extraction and quantification protocols;
(ii) assess the applicability of methanogenic cofactors in both short– and long-term monitoring applications by unravelling the link between cofactor content and methanogenic activity;
(iii) compare cofactor monitoring with other commonly used monitoring methods, and;
(iv) screen for potential industrial applications of methanogenic cofactor monitoring.

Cofactor extraction and quantification procedures were refined and validated

In **Chapter 4**, the adaptation and refinement of cofactor extraction and quantification protocols from literature, was discussed. Various tests were performed and the following conclusions with respect to the **cofactor F_{430} extraction procedure** were drawn:

(i) excessive contact with air degrades the native cofactor;
(ii) heating causes thermodegradation of native F_{430};
(iii) cell lysis by means of bead beating outperformed ultrasonication;
(iv) an anion exchange resin for additional purification is not required, and;
(v) the use of a vortexer and a vacuum extraction manifold allowed the parallel extraction and purification of 12 samples.

Quantification was performed using both spectrophotometry and high-performance liquid chromatography (HPLC) and the combined extraction-quantification procedures were validated using samples from the experiments described in Chapters 5 to 7. **Identification** using ultra-high-performance liquid chromatography coupled with high-resolution mass spectrometry (UHPLC-HRMS) confirmed the presence of the native cofactor based on its exact mass (*m/z*). The most common F_{430} degradation products, i.e., 12,13-didehydro-F_{430} (or F_{560}) and 13-epi and 12,13-diepi-F_{430}, were less abundant, confirming the validity of the developed protocol.

A **cofactor F_{430} standard** was tentatively prepared using preparative UHPLC-HRMS. The F_{430} degradation products were present in higher concentrations than in the experimental samples (i.e., up to 30% impurity). Nevertheless, the highly concentrated standard allowed a calibration curve to be constructed for the HPLC quantification, hence allowing the determination of approximate absolute cofactor F_{430} concentrations for comparison with literature values.

Three different **cofactor F_{420} quantification methods** were compared in this work:

(i) extraction and *ex-situ* quantification using fluorimetry;
(ii) *in-situ* quantification using fluorescence microscopy, and;
(iii) *in situ* quantification using flow cytometry.

Based on the results, the *ex-situ* fluorimetric quantification was deemed the most appropriate for total F_{420} fluorescence quantification. The fluorescence microscopy method did not produce satisfactory results in its current form, whereas the flow cytometric method showed potential for at-line quantification of relative F_{420} fluorescence and methanogenic community fingerprinting.

Future perspectives for the developed protocols. Although the **cofactor F_{430} protocol** allowed the dynamics to be determined quite accurately (experimental variability of 4 – 11%) the following optimizations should be considered. First, a *standard of higher purity* should be synthetized. To this end, the use of recently extracted samples is preferred and more care should be taken to reduce contact with air and excessive temperatures. Furthermore, it should be investigated whether the UHPLC procedure can be adapted in order to separate the main impurities based on their different retention times. Second, since also the HPLC procedure did not always allow the F_{430} epimers to be separated from the native form, the procedure should be adapted in order to optimize the separation and its repeatability. Furthermore, *adapting the HPLC procedure* may allow other interesting methanogenic cofactors such as methanopterin (MPT) and sarcinapterin (SPT) (see Section 2.1.5) to be quantified as well. Gorris *et al.* (1988) developed an HPLC method (System II) optimized for the combined quantification of these cofactors and the different cofactor F_{420} forms. In addition to quantifying the total F_{420} content by means of fluorimetry, this HPLC method could be used for the assessment of the relative importance of acetotrophic (SPT, F_{420}-4 and F_{420}-5) and hydrogenotrophic (MPT and F_{420}-2) methanogenic activity. Third, once a sufficiently pure standard is available, combining quantification and identification directly through *the use of UHPLC-HRMS* should be considered because of its lower detection limit and since detection by means of the exact mass leaves only the native form and the two epimers to be separated on the column. Finally, if sufficient care is taken to reduce contact with air and excessive temperatures, quantification of the nickel concentration by means of *ICP-MS* provides a reliable indication of the cofactor concentration (without the requirement of a cofactor standard). However, the purity of the samples should be checked from time to time in order to assure that the native cofactor form is measured. With respect to the **cofactor F_{420}** quantification methods, the reliability of the *fluorescence microscopy* would be greatly enhanced if the excitation wavelength could be selected more precisely.

<u>Cofactor quantification meets the requirements for methanogenic activity monitoring</u>

In order for cofactor F_{430} and F_{420} to be used as reliable monitoring tools for methanogenesis, the following requirements need to be met: (*i*) they need to be present in, and restricted to, methanogens (*ii*) they should be related to methanogenic activity, and (*iii*) follow its dynamics.

The *first requirement* was assessed based on the available literature and discussed in detail in Section 2.1.5. A preference for monitoring cofactor F_{430} was established based on

its incidence in all types of methanogens. Nonetheless, the higher incidence of cofactor F_{420} in hydrogenotrophic methanogens can be seen as an opportunity rather than a limitation, since it may allow these methanogens to be specifically targeted. Both F_{420} and F_{430} have been found in non-methanogenic species (i.e., in *Actinobacteria* and anaerobic methane oxidizers, respectively). However, presence of these microorganisms in mixed bioreactor samples is expected to be negligible. The presence of both cofactors was confirmed in the experiments, allowing to conclude that the first requirement is met.

With respect to the *second requirement*, the observations support the hypothesis that the cofactor contents are related to the activity of methanogens rather than solely their presence. Indeed, the significant short-term cofactor content variations that were recorded in **Chapters 5 and 6** could not be attributed to methanogen growth or death on these short time scales. Moreover, from the data presented in **Chapter 6**, it is clear that the cofactors significantly correlated with methanogenic activity. Therefore, in general, the second requirement is met in the relatively short-term experiments that were performed. However, some remarks for long-term bioreactor monitoring are in order and are highlighted in the next section.

With respect to the *third requirement*, it is important to stress that the prevailing cofactor content is the net result of production and degradation. Ideally, increased or decreased cofactor production occurs within the same time-scale as increased or decreased methane production. In fact, from a monitoring perspective, the cofactors would be even more useful if their concentration would predict future methane productivity. The results from **Chapter 6** do not support the latter, indicating that the cofactors will generally not reveal how the future methane productivity will evolve. In general, with respect to their dynamics, both cofactors seem to be: (*i*) quickly produced in response to increased substrate availability and (*ii*) degraded within days after inhibition of methanogenesis at an exponential rate (pseudo-first order kinetics with a 1.6 days half-life for cofactor F_{430}). Keeping in mind these observations, snapshots of cofactor content do not always relate to the amount of active methanogens, thus previous reactor performances should be taken into account for a correct interpretation. Particularly during the start-up period, cofactor contents were shown to often have an opposite trend compared to the methane production. The high concentration of cofactor in the (generally granular) inocula, combined with a too limited supply of substrates reaching the methanogens, is proposed as an explanation. Therefore, the final requirement is partly met and depends, amongst others, on the time span of the monitoring period and the sampling frequency.

<u>Monitoring the long-term performance of anaerobic bioreactors poses challenges to cofactor measurements</u>

As mentioned in the previous paragraphs and in **Chapter 7**, limitations of cofactor monitoring arose during the long-term follow-up of the methanogenic activity in anaerobic bioreactors. In two experiments exceeding 150 days of operation, the link between the cofactor content and methanogenic activity and its dynamics could not be confirmed. One proposed explanation is related to changes in the sludge matrix. Since the cofactor extraction and quantification protocols cannot include controls for the extraction efficiency, *changes in sludge morphology and physico-chemical characteristics* may affect the measured cofactor contents. Moreover, the changes in the sludge matrix may be driven

by *shifts in the (methanogenic) community* over these longer time spans. The initial hypothesis assumed that the cofactor F_{430} content would be independent of the methanogenic community structure and, hence, solely linked to function (i.e., methane production). However, the results from these long-term experiments indicate that different methanogenic communities may require different amounts of cofactor to produce the same amount of methane. Otherwise said, one F_{430} molecule may be used more efficiently by some species (or under certain conditions), therefore allowing more methane to be produced per cofactor molecule. This contradicts the initial hypothesis, which assumed that a given amount of cofactor would always lead to, or be able to sustain, a certain methane productivity. Nonetheless, it should be noted that in the long-term experiment with the phenolic wastewater during which changes in the methanogenic community occurred, cofactor F_{430} was still able to reflect well the inhibition of methanogenesis. Therefore, cofactor monitoring is still expected to provide an added value during long-term operation when process upsets occur. **Future experiments** should focus on linking (shifts in) the methanogenic community structure (ideally RNA based in order to capture activity instead of presence) to the measured cofactor contents. More fundamental research on differences in the mechanism of the cofactor F_{430}-MCR complex may help in explaining why certain communities seem to more effectively use a given cofactor content.

Cofactor monitoring can compete with, or complement, existing monitoring methods

pH, VFAs and methane production. In Part I, the three most commonly followed-up parameters during anaerobic bioreactor operation (i.e., pH, VFAs and methane production) were complemented with cofactor measurements. Because of its direct role in methanogenesis, cofactor F_{430}, in particular, yields important additional information that is directly related to the activity of methanogens. Based on the combined results, a decision-tree was made, highlighting the added value of cofactor measurements. This tool, depicted in Figure 9.1, provides a preliminary diagnosis and further recommendations for reactor operation based on the commonly measured parameters (methane production, VFAs, COD load), complemented with cofactor measurements. In the flow-scheme, seven different diagnoses are depicted all reflecting a different combination of methane production, VFA concentration and cofactor F_{430} content. Each diagnosis is linked with a recommendation for the bioreactor operation. The colour code reflects both the status of the reactor performance (decreasing from green to red) and the urgency of intervening in the process (increasing from green to red).

Since the cofactor's production is linked to the supply of substrate to the methanogens, a low cofactor content can mean one of two things: (*i*) insufficient substrate is supplied to the methanogens or (*ii*) too much substrate was supplied to the methanogens, causing inhibition. *In the first case*, VFAs will generally be low and the pH stable. If methane production is also low compared to the supplied COD load, the bottleneck in the process is located prior to the methanogenesis and acidogenesis. In this case (#2 in Figure 9.1), hydrolysis is likely limiting and it is best to reduce the loading to the reactor until this issue is addressed (e.g., by increasing the temperature if possible). Alternatively, if the COD load to the reactor is low, this situation may simply indicate (long-term) underfeeding of the reactor which explains the low methane production, VFAs and cofactor content. In such a case (#1 in Figure 9.1), it is advised to gently increase the loading rate.

In the second case, the VFAs will generally be high and the low cofactor content reflects the hampered methanogenesis and a lack of resilience. In such cases (#4 in Figure 9.1) it is advised to immediately halt the feeding. In the rare case of high methane production, high VFA concentrations and low F_{430} content, the low cofactor content is not expected to be able to sustain the (disproportionally) high methane production for long as also the accumulating VFAs indicate that the methanogens are struggling to keep converting the incoming substrates to methane. Therefore, the reactor is likely very close to its limit and reducing the loading may avoid the imminent reactor failure (#7 in Figure 9.1).

High cofactor F_{430} content can also indicate one of two things: (*i*) sufficient substrate is being supplied to the methanogens or (*ii*) residual cofactor content is present in the biomass. *In the first case*, a well-balanced process will be reflected by high methane production and low VFA and stable pH values. The high supply of methanogenic substrates drives the methane production and pushes the methanogens to maintain their high cofactor content. In such cases, the loading rate can be increased confidently (#6 in Figure 9.1). *In the second case*, the methane production is lower than what is expected based on the cofactor measurement. Therefore, the F_{430} content does not reflect well the current methanogenic activity. In such cases, the residual cofactor F_{430} reflects previous methanogenic activity. This may be attributable to the inoculum (i.e., during reactor start-up or after re-inoculation), or to a rather sudden decrease in methanogenic activity. If, in combination with the low methane production, the VFA concentrations are high, this situation (#5 in Figure 9.1) indicates a process upset and the high cofactor F_{430} content then reflects (temporary) resilience during the shock period. Despite the high cofactor content it is advised to reduce the loading and find and alleviate the process upset. It is in this case that cofactor measurements are particularly useful. Indeed, in Chapter 6, residual cofactor concentrations after process upsets reflected well the reactor's resilience towards process upsets. As long as sufficient cofactor is present and the cause of the process upset can be alleviated (e.g., feeding error or toxic components in the feed), the reactor's performance will be able to bounce back. Therefore, in a situation where methane production is low, but VFAs are low as well and residual cofactor content is present (#3 in Figure 9.1), the loading rate can be increased since either the process upset has been alleviated and the methanogens have proven to be resilient, or the situation reflects a start-up phase as described above. Note that cofactor F_{420} measurements can additionally be performed in order to pinpoint the group of methanogens that are limiting the reactor performance. Of course, these measurements can be performed during stable periods as well in order to assess the importance of the hydrogenotrophic methanogenesis. Since this decision-tree was drawn up from a limited number of lab-scale experiments, **future experiments** should validate or fine-tune the proposed diagnoses and actions. Pilot-scale reactors in the start-up phase or reactors treating challenging wastewaters are particularly interesting to follow-up using the proposed flow scheme.

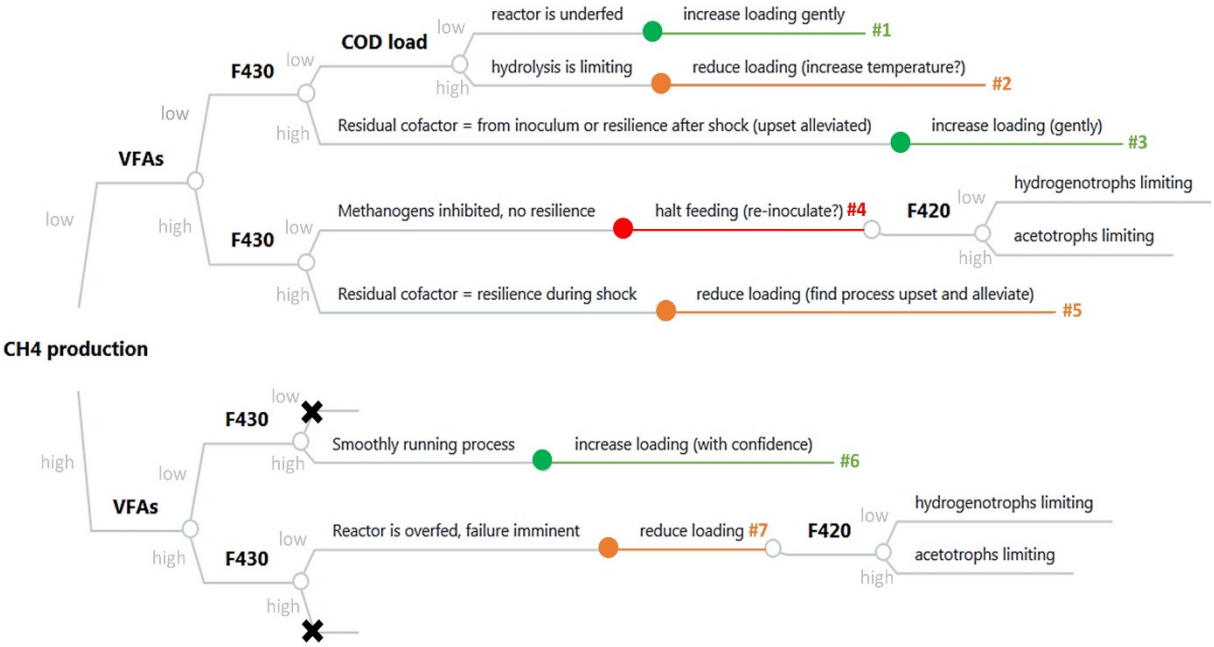


Figure 9.1 A decision-tree highlighting the potential added value of cofactor measurements during anaerobic bioreactor operation and troubleshooting. The crosses indicate situations which were not observed in this PhD thesis and are unlikely to occur. The colour code reflects both the status of the reactor performance (decreasing from green to red) and the urgency of intervening in the process (increasing from green to red). Note that complementing the VFA concentration measurement by the total alkalinity provides additional information on the buffer capacity of the system.

SMA and *mcrA* gene monitoring. In Chapters 6 and 7, two additional monitoring methods were evaluated and compared to the cofactor measurements. The *SMA tests* are supposed to reflect the (potential) methanogenic activity of the bioreactor sludge based on an *ex-situ* test using various (methanogenic) substrates. One of its drawbacks is that, in order to allow reproducibility, the methods are usually standardized and therefore the conditions do not represent the actual conditions prevailing in the bioreactor. The results in **Chapter 7**, indicate that SMA tests on acetate do not capture the trend in methanogenic activity well in bioreactors fed with synthetic dairy wastewater. Because of the importance of the hydrogenotrophic pathway for these types of substrates, SMA tests on H_2/CO_2 are expected to correlate better but were not performed initially. However, in a subsequent experiment, also these measurements only partly captured an increasing trend in methanogenic activity. The cofactor measurements, on the other hand, did not clearly outperform the SMA tests and showed limitations of their own. The remarks for the follow-up of long-term performance are applicable here because of the duration of these experiments. Nonetheless, in one of the two experiments cofactor F_{430} captured part of an increasing trend in methane production which was thought to be due to increased activity of hydrogenotrophic methanogens. **Future experiments** should more closely follow-up both cofactor F_{430} and F_{420} concentrations, as well as the SMAs on H_2/CO_2 and acetate in reactors that shift from predominantly using one methanogenic pathway to another. The added value of cofactor measurements may then be more thoroughly assessed.

In contrast to SMA tests, *monitoring on the mcrA gene level* is more closely linked to the *in-situ* methanogenic activity. The *mcrA* gene encodes for a specific methanogenic enzyme called Methyl-Coenzyme M reductase (MCR) and therefore its copy and transcript

numbers should be closely linked to the presence and activity of methanogens, respectively. In **Chapter 6**, the importance of including transcript quantification (on cDNA) was highlighted, since the copy numbers do not provide sufficient information on short-term dynamics in methanogenic activity. The *mcrA* transcripts showed a strong correlation with methane production rate confirming their suitability for monitoring purposes (as expected from literature). However, monitoring on the cofactor level provides the potential benefit of detecting remaining methanogenic potential. Due to their faster degradation rate, *mcrA* transcripts disappear very quickly upon inhibition whereas the slower degradation of the cofactors allow them to remain present for a longer period of time. Since the methanogens need cofactor F_{430} as an essential part of the MCR enzyme, its presence indicates that methanogenesis is likely to be resumed as soon as inhibiting conditions (e.g., high VFA concentrations and low pH) are alleviated (see also Figure 9.1). Furthermore, quantification of the *mcrA* transcripts entails a more complicated measurement than cofactor quantification. In **future experiments**, it would be interesting to determine the production and degradation kinetics of the *mcrA* gene on shorter time scales.

Most promising applications for cofactor monitoring in anaerobic bioreactors

Based on the results acquired in Part I of this PhD thesis, the most promising potential applications for cofactor monitoring were selected.

Monitoring process upsets. As discussed in the previous sections (and in **Chapter 5 and 6**), one of the most promising applications of cofactor monitoring is the diagnosis of process upsets. Reduced methane production prompts further investigation and using the decision-tree (Figure 9.1) in the troubleshooting process allows the suspected cause (e.g., hydrolysis or methanogenesis limitation) to be pinpointed more easily and relatively quickly. In addition, including cofactor F_{420} measurements may point to the types of methanogens (hydrogenotrophs or acetotrophs) that are limiting the reactor performance.

Start-up monitoring and inoculum screening. Since one of the main costs and most labour intensive tasks for starting up full-scale anaerobic bioreactors is the transportation and preparation of the inoculum, reducing its amount while ensuring sufficient activity is of paramount importance. The importance of a sufficiently active inoculum was also demonstrated in **Chapter 7**. Based on the results obtained in Sections 7.4 and 7.5, using cofactor content as an additional constraint during inoculum selection is proposed. This may lead to faster and more robust start-ups, reducing the likelihood of reactor failure. Assuming that both the measured methane production (which indicates best its current methanogenic activity) and cofactor F_{430} content (which may additionally indicate potential future methanogenic activity) are important, graphs like the one depicted in Figure 9.2 may be used to select appropriate inocula. Such two-dimensional graphs could be divided into four zones based on threshold values of methane production or yield and cofactor content, which would simplify the inoculum choice. Sludge samples in the top right part of this graph correspond to preferred inoculum sources. Based on the experiences with the bioreactor experiments and cofactor F_{430} measurements, a cofactor F_{430} content of at least 150 nmol $gVSS^{-1}$ seems to be an absolute minimum in order to allow for a smooth and swift bioreactor start-up. For the yield a threshold of e.g., 300 mL CH_4 $gCOD\ fed^{-1}$ (which corresponds to about 80% of the theoretical yield) could be proposed.

Note that the type of two-dimensional graphs introduced here, could be extended to three dimensions by adding an additional parameter potentially linked to methanogenic activity, such as, e.g., F_{420} content or *mcrA* transcripts.

Although the decision-tree proposed in this chapter was not validated for the step-wise increase of loading rates (i.e., during reactor start-up), it provides a basis for **further experiments** with respect to this operational task. Based on the proposed flow scheme, and using the additional cofactor quantification, process upsets due to too high applied loading rates or long start-up times due to too conservative feeding regimes may be avoided. Therefore, by continuing to monitor the cofactor contents throughout the start-up period, it is suspected that bioreactors would be less likely to fail during the ramping up of the organic loading rates.

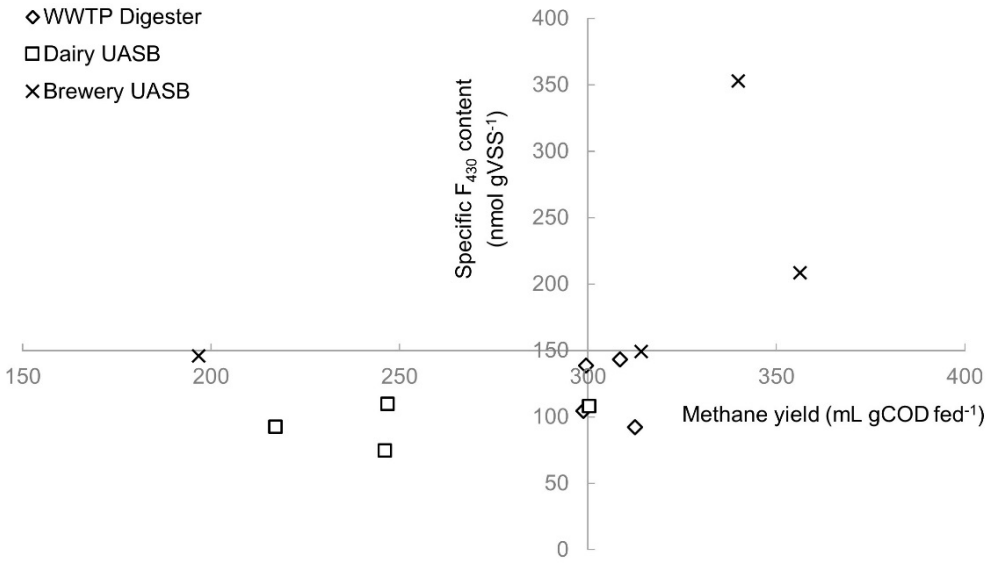


Figure 9.2 An example of how the cofactor content quantification of different inoculum sources can be used to select the most suitable inoculum for bioreactor start-up (using the data from Section 7.5). The selection of suitable thresholds for cofactor F_{430} content and methane yield, divides the graph in four parts. Samples in the top right part originate from preferred inoculum sources.

General outlook for methanogenic cofactor monitoring

The monitoring of methanogenic cofactors was applied in this PhD thesis to anaerobic bioreactors intended for methane production. While this is an obvious choice, their **use as a negative control** is also interesting. In reactors intended for VFA production, cofactor measurements (with sensitive detection techniques such as mass spectrometry) can confirm the absence of methanogens. Additionally, cofactor measurements provide exciting prospects for applications where *in-situ* methane production cannot be determined. The application of sampling at different heights in stratified reactors was already discussed in this thesis. Furthermore, e.g., in psychrophilic anaerobic wastewater treatment, a large fraction of the methane production is expected to take place in biofilms that grow on carriers or membrane surfaces under these conditions. Measuring the cofactor content in these biofilms and in the bulk section of such reactors can provide insights on the methanogenic activity at these locations. Cofactor F_{430} measurements have already been used to confirm the presence and activity of methanogens or anaerobic methane oxidizers in natural samples (i.e., swamps) and at remote locations (i.e., deep sea sediments). **Cofactor F_{430} measurements in permafrost samples** that are prone to thawing

because of changing climate conditions, may help in mapping the methane producing potential of certain regions, which is still difficult to estimate (Metje & Frenzel, 2007). Due to the high greenhouse gas potential of methane gas, such thawing may contribute to additional global warming (through so-called positive feedback) and cofactor F_{430} measurements could prove to be a relatively simple and quick monitoring method in these important regions of interest. Researchers have already targeted the *mcrA* gene for this purpose (e.g., Freitag & Prosser, 2009) and considering the correlation between transcripts of this gene and cofactor F_{430} concentrations found in the current work, the cofactor may be a suitable candidate for a faster, but equally informative, analysis of methane production potential.

In Chapter 2, one of the most promising monitoring tools that has been proposed in recent literature, the **BEAP test**, was discussed (Refai *et al.*, 2017) (see Section 2.1.3). Through supplementation of different substrates, the bottleneck of the anaerobic digestion process and potential future process upsets are determined. A very interesting experiment would be to quantify the methanogenic cofactors in the beginning and end of this test. As such, in less than 24 hours a large amount of complementary information could be obtained.

The more widespread application of cofactor F_{430} as a monitoring tool is hampered by the requirement for its extraction from the sludge and its thermal and oxidative instability. Although the protocol used in this PhD thesis provided a quantification within half a working day, for rapid process troubleshooting, this may still be too long. Furthermore, some equipment is required which is generally not available on-site or even at some R&D facilities of anaerobic technology providers. Therefore, it would be interesting to **design and validate a simplified version of the current extraction and quantification protocol**. Ideally, a method similar to the Hach's cuvette test kits could be designed. For the extraction, cell lysis by means of bead beating could be performed as proposed in this thesis, by means of a vortexer. Next, centrifugation steps could be replaced by filtration in order to retain the cells or recover the supernatant (i.e., the filtrate). With the use of a vacuum manifold and widely available C18 cartridges, the additional purification of the cofactor could also be performed quite easily. Subsequently, quantification of the yellow absorbance (at 430 nm) by means of spectrophotometry could be performed. Alternatively, the "yellowness" of the extract could be used visually (e.g., by comparing with different hues of yellow on a pH-strip-like paper) for rapid semi-quantitative assessment of cofactor concentration and, thus, presence and activity of methanogens.

Another interesting prospect with this respect would be to use **a cuvette test for nickel quantification**. The extraction would still be required, but relatively rapid quantification without additional purification may be possible. The possible interference of other ions present in the lysate should be investigated. Furthermore, considering that the test kit manual states that for the quantification of undissolved or complexly bound ions, an additional pre-treatment is required (i.e., by using their so-called "crack-set"), such an additional step might be necessary. For on-site quantification of the nickel concentration, electrochemical sensors have been developed and their use has already been proposed for dynamic trace metal dosing (Fermoso, 2008). A simple, **automated lysis method** (e.g., heating would be suitable since total nickel concentration is measured) **combined with *on-***

***line* quantification of the nickel concentration** by means of an electrochemical sensor, is an exciting prospect.

9.2 Part II – Assessing membrane fouling (potential) through bioflocculation monitoring

In the second part of this PhD thesis the focus was shifted from monitoring the biological status in various types of anaerobic bioreactors towards monitoring the membrane filtration performance in anaerobic membrane bioreactors (AnMBRs). Membrane fouling still entails important costs in MBR operation and even more so in the anaerobic variant where higher sludge concentrations often lead to more significant fouling. However, the impact of sludge concentration and parameters such as extracellular polymeric substances (EPS) is ambiguous in literature and often the impact of the sludge's microscopic morphology (i.e., its bioflocculation status) is overlooked. Based on results obtained in aerobic MBRs in our own research group (Van den Broeck *et al.*, 2012), the solids retention time (SRT) was selected as an operational parameter which may influence the bioflocculation status and allow the assessment of its importance in cross-flow operated AnMBRs. The objectives of this part can be summarized as follows:

(i) validate the use of the in-house developed activated sludge image analysis software for anaerobic sludges;
(ii) assess the effect of the solids retention time (SRT) on the dynamic bioflocculation process;
(iii) investigate the impact of sludge morphology on membrane filterability in cross-flow operated AnMBRs, and;
(iv) evaluate the impact of bioflocculation on syntrophic interactions.

<u>Limitations of the activated sludge automated image analysis programme (ASIAP)</u>

During the experiments, certain limitations of ASIAP were uncovered. The *increased abundance of fragments* reduced the brightness of the images and affected the segmentation and recognition process when using images at 10 times magnification. As a result, individual sludge fragments were grouped together and the number of flocs and filaments was greatly overestimated. The manual optimization of brightness and contrast temporarily restored ASIAP's performance but did not provide satisfactory results on the long term. In the end, images taken at 20 times magnification were used and reasonable results were obtained after manual brightness and contrast optimization and the use of manual thresholding in the ASIAP code. The final processed images had two distinct limitations: (*i*) less surface per sample was covered due to the higher magnification, reducing the representability and (*ii*) a fraction of the filaments was recognized as fragments, hereby underestimating this group of objects. These results highlight that **future experiments** need to focus on optimization of the image acquisition procedure and ASIAP code for the quantification of sludge samples containing large amounts of fragments.

The operation at prolonged SRT (indirectly) promoted the growth of filament-forming microorganisms

The results indicated that *significantly more filaments were present in the reactor operated at an SRT of 40 days* compared to operation at an SRT of 20 days. The longer SRT caused an increase in biomass concentration which, in turn, led to reduced sludge loading rates. As a result the food over microorganism ratio was lower, creating substrate limiting conditions. These conditions promoted the growth of filament forming bacteria because of their higher substrate affinity (as a result from their larger specific surface area) as explained by the kinetic selection theory.

The effect of SRT on filtration performance was overshadowed by the effect of shear

The increased amount of filaments was expected to affect the membrane permeability. However, an increased amount of fragments correlated better with reduced filterability. The increase in fragment number was unrelated to the change in SRT but rather a result of *prolonged operation in cross-flow filtration mode*. The continuous shear-stress imposed on the flocs led to floc erosion and floc breakage, causing more severe membrane fouling due to the release of fragments. Despite the deflocculation, the reactor's biological performance was unaffected, indicating that the syntrophic interactions, requiring short inter-microbial distances, remained largely intact. From the abovementioned observations, it is concluded that for the operation of side-stream AnMBRs, the *selection of a suitable cross-flow velocity* (which determines the shear rate) is crucial in order to limit disintegration of flocs while still providing sufficient shear across the membrane surface. In the tested range, the SRT was not the determining factor with respect to membrane filterability, although it did impact the sludge bioflocculation process. **Future experiments** should focus on different ranges of the cross-flow velocity and the SRT, since the relative importance of these parameters may shift.

In conclusion, monitoring the evolution of sludge morphology through the use of automated microscopic image analysis proved to be a valuable tool for the long-term follow-up of anaerobic membrane bioreactors. The procedure allowed the changes in morphology to be numerically substantiated and linked to the reduced filterability.

General outlook for bioflocculation monitoring

In conventional activated sludge (CAS) systems and aerobic MBRs, the past decades have learned that a good balance between floc forming and filamentous microorganisms is crucial in order to achieve good settleability or filterability. However, because of the successful development of high-rate anaerobic bioreactor systems predominantly using granulation as the sludge retention mechanism, researchers have generally focused on the mechanisms of the granulation process in anaerobic wastewater treatment. Although the recent implementation of AnMBRs omits the need for successful granule formation (hence its application for "niche" wastewaters that hamper the granulation process), the process of bioflocculation is still an important factor affecting the membrane filtration performance. The aforementioned ideal balance of flocs and filaments has been shown to be achieved by applying spatial or temporal substrate gradients in aerobic systems (Chiesa *et al.*, 1985). However, this approach has not sufficiently been investigated in anaerobic systems, whereas it is important for granule formation as well (Ehlers & Turner, 2013).

Therefore, more research is required regarding the impact of substrate gradients (i.e., feast/famine cycles) on the performance of flocculant and granular anaerobic bioreactor systems. In addition to using substrate gradients, oxygen gradients may also have a positive effect on anaerobic sludge flocculation. Although typically the oxygen concentration in anaerobic bioreactors should be reduced to a minimum, researchers have applied micro-aeration for the removal of hydrogen sulphide (Krayzelova *et al.*, 2014) or the improvement of hydrolysis (Johansen & Bakke, 2006). At the applied low supply rate of air, no adverse effects on the physical properties or methanogenic activity of granular sludge was found by Krayzelova and colleagues. In addition, with anecdotal reports of improved membrane filterability when leaks are present in AnMBR systems (personal communication), the abovementioned research results warrant further research regarding the effect of microaeration on bioflocculation and filterability performance in AnMBRs.

Bibliography

Ahn Y, Lee YJ, Kim H-S, Park S (2000) Monitoring of specific methanogenic activity of granular sludge by confocal laser scanning microscopy during start-up of thermophilic upflow anaerobic sludge blanket reactor. *Biotechnol Lett* 22:1591–1596.

Allen KD, Wegener G, White RH (2014) Discovery of multiple modified F430 coenzymes in methanogens and anaerobic methanotrophic *archaea* suggests possible new roles for F430 in nature. *Appl Environ Microbiol* 80:6403–6412.

Alvarado A, Montañez-Hernández LE, Palacio-Molina SL, Oropeza-Navarro R, Luévanos-Escareño MP, Balagurusamy N (2014) Microbial trophic interactions and mcrA gene expression in monitoring of anaerobic digesters. *Front Microbiol* 5:1–14.

Alves MM, Pereira MA, Sousa DZ, Cavaleiro AJ, Picavet M, Smidt H, Stams AJM (2009) Waste lipids to energy: How to optimize methane production from long-chain fatty acids (LCFA). *Microb Biotechnol* 2:538–550.

Ankel-Fuchs D, Thauer RK (1986) Methane formation from methyl-coenzyme M in a system containing methyl-coenzyme M reductase, component B and reduced cobalamin. *Eur J Biochem* 156:171–177.

Anthonisen AC, Srinath EG, Loehr RC, Prakasam TBS (1976) Inhibition of nitrification and nitrous acid compounds. *J Water Pollut Control Fed* 48:835–852.

APHA (2005) Standard Methods for the Examination of Water and Wastewater (1995) 21st edn. American Public Health Association/American Water Works Association/Water Environment Federation, Washington DC.

Appels L, Baeyens J, Degrève J, Dewil R (2008) Principles and potential of the anaerobic digestion of waste-activated sludge. *Prog Energy Combust Sci* 34:755–781.

Arabi S, Nakhla G (2009) Impact of cation concentrations on fouling in membrane bioreactors. *J Memb Sci* 343:110–118.

Balmelle B, Nguyen KM, Capdeville B, Cornier JC, Deguin A (1992) Study of factors controlling nitrite build-up in biological processes for water nitrification. *Water Sci Technol* 26:1017–1025.

Bashiri G, Rehan AM, Greenwood DR, Dickson JMJ, Baker EN (2010) Metabolic engineering of cofactor F420 production in Mycobacterium smegmatis. *PLoS One* 5:e15803.

Bates, BC, Kundzewicz ZW, Wu S, Palutikof JP (2008) Climate Change and Water. Technical Paper of the Intergovernmental Panel on Climate Change, IPCC Secretariat, Geneva, 210 pp.

Bäumer S, Murakami E, Brodersen J, Gottschalk G, Ragsdale SW, Deppenmeier U (1998) The $F_{420}H_2$:heterodisulfide oxidoreductase system from *Methanosarcina* species: 2-Hydroxyphenazine mediates electron transfer from $F_{420}H_2$ dehydrogenase to heterodisulfide reductase. *FEBS Lett* 428:295–298.

Bialek K, Cysneiros D, O'Flaherty V (2014) Hydrolysis, acidification and methanogenesis during low-temperature anaerobic digestion of dilute dairy wastewater in an inverted fluidised bioreactor. *Appl Mircobiol Biotechnol* 98:8737–8750.

Boe K, Batstone DJ, Angelidaki I (2006) An Innovative Online VFA Monitoring System for the Anerobic Process, Based on Headspace Gas Chromatography. *Biotechnol Bioeng* 96:712–721.

Brankatschk R, Bodenhausen N, Zeyer J, Burgmann H (2012) Simple absolute quantification method correcting for quantitative PCR efficiency variations for microbial community samples. *Appl Environ Microbiol* 78:4481–4489.

Brockmann M, Seyfried CF (1996) Sludge activity and cross-flow microfiltration - A non-beneficial relationship. *Water Sci Technol* 34:205–213.

Bruus JH, Nielsen PH, Keiding K (1992) On the stability of activated sludge flocs with implications to dewatering. *Water Res* 26:1597–1604.

Bühligen F, Lucas R, Nikolausz M, Kleinsteuber S (2016) A T-RFLP database for the rapid profiling of methanogenic communities in anaerobic digesters. *Anaerobe* 39:114–116.

Cao TA (2016) Integrating activated sludge floc size information in Membrane Bioreactor (MBR) fouling modeling. PhD thesis, KU Leuven.

Carmona M, Zamarro MT, Blazquez B, Durante-Rodriguez G, Juarez JF, Valderrama JA, Barragan MJL, Garcia JL, Diaz E (2009) Anaerobic Catabolism of Aromatic Compounds: a Genetic and Genomic View. *Microbiol Mol Biol Rev* 73:71–133.

Cavaleiro AJ, Salvador AF, Alves JI, Alves M (2009) Continuous High Rate Anaerobic Treatment of Oleic Acid Based Wastewater is Possible after a Step Feeding Start-Up. *Environ Sci Technol* 43:2931–2936.

Cenens C, Jenné R, Van Impe JF (2002) Evaluation of different shape parameters to distinguish between flocs and filaments in activated sludge images. *Water Sci Technol* 45:85–91.

Cenens C, Smets IY, Van Impe JF (2000) Modeling the Competition Between Floc- Forming and Filamentous Bacteria in Activated Sludge Waste Water Treatment Systems-II. A Prototype Mathematical Model Based on Kinetic Selection and Filamentous Backbone Theory. *Water Res* 34:2535–2541.

Cheeseman P, Toms-Wood A, Wolfe RS (1972) Isolation and Properties of a Fluorescent Compound, Factor F420, from *Methanobacterium* Strain M.o.H. *Microbiology* 112:527–531.

Chen, G. W., Lin, W. W., Lee DJ (1996) Capillary Suction Time As A Measure Of Sludge Dewaterability. *Water Sci Technol* 34:443–448.

Chiesa SC, Irvine RL, Manning JF (1985) Feast/famine growth environments and activated sludge population selection. *Biotechnol Bioeng* 27:562–568.

Cho YT, Young JC, Jordan JA, Moon HM (2005) Factors affecting measurement of specific methanogenic activity. *Water Sci Technol* 52:435–440.

Choi JG, Bae TH, Kim JH, Tak TM, Randall AA (2002) The behavior of membrane fouling initiation on the crossflow membrane bioreactor system. *J Memb Sci* 203:103–113.

Chomczynski P, Sacchi N (1987) Single-Step Method of RNA Isolation by Acid Guanidinium Thiocyanate-Phenol-Chloroform Extraction. *Anal Biochem* 162:156–159.

Choo K-H, Lee C-H (1996) Membrane fouling mechanisms in the membrane-coupled anaerobic bioreactor.

Chudoba J, Grau P, Ottová V (1973) Control of activated-sludge filamentous bulking-II. Selection of microorganisms by means of a selector. *Water Res* 7:1389–1406.

Coates JD, Coughlan MF, Colleran E (1996) Simple method for the measurement of the hydrogenotrophic methanogenic activity of anaerobic sludges. *J Microbiol Methods* 26:237–246.

Colleran E, Concannon F, Golden T, Geoghegan F, Crumlish B, Killilea E, Henry M, Coates J (1992) Use of Methanogenic Activity Tests to Characterize Anaerobic Sludges, Screen for Anaerobic Biodegradability and Determine Toxicity Thresholds against Individual Anaerobic Trophic Groups and Species. *Water Sci Technol* 25:31–40.

Conklin A, Stensel HD, Ferguson J (2006) Growth kinetics and competition between Methanosarcina and Methanosaeta in mesophilic anaerobic digestion. *Water Environ Res* 78:486–496.

Costa JC, Mesquita DP, Amaral AL, Alves MM, Ferreira EC (2013) Quantitative image analysis for the characterization of microbial aggregates in biological wastewater treatment: a review. *Environ Sci Pollut Res* 20:5887–5912.

Craft JL, Horng YC, Ragsdale SW, Brunold TC (2004) Nickel Oxidation States of F430 Cofactor in Methyl-Coenzyme M Reductase. *J Am Chem Soc* 126:4068–4069.

D'Abzac P, Bordas F, Joussein E, Van Hullebusch E, Lens PNL, Guibaud G (2010) Characterization of the mineral fraction associated to extracellular polymeric substances (EPS) in anaerobic granular sludges. *Environ Sci Technol* 44:412–418.

David J, Sierra M, Lafita C, Gabaldón C, Spanjers H, Van Lier JB (2017) Trace metals supplementation in Anaerobic membrane bioreactors treating highly saline phenolic wastewater. *Bioresour Technol* 234:106–114.

Davidson M and Abramowitz M (1999) Optical microscopy review article. Technical report, Olympus America Inc, Scientific Equipment Division.

De Bok FAM, Plugge CM, Stams AJM (2004) Interspecies electron transfer in methanogenic propionate degrading consortia. *Water Res* 38:1368–1375.

De Standaard 21/06/2017, "Schauvliege verbiedt waterverspilling in heel Vlaanderen" <http://www.standaard.be/cnt/dmf20170621_02934619>. Last accessed May 1, 2018.

De Temmerman L, Maere T, Temmink H, Zwijnenburg A, Nopens I (2014) Salt stress in a membrane bioreactor: Dynamics of sludge properties, membrane fouling and remediation through powdered activated carbon dosing. *Water Res* 63:112–124.

De Temmerman L, Maere T, Temmink H, Zwijnenburg A, Nopens I (2015) The effect of fine bubble aeration intensity onmembrane bioreactor sludge characteristics and fouling. *Water Res* 76:99–109.

De Vrieze J, Verstraete W, Boon N (2013) Repeated pulse feeding induces functional stability in anaerobic digestion. *Microb Biotechnol* 6:414–424.

De Zeeuw W (1984) Acclimimation of anaerobic sludge for UASB reactor start-up. PhD thesis, Landbouwhogeschool Wageningen.

Delafontaine MJ, Naveau HP, Nyns EJ (1979) Fluorimetric monitoring of methanogenesis in anaerobic digestors. *Biotechnol Lett* 1:71–74.

del Pozo DF, Mitiku Tobo Y, Van Geem K, de Kreuk MK, van Lier JB, Nopens I (2017) Characterization of full-scale sludge viscosity and density: Testing the stratification hypothesis. *15th IWA World Conference on Anaerobic Digestion.*

Demirel B, Scherer P (2008) The roles of acetotrophic and hydrogenotrophic methanogens during anaerobic conversion of biomass to methane: A review. *Rev Environ Sci Biotechnol* 7:173–190.

Dereli RK, Ersahin ME, Ozgun H, Ozturk I, Jeison D, van der Zee F, van Lier JB (2012) Potentials of anaerobic membrane bioreactors to overcome treatment limitations induced by industrial wastewaters. *Bioresour Technol* 122:160–70.

Dereli RK, Grelot A, Heffernan B, van der Zee FP, van Lier JB (2014) Implications of changes in solids retention time on long term evolution of sludge filterability in anaerobic membrane bioreactors treating high strength industrial wastewater. *Water Res* 59:11–22.

Diekert G, Konheiser U, Piechulla K, Thauer RK (1981) Nickel requirement and factor F430 content of methanogenic bacteria. *J Bacteriol* 148:459–464.

Diekert G, Weber B, Thauer RK (1980) Nickel Dependence of Factor F430 Content in *Methanobacterium thermoautotrophicum**. *Arch Microbiol* 127:273–278.

Dignac M-F, Urbain V, Rybacki D, Brcuhet A, Snidaro D, Scribe P (1998) Chemical description of extracellular polymers: implication on activated sludge floc structure. *Water Sci Technol* 38:45–53.

DiMarco AA, Bobik TA, Wolfe RS (1990) Unusual Coenzymes of Methanogenesis. *Annu Rev Biochem* 59:355–394.

Doddema HJ, Vogels GD (1978) Improved identification of methanogenic bacteria by Improved Identification of Methanogenic Bacteria by Fluorescence Microscopy. *Appl Enviromental Microbiol* 36:752–754.

Dogan T, Ince O, Oz NA, Ince BK (2005) Inhibition of volatile fatty acid production in granular sludge from a UASB reactor. *J Environ Sci Health A Tox Hazard Subst Environ Eng* 40:633–644.

Dolfing J, Mulder JW (1985) Comparison of methane production rate and coenzyme F420 content of methanogenic consortia in anaerobic granular sludge. *Appl Environ Microbiol* 49:1142–5.

Dolfing J, Bloeman WGBM (1985) Acitivity measurements as a tool to characterize the microbial composition of methanogenic environments. *J Microbiol Methods* 4:1–12.

Duin EC (2009) Role of Coenzyme F430 in Methanogenesis. Landes Bioscience and Springer Science+Business Media

Dvořák L, Gó Mez M, Dolina J, Ernín AČ (2016) Anaerobic membrane bioreactors—a mini review with emphasis on industrial wastewater treatment: applications, limitations and perspectives. *Desalin Water Treat* 57:19062–19076.

Egusa G, Brady DW, Grundy SM, Howard BV (1983) Isopropanol precipitation method for the determination of apolipoprotein B specific activity and plasma concentrations during metabolic studies of very low density lipoprotein and low density lipoprotein apolipoprotein B. *J Lipid Res* 24:1261–1267.

Eirich LD, Vogels GD, Wolfe RS (1979) Distribution of coenzyme F420 and properties of its Distribution of Coenzyme F420 and Properties of Its Hydrolytic Fragments. *J Bacteriol* 140:20–27.

Eirich LD, Vogels GD, Wolfe RS (1978) Proposed structure for coenzyme F_{420} from *Methanobacterium*. *Biochemistry* 17:4583–4593.

Eker APM, Eker Hessels JKC, Van De Velde J (1988) Photoreactivating Enzyme from the Green Alga *Scenedesmus acutus*. Evidence for the Presence of Two Different Flavin Chromophores. *Biochemistry* 27:1758–1765.

Eker APM, Kooiman P, Hessels JKC, Yasui A (1990) DNA photoreactivating enzyme from the cyanobacterium *Anacystis nidulans*. *J Biol Chem* 265:8009–8015.

Ellefson WL, Whitman WB, Wolfe RS (1982) Nickel-containing factor F430: chromophore of the methylreductase of *Methanobacterium*. *Proc Natl Acad Sci U S A* 79:3707–3710.

Erickson RJ (1985) An evaluation of mathematical models for the effects of pH and temperature on ammonia toxicity to aquatic organisms. *Water Res* 19:1047–1058.

Ermler U, Grabarse W, Shima S, Goubeaud M, Thauer RK (1997) Crystal structure of methyl-coenzyme M reductase: the key enzyme of biological methane formation. *Science* 278:1457–1462.

Ersahin ME, Ozgun H, Tao Y, Van Lier JB (2014) Applicability of dynamic membrane technology in anaerobic membrane bioreactors. *Water Res* 48:420–9.

Fan F, Zhou H, Husain H (2006) Identification of wastewater sludge characteristics to predict critical flux for membrane bioreactor processes. *Water Res* 40:205–212.

Fang HHP (2000) Microbial distribution in UASB granules and its resulting effects. *Water Sci Technol* 42:201–208.

Faust L, Temmink H, Zwijnenburg A, Kemperman AJB, Rijnaarts HHM (2014) High loaded MBRs for organic matter recovery from sewage: Effect of solids retention time on bioflocculation and on the role of extracellular polymers. *Water Res* 56:258–266.

Fdez-Güelfo LA, Álvarez-Gallego C, Sales D, Romero LI (2012) New indirect parameters for interpreting a destabilization episode in an anaerobic reactor. *Chem Eng J* 180:32–38.

Fermoso FG (2008) Metal supplementation to anaerobic granular sludge bed reactors□: An environmental engineering approach. PhD thesis, Wageningen University.

Ferry JG (2010) The chemical biology of methanogenesis. *Planet Space Sci* 58:1775–1783.

Field RW, Wu D, Howell J a., Gupta BB (1995) Critical flux concept for microfiltration fouling. *J Memb Sci* 100:259–272.

Field RW, Pearce GK (2011) Critical, sustainable and threshold fluxes for membrane filtration with water industry applications. *Adv Colloid Interface Sci* 164:38–44.

Forouhar F, Abashidze M, Xu H, Grochowski LL, Seetharaman J, Hussain M, Kuzin A, Chen Y, Zhou W, Xiao R, Acton TB, Montelione GT, Galinier A, White RH, Tong L (2008) Molecular insights into the biosynthesis of the F420 coenzyme. *J Biol Chem* 283:11832–40.

Freitag TE, Prosser JI (2009) Correlation of methane production and functional gene transcriptional activity in a peat soil. *Appl Environ Microbiol* 75:6679–6687.

Freitag TE, Toet S, Ineson P, Prosser JI (2010) Links between methane flux and transcriptional activities of methanogens and methane oxidizers in a blanket peat bog. *FEMS Microbiol Ecol* 73:157–165.

Frølund B, Palmgren R, Keiding K, Nielsen PH (1996) Extraction of extracellular polymers from activated sludge using a cation exchange resin. *Water Res* 30:1749–1758.

Gabris C, Bengelsdorf FR, Dürre P (2015) Analysis of the key enzymes of butyric and acetic acid fermentation in biogas reactors. *Microb Biotechnol* 8:865–873.

Gao WJ, Han MN, Qu X, Xu C, Liao BQ (2013) Characteristics of wastewater and mixed liquor and their role in membrane fouling. *Bioresour Technol* 128:207–214.

Gasch C, Hildebrandt I, Rebbe F, Röske I (2013) Enzymatic monitoring and control of a two-phase batch digester leaching system with integrated anaerobic filter. *Energy Sustain Soc*.

Gassert, F, Landis M, Luck M, Reig P, and Shiao T (2014) Aqueduct Global Maps 2.1. Working Paper. Washington, DC: World Resources Institute. Available online at <http://www.wri.org/publication/aqueduct-global-maps-21>. Last accessed May 1, 2018.

Gehring T, Klang J, Niedermayr A, Berzio S, Immenhauser A, Klocke M, Wichern M, Lu¨ M (2015) Determination of Methanogenic Pathways through Carbon Isotope (δ 13 C) Analysis for the Two-Stage Anaerobic Digestion of High-Solids Substrates. *Environ Sci Technol* 49:4705–4714.

Ghyoot WR, Verstraete WH (1997) Coupling membrane filtration to anaerobic primary sludge digestion. *Environ Technol* 18:569–580.

Glód BK (1997) Ion exclusion chromatography: Parameters influencing retention. *Neurochem Res* 22:1237–1248.

Gorris LGM, van der Drift C, Vogels GD (1988) Separation and quantification of cofactors from methanogenic bacteria by high-performance liquid chromatography: optimum and routine analyses. *J Microbiol Methods* 8:175–190.

Govoreanu R, Saveyn H, Van der Meeren P, Vanrolleghem P a (2004) Simultaneous determination of activated sludge floc size distribution by different techniques. *Water Sci Technol* 50:39–46.

Graham DE, White RH (2002) Elucidation of methanogenic coenzyme biosyntheses: from spectroscopy to genomics. *Nat Prod Rep* 19:133–147.

Grijspeerdt K, Verstraete W (1997) Image analysis to estimate the settleability and concentration of activated sludge. *Water Res* 31:1126–1134.

Guebitz GM, Bauer A, Bochmann G, Gronauer A, Weiss Editors S (2015) Microbiology and Molecular Biology Tools for Biogas Process Analysis, Diagnosis and Control. In: Biogas Science and Technology. pp 1–40

Gunsalus RP, Wolfe RS (1978) Chromophoric factors F342 and F430 of *Methanobacterium thermoautotrophicum*. *FEMS Microbiol Lett* 3:191–193.

GWI (Global Water Intelligence) (2015) Industrial Water Technology Markets 2015: Meeting Industrial Needs in Process Water Treatment and Wastewater Reuse. Oxford, United Kingdom, GWI.

Halkjaer Nielsen P, Marc Saunders A, Anna Hansen A, Larsen P, Lund Nielsen J, Terry Hazen by C, Wuertz S (2012) Microbial communities involved in enhanced biological phosphorus removal from wastewater — a model system in environmental biotechnology. *Curr Opin Biotechnol* 23:452–459.

Hammes F, Berney M, Wang Y, Vital M, Egli T (2008) Flow-cytometric total bacterial cell counts as a descriptive microbiological parameter for drinking water treatment processes. *Water Res* 42:269–277.

Hänni C, Brousseau T, Laudet V, Stehelin D (1995) Isopropanol precipitation removes PCR inhibitors from ancient bone extracts. *Nucleic Acids Res* 23:881–882.

Hendrickson EL, Leigh JA (2008) Roles of Coenzyme F420 -Reducing Hydrogenases and Hydrogen- and F420 -Dependent Methylenetetrahydromethanopterin Dehydrogenases in Reduction of F420 and Production of Hydrogen during Methanogenesis. *J Bacteriol* 190:4818–4821.

Hettich RL, Pan C, Chourey K, Giannone RJ (2013) Metaproteomics: Harnessing the power of high performance mass spectrometry to identify the suite of proteins that control metabolic activities in microbial communities. *Anal Chem* 85:4203–4214.

Higgins MJ, Novak JT (1997) The effect of cations on the settling and dewatering of activated sludges: Laboratory results. *Water Environ Res* 69:215–224.

Holm-Nielsen JB, Andree H, Lindorfer H, Esbensen KH (2007) Transflexive embedded near infrared monitoring for key process intermediates in anaerobic digestion/ biogas production. *J Near Infrared Spectrosc* 15:123–135.

Holohan BC (2018) Unpublished PhD thesis, National University of Ireland Galway (NUIG).

Hoyos-Hernandez C, Hoffmann M, Guenne A, Mazeas L (2014) Chemosphere Elucidation of the thermophilic phenol biodegradation pathway via benzoate during the anaerobic digestion of municipal solid waste. *Chemosphere* 97:115–119.

Huang Z, Ong SL, Ng HY (2011) Submerged anaerobic membrane bioreactor for low-strength wastewater treatment: Effect of HRT and SRT on treatment performance and membrane fouling. *Water Res* 45:705–713.

Huang Z, Ong SL, Ng HY (2013) Performance of submerged anaerobic membrane bioreactor at different SRTs for domestic wastewater treatment. *J Biotechnol* 164:82–90.

Hüster R, Gilles HH, Thauer RK (1985) Is coenzyme M bound to factor F430 in methanogenic bacteria? Experiments with *Methanobrevibacter ruminantium*. *Eur J Biochem* 148:107–111.

Hutschemackers J, Delafontaine M, Naveau HP, Nyns E (1982) An improved method for the quantitative evaluation of the potential for methane production of mixed microbial communities in digestion mixed liquors trough the determination of the content in coenzyme F420. *Biomass* 2:115–125.

Ince O, Anderson GK, Kasapgil B (1995) Control of organic loading rate using the specific methanogenic activity test during start-up of an anaerobic digestion system. *Water Res* 29:349–355.

Ince O, Ince BK, Yenigun O (2001) Determination of potential methane production capacity of a granular sludge from a pilot-scale upflow anaerobic sludge blanket reactor using a specific methanogenic activity test. *J Chem Technol Biotechnol* 76:573–578.

Ivanovic I, Leiknes TO, Ødegaard H (2008) Fouling control by reduction of submicron particles in a BF-MBR with an integrated flocculation zone in the membrane reactor. *Sep Sci Technol* 43:1871–1883.

Jeison D, Telkamp P, Van Lier JB (2009) Thermophilic Sidestream Anaerobic Membrane Bioreactors: The Shear Rate Dilemma. *Water Environ Res* 81:2372–2380.

Jenné R, Cenens C, Geeraerd AH, Impe JF Van (2002) Towards on-line quantification of flocs and filaments by image analysis. *Biotechnol Lett* 24:931–935.

Jenné R, Banadda EN, Smets I, Deurinck J, Van Impe J (2007) Detection of filamentous bulking problems: developing an image analysis system for sludge composition monitoring. *Microsc Microanal* 13:36–41.

Jensen PD, Yap SD, Boyle-Gotla A, Janoschka J, Carney C, Pidou M, Batstone DJ (2015) Anaerobic membrane bioreactors enable high rate treatment of slaughterhouse wastewater. *Biochem Eng J* 97:132–141.

Jiang B (2006) The Effect of Trace Elements on the Metabolism of Methanogenic Consortia. PhD thesis, Wageningen University

Jin B, Wilén BM, Lant P (2003) A comprehensive insight into floc characteristics and their impact on compressibility and settleability of activated sludge. *Chem Eng J* 95:221–234.

Jobling Purser BJ, Thai SM, Fritz T, Esteves SR, Dindale RM, Guwy a. J, Purser BJJ, Thai SM, Fritz T, Esteves SR, Dinsdale RM, Guwy AJ (2014) An improved titration model reducing over estimation of total volatile fatty acids in anaerobic digestion of energy crop, animal slurry and food waste. *Water Res* 61:162–170.

Jorand F, Zartarian F, Thomas F, Block JC, Bottero JY, Villemin G, Urbain V, Manem J (1995) Chemical and structural (2D) linkage between bacteria within activated sludge flocs. *Water Res* 29:1639–1647.

Juteau P, Rie V, Té C, Duckett M-F, Beaudet RJ, Lé FO, Villemur R, Bisaillon Correspondence J-G (2005) *Cryptanaerobacter phenolicus* gen. nov., sp. nov., an anaerobe that transforms phenol into benzoate via 4-hydroxybenzoate. *Int J Syst Evol Microbiol* 55:245–250.

Kampmann K, Ratering S, Baumann R, Schmidt M, Zerr W, Schnell S (2012) Hydrogenotrophic methanogens dominate in biogas reactors fed with defined substrates. *Syst Appl Microbiol* 35:404–413.

Kaneko M, Takano Y, Ohkouchi N, Sakata S (2017) Does intact coenzyme F430 accumulate? Implication for its use as proxies for methane production and consumption. In: 28th International Meeting on Organic Geochemistryh International Meeting on Organic Geochemistry.

Kaneko M, Takano Y, Chikaraishi Y, Ogawa NO, Asakawa S, Watanabe T, Shima S, Krüger M, Matsushita M, Kimura H, Ohkouchi N (2014) Quantitative analysis of coenzyme F430 in environmental samples: A new diagnostic tool for methanogenesis and anaerobic methane oxidation. *Anal Chem* 86:3633–3638.

Kaneko M, Takano Y, Ogawa NO, Sato Y, Yoshida N, Ohkouchi N (2016) Estimation of methanogenesis by quantification of coenzyme F430 in marine sediments. *Geochem J* 50:1–8.

Kangle KM, Kore S V, Kore VS, Kulkarni GS (2012) Recent Trends in Anaerobic Codigestion: A Review. *Univers J Environ Res Technol* 2:210–219.

Keltjens JT, Huberts MJ, Laarhoven WH, Vogels GD (1983) Structural elements of methanopterin, a novel pterin present in *Methanobacterium thermoautotrophicum*. *Eur J Biochem* 130:537–544.

Keltjens JT, Whitman WB, Caerteling CG, van Kooten AM, Wolfe RS, Vogels GD (1982) Presence of coenzyme M derivatives in the prosthetic group (coenzyme MF430) of methylcoenzyme M reductase from *Methanobacterium thermoautotrophicum*. *Biochem Biophys Res Commun* 108:495–503.

Kern T, Theiss J, Röske K, Rother M (2016) Assessment of hydrogen metabolism in commercial anaerobic digesters. *Appl Microbiol Biotechnol* 100:4699–4710.

Ketheesan B, Stuckey DC (2015) Effects of Hydraulic/Organic Shock/Transient Loads in Anaerobic Wastewater Treatment: A Review. *Crit Rev Environ Sci Technol* 45:2693–2727.

Kida K, Shigematsu T, Kijima J, Numaguchi M, Mochinaga Y, Abe N, Morimura S (2001) Influence of Ni2+ and Co2+ on methanogenic activity and the amounts of coenzymes involved in methanogenesis. *J Biosci Bioeng* 91:590–5.

Kida K, Yorikazu Sonoda I, Kawase M, Nomura T (1991) Influence of mineral nutrients on high performance during anaerobic treatment of wastewater from a beer brewery. *J Ferment Bioeng* 72:54–57.

Klindworth A, Pruesse E, Schweer T, Peplies J, Quast C, Horn M, Glöckner FO (2013) Evaluation of general 16S ribosomal RNA gene PCR primers for classical and next-generation sequencing-based diversity studies. *Nucleic Acids Res* 41:1–11.

Krüger M, Meyerdierks A, Glöckner FO, Amann R, Widdel F, Kube M, Reinhardt R, Kahnt J, Böcher R, Thauer RK, Shima S (2003) A conspicuous nickel protein in microbial mats that oxidize methane anaerobically. *Nature* 426:878–881.

Kunacheva C, Stuckey DC (2014) Analytical methods for soluble microbial products (SMP) and extracellular polymers (ECP) in wastewater treatment systems: A review. Water Res. 61:

Lambrecht J, Cichocki N, Hübschmann T, Koch C, Harms H, Müller S (2017) Flow cytometric quantification, sorting and sequencing of methanogenic *archaea* based on F 420 autofluorescence. *Microb Cell Fact*.

Larson DR, Singer RH, Zenklusen D (2009) A single molecule view of gene expression. *Trends Cell Biol* 19:630–637.

Lemoine L (2018) Unpublished PhD thesis, KU Leuven.

Lettinga G, van Velsen AFM, Hobma SW, de Zeeuw W, Klapwijk A (1980) Use of the upflow sludge blanket (USB) reactor concept for biological wastewater treatment, especially for anaerobic treatment. *Biotechnol Bioeng* 22:699–734.

Levén L, Nyberg K, Korkea-aho L, Schnürer A (2006) Phenols in anaerobic digestion processes and inhibition of ammonia oxidising bacteria (AOB) in soil. *Sci Total Environ* 364:229–238.

Levén L, Nyberg K, Schnürer A (2012) Conversion of phenols during anaerobic digestion of organic solid waste - A review of important microorganisms and impact of temperature. *J Environ Manage* 95:S99–S103.

Li W, Chou S, Khullar A, Gerratana B (2009) Cloning and characterization of the biosynthetic gene cluster for tomaymycin, an SJG-136 monomeric analog. *Appl Environ Microbiol* 75:2958–2963.

Li XY, Yang SF (2007) Influence of loosely bound extracellular polymeric substances (EPS) on the flocculation, sedimentation and dewaterability of activated sludge. *Water Res* 41:1022–1030.

Liao BQ, Allen DG, Droppo IG, Leppard GG, Liss SN (2001) Surface properties of sludge and their role in bioflocculation and settleability. *Water Res* 35:339–350.

Liao B-Q, Kraemer JT, Bagley DM (2006) Anaerobic Membrane Bioreactors: Applications and Research Directions.

Lin H, Chen J, Wang F, Ding L, Hong H (2011) Feasibility evaluation of submerged anaerobic membrane bioreactor for municipal secondary wastewater treatment. *Desalination* 280:120–126.

Lin H, Peng W, Zhang M, Chen J, Hong H, Zhang Y (2013) A review on anaerobic membrane bioreactors: Applications, membrane fouling and future perspectives. *Desalination* 314:169–188.

Lin H, Zhang M, Wang F, Meng F, Liao BQ, Hong H, Chen J, Gao W (2014) A critical review of extracellular polymeric substances (EPSs) in membrane bioreactors: Characteristics, roles in membrane fouling and control strategies. J. Memb. Sci. 460:

Lin XL, White RH (1986) Occurrence of coenzyme F420 and its□γ-monoglutamyl derivative in nonmethanogenic archaebacteria. *J Bacteriol* 168:444–448.

Liu Y, Fang HHP (2003) Influences of Extracellular Polymeric Substances (EPS) on Flocculation, Settling, and Dewatering of Activated Sludge. *Crit Rev Environ Sci Technol* 33:237–273.

Lomborg CJ, Holm-Nielsen JB, Oleskowicz-Popiel P, Esbensen KH (2009) Near infrared and acoustic chemometrics monitoring of volatile fatty acids and dry matter during co-digestion of manure and maize silage. *Bioresour Technol* 100:1711–1719.

Lozano CJS, Mendoza MV, de Arango MC, Monroy EFC (2009) Microbiological characterization and specific methanogenic activity of anaerobe sludges used in urban solid waste treatment. *Waste Manag* 29:704–711.

Lueders T, Chin KJ, Conrad R, Friedrich M (2001) Molecular analyses of methyl-coenzyme M reductase□α-subunit (*mcrA*) genes in rice field soil and enrichment cultures reveal the methanogenic phenotype of a novel *archaeal* lineage. *Environ Microbiol* 3:194–204.

Luton PE, Wayne JM, Sharp RJ, Riley PW (2002) The *mcrA* gene as an alternative to 16S rRNA in the phylogenetic analysis of methanogen populations in landfill. *Microbiology* 148:3521–3530.

Ma K, Conrad R, Lu Y (2012) Responses of methanogen *mcrA* genes and their transcripts to an alternate dry/wet cycle of paddy field soil. *Appl Environ Microbiol* 78:445–454.

Madsen M, Holm-Nielsen JB, Esbensen KH (2011) Monitoring of anaerobic digestion processes: A review perspective. *Renew Sustain Energy Rev* 15:3141–3155.

Mayr S, Latkoczy C, Krüger M, Günther D, Shima S, Thauer RK, Widdel F, Jaun B (2008) Structure of an F430 variant from *archaea* associated with anaerobic oxidation of methane. *J Am Chem Soc* 130:10758–10767.

Meng F, Yang F (2007) Fouling mechanisms of deflocculated sludge, normal sludge, and bulking sludge in membrane bioreactor. *J Memb Sci* 305:48–56.

Meng F, Zhang H, Yang F, Zhang S, Li Y, Zhang X (2006) Identification of activated sludge properties affecting membrane fouling in submerged membrane bioreactors. *Sep Purif Technol* 51:95–103.

Mesquita DP, Amaral AL, Ferreira EC (2011) Identifying different types of bulking in an activated sludge system through quantitative image analysis. *Chemosphere* 85:643–652.

Metje M, Frenzel P (2007) Methanogenesis and methanogenic pathways in a peat from subarctic permafrost. *Environ Microbiol* 9:954–964.

Metzker ML (2010) Sequencing technologies — the next generation. *Nat Rev Genet* 11:31–46.

Moore SJ, Sowa ST, Schuchardt C, Deery E, Lawrence AD, Ramos JV, Billig S, Birkemeyer C, Chivers PT, Howard MJ, Rigby SEJ, Layer G, Warren MJ (2017) Elucidation of the biosynthesis of the methane catalyst coenzyme F430. *Nature*.

Morris RL, Schauer-Gimenez A, Bhattad U, Kearney C, Struble CA, Zitomer D, Maki JS (2013) Methyl coenzyme M reductase (*mcrA*) gene abundance correlates with activity measurements of methanogenic H2/CO2-enriched anaerobic biomass. *Microb Biotechnol* 7:77–84.

Morris RL, Tale VP, Mathai PP, Zitomer DH, Maki JS (2016) *mcrA* Gene abundance correlates with hydrogenotrophic methane production rates in full-scale anaerobic waste treatment systems. *Letters in applied microbiology*, *62*(2), 111-118.

Moura I, Moura JJG, Santos H, Xavier A V., Burch G, Peck HD, LeGall J (1983) Proteins containing the factor F430 from *methanosarcina barkeri* and *methanobacterium thermoautotrophicum*. Isolation and properties. *Biochim Biophys Acta (BBA)/Protein Struct Mol* 742:84–90.

Mulat DG, Jacobi HF, Feilberg A, Peter A, Adamsen S, Richnow H-H, Nikolausz M (2016) Changing Feeding Regimes To Demonstrate Flexible Biogas Production: Effects on Process Performance, Microbial Community Structure, and Methanogenesis Pathways. *Appl Environ Microbiol* 82:438–449.

Mulat DG, Ward AJ, Peter A, Adamsen S, Voigt NV, Nielsen JL, Feilberg A (2014) Quantifying Contribution of Synthrophic Acetate Oxidation to Methane Production in Thermophilic Anaerobic Reactors by Membrane Inlet Mass Spectrometry. *Environ Sci Technol* 48:2505–2511.

Munk B, Bauer C, Gronauer A, Lebuhn M (2012) A metabolic quotient for methanogenic *Archaea*. *Water Sci Technol* 66:2311–2317.

Nagaoka H, Ueda S, Miya A (1996) Influence of bacterial extracellular polymers on the membrane separation activated sludge process. Water Sci. Technol. 34:165–172.

Nettmann E, Bergmann I, Mundt K, Linke B, Klocke M (2008) *Archaea* diversity within a commercial biogas plant utilizing herbal biomass determined by 16S rDNA and *mcrA* analysis. *J Appl Microbiol* 105:1835–1850.

Ney B, Carere CR, Sparling R, Jirapanjawat T, Stott MB, Jackson CJ, Oakeshott JG, Warden AC, Greening C (2017) Cofactor Tail Length Modulates Catalysis of Bacterial F420-Dependent Oxidoreductases. *Front Microbiol*.

Neyens E, Baeyens J, Dewil R, De Heyder B (2004) Advanced sludge treatment affects extracellular polymeric substances to improve activated sludge dewatering. *J Hazard Mater* 106:83–92.

Nguyen D, Gadhamshetty V, Nitayavardhana S, Khanal SK (2015) Automatic process control in anaerobic digestion technology: A critical review. *Bioresour Technol* 193:513–522.

Nguyen TP, Hankins NP, Hilal N (2007) Effect of chemical composition on the flocculation dynamics of latex-based synthetic activated sludge. *J Hazard Mater* 139:265–274.

Nielsen PH, Jahn A (1999) Extraction of EPS. In: Wingender J, Neu TR, Flemming H-C (eds) Microbial Extracellular Polymeric Substances: Characterization, Structure and Function. Springer Berlin Heidelberg, Berlin, Heidelberg, pp 49–72.

Nikolausz M, Walter RFH, Sträuber H, Liebetrau J, Schmidt T, Kleinsteuber S, Bratfisch F, Günther U, Richnow HH (2013) Evaluation of stable isotope fingerprinting techniques for the assessment of the predominant methanogenic pathways in anaerobic digesters. *Appl Microbiol Biotechnol* 97:2251–2262.

Nordberg Å, Hansson M, Sundh I, Nordkvist E, Carlsson H, Mathisen B (2000) Monitoring of a biogas process using electronic gas sensors and near-infrared spectroscopy (NIR). *Water Sci Technol* 41:1–8.

Omil F, Mendez R, Lema JM (1995) Anaerobic treatment of saline wastewaters under high sulphide and ammonia content. *Bioresour Technol* 54:269–278.

Ozgun H, Dereli RK, Ersahin ME, Kinaci C, Spanjers H, Van Lier JB (2013) A review of anaerobic membrane bioreactors for municipal wastewater treatment: Integration options, limitations and expectations. *Sep Purif Technol* 118:89–104.

Pacheco-Ruiz S, Heaven S, Banks CJ (2017) Effect of mean cell residence time on transmembrane flux, mixed-liquor characteristics and overall performance of a submerged anaerobic membrane bioreactor. *Environ Technol* 38:1263–1274.

Parawira W, Murto M, Read JS, Mattiasson B (2005) Profile of hydrolases and biogas production during two-stage mesophilic anaerobic digestion of solid potato waste. *Process Biochem* 40:2945–2952.

Passaris I, Van Gaelen P, Cornelissen R, Simoens K, Grauwels D, Vanhaecke L, Springael D, Smets I (2018) Cofactor F430 as a biomarker for methanogenic activity: application to an anaerobic bioreactor system. *Appl Microbiol Biotechnol* 102:1191–1201.

Peck MW, Chynoweth DP (1992) On-line fluorescence-monitoring of the methanogenic fermentation. *Biotechnol Bioeng* 39:1151–1160.

Pfaltz, A., Jaun, B., Fassler, A., Eschenmoser, A., Jaenchen, R., Gilles, H. H., Diekert, G., Thauer, R. K. (1982). Zur Kenntnis des Faktors F430 aus methanogenen Bakterien: Struktur des porphinoiden Ligandsystems. *Helvetica Chimica Acta*, 65, 828–865.

Pfaltz A, Kobelt A, Hüster R, Thauer RK (1987) Biosynthesis of coenzyme F430 in methanogenic bacteria. Identification of 15,17(3)-seco-F430-17(3)-acid as an intermediate. *Eur J Biochem* 170:459–467.

Pfaltz DA, Jaun B, Diekert G, Thauer RK, Eschenmoser A (1985) Zur kenntnis des faktors F430 aus methanogenen bakterien: Über die natur der isolierungsartefakte van F430, ein beitrag zur shemie von F430 und zur konformationellen stereochemie der ligandperipherie von hydroporphinoiden nickel(II)-komplex. *Helv Chim Acta* 68:1338–1358.

Pind PF, Angelidaki I, Ahring BK (2002) A New VFA Sensor Technique for Anaerobic Reactor Systems. *Biotechnol Bioeng* 82:54–61.

Polag D, May T, Müller L, König H, Jacobi F, Laukenmann S, Keppler F (2015) Online monitoring of stable carbon isotopes of methane in anaerobic digestion as a new tool for early warning of process instability. *Bioresour Technol* 197:161–170.

Qiu G, Song Y hui, Zeng P, Duan L, Xiao S (2013) Characterization of bacterial communities in hybrid upflow anaerobic sludge blanket (UASB)-membrane bioreactor (MBR) process for berberine antibiotic wastewater treatment. *Bioresour Technol* 142:52–62.

Qiu Y, Imachi H, Ohashi A, Harada H (2003) *Sporotomaculum syntrophicum* sp. nov., a novel anaerobic, syntrophic benzoate-degrading bacterium isolated from methanogenic sludge treating wastewater from terephthalate manufacturing. *Arch Microbiol* 179:242–419.

Ramos C, García A, Diez V (2014) Performance of an AnMBR pilot plant treating high-strength lipid wastewater: Biological and filtration processes. *Water Res* 67:203–215.

Refai S, Berger S, Wassmann K, Deppenmeier U (2014) Quantification of methanogenic heterodisulfide reductase activity in biogas sludge. *J Biotechnol* 180:66–69.

Refai S, Berger S, Wassmann K, Hecht M, Dickhaus T, Deppenmeier U (2017) BEAP profiles as rapid test system for status analysis and early detection of process incidents in biogas plants. *J Ind Microbiol Biotechnol* 44:465–476.

Reynolds PJ, Colleran E (1987) Evaluation and improvement of methods for coenzyme F420 analysis in anaerobic sludges. *J Microbiol Methods* 7:115–130.

Rivière D, Desvignes V, Pelletier E, Chaussonnerie S, Guermazi S, Weissenbach J, Li T, Camacho P, Sghir A (2009) Towards the definition of a core of microorganisms involved in anaerobic digestion of sludge. *ISME J* 3:700–714.

Rozzi A, Remigi E (2004) Methods of assessing microbial activity and inhibition under anaerobic conditions: A literature review. *Rev Environ Sci Biotechnol* 3:93–115.

Ruhsing Pan J, Su Y-C, Huang C, Lee H-C (2010) Effect of sludge characteristics on membrane fouling in membrane bioreactors. *J Memb Sci* 349:287–294.

Salama Y, Chennaoui M, Sylla A, Mountadar M, Rihani M, Assobhei O (2016) Characterization, structure, and function of extracellular polymeric substances (EPS) of microbial biofilm in biological wastewater treatment systems: a review. *Desalin Water Treat* 57:16220–16237.

Sandberg M, Ahring BK (1992) Anaerobic treatment of fish meal process waste-water in a UASB reactor at high pH. *Appl Microbiol Biotechnol* 36:800–804.

Schink B (1997) Energetics of Syntrophic Cooperation in Methanogenic Degradation. *Microbiol Mol Biol Rev* 61:262–280.

Schöcke L, Schink B (1999) Energetics and biochemistry of fermentative benzoate degradation by *Syntrophus gentianae*. *Arch Microbiol* 171:331–337.

Schönheit P, Keweloh H, Thauer RK (1981) Factor F420 degradation in *Methanobacterium thermoautotrophicum* during exposure to oxygen. *FEMS Microbiol Lett* 12:347–349.

Shen L-G, Lei Q, Chen J-R, Hong H-C, He Y-M, Lin H-J (2015) Membrane fouling in a submerged membrane bioreactor: Impacts of floc size. *Chem Eng J* 269:328–334.

Sheng G, Yu H, Li X (2010) Extracellular polymeric substances (EPS) of microbial aggregates in biological wastewater treatment systems: A review. *Biotechnol Adv* 28:882–894.

Shiemke AK, Hamilton CL, Scott RA (1988) Structural heterogeneity and purification of protein-free F430 from the cytoplasm of *Methanobacterium thermoautotrophicum*. *J Biol Chem* 263:5611–5616.

Shigematsu T, Era S, Mizuno Y, Ninomiya K, Kamegawa Y, Morimura S, Kida K (2006) Microbial community of a mesophilic propionate-degrading methanogenic consortium in chemostat cultivation analyzed based on 16S rRNA and acetate kinase genes. *Appl Microbiol Biotechnol* 72:401–415.

Shigematsu T, Tang Y, Kobayashi T, Kawaguchi H, Morimura S, Kida K (2004) Effect of dilution rate on metabolic pathway shift between aceticlastic and nonaceticlastic methanogenesis in chemostat cultivation. *Appl Environ Microbiol* 70:4048–4052.

Sobeck DC, Higgins MJ (2002) Examination of three theories for mechanisms of cation-induced bioflocculation. *Water Res* 36:527–538.

Souto TF, Aquino SF, Silva SQ, Chernicharo CAL (2010) Influence of incubation conditions on the specific methanogenic activity test. *Biodegradation* 21:411–24.

Sowers KR, Baron SF, Ferry JG (1984) *Methanosarcina acetivorans* sp. nov., an acetotrophic methane-producing bacterium isolated from marine sediments. *Microbiology* 47:971–978.

Spanjers H, van Lier JB (2006) Instrumentation in anaerobic treatment - research and practice. *Water Sci Technol* 53:63–76.

Springer E, Sachs MS, Woese CR, Boone DR (1995) Partial gene sequences for the A subunit of methyl-coenzyme M reductase (*mcrI*) as a phylogenetic tool for the family *Methanosarcinaceae*. *Int J Syst Bacteriol* 45:554–559.

Steinberg LM, Regan JM (2009) *mcrA*-Targeted Real-Time Quantitative PCR Method To Examine Methanogen Communities. *Appl Environ Microbiol* 75:4435–4442.

Steyer, J.P., Bouvier, J.C., Conte, T., Gras, P., Harmand, J., y Delgenes JP (2002) On-line measurement of COD , TOC , VFA , total and partial alkalinity in anaerobic processes using infra-red spectrometry. *Water Sci Technol* 45:133–138.

Sträuber H, Lucas R, Kleinsteuber S (2016) Metabolic and microbial community dynamics during the anaerobic digestion of maize silage in a two-phase process. *Appl Microbiol Biotechnol* 100:479–491.

Suez Water Technologies & Solutions, InSight: Asset Performance Management for Water, <https://www.suezwatertechnologies.com/insight>. Last accessed May 1, 2018.

Suez Water Technologies & Solutions, ModuleTrac: Track, monitor and analyze ZeeWeed membranes, <https://www.suezwatertechnologies.com/moduletrac>

Switzenbaum MS, Giraldo-Gomez E, Hickey RF (1990) Monitoring of the anaerobic methane fermentation process. *Enzyme Microb Technol* 12:722–730.

Switzenbaum MS, Eimstad RB (1987) Analysis of anaerobic biofilms. *Environ Technol Lett* 8:21–32.

Takano Y, Kaneko M, Kahnt J, Imachi H, Shima S, Ohkouchi N (2013) Detection of coenzyme F430 in deep sea sediments: A key molecule for biological methanogenesis. *Org Geochem* 58:137–140.

Ten Brummeler E, Hulshoff Pol LW, Dolfing J (1985) Methanogenesis in an upflow anaerobic sludge blanket reactor at pH 6 on an acetate-propionate mixture. *Appl Environ Microbiol* 49:1472–1477.

Thauer RK, Kaster A-K, Seedorf H, Buckel W, Hedderich R (2008) Methanogenic *archaea*: ecologically relevant differences in energy conservation. *Nat Rev Microbiol* 6:579–591.

TNAV, Vlaams Netwerk Watertechnologie, Over Intelsens, <https://www.tnav.be/over-intelsens>. Last accessed May 1, 2018.

United Nations (2015). Transforming our world: the 2030 agenda for sustainable development.

United Nations World Water Assessment Programme (WWAP) (2017) The United Nations World Water Development Report 2017. Wastewater: The Untapped Resource. Paris, UNESCO.

Van Beelen P, Labro JF, Keltjens JT, Geerts WJ, Vogels GD, Laarhoven WH, Guijt W, Haasnoot CA (1984) Derivatives of methanopterin, a coenzyme involved in methanogenesis. *Eur J Biochem* 139:359–65.

Van Beelen P, Geerts WJ, Pol A, Vogels GD (1983) Quantification of coenzymes and related compounds from methanogenic bacteria by high-performance liquid chromatography. *Anal Biochem* 131:285–290.

Van De Staey G, Gins G, Smets I (2016) Bioflocculation and Activated Sludge Separation: A PLS Case Study. *IFAC-PapersOnLine* 49:1151–1156.

Van De Staey G (2016) What is the role of activated sludge flocs in membrane fouling in membrane bioreactors (MBRs)? PhD thesis, KU Leuven.

Van De Staey G, Smits K, Smets I (2015) An experimental study on the impact of bioflocculation on activated sludge separation techniques. *Sep Purif Technol* 141:94–104.

Van den Broeck R, Krzeminski P, Van Dierdonck J, Gins G, Lousada-Ferreira M, Van Impe JFM, van der Graaf JHJM, Smets IY, van Lier JB (2011) Activated sludge characteristics affecting sludge filterability in municipal and industrial MBRs: Unraveling correlations using multi-component regression analysis. *J Memb Sci* 378:330–338.

Van den Broeck R, Van Dierdonck J, Caerts B, Bisson I, Kregersman B, Nijskens P, Dotremont C, Van Impe JF, Smets IY (2010) The impact of deflocculation-reflocculation on fouling in membrane bioreactors. *Sep Purif Technol* 71:279–284.

Van den Broeck R, Van Dierdonck J, Nijskens P, Dotremont C, Krzeminski P, van der Graaf JHJM, van Lier JB, Van Impe JFM, Smets IY (2012) The influence of solids retention time on activated sludge bioflocculation and membrane fouling in a membrane bioreactor (MBR). *J Memb Sci* 401–402:48–55.

Van Dierdonck J, Van den Broeck R, Vervoort E, D'haeninck P, Springael D, Van Impe J, Smets I (2012) Does a change in reactor loading rate affect activated sludge bioflocculation? *Process Biochem* 47:2227–2233.

Van Dierdonck J, Van den Broeck R, Vervoort E, Van Impe J, Smets I (2013) The effect of alternating influent carbon source composition on activated sludge bioflocculation. *J Biotechnol* 167:225–234.

Van Lier JB, Van der Zee FP, Frijters CTMJ, Ersahin ME (2015) Celebrating 40 years anaerobic sludge bed reactors for industrial wastewater treatment. *Rev Environ Sci Bio/Technology* 14:681–702.

Vanwonterghem I, Jensen PD, Ho DP, Batstone DJ, Tyson GW (2014) Linking microbial community structure, interactions and function in anaerobic digesters using new molecular techniques. *Curr Opin Biotechnol* 27:55–64.

Veeresh GS, Kumar P, Mehrotra I (2005) Treatment of phenol and cresols in upflow anaerobic sludge blanket (UASB) process: a review. *Water Res* 39:154–170.

Veolia Water Technologies, AQUAVISTA for smarter water solutions <https://www.veoliawatertechnologies.com/en/aquavista-smarter-water-solutions>. Last accessed May 1, 2018.

Visvanathan C, Abeynayaka A (2012) Developments and future potentials of anaerobic membrane bioreactors (AnMBRs). *Membr Water Treat* 3:1–23.

Vlaamse Overheid 2009, MIRA-T Milieurapport Vlaanderen 2008. Indicatorraport, <https://www.vlaanderen.be/nl/publicaties/detail/mira-t-milieurapport-vlaanderen-indicatorrapport-08>. Last accessed May 1, 2018.

Wang B Bin, Peng DC, Hou YP, Li HJ, Pei LY, Yu LF (2014) The important implications of particulate substrate in determining the physicochemical characteristics of extracellular polymeric substances (EPS) in activated sludge. *Water Res* 58:1–8.

Wang L, Shammas N, Hung Y-T (2009) Advanced Biological Treatment Processes, 9th edn. Humana Press, New York

Watanabe T, Kimura M, Asakawa S (2009) Distinct members of a stable methanogenic *archaeal* community transcribe *mcrA* genes under flooded and drained conditions in Japanese paddy field soil. *Soil Biol Biochem* 41:276–285.

Weiland P (2010) Biogas production: Current state and perspectives. *Appl Microbiol Biotechnol* 85:849–860.

Whitman WB, Wolfe RS (1980) Presence of nickel in Factor F430 from *Methanobacterium bryantii*. *Biochem Biophys Res Commun* 92:1196–1201.

Whitmore TN, Etheridge SP, Stafford DA, Leroff UEA, Hughes D (1986) The evaluation of anaerobic digester performance by coenzyme F420 analysis. *Biomass* 9:29–35.

Wirth B, Krebs M, Andert J (2015) Anaerobic degradation of increased phenol concentrations in batch assays. *Environ Sci Pollut Res* 22:19048–19059.

Worm P, Fermoso FG, Stams AJM, Lens PNL, Plugge CM (2011) Transcription of *fdh* and *hyd* in *Syntrophobacter* spp. and *Methanospirillum* spp. as a diagnostic tool for monitoring anaerobic sludge deprived of molybdenum, tungsten and selenium. *Environ Microbiol* 13:1228–1235.

Yu Y, Lee C, Kim J, Hwang S (2005) Group-specific primer and probe sets to detect methanogenic communities using quantitative real-time polymerase chain reaction. *Biotechnol Bioeng* 89:670–679.

Yu Z, Wen X, Xu M, Huang X (2012) Characteristics of extracellular polymeric substances and bacterial communities in an anaerobic membrane bioreactor coupled with online ultrasound equipment. *Bioresour Technol* 117:333–340.

Zehnder AJB, Huser BA, Brock TD, Wuhrmann K (1980) Characterization of an Acetate-Decarboxylating, Non-Hydrogen-Oxidizing Methane Bacterium. *Arch Microbiol* 124:1–11.

Zeikus JG, Kenealy W, Fuchs G, Thauer RK (1977) Oxidoreductases involved in cell carbon synthesis of *Methanobacterium thermoautotrophicum*. *J Bacteriol* 132:604–613.

Zhang C, Yuan Q, Lu Y (2014) Inhibitory effects of ammonia on methanogen *mcrA* transcripts in anaerobic digester sludge. *FEMS Microbiol Ecol* 87:368–377.

Zhang TC, Noike T (1994) Influence of retention time on reactor performance and bacterial trophic populations in anaerobic digestion processes. *Water Res* 28:27–36.

Zhou J, Bruns MANN, Tiedje JM (1996) DNA Recovery from Soils of Diverse Composition. *Appl Enviromental Microbiol* 62:316–322.

Alfred Delaunoislaan 6 – box 2
3001 Heverlee, Belgium

+32497237354
Iason.Passaris@gmail.com

Born 25th of August 1990
in Luxembourg

Curriculum Vitae

Education

2013 – 2018	**PhD in chemical engineering**
KU Leuven, Belgium	*Development and validation of biological monitoring tools for anaerobic (membrane) bioreactors*
2011 - 2013	**MSc in Bio-Engineering – Environmental Technology**
KU Leuven, Belgium	Grade: 79%, cum laude Thesis: *Cultivation and harvesting of microalgal biomass in a lab-scale membrane photo bioreactor* Awarded with 3rd place at the TNAV awards for master thesis research
	Degree environmental coordinator A
	Grade: 79%, cum laude
2008 – 2011	**BSc in Bio-Engineering**
University of Antwerp, Belgium	Grade: 78%, cum laude Presented the bachelor project *Applications for biomass out of bamboo: pyrolysis oil, activated carbon and pretreatments for digestion* at the 9th World Bamboo Congress

Additional courses

Arenberg Doctoral school (2013 – 2018)	Project planning and management • Time-management • Networking Entrepreneurship • Intellectual Property Management Effective Graphical Displays • Identification of personal strengths and weaknesses

Teaching and tutor activities

Thesis students	Tutored five MSc students
Bachelor students	Supervised three groups of bachelor students for P&O projects
Internships	Supervised a Japanese intern for a period of 3 months
Thesis assessment	Took part in the jury of three (additional) MSc theses
Practical sessions	Supervised practical sessions of the course *Wastewater Treatment Technology*

Publications

Peer-reviewed papers	Passaris I., Van Gaelen P., Cornelissen R., Simoens K., Grauwels D., Vanhaecke L., Springael D., Smets I. (2017). Cofactor F430 as a biomarker for methanogenic activity: application to an anaerobic bioreactor system. *Applied Microbiology and Biotechnology*, *102*(3), 1191-1201. Marbelia, L., Bilad, M. R., Passaris, I., Discart, V., Vandamme, D., Beuckels, A. Muylaert , K., & Vankelecom, I. F. (2014). Membrane photobioreactors for integrated microalgae cultivation and nutrient remediation of membrane bioreactors effluent. *Bioresource technology*, *163*, 228-235.
Conferences	Passaris I., Szabo-Corbacho A., Goossens K., Van Gaelen P., Grauwels D., Simoens K., Springael D., Smets I., Van Lier J. (2017). Live biomass fraction and cofactor F430 measurement complementing SMA tests in anaerobic membrane bioreactors? *The 15th*

IWA World Conference on Anaerobic Digestion: Conference Proceedings: Vol. 15. World Conference on Anaerobic Digestion. Beijing, 17-20 October 2017 (pp. 537-540).

Passaris I., Van Gaelen P., Cornelissen R., Simoens K., Springael D., Vanhaecke L., Smets I. (2017). Cofactor F430 content as a potential biomarker for methanogenic activity: application to an anaerobic membrane bioreactor system.

BENELUX Young Water Professionals regional conference. Ghent, Belgium, 5-7 July 2017.

Passaris I., Van Gaelen P., Cornelissen R., Simoens K., Vanhaecke L., Smets I. (2017). Cofactor F430 in AnMBRs: a potential biomarker for methanogenic activity? *IWA Specialized Conference on Instrumentation, Control and Automation*. Québec, Canada, 11-14 June 2017.

Hubeau, M., Passaris, I., Rogiers, G., Bollaerts, M., Brems, A., Appels, L., Dewil, R. & Potters, G. (2012). Applications for biomass out of bamboo: Pyrolysis oil, activated carbon, pretreatments for digestion. In *9th World Bamboo Congress Proceedings* (pp. 361-373). World Bamboo Organization.

Posters

Passaris I., Simoens K., Smets I. (2015). Co-factor F430 monitoring as a manageable tool for methanogenic activity assessment in anaerobic (membrane) bioreactors.
The 14th IWA World Congress on Anaerobic Digestion. Vina del Mar, Chile, 15-18 November 2015.